Investigating the therapeutic potential of REV-ERBα activation in chronic inflammatory diseases

by

Sangeet Makhija

A dissertation submitted to the Graduate Faculty of

Auburn University

In partial fulfillment of the

Requirements for the Degree of

Doctor of Philosophy

Auburn, Alabama

May 4, 2024

Approved by

Kristine Griffett, Chair, Assistant Professor

Robert Judd, Boshell Professor

Bruce F. Smith, Professor

Russell Cattley, Tyler & Frances Young Professor Emeritus

Maninder Sandey, Associate Professor

Amol Suryawanshi, Assistant Professor

Abstract

Metabolic-associated steatohepatitis (MASH) is a metabolic disease of the liver, that manifests itself as steatohepatitis, inflammation, and fibrosis. It has the potential to progress to cirrhosis and hepatocellular carcinoma if uncontrolled. Currently, there is no effective treatment strategy except lifestyle changes. It is imperative to develop therapeutics against MASH and alleviate the leading cause of liver transplants across the world. We and others have shown that nuclear receptor REV-ERB plays a significant protective role in liver biology by acting as a transcriptional repressor of important genes involved in metabolism, inflammation, and fibrosis. While we have shown that in-vivo administration of REV-ERB agonist SR9009 is able to alleviate symptoms of MASH such as inflammation and fibrosis, we are yet to find out its mechanism of action. Additionally, SR9009 has its limitations in terms of solubility and efficacy. In this dissertation, we utilize a relatively novel REV-ERB agonist STL1267 and explore its efficacy in the treatment of MASH. We also explore its mechanism of action using in-vitro and in-vivo mouse models. We found that STL1267 is more effective in treating MASH, with increased reduction in triglycerides, inflammation, and fibrosis. We were able to show that REV-ERB agonism acts via metabolically reprogramming energy metabolism in cells associated with MASH. It reduces mitochondrial metabolism, and alleviates metabolic stress, reducing the further downstream effects such as oxidative stress, mitochondrial dysfunction, inflammation, and fibrosis in cells such as hepatocytes, stellate cells, and macrophages.

Acknowledgements

I would like to express my sincere gratitude to Dr. Griffett for her unwavering support, invaluable mentorship, and for fostering an exceptional learning environment throughout my doctoral journey. A special thanks to Josh for his consistent assistance in experiments and beyond. I am also deeply grateful to all members of the Griffett Lab for their friendship, camaraderie, and unwavering support throughout this endeavor.

I extend my heartfelt appreciation to my committee for their encouragement and guidance. Their expertise and insights have been invaluable in shaping this thesis.

Chapters 2-4 will be submitted as a manuscript. I would like to acknowledge the collaborative efforts with UC Davis for tissue RNAseq and Metabolomics analysis, and Dr. Mitra at the Center for Pharmacogenomics and Single-Cell Omics, Auburn University, for conducting Cell RNAseq. I am grateful to Ms. Melissa Kazantzis at Scripps, Florida, for her expertise in serum analysis, Dr. Kyle McCommis at SLU for his help with experimental design and to Dr. Emily Graff of Auburn University for her assistance with histological assessments. All schematics were created with www.biorender.com.

I am profoundly thankful to Guru ji, my grandparents; parents; and sisters, whom I strive to make proud for their unwavering support, encouragement, and

understanding throughout this journey. Their love and encouragement have been my pillars of strength.

Lastly, I am indebted to Late Dr. Kusum R Gupta for igniting my interest in research and providing me with the initial guidance that set me on this path.

Thank you all for being an integral part of this journey.

Table of Contents

LIST OF FIGURES

List of Abbreviations

LBD: Ligand Binding Domain

RXR: Retinoid X Receptor

RAR: Retinoic Acid Receptors

PPAR: Peroxisome Proliferator-Activated Receptor

LXR: Liver X Receptors

FXR: Farnesoid X Receptor

VDR: Vitamin D Receptor

TR: Thyroid Hormone Receptor

NR: Nuclear Receptor

ER: Estrogen Receptor

cDNA: Complimentary DNA

TTFL: Transcription-Translation Feedback Loop

PR: Progesterone Receptor

ChIP: Chromatin Immunoprecipitation

NCoR: Nuclear Hormone Receptor Co-Repressor

DBD: DNA-Binding Domain

ROR: RA Related Orphan Receptor

RORE: ROR Response Element

HDAC3: Histone Deacetylase 3

HNF: Hepatocyte Nuclear Factor

TF: Transcription Factors

G6PC: Glucose-6-Phosphatase

PCK1: Phosphoenolpyruvate Carboxykinase 1

BMAL1: Brain and Muscle ARNT-like 1

PPARG: Peroxisome Proliferator-Activated Receptor Gamma

PGC1a: Peroxisome Proliferator-Activated Receptor Gamma Coactivator 1-alpha

GSK: Glycogen Synthase Kinase

FRET: Fluorescence Resonance Energy Transfer

SAR: Structure-Activity Relationship

SCN: Suprachiasmatic Nucleus

bHLH: Basic Helix-Loop-Helix

Npas2: Neuronal PAS Domain Protein 2

CLOCK: Circadian Locomotor Output Cycles Kaput

BMDM: Bone Marrow-Derived Macrophages

Nfil3: Nuclear Factor Interleukin-3 Regulated Protein

ILC3: Innate Lymphoid Cells type 3

EAE: Experimental Autoimmune Encephalomyelitis

TLR4: Toll-Like Receptor 4

CCL2: Chemokine (C-C motif) Ligand 2

MMP9: Matrix Metalloproteinase 9

CX3CR1: Chemokine (C-X3-C motif) Receptor 1

IL6: Interleukin 6

KO: Knockout

SREBP: Sterol Regulatory Element Binding Proteins

NASH: Nonalcoholic Steatohepatitis

NAFLD: Nonalcoholic Fatty Liver Disease

MASLD: Metabolic Associated Fatty Liver Disease

MASH: Metabolic Associated Steatohepatitis

TG: Triglycerides

WAT: White Adipose Tissue

DNL: De Novo Lipogenesis

IR: Insulin Resistance

ACC: Acetyl-CoA Carboxylase

FAS: Fatty Acid Synthase

JNK: c-Jun N-terminal Kinase

FAO: Fatty Acid Oxidation

HSC: Hepatic Stellate Cells

KC: Kupffer Cells

LDL: Low-Density Lipoprotein

FFA: Free Fatty Acids

OA: Oleic Acid

PA: Palmitic Acid

mtDNA: Mitochondrial DNA

TCA: Tricarboxylic Acid Cycle

ETC: Electron Transport Chain

MPTP: 1-Methyl-4-Phenyl-1,2,3,6-Tetrahydropyridine

DAMP: Damage-Associated Molecular Pattern

HCC: Hepatocellular Carcinoma

OS: Oxidative Stress

LPS: Lipopolysaccharide

PDGF: Platelet-Derived Growth Factor

NK: Natural Killer Cells

MetS: Metabolic Syndrome

CVD: Cardiovascular Disease

T2DM: Type 2 Diabetes Mellitus

TG: Triglycerides

VLDL: Very Low-Density Lipoprotein

mTORC1: Mammalian Target of Rapamycin Complex 1

LD: Lipid Droplets

ROS: Reactive Oxygen Species

PDC: Pyruvate Dehydrogenase Complex

LDH: Lactate Dehydrogenase

MRC: Mitochondrial Respiratory Chain

HFD: High-Fat Diet

PMA: Phorbol 12-Myristate 13-Acetate

CNS: Central Nervous System

List of Tables

Chapter 1: Introduction

1.1 Nuclear Receptors

Nuclear receptors (NR) are transcription factors (TF), that regulate transcription via either promoting or repressing target genes. They can bind DNA as monomers, homodimers, or heterodimers at specific DNA recognition sequences in the promoter regions of target genes. This action is often in response to of the receptors endogenous ligand(s), that are often hydrophobic entities that promote conformational changes in the receptor to allow the formation of multi-protein complexes for transcriptional regulation (Alexander et al., 2021; Aranda & Pascual, 2001).

Nuclear receptors with identified endogenous ligands, are divided in two sub-groups: steroid hormone receptors and non-steroid hormone receptors. Steroid hormone receptors primarily exist outside of the nucleus, in a complex with chaperone proteins. Upon binding with a ligand, these chaperone proteins are liberated, allowing for the migration of the receptor to the nucleus for transcription regulation. A conformational shift in the ligand-binding domain, or LBD, brought on by the binding of ligands, sets off a series of subsequent events. These events include the receptor's separation from heat shock proteins and its translocation from the cytoplasm to the nucleus for some nuclear receptors, notably the glucocorticoid receptor and other steroid receptors. When a ligand binds to a

receptor, it undergoes a conformational change that allows for the recruitment of transcriptional co-regulatory proteins to receptor-specific gene promoter complexes to activate or inhibit transcription (Xiao & DeFranco, 1997).

Non-steroid hormone receptors are typically within the nucleus also in the apo state, but often form heterodimers with other nuclear receptors and/or transcriptional regulators. Non-steroid hormone receptors, also known as nuclear receptors, play crucial roles in regulating gene expression and various cellular processes. These receptors are typically found within the nucleus, even in their unbound or apo state, where they can modulate gene transcription in response to ligand binding (Sever & Glass, 2013). While many of these receptors can function as homodimers (two identical subunits) in their activated state, they often form heterodimers (two different subunits) with other nuclear receptors or transcriptional regulators, expanding their regulatory capabilities and specificity (Bookout et al., 2006).

One common partner for heterodimerization is the Retinoid X Receptor (RXR), which is itself a nuclear receptor. When nuclear receptors form heterodimers with RXR, they can influence specific pathways beyond those associated with classical hormone signaling. RXR serves as a versatile partner due to its ability to interact with various ligands, including those derived from dietary sources or synthetic compounds, in addition to hormones. There are various ligands that bind to nuclear receptors partnering with RXR (Chambon, 1996; Ghyselinck & Duester, 2019).

Retinoic acid is a metabolite of vitamin A and serves as a ligand for several nuclear receptors, including the retinoic acid receptors (RARs) and peroxisome proliferator-activated receptor beta/delta (PPARβ/δ), which heterodimerize with RXR. These receptors regulate processes such as cell growth, differentiation, and metabolism. Oxysterols are oxidized derivatives of cholesterol (Chandra et al., 2008). Liver X receptors (LXRs) are nuclear receptors that form heterodimers with RXR and are activated by oxysterols. LXRs play essential roles in lipid metabolism, inflammation, and cholesterol homeostasis (Tontonoz & Mangelsdorf, 2003). Fatty acids and their derivatives, such as prostaglandins, can act as ligands for nuclear receptors like the peroxisome proliferator-activated receptors (PPARs), which can heterodimerize with RXR. PPARs regulate various metabolic processes, including lipid metabolism and inflammation (Berger & Moller, 2002). Bile acids, synthesized from cholesterol in the liver, serve as ligands for the farnesoid X receptor (FXR) and the vitamin D receptor (VDR), both of which can heterodimerize with RXR. FXR regulates bile acid homeostasis, lipid metabolism, and glucose metabolism, while VDR plays a role in calcium homeostasis and immune function (Saeed et al., 2019).

These examples illustrate the diverse range of ligands and pathways regulated by nuclear receptors that heterodimerize with RXR. By partnering with RXR, these receptors can respond to various signaling molecules beyond classical steroid hormones, allowing for precise control of gene expression and cellular responses in diverse physiological contexts.

Nuclear receptors can regulate transcriptional activation by binding DNA at canonical consensus sequences. Binding at these sequences can occur in varied patterns, which allows for selectivity in gene regulation. These sequences are typically short stretches of DNA that exhibit a high degree of similarity across different genes or genomes. Nuclear receptors utilize these consensus sequences as recognition sites to bind to specific regions of DNA and regulate gene expression (Penvose et al., 2019). The ability of nuclear receptors to bind to these consensus sequences in varied patterns contributes to their selectivity in gene regulation. This selectivity arises from several factors. While consensus sequences represent a general pattern of nucleotides recognized by a particular DNA-binding protein, there is often variability in the exact sequence surrounding the consensus motif. This variability allows nuclear receptors to recognize and bind to a diverse array of sequences that contain variations of the consensus motif (Fang et al., 2012). As a result, nuclear receptors can regulate different sets of target genes by binding to similar but not identical sequences (Sever & Glass, 2013).

Nuclear receptors do not act alone in regulating gene expression; they often interact with coactivators or corepressors, which influence their DNA-binding specificity and transcriptional activity (Lonard & O'Malley, 2006). These cofactors can modulate the binding affinity of nuclear receptors for specific DNA sequences or stabilize receptor-DNA complexes. By interacting with different cofactors, nuclear receptors can exhibit selective binding to distinct subsets of DNA

sequences, leading to differential gene regulation (Aagaard et al., 2011). Nuclear receptors are dynamic proteins that can adopt multiple conformational states upon ligand binding. Ligand binding induces structural changes in the receptor, altering its interaction with DNA and cofactors. This conformational flexibility allows nuclear receptors to bind to DNA sequences with varying affinities and specificities depending on the ligand present (Khan et al., 2022). Different ligands may stabilize distinct receptor conformations that preferentially interact with specific DNA sequences, thereby influencing the selectivity of gene regulation (de Vera et al., 2017). As previously mentioned, nuclear receptors can form heterodimers with other nuclear receptors or transcription factors, such as RXR. Heterodimerization expands the repertoire of DNA sequences that nuclear receptors can bind to, as it allows them to recognize composite response elements composed of motifs recognized by both partners. By partnering with different heterodimerization partners, nuclear receptors can regulate gene expression in a highly selective manner, targeting specific sets of genes involved in different biological processes (Butt & Walfish, 1996).

In summary, the selectivity of gene regulation by nuclear receptors arises from the combined effects of variability in DNA binding motifs, interactions with cofactors, conformational flexibility, and heterodimerization with other transcription factors. These mechanisms allow nuclear receptors to bind to diverse DNA sequences and regulate the expression of specific target genes in response to various physiological and environmental cues.

1.1.1 Ligand regulation of nuclear receptors

Most nuclear receptors will typically function as ligand-dependent transcription factors. Each gene has promoter/enhancer regions rich with specific DNA-response elements that are recognized by nuclear receptors. Nuclear receptors can alter the recruitment and binding of other transcription factors that might regulate gene expression. All 48 members of the nuclear receptor family have specific and distinct DNA response elements as well as ligands that they bind to, attributing to their distinct functions (Fischer & Smiesko, 2019). Most nuclear receptors can function both in presence and absence of ligands, however, their degree of gene regulation may vary. An example of this is thyroid hormone receptor (TR), which functions as a transcriptional repressor in the absence of its ligand, thyroid hormone. However, in its presence, it exerts its function as a transcriptional activator (Grontved et al., 2015; Horlein et al., 1995). Often, ligand binding induces structural conformations, possibly in the LBD thus altering the binding of protein cofactors to which the NR binds.

Structural studies have shown that NR LBDs have a conserved tertiary structure composed of alpha-helices arranged as a three-layer sandwich. This domain is largely globular, and the ligand binding pocket exists in its interior, consistent with its hydrophobic characteristic. Within the domain, there are 11 helices, and helix 12 (H12) forms a mobile lid over the ligand binding pocket (Hill et al., 2012). This

serves as a critical site for the binding of ligand-recruited co-activator proteins (Fig 1.1). In the absence of H12, such as in NR REV-ERBα (NR1D1), the ability to recruit and bind co-activators is lost, and thus, REV-ERBα can only act as a transcriptional repressor (Renaud et al., 2000).

1.1.2 Why study nuclear receptors?

There has been a great deal of interest in finding natural or synthetic ligands for the orphan members of the superfamily that could be used as chemical tools to probe receptor function and to elucidate the potential therapeutic value of these receptors. Numerous drugs on the market target nuclear receptors. In fact, nuclear receptors are second to GPCRs which are the most targeted family of receptors for drug discovery. Since nuclear receptors are involved in numerous physiological processes, drug discovery and development has focused extensively on several of these receptors. Drugs targeting nuclear receptors play significant roles in various therapeutic areas, including metabolic disorders, cancer, and inflammatory diseases. Examples of drugs targeting nuclear receptors include Rosiglitazone and Pioglitazone which target peroxisome proliferator-activated receptor gamma (PPARγ) (Orasanu et al., 2008). These are used in the treatment of type 2 diabetes mellitus by improving insulin sensitivity and glucose metabolism (Doggrell, 2008). Another prominent example is Tamoxifen, which targets estrogen receptor (ER), and is used in the treatment of ER positive breast cancer (Cuzick et al., 2015). These examples demonstrate the diverse therapeutic applications of drugs targeting nuclear receptors across various medical conditions.

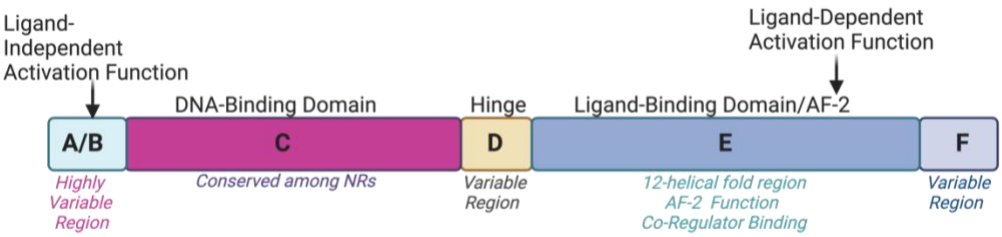

Figure 1.1 **Canonical nuclear receptor structure and modular domains.** At the core of NR structure lies the DNA-binding domain (DBD), which typically consists of two zinc finger motifs responsible for recognizing specific DNA sequences known as response elements. Adjacent to the DBD is a highly variable region, which confers specificity in DNA binding and ligand recognition. Following the DBD, NRs possess a flexible hinge region, often termed the variable region, which facilitates conformational changes upon ligand binding. The ligand-binding domain (LBD) contains a conserved 12-helical fold region responsible for ligand binding and receptor activation. Within the LBD, the activation function 2 (AF-2) helix serves as a docking site for coactivator proteins, facilitating the recruitment of the transcriptional machinery and gene activation. This modular structure of NRs allows for versatile regulation of gene expression in response to diverse physiological signals, highlighting their importance in cellular homeostasis and adaptation.

1.2 NR REV-ERBs - Importance in Physiology

1.2.1 History

The discovery of REV-ERBα represents a pivotal milestone in our understanding of the intricate molecular mechanisms governing circadian rhythm regulation. Through a series of landmark discoveries, researchers have unraveled the multifaceted roles of REV-ERBα in orchestrating the circadian clock. In 1989, Nobuyuki Miyajima and colleagues identified two orthologs of erbA on human chromosome 17, setting the stage for the discovery of REV-ERBα (Miyajima et al., 1989). These orthologs, transcribed from opposite DNA strands at the same locus, laid the groundwork for understanding the molecular basis of circadian rhythm regulation. Subsequent efforts led to the isolation of REV-ERBα complementary DNA (cDNA) from a human fetal skeletal muscle library in 1990 by Mitchell A. Lazar, Karen E. Jones, and William W. Chin (Lazar et al., 1989). This pivotal discovery provided the first insights into the genetic structure of REV-ERBα and its relationship with hormone receptors.

The involvement of REV-ERBα in circadian rhythm regulation was first suggested in 1998 by Ueli Schibler's group (Balsalobre et al., 1998). Through meticulous experiments, they demonstrated the daily rhythmic expression of REV-ERBα in rat fibroblasts, hinting at its potential role in the circadian clock. This discovery marked the beginning of a new era in circadian biology, as researchers began to unravel

the molecular mechanisms underlying REV-ERBα's circadian function. The pivotal role of REV-ERBα in the transcription-translation feedback loop (TTFL) was further elucidated in 2002, representing a major breakthrough in our understanding of circadian rhythm regulation. Through a series of elegant experiments, researchers demonstrated that REV-ERBα acts as a transcriptional repressor, suppressing the expression of the Bmal1 gene, a key component of the positive arm of the circadian clock (Preitner et al., 2002). Furthermore, the expression of REV-ERBα itself was found to be regulated by other components of the TTFL, establishing it as a critical link between the positive and negative regulatory arms of the circadian rhythm.

The discovery of REV-ERBα has had profound implications for our understanding of circadian biology and its potential therapeutic applications. By elucidating the molecular mechanisms underlying circadian rhythm regulation, researchers have gained insights into various physiological processes influenced by the circadian clock, including metabolism, sleep-wake cycles, and immune function. Moreover, REV-ERBα has emerged as a promising target for the development of novel therapeutics for circadian rhythm disorders and related metabolic conditions. For many years, science and medicine have been greatly impacted by historical discoveries pertaining to nuclear hormone receptors, such as the ER, progesterone receptor (PR), TRs, RARs, and RXRs. The framework for comprehending hormone action was established by Elwood V. Jensen's seminal discovery of the ER in 1958 (Jensen et al., 1967; Jensen et al., 1968). This was especially true in the field of breast cancer research, where treatment tactics were

driven by the contrasts between ER-positive and ER-negative cells. In a similar vein, John Gorski's 1968 discovery of the PR clarified its crucial function in reproductive biology as well as its connection to breast and endometrial malignancies (Gorski et al., 1968). The 1970s saw the characterization of TRs, which demonstrated their crucial role in the control of metabolism and the processes involved in development.

The identification of RXRs and RARs in the 1980s led to new insights into the development of the embryo and opened up new treatment options for conditions like acute promyelocytic leukemia (Benbrook et al., 2014). These groundbreaking discoveries open the door for focused treatment approaches across a range of medical specialties by highlighting the significance of nuclear hormone receptors in physiological homeostasis and disease pathogenesis. Understanding the structure and function of REV-ERBs required the identification and characterization of several nuclear receptors, including PPARs, RARs, and TRs. Through contrasting the structural patterns and functional characteristics of recognized NRs with REV-ERBs, scientists were able to obtain important understandings of their possible functions in cellular physiology. The identification of shared domains within REV-ERBs was made possible by the structural homology between these receptors, which offered insights into their possible connections and mode of action with other cellular components. Furthermore, possible activities for REV-ERBs, such as metabolism and circadian rhythm regulation, were deduced using functional analogies derived from the roles of TRs,

RARs, and PPARs in transcriptional regulation. Research on other NRs provided information on gene regulation mechanisms and ligand binding specificity, which made it easier to investigate the ligand-dependent transcriptional activities of REV-ERBs and how they affect target gene expression. In general, the earlier knowledge of NR biology offered a strong basis for clarifying the functions of REV-ERBs in cellular functions and their possible effects on health and illness.

REV-ERBβ was discovered in 1994 (Dumas et al., 1994). This discovery provided the foundation for further characterization of REV-ERBs and their biological functions. Subsequent studies focused on elucidating the biological functions of REV-ERBs and their role in gene regulation (Burke et al., 1996; Renaud et al., 2000). Researchers employed molecular biology techniques, such as gene expression analysis, protein-protein interaction assays, and chromatin immunoprecipitation (ChIP) experiments, to investigate the transcriptional activities and binding properties of REV-ERBs. These studies revealed that REV-ERBs functioned as transcriptional repressors involved in the regulation of circadian rhythm and metabolic pathways (Guillaumond et al., 2005; Laitinen et al., 2005; Ramakrishnan & Muscat, 2006; Teboul & Delaunay, 2003).

Another key aspect of REV-ERB discovery was the identification of their endogenous ligand, heme. Researchers uncovered the ability of REV-ERBs to bind heme, a crucial molecule involved in various cellular processes, including oxygen transport, oxidative metabolism, and circadian rhythm regulation. The

identification of heme as the endogenous ligand for REV-ERBs provided insights into the mechanisms underlying their activity and regulation (Raghuram et al., 2007). Both REV-ERBα and REV-ERBβ are similar in their function, tissue distribution, as well as structure. Studies using knockout mice have shown that they have redundant roles with the ability to compensate for each other's functional loss. However, it has also been shown that REV-ERBα is the dominant isotype. (Bugge et al., 2012; Janich et al., 2015; Pariollaud et al., 2018)

1.2.2 Expression Profile

REV-ERBα is ubiquitously expressed as a single 3 kb mRNA in mammals. Extremely low amounts are seen in the testis, lung, and hypothalamus, moderate levels in the pituitary and kidney, and strong expression in the brain, liver, heart, and brown fat (Raza et al., 2022). It has been revealed that B lymphocyte lineage cell lines also express REV-ERBα. REV-ERBα expression begins in the heart at E 10.5 during development, moves to the eyes the next day, and then increases during the second week of life. High expression was seen in the brain's cerebral cortex, hippocampus, olfactory granule cells, and cerebellar Purkinje cells. Research has demonstrated that the expression of REV-ERBα increases during the differentiation of adipocytes and decreases during myogenic differentiation.

1.2.3 REV-ERBs are Transcriptional Repressors

REV-ERBs exert their transcriptional control by binding to specific DNA sequences known as RevRE or RORE sites (Giguere et al. 1994). These sites typically consist of an AGGTCA half-site flanked by an A/T-rich region. REV-ERBα, binds to these sequences, specifically targeting the major groove of the AGGTCA half-site (Harding and Lazar, 1993). While REV-ERBs bind to this site as monomers, they bind even more tightly as a dimer, when the sequence is repeated with a 2bp spacer, called the REVDR2 (Harding and Lazar 1995). This sequence-specific binding is crucial for the subsequent steps in the repression process. A key aspect of REV-ERB-mediated transcriptional repression is its constitutive interaction with Nuclear Corepressor 1 (NCoR) (Horelein et al. 1995; Zamir et al. 1996). NCoR is a large protein that possesses inherent repressive functions. The interaction between REV-ERB and NCoR is facilitated by specific domains within NCoR, known as corepressor-NR (CoRNR) boxes, which specifically interact with NRs like REV-ERBs (Hu and Lazar 1999). Additionally, the stability of this interaction is enhanced by heme, which also serves as a sensor for REV-ERB activity (Raghuram et all 2007; Yin et al 2007). Upon binding to NCoR, REV-ERB initiates the assembly of a multiprotein repressor complex. This complex includes various components such as Transducin Beta-Like 1 (TBL1), G-protein Pathway Suppressor 2 (GPS2), and Histone Deacetylase 3 (HDAC3). These proteins collaborate to establish a repressive environment at the target gene loci. HDAC3, a critical component of the repressor complex, plays a pivotal role in modifying the chromatin structure. HDAC3 catalyzes the removal of acetyl groups from lysine residues in the histone proteins associated with the DNA. (Haberland et al 2009)

This process, known as histone deacetylation, results in a more condensed chromatin structure that is less accessible to transcriptional machinery. The repressive chromatin environment established by HDAC3-mediated histone deacetylation, combined with the recruitment of other factors within the repressor complex, effectively inhibits the activity of core transcriptional factors and RNA polymerase II. As a result, the transcription of target genes at REV-ERB binding sites is repressed (Fig 1.2).

There is also a feedback loop connecting the REV-ERBs and RORs. RevRE, that allows for both autoregulation and ROR control is present in the NR1D1 gene promoter (Burris et al., 2023). In turn, REV-ERB also modulates the NR1F1 (RORα) gene. However, it has been observed that REV-ERB is able to bind to the genome in a tissue-specific manner even when the RORE motif is lacking. While the classical mode of REV-ERB action involves binding to ROREs to regulate target gene transcription, several studies have revealed additional mechanisms through which REV-ERB can exert its regulatory effects in a context-dependent manner. REV-ERB can interact with and modulate the activity of other transcription factors, thereby influencing gene expression indirectly. This happens through various mechanisms.

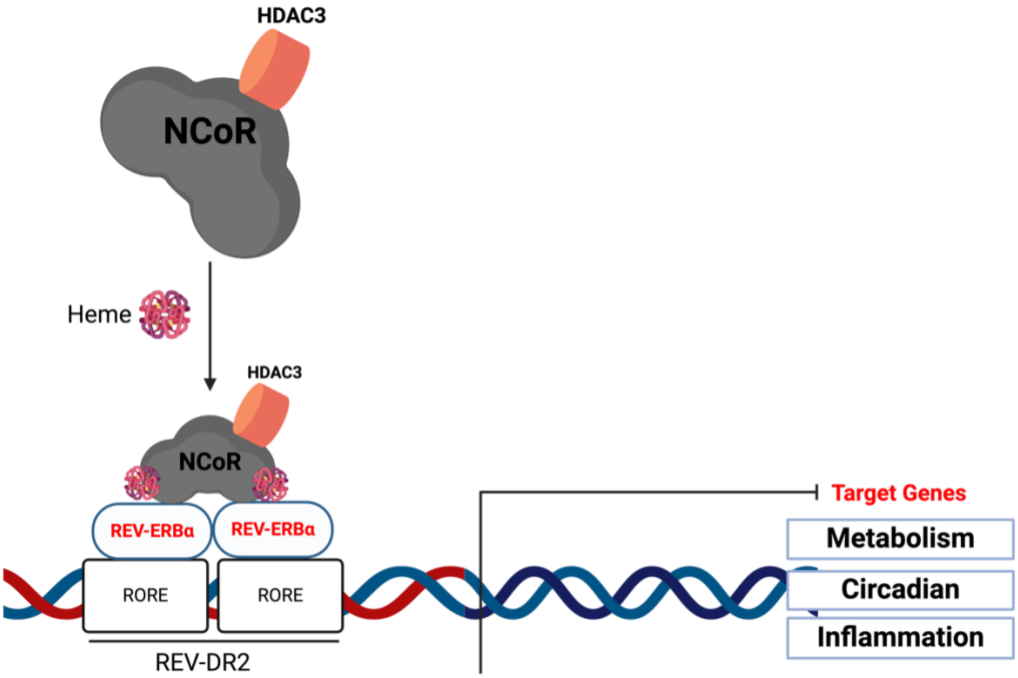

Figure 1.2 REV-ERBα is a transcriptional repressor. RORE repeat elements form REV-DR2, a specific binding site for REV-ERBα to dimerize at. NCoR binds to REV-ERBα through CoRNR boxes, and is stabilized by interaction with its natural ligand, heme. Upon binding to NCoR, REV-ERB initiates the assembly of a multiprotein repressor complex, including HDAC3. HDAC3 condenses the chromatin structure through histone deacetylation, resulting in effective transcriptional repression of various target genes such as in metabolism, circadian, and inflammatory pathways.

REV-ERB has also been shown to interact with nuclear receptors such as the RORs and LXRs, which themselves bind to specific DNA motifs (Fontaine et al., 2008). By forming complexes with these transcription factors, REV-ERB can influence their transcriptional activity and target gene specificity, even in the absence of canonical RORE motifs. For example, the REV-ERBs bind to the NF-Y transcription factor to reduce the production of myogenic regulatory factors in proliferating myoblasts (Welch et al., 2017), and they bind to hepatocyte nuclear factor 4a and 6 (Hnf) to suppress genes involved in liver metabolism. This type of non-canonical binding to other TFs gives REV-ERB the ability to reprogram gene expression in a tissue-specific manner. These interactions can occur independently of DNA binding and may facilitate the recruitment of REV-ERB to specific genomic regions or modulate its transcriptional activity. It has also been observed that REV-ERB-mediated gene regulation can involve long-range chromatin interactions that bring distal regulatory elements, such as enhancers or silencers, into proximity with target gene promoters. These interactions can be mediated by chromatin looping mechanisms and may occur independently of direct DNA binding by REV-ERB (Papazyan et al., 2016).

1.2.4 REV-ERB ligands

Like other nuclear receptors, REV-ERB receptors contain a distinct ligand binding domain and can bind specific endogenous and small molecule ligands. Recent years have witnessed discovery of an array of new REV-ERBα ligands most of which have pharmacological activities in vivo. It is noteworthy that all these REV-

ERBα ligands most likely also act on its paralog REV-ERBβ, due to the high degree of homology in the ligand binding domains of these two receptors. These ligands are described in the following section.

1.2.4.1 Natural- Heme

It has been shown through various biochemical and binding assays, that heme binds directly to REV-ERBs (Raghuram et al., 2007). Mutation studies further showed the amino acids in REV-ERBα that were necessary for heme binding and transcriptional repression effector function (Carter et al., 2016). REV-ERB mediated transcriptional repression of target genes such as glucose-6-phosphatase catalytic subunit (G6PC), phosphoenolpyruvate carboxykinase 1 (PCK1) and basic helix-loop-helix ARNT like 1 (BMAL1) was reduced with decreased heme levels, as shown by decreased levels of REV-ERB/NCoR complex as well as decreased recruitment of NCoR to promoters of target genes (Raghuram et al., 2007).

Physiologically, heme regulates adipogenesis. It has been shown that intracellular levels of heme increase during adipogenesis, and decreased levels inhibit the process. Additionally, heme has also been implicated in playing a role in the regulation of circadian rhythm, as heme levels are regulated in a circadian manner (Kumar et al., 2010). REV-ERB can modulate heme levels through several mechanisms. During adipogenesis, REV-ERB can repress heme levels through

modulation of PPAR gamma (PPARG) by directly repressing PPARG coactivator 1 alpha (PGC1a) (Wu et al., 2009). REV-ERB is also regulated in a circadian manner. It has been shown that oscillations in the levels of heme may regulate the activity of REV-ERBβ (Freeman et al., 2019).

1.2.4.2 Heme-REV-ERB binding – Structural basis

REV-ERBβ ligand binding domain is the same as other nuclear receptors as seen in REV-ERBβ-heme bound structure. Mutations in histidine on helix 11 and cysteine on helix 3 in heme, prevent it from binding to REVERB and reduces REV-ERB activity (Pardee et al., 2009). Heme binding is accommodated due to expansion of ligand binding domain, where hydrophobic residues in LBD form bonds with hydrophobic porphyrin ring of the heme molecule.

REV-ERB's binding with heme, leads to recruitment of co-repressors such as NCoR (Yin et al., 2010). It has been shown that the crystal structure of apo REV-ERBα is able to complex with NCoR (Phelan et al., 2010). However, in cell-based studies, NCoR recruitment increases with heme binding, leading to increased transcriptional repression. On the other hand, biochemical studies show the opposite, suggesting heme binding reduces co-repressor binding (Wu et al., 2009). The biochemical studies, however, are not physiologically relevant pertaining to the use of isolated LBDs and peptide fragments of NCoR. Nevertheless, this leaves the mechanism of action of heme mediated REVERB activity unknown.

1.2.4.3 Synthetic

In general terms, synthetic ligands for REVERB can be either agonists or antagonists. Agonists are molecules that bind to the NR and induce conformational changes, favoring the binding of co-regulatory proteins, ultimately leading to increased receptor activity. Antagonists, compete with agonists to bind LBD, and repress transcriptional activity by preventing co-regulatory protein binding. Further, ligands that can repress NR activity below basal activity, are called inverse agonists.

It is of note, however, that since REVERB can only act as a transcriptional repressor, agonists increase its activity, ultimately causing a reduction in target gene expression. There are a few synthetic agonists and antagonists that have been developed for REV-ERB. Of pharmacological importance, since the REV-ERB receptors lack Helix 12 and cannot bind co-activators, inverse agonists cannot exist for these NRs.

1.2.4.3.1 Agonists

The endogenous activator of REV-ERB, heme, presents challenges due to its interaction with multiple non-specific binding sites, rendering it unsuitable for developing synthetic ligands (Pardee et al., 2009). The first synthetic ligand for REV-ERB was discovered by GlaxoSmithKline (GSK), using a fluorescence resonance energy transfer (FRET) assay to assess recruitment of NCoR. This

compound, GSK4112 (1,1-dimethylethyl N-[(4-chlorophenyl)methyl]-N-[(5-nitro-2-thienyl) methyl]glycinate), acted as a dual agonist for REV-ERBα and REV-ERBβ (Grant et al., 2010). However, its pharmacokinetic profile was suboptimal for in vivo use. In response, further investigations led to the development of structurally modified compounds with improved potency, efficacy, and pharmacokinetics, notably SR9009 and SR9011 (Solt et al., 2012). These compounds demonstrated robust effects on circadian rhythm, metabolism, and energy expenditure in vivo and exhibited no off-target activity among 48 nuclear receptors when used at concentrations near the EC_{50} (600-900 μM; assay dependent).

Recognizing the toxic liability associated with the nitrothiophene group in SR9009 and SR9011, researchers explored alternative scaffolds. The Scripps Research Institute proposed a series of tetrahydroisoquinolines designed to enhance compound performance by restricting scaffold rotation (Noel et al., 2012). Among these, SR12418 emerged as a promising candidate, displaying superior potency and plasma exposure compared to SR9009/SR9011 (Amir et al., 2018). Additionally, other groups introduced novel chemical scaffolds, including triazolopyridazine and structurally similar compounds (Westermaier et al., 2017). More recently, a unique REV-ERB agonist scaffold STL1267, providing the first X-ray crystal structure of a synthetic ligand bound to the REV-ERB LBD was described (Murray et al., 2022).

Research continues to focus on developing REV-ERB agonists, aiming to elucidate their structure-function relationship and therapeutic potential. Rodent studies have demonstrated the efficacy of REV-ERB agonists in mitigating inflammatory diseases and improving metabolic profiles. Although no REV-ERB agonists have entered clinical trials, SR9009 is illicitly marketed as a performance-enhancing drug under the name "stenabolic." Efforts to discourage its misuse include exploring potential metabolites and developing assays for detection (Geldof et al., 2016; Mazzarino et al., 2018).

Recently, Murray et al (2022) characterized a novel synthetic agonist, STL1267. This ligand was identified through structure-activity relationship (SAR) studies, molecular modeling, and mutational analysis. STL1267 was found to exhibit high potency and selectivity for REV-ERB activation (K_i = 0.16uM), with favorable pharmacokinetic properties suitable for in vivo studies. This ligand represents a promising candidate for further investigation and potential therapeutic development targeting REV-ERB-mediated pathways.

STL1267 and SR9009 are both synthetic agonists of the nuclear receptor REV-ERB, but they may differ in several aspects, including potency, selectivity, pharmacokinetics, and structural features. STL1267 exhibits higher potency and selectivity for REV-ERB activation compared to SR9009. This means that it can more effectively activate REV-ERB and may have fewer off-target effects on other receptors or pathways, thus STL1267 may have a more favorable safety profile

than SR9009, with reduced potential for adverse effects or toxicity. Further, factors such as absorption, distribution, metabolism, and elimination, leading to enhanced bioavailability and duration of action, are more enhanced in STL1267 as compared to SR9009. Preclinical studies may demonstrate that STL1267 exhibits superior efficacy compared to SR9009 in relevant disease models. This could include studies on circadian rhythm regulation, metabolism, inflammation, and other REV-ERB-mediated pathways (Makhija et al., 2023; Murray et al., 2022).

While cobalt and zinc protoporphyrin have been identified as natural antagonists for REV-ERB (Matta-Camacho et al., 2014), the first synthetic antagonist, SR8278, was also derived from the GSK4112 scaffold while screening for REV-ERB agonists (Kojetin et al., 2011). Through its mechanism of action, SR8278 increases the transcription of REV-ERB target genes, thereby exerting its biological effects. Preclinical research has demonstrated promising anti-cancer effects of SR8278 in various cancer models. For example, studies have shown that SR8278 can inhibit tumor growth and metastasis in breast cancer, prostate cancer, and melanoma models. Additionally, SR8278 has been reported to sensitize cancer cells to chemotherapy and radiation therapy, potentially enhancing treatment efficacy (Kim et al., 2022; Lee et al., 2020).

Following this discovery, additional antagonist scaffolds were developed, including ARN5187, a spirocyclic cyclopentane scaffold, identified through virtual screening by the Istituto Italiano di Tecnologia (De Mei et al., 2015). ARN5187 interacts

directly with the ligand-binding domain (LBD) of REV-ERBβ, functioning as an antagonist according to research. Furthermore, ARN5187 acts as a dual inhibitor, targeting both REV-ERB and autophagy. The use of this compound with dual inhibitory effects could be a promising approach for inducing cytotoxicity in cancer cells. GSK1362 was introduced as an oxazole REV-ERB antagonist, inhibiting NCoR recruitment in cell-based assays but displaying limited pharmacokinetics (Pariollaud et al., 2018). Pariollaud and colleagues introduced GSK1362, a novel selective inverse agonist targeting REV-ERBs, in their study. They demonstrated its inhibition of REV-ERBα interactions with NCoR1 and SMRT2 peptides through FRET assays (Pariollaud et al., 2018). Structures of each ligand are depicted in Fig 1.7.

1.2.5 REV-ERBs in various diseases

The REV-ERB receptors are core circadian clock components, and play a direct role in the modulation metabolism, inflammation, and other physiological processes. As such, it has extensively been researched as a therapeutic tool in sleep disorders and metabolic disorders. However, recently, a broad role of REV-ERBα has been uncovered in various pathologies such inflammatory diseases, cardio-vascular diseases, and cancer. Further insight into the role of REV-ERB in regulation of various pathologies is provided by REV-ERBα knockouts, where in disturbances in genome-wide gene expression are observed. These differentially expressed genes are involved in pathways that regulate various diseases.

1.2.5.1 Circadian rhythm

The suprachiasmatic nucleus (SCN) is the circadian molecular clock within the hypothalamus of all vertebrates, and it synchronizes the circadian rhythm to light-dark cycles. The SCN projects outputs to several brain areas containing local circadian clocks that direct behavioral, autonomic, and neuroendocrine rhythms.

Circadian gene expression in peripheral tissues are synchronized with the central clock through signals such as feeding-fasting, temperature variations, or hormone rhythms (Papazyan et al., 2016). A circadian loop is regulated by positive and

negative feedback loops. Each loop dominates operations in either light or dark cycles. Bmal1, a basic helix-loop-helix (bHLH) protein, makes up the positive arm of the core circadian clock. It forms a heterodimer with other bHLH proteins, such as neuronal PAS domain protein 2 (Npas2) or circadian locomotor output cycles kaput (CLOCK) (Pett et al., 2016). The resultant heterodimer upregulates rhythmically expressed genes, particularly those encoding negative arm proteins, by binding to E-boxes (CACGTG). The negative arm proteins PER and CRY interact with the BMAL1 heterodimers to suppress the expression of their target genes (Pett et al., 2016).

One of the methods for circadian gene regulation is the secondary loop which actively involves REV-ERB. Where in, the nuclear receptor ROR upregulates circadian gene expression, REV-ERB represses it, due to their competitive binding. Their abundance on gene regulatory sites dictates the expression. For repression of this positive regulatory arm at the end of its cycle, BMAL1 heterodimers can interact with the REV-ERB promoter via E-boxes, thus increasing REV-ERB transcription. The resulting REV-ERB protein binds ROREs in the Bmal1 promoter to inhibit positive circadian transcription, initiating the negative arm (Guillaumond et al., 2005; Hunter et al., 2020) (Fig 1.3).

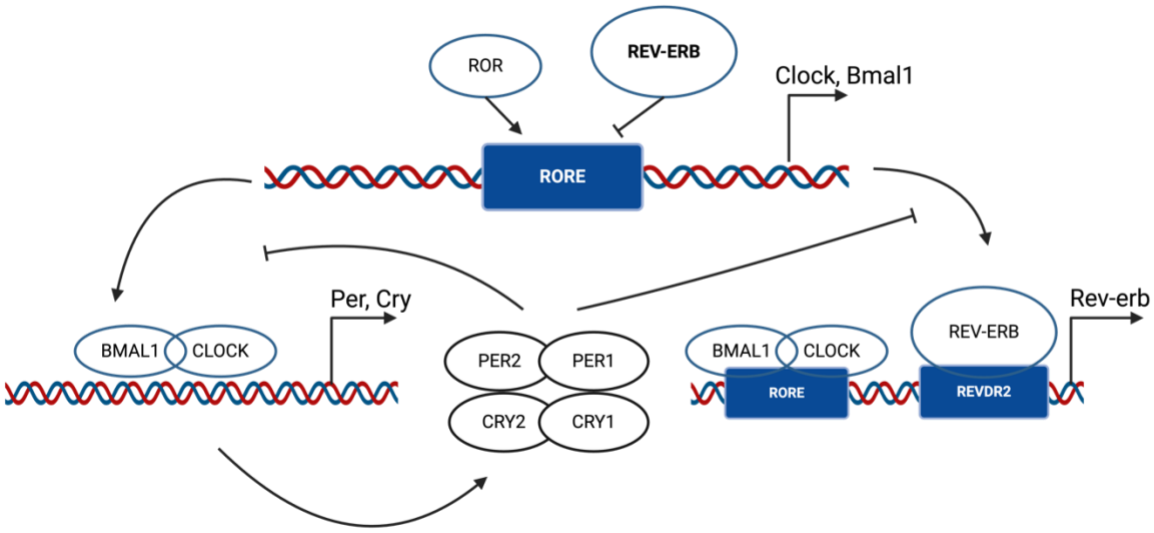

Figure 1.3 ***REV-ERBs play an important role in circadian rhythm.*** During the negative phase of the circadian cycle, REV-ERBs inhibit the expression of BMAL1 and CLOCK genes by binding to their respective promoters, thereby suppressing their transcriptional activity. PER and CRY proteins form complexes that translocate into the nucleus and inhibit the transcriptional activity of BMAL1/CLOCK heterodimers. This repression of BMAL1/CLOCK activity contributes to the suppression of their own transcription, completing the negative feedback loop. Conversely, during the positive phase of the cycle, BMAL1/CLOCK heterodimers activate the transcription of REV-ERB genes, creating a rhythmic oscillation of gene expression. This intricate feedback loop between REV-ERB and BMAL1/CLOCK ensures the precise timing and coordination of circadian rhythms across various biological processes, including metabolism, sleep-wake cycles, and hormone regulation.

1.2.5.2 Inflammation

Nr1d1$^{-/-}$ mice consistently exhibit exacerbated inflammatory states. Innate immune response regulation by REV-ERBα is well established, with direct roles in immune cell activation, development, NFκb signaling, and NLRP3 inflammasome activation (Adlanmerini & Lazar, 2023; Amir et al., 2018; Griffin et al., 2019; Guo et al., 2019; Pariollaud et al., 2018; Pourcet et al., 2018; Reitz et al., 2019; Stujanna et al., 2017; S. Wang et al., 2021; Wang et al., 2018; L. Zhang et al., 2017). NLRP3 inflammasome results in the release of IL-1β and IL-18. In macrophages, REV-ERB directly regulates the circadian control of genes *Nlrp3, IL1β, and IL-18*. In fact, it has been shown, that bone marrow-derived macrophages (BMDM) from REV-ERBα null mice, have increased inflammasome activation and higher pro-inflammatory cytokine levels (Pourcet et al., 2018) . This is intriguing because multiple diseases such as atherosclerosis, gout and Alzheimer's disease are NLRP3 dependent, and REV-ERB is a potential target for their treatment.

REV-ERB plays a major role in Th17 cells as well. RORγt, an isotype of ROR, is the TF responsible for Th17 cell differentiation. At low levels, REV-ERB inhibits nuclear factor interleukin-3 regulated protein (Nfil3) which represses the transcription of RORγt, thus, indirectly promoting Th17 cell differentiation (Yu et al., 2013). However, at high levels, REV-ERB competes with RORγt binding to Th17 cell genes, effectively inhibiting Th17 effector function (Chang et al., 2019). Additionally, ROR regulates the expression of IL-17a and IL-17f in gdT cells, as

well as the differentiation of innate lymphoid cells (ILC3s). REV-ERB can compete with and repress these ROR mediated processes. This further makes REV-ERB an attractive target for the treatment of diseases that involve Th17 cells, for instance, auto-immune disorders as show using models of experimental autoimmune encephalomyelitis (EAE).

In macrophages, REV-ERB controls the expression of numerous inflammatory genes, such as toll-like recptor-4 (Tlr4), p65, chemokine C-C motif ligand 2 (Ccl2), matrix metalloproteinase 9 (Mmp9), and C-X3-C Motif Chemokine Receptor 1 (Cx3cr1), and interleukin-6 (Il-6) (Guo et al., 2019). Thus, REV-ERB and ROR regulate a broad range of inflammatory genes. Since, ROR and REV-ERB are ligand-regulated transcription factors, it is more viable to pharmaceutically modulate their roles for the treatment of all inflammatory diseases.

1.2.5.3 Metabolism

REV-ERBα knockout mice (KO) display a tendency towards obesity, characterized by increased fat accumulation and decreased energy expenditure compared to wild-type mice (Delezie et al., 2012; Woldt et al., 2013). Placing REV-ERBα KO mice on a high-fat diet exacerbates the difference in fat mass between KO and wild-type mice (Hunter et al., 2021). In KO mice, the expression of several lipid metabolic genes in the liver and white adipose tissue is elevated at ZT12, a time when REV-ERBα levels are typically high (Y. Zhang et al., 2017). This upregulation

of lipoprotein lipase, which facilitates lipid storage, worsens fat accumulation (Delezie et al., 2012). Additionally, REV-ERBα KO mice exhibit decreased energy expenditure, attributed to reduced mitochondrial function and oxidative capacity in skeletal muscle, limiting their exercise capacity (Woldt et al., 2013). Interestingly, these effects seem to be specific to the REV-ERBα isotype, as REV-ERBβ KO mice do not exhibit increased fat mass or suppressed oxidative and metabolic genes compared to wild-type mice (Amador et al., 2018).

In contrast to skeletal muscle, there is considerable functional redundancy between REV-ERBα and REV-ERBβ in the liver (Bugge et al., 2012; Cho et al., 2012). While REV-ERBα KO mice show moderate hepatic steatosis, silencing REV-ERBβ in these mice exacerbates the severity of the condition, indicating a compensatory role for REV-ERBβ (Bugge et al., 2012). ChIP-seq experiments targeting hepatic REV-ERBα and REV-ERBβ reveal overlapping peaks near regulatory regions of lipid metabolic genes, consistent with their shared regulation of lipid metabolism (Bugge et al., 2012; Cho et al., 2012). This regulation extends to cholesterol synthesis genes, such as Insig2, where elevated REV-ERB levels repress Insig2 transcription, promoting the activity of sterol regulatory element binding proteins (SREBPs) and rhythmic cholesterol synthesis (Le Martelot et al., 2009).

REV-ERB also governs peripheral circadian rhythms which influence glucose metabolism and other metabolic pathways. It enhances the expression of

exocytosis genes in pancreatic alpha and beta cells, enabling appropriate secretion of glucagon or insulin in response to serum glucose levels (Vieira et al., 2012; Vieira et al., 2013) A HFD induces leptin release, disrupting REV-ERB expression rhythms in pancreatic beta cells via a MAPK-dependent mechanism, thereby affecting glucose-stimulated insulin secretion (Vieira et al., 2012). Furthermore, hepatic insulin sensitivity peaks upon waking when REV-ERB expression is highest. REV-ERBα and REV-ERBβ in SCN GABAergic neurons regulate neuronal firing, correlating with insulin-mediated suppression of hepatic glucose production. SCN GABAergic REV-ERB double KO mice lose this peak in insulin sensitivity, resulting in excessive hyperglycemia upon awakening, akin to the "dawn phenomenon" observed in some patients with type 2 diabetes (Ding et al., 2021). Notably, peripheral blood macrophages from these patients exhibit aberrant REV-ERB rhythms.

1.2.6 Knowledge gap

Based on its prominent role in the regulation of metabolism and inflammation, REV-ERB likely plays a crucial role in Metabolic-Associated Steatohepatitis (MASH; previously Non-Alcoholic Steatohepatitis, NASH), a severe form of Metabolic dysfunction-associated steatotic liver disease (MASLD; formerly nonalcoholic fatty liver disease, NAFLD), due to its above-mentioned functions in lipid metabolism, inflammation, and circadian rhythm. Dysregulation of lipid metabolism is a hallmark of MASH, characterized by excessive accumulation of

triglycerides and free fatty acids in hepatocytes. REV-ERB's modulation of lipid metabolism pathways could influence the development and progression of MASH.

In MASH, inflammation plays a critical role in driving disease progression, leading to hepatocyte injury, fibrosis, and eventually cirrhosis. REV-ERB's ability to modulate inflammatory pathways may impact the inflammatory milieu within the liver and influence MASH pathogenesis. Disruption of circadian rhythm, has been associated with metabolic disorders, including MASLD and MASH. Altered circadian rhythm can affect liver function, metabolism, and inflammatory responses, exacerbating the development and progression of MASH.

Identifying the knowledge gap in this context involves understanding the specific mechanisms by which REV-ERB dysregulation contributes to MASH pathogenesis and progression. While studies have implicated REV-ERB in lipid metabolism, inflammation, and circadian rhythm regulation, the precise molecular mechanisms underlying its involvement in MASH remain incompletely understood. In addition to its broader physiological functions, REV-ERB exhibits cell-specific and tissue-specific effects that may be relevant to MASH. Several signaling pathways implicated in MASH, such as insulin resistance, oxidative stress, and hepatic stellate cell activation have been associated with REV-ERB. Thus, exploring the cell-specific and tissue-specific effects of REV-ERB in MASH represents a critical knowledge gap in understanding disease pathogenesis and identifying potential therapeutic targets. Elucidating the molecular mechanisms underlying REV-ERB's

actions in different cell types within the liver and adipose tissue, will aid in gaining insights into its role in MASH and develop targeted interventions to mitigate progression of this disease for which now treatments are yet available.

1.3 Metabolic dysfunction-associated steatotic liver disease (MASLD)

MASLD is a chronic disease of the liver, characterized by hepatic steatosis, in absence of secondary causes of fat accumulation such as in excessive alcohol consumption. MASLD lies on a spectrum with the most benign form being hepatic steatosis, but the more severe end being marked by inflammation, fibrosis, and cirrhosis. The severe form of the disease is called metabolic dysfunction-associated steatohepatitis (MASH).

In recognition of the metabolic nature of the disease, and the stigmatizing former nomenclature, the global liver community coalesced around the world in 2023, to improve the nomenclature focusing on the characteristics of the disease in a non-stigmatizing way to enhance research and funding. However, it is to be noted that the natural history, staging and clinical trials for the disease remains the same.
Clinically, MASLD is defined as >5% fat accumulation in the liver, not caused by secondary causes such as alcohol/drug consumption or viral induced steatosis. MASLD patients may also exhibit elevated liver enzymes (Kim et al., 2023).

1.3.1 Pathophysiology

1.3.1.1 Lipid accumulation

MASLD is a typical example of a disease with exhibition of ectopic accumulation of lipids. A common characteristic of MASLD is the excessive triglyceride (TG) synthesis in hepatocytes, often because of high energy intake as compared to consumption. 60% of the substrates for TG synthesis come from white adipose tissue (WAT) whereas the remaining substrates are derived from de novo lipogenesis (DNL) and external diet containing high fats and/or high sugars.

Insulin tends to play a major role in MASLD patients, as it is responsible for mediating TG storage in AT, as well as promotes the storage of fatty acids in form of lipid droplets in AT, often termed as lazy lipid reservoirs (Perry et al., 2014). Insulin resistance (IR) and DNL are closely related, thus forming a complicated link between IR and MASLD, as DNL is the main pathway for lipid accumulation. *Sterol regulatory element binding protein 1c* (*SREBP-1c*) and *carbohydrate response element-binding protein* (*ChREBP*) promote DNL in hepatocytes in MASLD (Foretz et al., 1999). While IR is responsible for the activation of SREBP-1c, excessive glucose substrates activate ChREBP to regulate the expression of *acetyl-coA carboxylase* (*ACC*) and *fatty acid synthase* (*FASN*) (Xu et al., 2013).

Dietary factors, thus, become a major contributing factor to the development, pathophysiology, and progression of MASLD to a more severe state. Studies have suggested that while a high fat diet alone induces obesity and some IR, the addition

of fructose to the diet triggers liver metabolism specific hepatic stressors, via *c-Jun N-terminal kinase* (*JNK*) and *IR* (Pereira et al., 2017). This leads to increased fat accumulation via lipogenesis and decreased fatty acid oxidation (FAO). Further, addition of fructose to the diet in humans and animal models induces gene expression of liver fibrosis, ER stress, and inflammation, all markers of severe MASLD, i.e., MASH (Park et al., 2023).

1.3.1.2 Lipotoxic stress

Roger Unger in 1994 first described lipotoxicity, and since, studies on hepatic and plasma lipidomics in MASLD have bloomed (Lee et al., 1994). Lipotoxicity can be defined as the toxic effect of consistently increased lipid concentrations in non-adipose tissues. In context of MASLD, hepatocytes are overburdened and are unable to transport these lipotoxic substances with a fast turnover, thus, exacerbating hepatocyte damage and facilitating the progression of MASLD to MASH, via activation of inflammation and fibrosis (Geng et al., 2021).

However, lipotoxicity largely has differential effects on cell populations. While hepatocytes are damaged from lipotoxic substances, hepatic stellate cells (HSC), the major contributor in hepatic fibrogenesis, are activated for fibrotic signaling via TLR4 signaling pathways (Zhang et al., 2021). Further, Kupffer cells (KC), the liver-resident macrophage population, is also activated to a pro-inflammatory state in presence of high concentrations of oxidized low-density lipoproteins (LDLs) (Bieghs et al., 2013).

However, the dichotomy of this complicated pathophysiological mechanism is that not all lipids are lipotoxic. It has been shown that TGs and free fatty acids (FFA) that contain unsaturated double bonds have protective effects against lipotoxic substance induced liver injury (Akazawa et al., 2010; Dongiovanni et al., 2015; Nogueira et al., 2016; Yamaguchi et al., 2007). In animal models of MASH, certain FAs such as monosaturated oleic acid (OA) have been shown to promote hepatic steatosis (Chen et al., 2018), however, are not as toxic as saturated FFAs such as palmitic acid (PA) and stearic acid. Other examples of lipotoxic FFAs are ceramides and free cholesterol.

Overall, lipotoxicity is a core influencing factor in MASLD, as it is potentially able to worsen pathology and promote a severe diseased state. It is not only able to induce apoptosis, fibrosis, inflammation, and cell damage, but further downstream effects also include mitochondrial dysfunction and endoplasmic reticulum (ER) stress.

1.3.1.3 Oxidative stress

Imbalances in the redox state and oxidative stress are distinctive characteristics of MASLD, with the ability to contribute towards major pathologies, such as steatosis, IR, fibrogenesis, and inflammation. The role of oxidative stress in the liver was first described by Comporti in 1965, where it was observed that carbon tetrachloride

(CCl4-) treated rats had increased lipid peroxidation, leading to the description of reactive oxygen species (ROS) in hepatic injury (Comporti & Saccocci, 1965).

Primary cell populations affected by oxidative stress in the liver are hepatocytes, however, other non-parenchymal cells such as KCs and HSCs are also affected (Allameh et al., 2023). HSC transdifferentiation is triggered by Cytochrome P4502E1- (CYP2E1-) induced free radicals. Antioxidant treatment, on the other hand, is able to prevent collagen production (Nieto et al., 2002), thus, suggesting a major role of ROS on fibrogenesis. This is further fortified by NOX-1 and NOX-2 deficient mice, which lack antioxidant pathways. They show exacerbated hepatic fibrosis in CCl4- treated animal models of fibrosis (Cui et al., 2011; Jiang et al., 2010; Paik et al., 2011). In KCs, oxidative stress has been implicated in increasing M1 polarization, which is a pro-inflammatory state of macrophages, therefore favoring MASLD progression to MASH (Svegliati-Baroni et al., 2001).

Oxidized phospholipids linked to oxidative stress build up and cause mitochondrial dysfunction in hepatocytes (Sun et al., 2020). Liver inflammation is brought on by the release of mitochondrial DNA (mtDNA) from damaged hepatocytes via activation of toll-like receptor 9 (TRL9) (Handa et al., 2016). One of the primary producers of ROS in cells is mitochondria, which are crucial for FAO and energy production. However, during this process, a significant amount of ROS is also generated. Thus, mitochondrial stress is a major characteristic of MASH and a target for therapy.

1.3.1.4 Mitochondrial dysfunction

The primary cause of hepatocellular damage in MASLD is oxidative stress, which leads to hepatic inflammation and fibrosis. Since mitochondrial dysfunction is a major cause of ROS generation, mitochondria play an inherent role in MASH pathogenesis. The nutrient overload in MASH, particularly increased FAs in hepatocytes, leads to elevated mitochondrial FA import and oxidation (Legaki et al., 2022). Thus, via TCA cycle and beta-oxidation, there is elevation in levels of NADH and FADH2. While these molecules contribute to the electron transport chain, approximately 2% of electrons are leaked from ETC leading to radicalized oxygen species (Satapati et al., 2015).

The DNA and membrane of the mitochondria undergo damage by ROS. mtDNA encodes respiratory chain polypeptides. Because of the proximity to the inner membrane, lack of protective histones, and inadequate DNA repair mechanisms in mtDNA, it is extremely vulnerable to oxidative damage. Reduced mitochondrial function will therefore result from any factor that affects mitochondrial integrity. On the other hand, free radicals also compromise the components of ETC, which lowers the amount of ATP produced and increases electron leakage from ETC, which increases ROS production to an even greater extent (Myint et al., 2023). This creates a vicious cascade. Hepatic inflammation, fibrosis, and the pathophysiology of hepatocyte death are all directly correlated with ROS.

ROS have a proinflammatory effect in that they can trigger the production of inflammatory cytokines including IL-1β, IL-6, and TNF-α by activating the nuclear factor-κB (NF-κB) and nucleotide-binding oligomerization domain-like receptor family, pyrin domain-containing 3 (NLRP3) inflammasome (Myint et al., 2023). Proinflammatory cytokines trigger apoptotic receptors on hepatocytes like TNF-related apoptosis inducing ligand (TRAIL) and Fas, which in turn cause hepatocyte apoptosis.

Further, ROS can damage mitochondrial membrane to form mitochondrial permeability transition pore (MPTP), which causes the release of mtDNA into the cytoplasm, where it can act as a damage associated molecular pattern (DAMP) (Xian et al., 2022). Downstream, this leads to NLRP3 inflammasome activation, pro-inflammatory cytokine secretion, and inflammation via KCs. MPTP formation in hepatocytes also marks them for necrosis and cell death (Elmore et al., 2001). Hepatocyte loss triggers progenitor cell proliferation in response, which produces regenerative nodules divided by fibrotic bands that are indicative of cirrhosis. Progenitor cells that proliferate in environments with persistent inflammation and ROS are susceptible to acquiring nuclear and mitochondrial anomalies which may result in a malignant transition into HCC (Yin et al., 2021). Furthermore, proinflammatory cytokines induce the activation of pro-oncogenic pathways, including (JNK), signal transducer and activator of transcription 3 (STAT3), and Janus kinase 2 (JAK2), leading to the malignant transformation of hepatocytes (Hin Tang et al., 2020) (Fig 1.4).

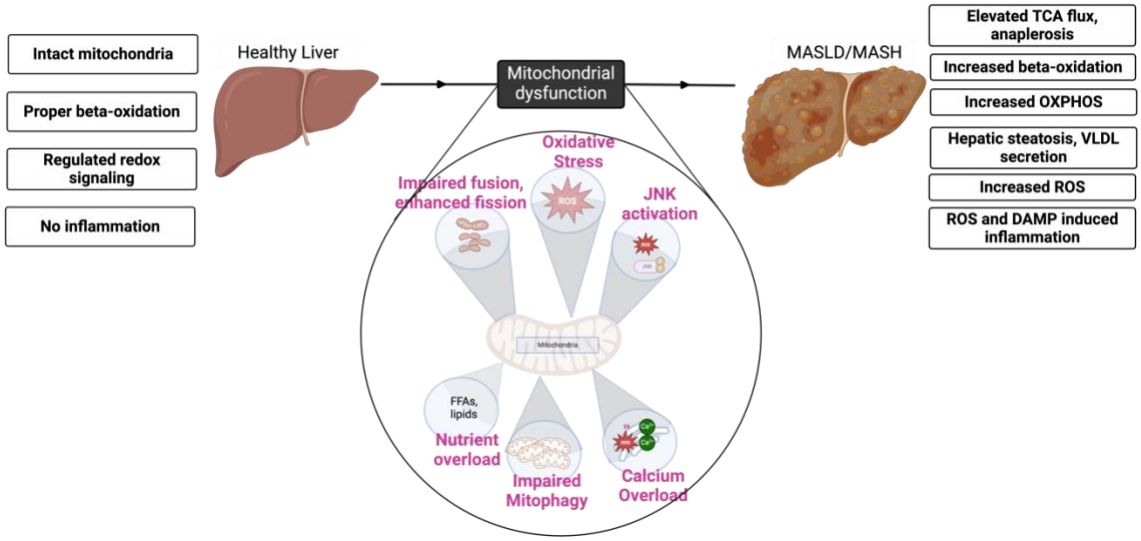

Figure 1.4 **Mitochondrial dysfunction plays a pivotal role in the pathogenesis of MASH.** Nutrient overload, such as elevated levels of free fatty acids and glucose, overwhelms mitochondrial capacity, leading to impaired mitochondrial function. This dysregulated mitochondrial metabolism results in increased oxidative stress, characterized by the overproduction of ROS, which further exacerbates cellular damage. Additionally, impaired mitophagy contributes to the accumulation of dysfunctional mitochondria. Activation of JNK signaling pathway, a key mediator of hepatic inflammation, is stimulated by mitochondrial dysfunction, further perpetuating liver injury. Moreover, mitochondrial dysfunction in NASH is associated with altered metabolic flux, including elevated TCA cycle flux, impaired beta-oxidation of fatty acids, and increased OXPHOS. These metabolic alterations not only disrupt energy homeostasis but also contribute to the generation of ROS, exacerbating oxidative stress and cellular damage in MASH. (c-Jun N-terminal kinase, JNK; TCA, Tricarboxylic acid; OXPHOS, oxidative phosphorylation;)

1.3.1.5 Inflammation

Systemic metabolic homeostasis and the overall inflammatory state are determined by immune cell-to-metabolic tissue crosstalk. According to current findings, immunologic abnormalities in the liver contribute to the persistence and exacerbation of inflammation in MASLD. MASH is defined by a strong influx of immune cells into the liver, where they become activated and can release inflammatory mediators.

NLRP3 inflammasome components are expressed at very low levels in healthy hepatocytes, however, in both animal models and humans, it is increased significantly in MASH. The NLRP3 inflammasome is mostly expressed in liver sinusoidal, endothelial cells, KCs, and damaged hepatocytes. Even in stellate cells, NLRP3 has been shown to play an important role in induction of fibrosis, but this is limited to animal models (Inzaugarat et al., 2019). However, in concurrence with that, pharmacological inhibition of NLRP3 is protective in MASH pathology, including inflammation, steatosis, and fibrosis (Yang et al., 2016). Macrophages and T-helper cells are the major cell types involved in MASH pathogenesis.

Macrophages play a crucial role in the pathogenesis and progression of MASH (Fig 1.5). Macrophages are key mediators of inflammation in MASH. They infiltrate the liver in response to various signals such as lipopolysaccharides (LPS), free fatty acids, chronic hyperglycemia, and damage-associated molecular patterns (DAMPs) released by injured hepatocytes. Once activated, macrophages produce

pro-inflammatory cytokines such as tumor necrosis factor-alpha (TNF-α), interleukin-6 (IL-6), and interleukin-1 beta (IL-1β), which contribute to hepatic inflammation and injury. In MASH, hepatocytes accumulate excessive lipid droplets, leading to lipotoxicity and cell death.

Macrophages, particularly Kupffer cells residing in the liver sinusoids, phagocytose these lipid-laden hepatocytes, contributing to the clearance of apoptotic cells and lipid debris (Xu et al., 2023). However, this process can also exacerbate inflammation and promote fibrosis through the release of inflammatory mediators. Further, macrophages secrete factors such as transforming growth factor-beta (TGF-B) and platelet-derived growth factor (PDGF), which stimulate the activation of HSCs (Liu et al., 2010).

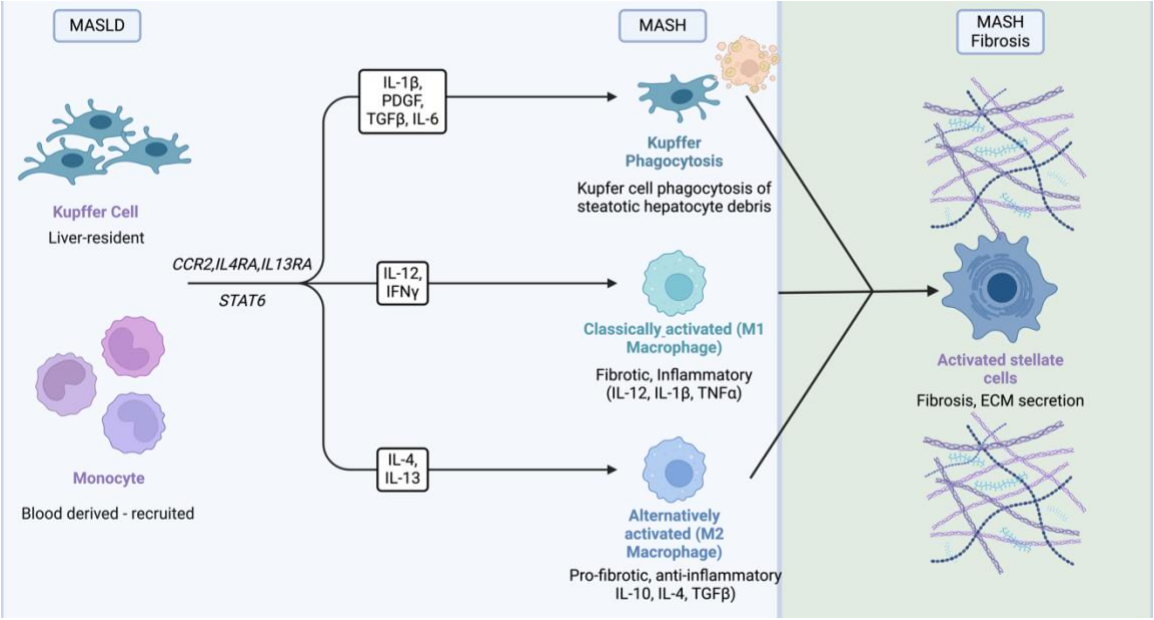

Figure 1.5 **The role of macrophages in pathogenesis of MASLD/MASH** This figure illustrates the dynamic involvement of macrophages, in progression of MASLD to MASH. Kupffer cells and infiltrating monocytes can be activated upon various stimuli and inflammatory cytokines. Kupffer cells play a role in phagocytosis of lipid-laden hepatocytes, however persistent activation and dysregulation lead to activation of HSCs. M1 macrophages contribute to inflammation in MASH, while M2 macrophages exert anti-inflammatory effects. Cytokines and chemokines from macrophages, activates HSCs for ECM secretion. (IL-1b, Interleukin-1 beta; IL-12, interleukin 12; TNFa, Tumor necrosis factor – alpha; IL10, Interleukin 10; TGFb, Transforming growth factor beta;)

Activated hepatic stellate cells (HSCs) are the primary producers of extracellular matrix proteins such as collagen, contributing to liver fibrosis. In the early stages of MASH, macrophages may also play a role in resolving inflammation through the secretion of anti-inflammatory cytokines such as interleukin-10 (IL-10) and by promoting tissue repair. However, in chronic or severe MASH, this resolution process is often impaired, leading to persistent inflammation and fibrosis. Macrophages interact with other immune cells such as T cells, B cells, and natural killer (NK) cells within the liver microenvironment, modulating the immune response in MASH. Dysregulated crosstalk between different immune cell populations can further exacerbate liver inflammation and fibrosis (Koyama & Brenner, 2017).

T cells, a type of lymphocyte, play various roles in the pathogenesis and progression of NASH. CD4+ T Cells (Helper T cells) such as Th1 cells produce pro-inflammatory cytokines such as interferon-gamma (IFN-γ) and TNFα, which contribute to hepatic inflammation and injury in MASH. Th17 cells produce interleukin-17 (IL-17) and interleukin-22 (IL-22), which promote inflammation and neutrophil recruitment to the liver, exacerbating liver damage in MASH. Regulatory T cells (Tregs) have anti-inflammatory properties and help maintain immune tolerance by suppressing excessive immune responses. In MASH, decreased Treg function or numbers may contribute to persistent inflammation and disease progression (Her et al., 2020; Rau et al., 2016; Sutti & Albano, 2020).

Dysregulation of CD4 T cell function is implicated in MASLD and MASH progression. Increased accumulation of inflammatory Th1 and Th17 cells is observed in both peripheral and intrahepatic leukocytes during MASH in humans and mouse models. Humanized mouse models on a high-fat, high-carbohydrate diet show a progressive increase in CD4 T cell frequency, and antibody-mediated depletion of total CD4 T cells reduces hepatic inflammation and fibrosis, indicating CD4 T cell dependence in MASH development. IFNγ deficiency attenuates MASH progression in mice, suggesting a role for Th1 cells in promoting inflammation. Recruitment of CD4 T cells into the liver involves α4β7-MAdCAM-1 interaction, which contributes to MASH pathogenesis. Blockade of this interaction reduces hepatic inflammation and fibrosis. Dysregulation of lipid metabolism during MASLD/MASH may cause a selective loss of CD4 T cells, impacting anti-tumor surveillance (Adams & Eksteen, 2006; Her et al., 2020; Rai et al., 2020). Increased Th17 cell accumulation is observed in MASH patients compared to those with MASLD, suggesting a potential role in disease progression.

Inhibition of IL-17 and its receptor protects against MASH in mouse models induced by high-fat or methionine-choline-deficient (MCD) diet (Harley et al., 2014; Rau et al., 2016; Tang et al., 2011). Few studies have focused on the role of Tregs, but there is evidence suggesting their involvement in preventing excessive immune cell activation. Conflicting findings exist regarding the frequency and function of Tregs in MASH, possibly due to differences in mouse models or their dual roles in early and late MASH progression and carcinogenesis (Ma et al., 2007; H. Wang et

al., 2021). Mechanisms underlying CD4 T cell activation and effector functions in MASH are not well understood. The liver microenvironment and cellular metabolism may influence CD4 T cell phenotypes, as seen with the inflammatory and glycolytic ihTh17 cells implicated in obesity and MASLD pathogenesis.

CD8+ T cells also play a role in MASH progression, where they recognize and eliminate hepatocytes expressing abnormal or stress-induced antigens, such as those related to lipotoxicity and cellular damage in MASH. However, excessive activation of CD8+ T cells can lead to hepatocyte injury and contribute to liver inflammation and fibrosis. Elevated numbers of CD8 T cells in MASH patients correlate with increased frequency of blood CD8 T cells expressing perforin, IFNγ, and TNFα, indicating systemic activation or crosstalk with other tissues. Experimental depletion of total CD8 T cells in animal models improves MASH and prevents transition to hepatocellular carcinoma (HCC), suggesting a direct role in disease progression. Type I interferons support the activation of cytotoxic CD8 T cells early during the transition from steatosis to MASH, leading to increased production of proinflammatory cytokines IFNγ and TNFα. Intrahepatic CD8 T cells from obese-hyperlipidemic mice with MASH express increased levels of IL-10 and can directly activate hepatic stellate cells (HSCs) ex vivo (Breuer et al., 2020).

Single-cell genomics reveal functionally distinct subsets of CD8 T cells in MASH. During established MASH, a subset of CXCR6+ CD8 T cells accumulates in the liver, exhibiting features of short-lived tissue-resident effector cells and an

activated exhausted phenotype. CXCR6+ CD8 T cells promote non-specific killing of hepatocytes and disease progression, and their accumulation may lead to impaired immune surveillance and the development of MASH-driven HCC. While evidence suggests a pathogenic role for CD8 T cells in MASH progression through the secretion of proinflammatory molecules and non-specific killing of hepatocytes, they may also use specific effector functions, such as perforin, to limit inflammation. Tissue-resident CD8 T cells are required for the resolution of murine MASH, suggesting a potential dichotomous role during disease progression and resolution (Bhattacharjee et al., 2017; Soares-da-Silva, 1986; Wolf et al., 2014).

NKT cells are a unique subset of T cells with both innate and adaptive immune functions. They recognize lipid antigens presented by CD1d molecules and produce cytokines such as IFNγ and TNFα. NKT cells can modulate hepatic inflammation and lipid metabolism in MASH. γδT cells are a minor subset of T cells with diverse functions. In MASH, γδT cells may contribute to liver inflammation through the production of pro-inflammatory cytokines and the activation of other immune cells. The number of intrahepatic γδ T cells and IL-17-producing γδ T cells increases significantly after mice are fed a high-fat diet. Despite no changes in obesity, mice lacking γδ T cells ($Tcrd^{-/-}$ mice) display reduced liver injury and lobular inflammation when subjected to high-fat (HF) or high-fat, high-cholesterol (HFHC) diet feeding, suggesting that γδ T cells promote MASH. IL-17 secretion by γδ T cells is proposed as a contributing factor to MASH development. This is supported by the observation that Tcrd-/- mice reconstituted with hepatic Il17a-

deficient γδ T cells show improved MASH symptoms compared to those receiving wild-type (WT) γδ T cells. In a different model using a methionine-choline-deficient (MCD) diet, Tcrd-/- mice also displayed attenuated liver steatosis, injury, and hepatic leukocyte infiltration, including a decrease in inflammatory monocyte influx. However, in this model, the pathogenic role of γδ T cells was independent of IL-17, indicating differences in disease pathogenesis induced by different MASH-inducing diets (Li et al., 2017; Torres-Hernandez et al., 2020)

1.3.2 MASLD is part of metabolic syndrome (MetS)

MetS has various components such as systemic hypertension, dyslipidemia, insulin resistance, and overt diabetes (Fig 1.6). Patients with MASLD, often exhibit one or more components of MetS as well (Kim et al., 2019). MetS is a known risk factor for cardiovascular disease (CVD) developments, and visceral obesity is a known risk factor for MASLD (Browning et al., 2004). Since cardiac and vascular diseases are often the leading cause of death in these patients, the limelight is often shifted from other underlying causes to them, however, it is important to note that the pathophysiological mechanisms connecting MASLD and cardiovascular diseases is unknown, and IR could perhaps be the link between them. This complex relationship between MetS and MASLD poses a major challenge for clinicians.

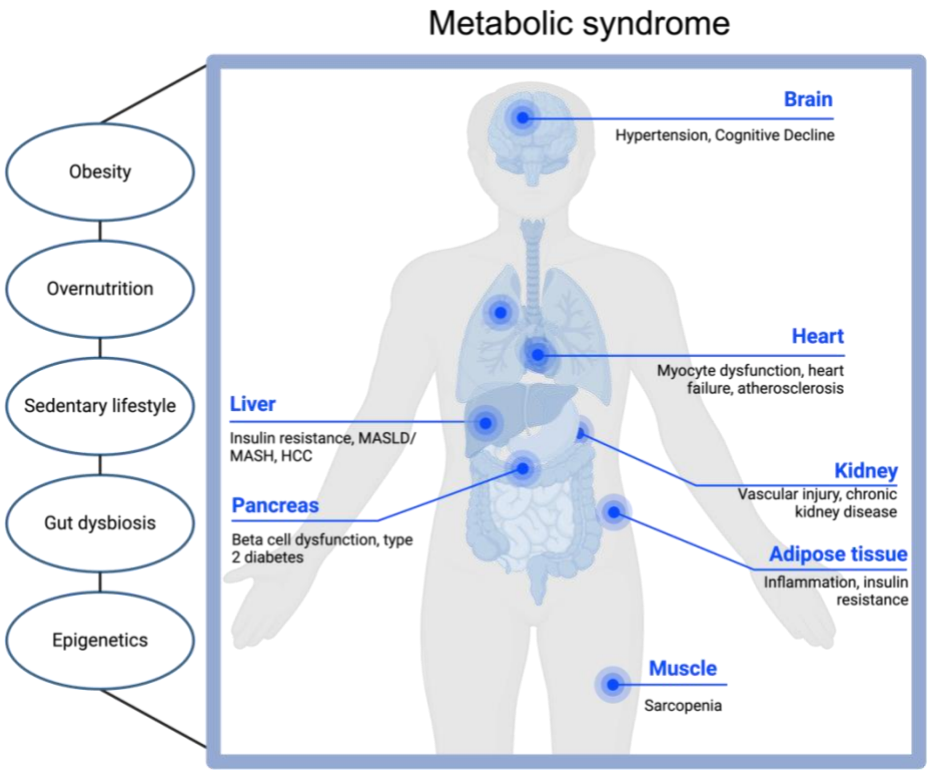

Figure 1.6 **Metabolic syndrome is a complex cluster of interconnected metabolic abnormalities** Factors such as obesity, overnutrition, sedentary lifestyle and gut dysbiosis can collectively increase the risk of cardiovascular disease, type 2 diabetes, MASLD/MASH, through factors such as dyslipidemia, insulin resistance, and chronic inflammation. This figure illustrates the diverse manifestations of metabolic syndrome across various organ systems.

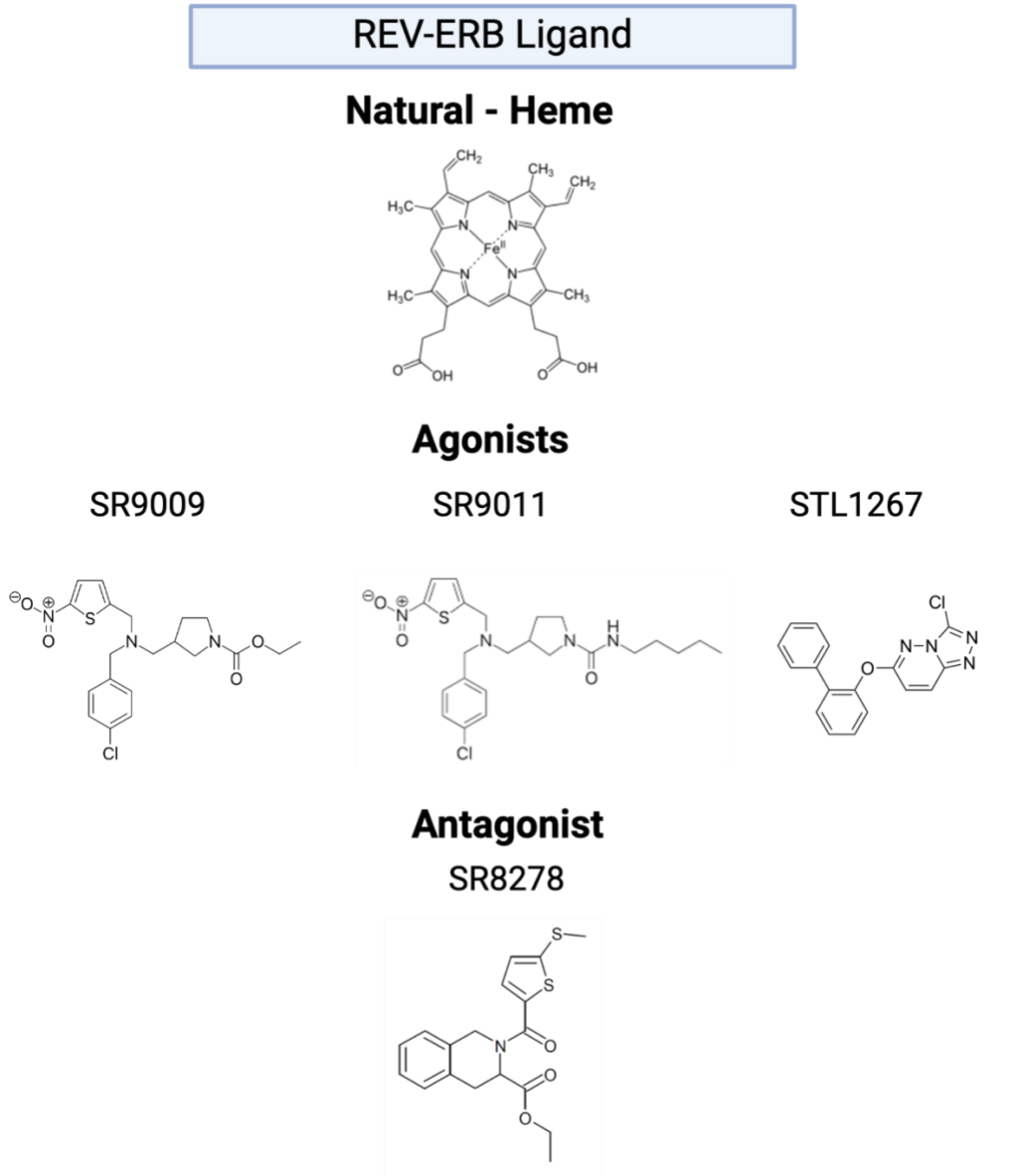

Figure 1.7 **Various REV-ERB ligands and their chemical structures**

1.3.3 MASLD – Epidemiology

Estimates suggest that between 25-30% of individuals worldwide suffer from MASLD, with prevalence rates varying across regions, from 13.5% in Africa to 31.8% in the Middle East. In the United States, MASLD stands as the leading chronic liver condition, impacting approximately 25% of adults. Of those affected by MASLD, around 20% progress to the more severe form MASH, which amounts to a significant 5% of the US adult population (Ray, 2021). Notably, individuals with metabolic or cardiovascular risk factors, such as type 2 diabetes, obesity, hypertension, dyslipidemia, and metabolic syndrome, are more likely to develop MASLD.

The prevalence of MASLD is expected to rise globally in tandem with increases in diabetes and obesity rates. Factors such as aging and lifestyle changes, including weight gain exacerbated by home confinement during the COVID-19 pandemic, contribute to this trend. The substantial numbers of individuals affected by MASLD pose a significant burden on patients, society, and the economy, particularly in later disease stages characterized by severe fibrosis (Schattenberg et al., 2021). Addressing these challenges requires prompt diagnosis and treatment to mitigate healthcare costs and improve patient outcomes. However, several obstacles hinder the effective management of MASLD. Limited understanding of the condition and its potential effects, disagreements over diagnostic methods, challenges in symptom recognition, and a lack of approved pharmaceutical treatments present significant barriers (European Association for the Study of the Liver. Electronic address et al., 2021; Said et al., 2013).

MASLD is often diagnosed incidentally through abnormal blood test or liver imaging results, highlighting the need for increased awareness and proactive screening efforts (Armstrong et al., 2012). Despite its prevalence and impact, MASLD remains underdiagnosed and underrecognized. Moreover, there is a lack of standardized or comprehensive models of care for managing the condition. Therefore, efforts to enhance knowledge, awareness, and diagnostic strategies for MASLD are essential. Establishing standardized care models and improving access to screening and treatment can help address the growing burden of this chronic liver condition and improve patient outcomes in the long term (Alexander et al., 2018; Blais et al., 2015; Lazarus et al., 2021; Patel et al., 2018).

1.3.4 Risk factors

Patients with MASLD commonly exhibit components of MetS, along with associated CVD risk factors (Anstee et al., 2013; Byrne & Targher, 2015). These components include obesity, type 2 diabetes mellitus (T2DM), and dyslipidemia. Notably, individuals with MASLD have an increased prevalence of CVD, underscoring the interconnectedness of metabolic and cardiovascular health (Bhatia et al., 2012; European Association for the Study of the et al., 2016). Moreover, those with T2DM and MASLD demonstrate a higher prevalence of vascular, cerebrovascular, and coronary diseases compared to those without MASLD, emphasizing the heightened cardiovascular risk associated with this condition (Targher et al., 2007).

The association between MASLD and an unhealthy lifestyle is evident, as lifestyle factors such as poor diet, lack of exercise, and excessive alcohol consumption are known contributors to the development and progression of MASLD. Therefore, interventions aimed at improving lifestyle habits, such as adopting a healthier diet and increasing physical activity, may prove beneficial in reducing MASLD progression and symptoms.

Interestingly, smoking, a well-established risk factor for various diseases including cancer, respiratory diseases, and CVD, has also been implicated in MASLD. Multiple studies have reported a significant association between smoking and MASLD, with smokers showing a higher risk of developing the condition compared to non-smokers (Al-Dayyat et al., 2018). Additionally, research suggests that smokers with MASLD tend to exhibit more advanced fibrosis compared to non-smokers, indicating a potential exacerbating effect of smoking on liver health (Ou et al., 2019). However, the link between smoking and MASLD remains somewhat controversial, and the underlying mechanisms connecting the two warrant further investigation. It is plausible that smoking may exacerbate liver inflammation and oxidative stress, contributing to the progression of MASLD. Moreover, smoking may interact with other risk factors such as obesity and T2DM to amplify the risk of liver disease.

In conclusion, MASLD is closely associated with metabolic syndrome and cardiovascular risk factors, highlighting the importance of comprehensive management strategies targeting both liver and cardiovascular health. Lifestyle modifications, including smoking cessation, along with appropriate medical interventions, play a crucial role in mitigating the progression of MASLD and reducing associated morbidity and mortality. Further research is needed to elucidate the precise mechanisms linking smoking and MASLD and to inform targeted interventions aimed at addressing this important public health issue.

1.4 Metabolic reprogramming in MASLD and MASH

De-novo lipogenesis (DNL) is a metabolic process in which circulating carbohydrates are converted into fatty acids within the liver. These fatty acids can then either be stored as triglycerides (TGs) or utilized for other lipid synthesis pathways. The liver relies on DNL or uptake of lipids for its lipid acquisition, which are subsequently either stored or utilized for energy production and ketogenesis. Neutral lipids such as TGs and cholesteryl esters are stored in lipid droplets within hepatocytes and can be released as FFAs through processes like lipolysis or lipophagy (Seebacher et al., 2020).

The metabolism of FFAs primarily occurs through mitochondrial β-oxidation and peroxisomal oxidation, generating energy for hepatocytes and substrates for ketogenesis (Rui, 2014). This metabolic process provides metabolic fuel, in the

form of very low-density lipoproteins (VLDLs), for extrahepatic tissues. The balance between lipid supply and metabolism is crucial, and an imbalance can lead to fat accumulation (steatosis), which is a key factor in the pathogenesis of MASLD and MASH.

Diet plays a significant role in this lipid imbalance, particularly foods high in fructose, which have been linked to increased lipid synthesis and hepatic steatosis (Lim et al., 2010). The conversion of glucose to fatty acids involves a series of enzymatic reactions facilitated by various enzymes, including glucokinase, pyruvate carboxylase, ATP-citrate lyase, malic enzyme, acetyl-CoA carboxylase, and fatty acid synthase. These enzymes catalyze the conversion of glucose to fatty acids, which are then used to synthesize TGs.

Excessive consumption of foods rich in sugar and high-fructose corn syrup has been associated with obesity, hepatic steatosis, and MASH. Fructose is absorbed by intestinal epithelial cells through the glucose transporter GLUT5 and rapidly phosphorylated by ketohexokinase (HK) upon reaching the liver (Ferraris et al., 2018). Fructose-1-phosphate, the product of this phosphorylation, serves as a substrate for DNL and activates glucokinase, thereby enhancing glycolytic flux in hepatocytes. Inhibiting fructokinase specifically in the liver has been shown to significantly reduce hepatic steatosis in mice fed a fructose-rich diet, highlighting the critical role of hepatic fructose metabolism in promoting fat accumulation in the liver under metabolic stress conditions (Ishimoto et al., 2013).

1.4.1 Lipid Regulation in MASLD/MASH

MASLD and its progressive form, MASH, are characterized by dysregulation of lipid metabolism within the liver. This section delves into the molecular intricacies involving key transcriptional regulators, insulin signaling, and hepatic lipid uptake, providing a comprehensive understanding of the processes driving hepatic steatosis.

1.4.2 Transcriptional Regulators:

Sterol Response Element–Binding Protein 1c (SREBP1c) and Carbohydrate Response Element–Binding Protein (ChREBP) emerge as pivotal players in the regulation of lipogenesis. SREBP1c responds to nutrient and hormonal cues, with Liver X receptor (LXR; NR1H3) activation stimulating lipogenic gene expression (Yoshikawa et al., 2001). Conversely, FXR; NR1H4 exerts opposite effects, highlighting the nuanced control over hepatic lipid synthesis (Watanabe et al., 2004). Aberrant activation of SREBP1c has been implicated in both murine models and human subjects with MASLD, underscoring its significance in disease progression (Kohjima et al., 2008).

ChREBP, a transcription factor that is highly responsive to glucose, fructose, and hormonal signals, undergoes multifaceted regulation at the gene expression, subcellular localization, and transcriptional activity levels. SREBP1c and ChREBP

engage with various transcriptional coactivators and corepressors, acting as a central hub for communication with the liver clock (Linden et al., 2018). This interaction contributes to the coordination of diurnal rhythms in hepatic lipid metabolism. The involvement of the transcription factor ZBTB20 further emphasizes the intricate regulatory network orchestrating lipogenesis in MASLD (Liu et al., 2017).

The convergence of AKT and mammalian target of rapamycin complex 1 (mTORC1) signaling stimulates DNL through both SREBP1c and ChREBP, elucidating the interconnected signaling pathways that contribute to the pathological lipid accumulation in hepatic cells (Yecies et al., 2011). Insulin, a central player in glucose and lipid homeostasis, exerts profound effects on hepatic lipid metabolism. Its stimulation of DNL in the liver and adipose tissue is mediated by the downstream AKT/mTORC1 pathway (Vander Haar et al., 2007). Insulin-induced upregulation of Slug in hepatocytes further exacerbates hepatic steatosis through an epigenetic mechanism, highlighting the multifaceted impact of insulin signaling in MASLD progression (Liu et al., 2020). Additionally, insulin stimulates glycolysis by inhibiting FOXO1, a repressor of glucokinase expression and glycolysis (Lee & Dong, 2017). In a state of insulin resistance, insulin retains its capacity to promote hepatic lipogenesis, despite a reduced ability to inhibit gluconeogenesis, pointing to the notion of selective insulin resistance. The initiation of pro-lipogenic signaling and the presence of abundant lipogenic

substrates are significant contributors to the development of hepatic steatosis in MASLD.

Hepatic lipid uptake constitutes a significant contributor to liver fat accumulation in MASLD. Plasma membrane FFA transporters, including CD36, FATP2, and FATP5, play pivotal roles in this process. Deletion of CD36 has been shown to mitigate diet-induced steatosis in murine models, underscoring its relevance in MASLD pathophysiology (Wilson et al., 2016).

TFs such as PPARγ, pregnane X receptor (PXR), aryl hydrocarbon receptor (AHR), and testicular receptor 4 (TR4) directly activate CD36 expression, promoting hepatic steatosis. PPARγ, in addition, enhances cellular lipid storage capacity by increasing the expression of lipid droplets (LDs) (Wolf Greenstein et al., 2017). Moreover, increased expression of CD36 in the liver is associated with the liberation of FFAs from white adipose tissue, aiding in the movement of lipids from adipose tissue to the liver in MASLD (Rui, 2014). In addition to FFAs circulating in the bloodstream, VLDL remnants offer supplementary lipid reservoirs for liver cells. In summary, the molecular landscape of lipid regulation in MASLD and MASH is intricate and multifaceted. The interplay of transcriptional regulators, insulin signaling, and hepatic lipid uptake underscores the complexity of hepatic steatosis development. Understanding these molecular mechanisms is critical for devising targeted therapeutic interventions aimed at mitigating the impact of these prevalent liver diseases on global health.

1.4.3 Neutral Lipid Storage and Heterogeneity of LDs:

Neutral lipids find their sanctuary within the core of LDs, structures enveloped by a monolayer of phospholipids and proteins. Originating from the endoplasmic reticulum, LDs exhibit heterogeneity in both size and lipid composition. This diversity underscores the dynamic nature of lipid storage within hepatocytes, a key aspect in the context of MASLD. Two prominent pathways contribute to lipid catabolism in the liver: lipase-mediated triglyceride hydrolysis and lipophagy, a specialized form of autophagy directing lipids towards lysosomal degradation. These processes play crucial roles in regulating lipid homeostasis and preventing the detrimental effects of lipid accumulation within hepatocytes.

Fatty acids released from LDs are metabolized markedly by peroxisomal and mitochondrial β-oxidation. This metabolic cascade generates acetyl-CoA, a versatile substrate that follows diverse pathways. Acetyl-CoA oxidation via the TCA cycle is a major metabolic fate, leading to ATP production (Alves-Bezerra & Cohen, 2017). Studies employing stable isotope tracers reveal elevated TCA cycle activity and acetyl-CoA oxidation in human MASLD livers (McCullough et al., 2018). This upregulation may represent an adaptive response to increased lipid and acetyl-CoA flux, highlighting the liver's attempt to manage the excess.

Gene	Gene Name	Function
Acly	Acetyl-CoA Lyase	Conversion of citrate to acetyl-CoA
Fas	Fatty Acid Synthase	Catalyzes the synthesis of LCFA from acetyl-CoA and malonyl-CoA.
Fasn	Fatty Acid Synthase	Fatty acid synthesis.
Fabp5	Fatty Acid Binding Protein 5	Transport and uptake of LCFA
Dgat2	Diacylglycerol O-Acyltransferase 2	Catalyzes the final step in triacylglycerol synthesis
Pparg	Peroxisome Proliferator-Activated Receptor Gamma	TF regulating lipid storage, glucose metabolism
Srebf1	Sterol Regulatory Element-Binding Transcription Factor 1	TF regulating cholesterol, fatty acid biosynthesis.
Acaca	Acetyl-CoA Carboxylase Alpha	Catalyzes synthesis of precursor for fatty acid synthesis.
Xbp1	X-Box Binding Protein 1	Genes of Lipid synthesis, LD formation, Fas
CD36	Cluster of Differentiation 36	Fatty acid translocase and scavenger receptor

Table 1.1 List of major genes in lipid metabolism and their roles.

The surplus adipose lipolysis and hepatic acetyl-CoA production contributes to heightened pyruvate carboxylase flux, resulting in increased hepatic gluconeogenesis. This mechanism becomes particularly relevant in the context of obesity with adipose tissue dysfunction, where insulin's inhibition of lipolysis is inadequate. Consequently, impaired insulin suppression of hepatic glucose production ensues, becoming a pivotal factor in the metabolic dysregulation associated with MASLD. An intriguing revelation comes from studies indicating that liver-specific activation of mitochondrial uncoupling can reverse hepatic steatosis in MASH (Caldeira da Silva et al., 2008; Perry et al., 2015). This phenomenon is postulated to occur through increased mitochondrial respiration and enhanced fat combustion. The potential therapeutic implications of targeting mitochondrial function shed light on innovative approaches in addressing MASLD and its advanced stages.

1.4.4 Fatty acid oxidation (FAO):

PPARα emerges as a pivotal player, acting as the master transcriptional regulator of the β-oxidation and ketogenesis gene programs. Hepatocyte-specific deletion of PPARα results in decreased liver β-oxidation and ketogenesis, leading to liver steatosis (Montagner et al., 2016). Transcriptional coactivators such as PGC-1α, BAF60a, SIRT1, and TBL1 converge on PPARα, influencing fatty acid oxidation and liver lipid content (Li et al., 2008). Additionally, factors like IRF9, GPS2, and

Astrocyte Elevated Gene 1 modulate PPARα activity, offering insights into potential therapeutic targets (Liang et al., 2019).

The Sirtuin (SIRT) family of enzymes, responsible for NAD+-dependent lysine deacetylation, plays a crucial role in posttranslational protein modifications. SIRT1 activates PGC-1α, enhancing β-oxidation, while SIRT2 and SIRT6 deletion exacerbates hepatic steatosis (Zhou et al., 2017). Mitochondrial SIRT3, crucial for β-oxidation and ketogenesis, sees reduced activity in obesity, contributing to hepatic lipid accumulation (Lombard et al., 2011). Dietary supplementation with the NAD+ precursor nicotinamide riboside demonstrates potential in reversing high-fat/high-sucrose-induced liver steatosis, highlighting the therapeutic implications of targeting SIRTs (Canto et al., 2012).

Contrary to the theoretical expectation of decreased FAO due to increased DNL, studies indicate enhanced mitochondrial β-oxidation in NASH and obesity (Moore et al., 2022). This paradoxical response is observed through the upregulation of fatty acid translocase (CD36/FAT) and consequently increased FFA uptake in hepatocytes. CD36/FAT expression is associated with levels of serum FFAs and apoptosis mediators**.** The altered respiratory exchange ratio (RER) and elevated oxygen consumption rate in HFD mice underscore the complexity of FAO regulation, emphasizing the need for a nuanced understanding of metabolic adaptations in different stages of MASLD progression.

The expression of genes involved in hepatic mitochondrial β-oxidation, including PPARα, PGC1α, and CPT1a, is elevated in fatty liver mouse models and MASLD patients (Kohjima et al., 2007; Liu et al., 2018; Pittala et al., 2019). However, a transition from simple steatosis to MASH may result in decreased expression of genes related to β-oxidation, suggesting a dynamic alteration in FAO capability during different stages of MASLD. Compensatory pathways such as ω-oxidation in the ER and β-oxidation in peroxisomes are upregulated in MASH, albeit with potential drawbacks such as increased reactive oxygen species (ROS) production and the accumulation of by-products hindering insulin signaling and promoting insulin resistance.

Gene Name	Function
Acyl-CoA Dehydrogenase, Long Chain (Acadl)	Catalyzes the initial step in the beta-oxidation pathway
Carnitine Palmitoyltransferase 2 (Cpt2)	Transports long-chain fatty acyl-CoA into the mitochondria for beta-oxidation
Acyl-CoA Oxidase 1 (Acox1)	Catalyzes the desaturation of acyl-CoA intermediates during peroxisomal beta-oxidation
Pyruvate Dehydrogenase Kinase 4 (Pdk4)	Inhibits pyruvate dehydrogenase
Carnitine Palmitoyltransferase 1A (Cpt1a)	Catalyzes the transfer of long-chain fatty acyl-CoA to carnitine
Fatty Acid Binding Protein 3 (Fabp3)	Involved in the transport of LCFAs
Peroxisome Proliferator-Activated Receptor Alpha (Ppara)	TF for genes in FAO
Fatty Acid Binding Protein 1 (Fabp1)	Uptake and transport of fatty acids within hepatocytes

Table 1.2 List of major genes in FAO and their roles

In summary, the paradoxical enhancement of FAO in the face of increased lipid synthesis adds a layer of sophistication to our understanding, prompting further investigation into the temporal dynamics of metabolic adaptations during MASLD progression.

1.4.5 Glycolysis

Metabolic dysregulation, particularly in glycolysis and pyruvate metabolism, plays a pivotal role in the pathogenesis of MASLD. This section explores the intricate regulation of glycolysis, focusing on key enzymes such as HK, phosphofructokinase (PFK), and pyruvate kinase (PK), and delves into the complex interplay between insulin signaling, glycolytic enzyme expression, and the downstream consequences in the context of MASLD.

Glycolysis, the metabolic pathway converting glucose to pyruvate, is tightly regulated by rate-limiting enzymes, such as HK. This enzyme, primarily regulated by insulin, is significant in postprandial blood glucose modulation. The insulin receptor substrate (IRS)/PI3K/AKT axis is central to insulin's regulation of glucose metabolism, highlighting the intricate signaling cascade that governs glycolytic activity.

Comparative studies between regular chow (RC)-fed and high-fat diet (HFD)-fed mice reveal an upregulation in the mRNA levels of key glycolysis-related enzymes

(HK2, PFKm, PKm) in the liver of HFD-fed mice (Liu et al., 2018). The PTEN-null mouse model further demonstrates that glycolytic enzymes are overexpressed via the P13K/AKT2/PPARγ axis, linking enhanced glycolysis to the susceptibility to fatty liver and hepatocellular carcinoma (Horie et al., 2004). Adenoviral-mediated overexpression of HK2 and PKM2 not only promotes liver growth but also induces liver steatosis, establishing a potential connection between increased glycolysis and hepatocarcinogenesis in fatty liver (Panasyuk et al., 2012).

The product of glycolysis, pyruvate, undergoes dehydrogenation to lactate or decarboxylation to acetyl-coenzyme A by the pyruvate dehydrogenase complex (PDC) in mitochondria. The reversible dephosphorylation and phosphorylation of PDC, regulated by pyruvate dehydrogenase phosphatase (PDP) and pyruvate dehydrogenase kinase (PDK1-4), respectively, dictate the complex's activity. The controversy surrounding PDC activity in hepatocytes of fatty liver is addressed, with studies indicating both decreased and enhanced PDC activity in obesity and MASLD (Bajotto et al., 2006; Go et al., 2016; Shannon et al., 2021). Yet, considering that only 5% of the liver TCA cycle is contributed by the acetyl-CoA produced through pyruvate oxidative decarboxylation (Cappel et al., 2019), the impact of this process on the pathological progression of fatty liver might not be a direct contributor. This necessitates a nuanced understanding of the multifaceted regulation of PDC in the pathological context.

Insulin sensitizer Metformin would normalize PDC activity and mitigates the flow of the tricarboxylic acid (TCA) cycle derived from pyruvate, and was investigated as a potential therapeutic (Haukeland et al., 2009; Van Wagner & Rinella, 2011). 6-12 months of metformin treatment supplemented with lifestyle changes was unable to improve MASH liver pathology. This could be attributed to the relatively low contribution of acetyl-CoA produced by pyruvate to the liver TCA cycle which raises questions about the direct involvement of pyruvate oxidative decarboxylation by PDC in the pathogenesis of fatty liver. Future research must unravel the complex interactions within glycolysis and pyruvate metabolism, providing valuable insights into potential therapeutic targets for MASLD. In summary, the dysregulation of glycolysis and pyruvate metabolism in MASLD is a multifaceted phenomenon influenced by insulin signaling, glycolytic enzyme expression, and the intricate balance between phosphorylation and dephosphorylation of PDC. The contradictory findings in PDC activity highlight the complexity of metabolic adaptations in fatty liver conditions. As research advances, a deeper understanding of these regulatory networks will pave the way for targeted interventions to alleviate the burden of MASLD.

1.4.6 Lactate production

The observation of significantly heightened lactate production in fatty liver, as indicated by studies conducted by Liu et al. (2018) and Wang et al. (2020), unveils a distinctive feature reminiscent of the Warburg effect (de la Cruz-Lopez et al.,

2019). This metabolic phenomenon, characterized by an increased reliance on glycolysis even in the presence of sufficient oxygen, adds a layer of complexity to the understanding of MASLD/MASH. One of the key contributors to the accumulation of lactate in MASLD is the P300/CBP-associated factor (PCAF)-mediated high acetylation level of lactate dehydrogenase-B (LDH-B) (T. Wang et al., 2021). This mechanism was recognized as a major cause for the elevated lactate levels observed in fatty liver conditions. Acetylated LDH-B exhibits reduced activity, impairing the hepatocyte's ability to efficiently dispose of lactate and leading to its accumulation within the liver.

The repercussions of increased lactate levels extend beyond the exacerbation of hepatic steatosis. The elevated lactate contributes to the acetylation of histone H3K9 by diminishing the activity of nuclear HDAC (Latham et al., 2012). This event, outlined by Wang et al. (2020), results in an augmented expression of genes involved in lipogenesis and fatty acid uptake. Consequently, the intricate interplay between lactate accumulation and epigenetic modifications further underscores the multifaceted nature of metabolic disturbances in MASLD.

In conclusion, the elevated lactate levels observed in fatty liver conditions signify not only a metabolic aberration but also a manifestation of the Warburg effect. The PCAF-mediated acetylation of LDH-B emerges as a crucial player in this scenario, shedding light on the intricacies of lactate dysregulation in MASLD. The consequences of heightened lactate extend to the epigenetic level, influencing

gene expression related to lipogenesis and fatty acid uptake. Understanding these intricate metabolic pathways is paramount for developing targeted interventions aimed at mitigating the impact of lactate accumulation in the context of liver diseases.

1.4.7 Tri-carboxylic cycle (TCA)

In the fasting state, spanning 12 and 24 hours, individuals with MASLD exhibit a notable increase in the flow of acetyl-CoA into the TCA cycle compared to those without the condition. This heightened acetyl-CoA flux is intricately linked to the liver's triglyceride content, gluconeogenesis rate, and blood glucose concentrations, establishing a positive correlation (Fletcher et al., 2019; Sunny et al., 2011). Despite observed mitochondrial damage, excess acetyl-CoA in NAFLD hepatocytes tends to be directed towards catabolism through the TCA cycle rather than ketogenesis, indicating a reduction in fat consumption. The TCA cycle operates constitutively in MASLD, with its activity seldom regulated by hormonal cues. Increased fat oxidation emerges as a primary driver for the observed enhancement of the TCA cycle in MASLD. Augmented gluconeogenesis, coupled with oxaloacetate enrichment activating pyruvate carboxylase, contributes to the hyperactive TCA cycle observed in MASLD.

Furthermore, mitochondrial TCA cycle flux is closely associated with ROS production, leading to oxidative stress. This oxidative stress contributes to the progression from liver steatosis to steatohepatitis. Inhibiting

anaplerotic/cataplerotic flow in the mitochondrial TCA cycle reduces oxidative metabolism, presenting a potential therapeutic avenue for inflammation and oxidative stress mitigation. The heightened activity of the TCA cycle in MASLD results in increased levels of intermediates, particularly citrate, which allosterically activates ACC and serves as a precursor for DNL through the citrate pyruvate cycle. This intricate interplay between TCA cycle dynamics and lipid metabolism underscores the complexity of metabolic adaptations in MASLD and offers insights crucial for developing targeted interventions aimed at modulating TCA flux and mitigating disease progression.

1.4.8 Mitochondrial respiratory chain (MRC)

The Mitochondrial Respiratory Chain (MRC), a vital component embedded in the inner mitochondrial membrane, comprises four protein complexes (CI, CII, CIII, CIV) responsible for transferring protons and electrons from NADH and FADH2. This intricate process eventually leads to the production of water when oxygen molecules accept electrons and hydrogen ions. During this electron delivery, protons are transported, creating a proton-motive force (PMF). This force is then harnessed to drive ATP generation, coupling the MRC with ATP synthesis. In the context of normal mitochondrial respiratory function, ROS are generated within a physiological range.

Most electrons delivered to the MRC are efficiently accepted by oxygen, forming water with protons catalyzed by cytochrome c oxidase (CIV). However, a small

fraction of electrons directly combines with oxygen, producing superoxide anion radicals (O2–) and other ROS, predominantly occurring in complex I and complex III (Guan et al., 2022).

In patients with MASH, alterations in MRC efficiency are evident. In the early stages, such as obesity or simple fatty liver, hepatic mitochondrial respiration increases as a compensatory mechanism (Hoene et al., 2021; Koliaki et al., 2015; Sunny et al., 2011). However, in patients with steatohepatitis, there is a decrease in hepatic mitochondrial respiratory levels, indicating a loss of this adaptive response (Perez-Carreras et al., 2003). This decrease in addition to consistently reduced activity in various MRC complexes, results in inadequate capture of excess electrons by oxygen. Consequently, MASLD progresses to MASH, accompanied by heightened ROS production, DNA damage, inflammation, and liver injury.

Additionally, in MASH patients as well as obese leptin deficient (ob/ob) mice, the expression of uncoupling protein-2 (UCP-2) elevates (Serviddio et al., 2008). This exacerbates mitochondrial uncoupling and proton leakage, reducing the efficiency of liver ATP synthesis. The impaired ATP synthesis is validated in obesity and MASLD patients, emphasizing the role of mitochondrial dysfunction in the disease progression. **Interestingly, the uncoupling of liver mitochondria, while contributing to impaired ATP synthesis, appears to play a protective role by accelerating energy expenditure.** Targeting this aspect, using adenine nucleotide translocase (ANT) inhibitor carboxyatractyloside, shows promise in

alleviating fatty liver and insulin resistance in mice by enhancing uncoupling. The complex interplay within the MRC in MASLD underscores the need for targeted interventions addressing mitochondrial dysfunction to mitigate the progression of the disease.

1.4.9 Ketogenesis

Within the liver, the acetyl-CoA pool, sourced from both FAO and glycolysis, undergoes three major fluxes: ketogenesis, the TCA cycle, and DNL. Ketone bodies, synthesized in hepatocytes from acetyl-CoA derived through FAO, serve as an alternative energy source for extrahepatic tissues, particularly when glucose availability is limited. However, a peculiar aspect is that ketone bodies cannot be utilized within the liver due to the absence of enzymes capable of their utilization. Hence, these ketone bodies are exported to extrahepatic tissues for terminal oxidation, providing a crucial alternative energy source, especially when glucose is scarce (Mooli & Ramakrishnan, 2022).

Ketogenesis is primarily regulated by the rate of mitochondrial β-oxidation, Carnitine Palmitoyl transferase 1 (CPT1) activity, TCA cycle flux and its intermediate’s concentrations, as well as hormonal influences such as glucagon and insulin. Elevated acetyl-CoA content resulting from increased β-oxidation or impaired glycolysis, reducing oxaloacetate derived from anaplerosis, strengthens ketogenesis as a consequential response.

Under normal physiological conditions, approximately 86 ± 2% of acetyl-CoA is utilized for ketone body production in the liver. However, in patients with MASLD, this percentage decreases to 77 ± 2% after a 24-hour fast, leading to a 30% reduction in serum β-hydroxybutyric acid concentration compared to the control group. Notably, this difference is not significant after overnight fasting.

Furthermore, the serum β-hydroxybutyric acid concentration exhibits a negative correlation with liver fat content in MASLD patients (Croci et al., 2016). Ketogenic insufficiency, observed in MASLD conditions, exacerbates hepatic inflammation and injury, as evidenced by studies in mice treated with 3-hydroxymethylglutaryl CoA synthase (HMGCS2) antisense oligonucleotide (ASO) after a High-Fat Diet (HFD) (Asif et al., 2022). Additionally, insufficient ketogenesis contributes to increased DNL as more acetyl-CoA is diverted towards citrate synthesis. Disruptions in the intricate balance of acetyl-CoA flux, particularly in the context of reduced ketogenesis, play a role in the pathophysiology of MASLD, influencing not only energy metabolism but also contributing to inflammation and hepatic injury.

In summary, there is a multifaceted metabolic dysregulation underlying MASLD, encompassing glycolysis, pyruvate metabolism, lactate production, TCA cycle, MRC function, and ketogenesis. Additionally, the role of REV-ERB, a key transcriptional regulator, likely impacts each process. It potentially influences ROS production by modulating mitochondrial function and MRC efficiency,

consequently affecting oxidative stress levels. REV-ERB's regulatory influence extends to TCA cycle dynamics, potentially impacting lipid metabolism and oxidative stress modulation. Moreover, its involvement in ketogenesis regulation suggests a broader role in energy homeostasis and inflammation, providing a potential therapeutic target for MASLD intervention.

Gene Abbreviation	Gene Name	Role in Cholesterol Metabolism
HMGCR	3-Hydroxy-3-Methylglutaryl-CoA Reductase	Cholesterol biosynthesis - Rate limiting step
CYP7A1	Cytochrome P450 Family 7 Subfamily A Member 1	Conversion of cholesterol to bile acids (cholesterol catabolism).
SREBF2	Sterol Regulatory Element-Binding Transcription Factor 2	Regulates genes in cholesterol biosynthesis and uptake
ABCA1	ATP-Binding Cassette Transporter A1	Efflux of cellular cholesterol to HDL particles.
AKT1	Protein Kinase B Alpha 1	Modulates SREBP activity
APOB	Apolipoprotein B	Essential component of VLDL and LDL particles
LDLR	Low-Density Lipoprotein Receptor	Uptake of LDL particles from the bloodstream
SREBF1	Sterol Regulatory Element-Binding Transcription Factor 1	Regulates genes involved in cholesterol and fatty acid biosynthesis.

Table 1.3 List of major genes in cholesterol metabolism and their roles

Gene Abbreviation	Gene Name	Role in Glucose Metabolism
SLC2A2	Solute Carrier Family 2 Member 2 (GLUT2)	Facilitates glucose transport in hepatocytes
SLC2A4	Solute Carrier Family 2 Member 4 (GLUT4)	Insulin-stimulated glucose uptake into muscle and adipose tissue
PKLR	Pyruvate Kinase, Liver and RBC	Conversion of phosphoenolpyruvate (PEP) to pyruvate in glycolysis
SLC2A5	Solute Carrier Family 2 Member 5 (GLUT5)	Fructose transport in various tissues
G6PC	Glucose-6-Phosphatase, Catalytic Subunit	Hydrolysis of G6P to glucose in the liver into blood
SLC2A1	Solute Carrier Family 2 Member 1 (GLUT1)	Basal glucose uptake in various tissues
PPARGC1	Peroxisome Proliferator-Activated Receptor Gamma Coactivator 1	Mitochondrial biogenesis and oxidative metabolism
HNF4A	Hepatocyte Nuclear Factor 4 Alpha	Regulates genes in glucose and lipid metabolism

Table 1.4 List of major genes in glucose metabolism and their roles

Chapter Two: Role of REV-ERBα in Metabolic Reprogramming of MASLD/MASH Cells *In Vitro*

2.1 Rationale and Experimental Design

Beyond their well-established roles in circadian regulation and Th17 cell differentiation, members of the NR family, specifically REV-ERBs, have emerged as key players in metabolic regulation. This chapter explores the capability of REV-ERBα agonism to alter metabolic phenotypes in cells of MASLD/MASH pathogenesis.

SR9009, a synthetic REV-ERB agonist, has demonstrated therapeutic utility in metabolic and liver-related conditions such as MASLD and MASH. In previous studies from our lab and others, SR9009 was shown to have a suppressive role in fibrosis in models of MASH, improving metabolic, biochemical, and histopathological indices. SR9009 is also a strong anti-inflammatory drug, however, despite the improvements in liver pathology, the mechanism of action of REV-ERBα -driven transcriptional repression in MASLD/MASH is still unclear. Given the poor solubility and low potency of SR9009, our lab worked in collaboration with the Elgendy lab at Washington University in St. Louis and the Burris lab at the University of Florida to characterize a more selective and potent REV-ERB agonist, STL1267. Based on previous studies using synthetic ligands for REV-ERB as well as genetic knockout experiments, it was hypothesized that REV-ERB exerts its protective role in MASLD/MASH via mitochondrial metabolic

reprogramming. *In vitro* experiments were conducted to assess the role of REV-ERB-mediated transcriptional repression in metabolic processes involved in the development of MASLD/MASH.

However, cell lines, although convenient and widely used, can exhibit genetic and phenotypic variations that deviate from the complexity of primary human cells. Primary human cells closely represent the in vivo physiological conditions, preserving the intricate interplay of signaling pathways, cellular responses, and microenvironmental influences. Thus, to ensure translational relevance and reliability of research outcomes, experiments were performed in primary human hepatocytes as well.

2.2 Results

Pharmacological activation of REV-ERB using STL1267 was found to significantly impact mitochondrial metabolism, suppressing mitochondrial respiration as measured by oxygen consumption rate in cells such as human hepatocellular carcinoma cell line HepG2, which is commonly used as a model of hepatocytes (Fig 2.1). This was further fortified in primary human hepatocytes, where STL1267 treatment was able to alleviate mitochondrial respiration, with significant reduction in basal metabolism, ATP production, non-mitochondrial respiration, and maximal respiration (Fig 2.2). To validate whether this was a mitochondria specific effect, or, if there is a presence of a compensatory mechanism where cells switch to glycolysis for energy, glycolytic stress test and glucose uptake tests were

performed on HepG2s (Fig 2.3). We found that there was no effect of REV-ERB agonism on either glycolytic stress or glucose uptake in HepG2s, suggesting a mitochondria specific effect in hepatocytes.

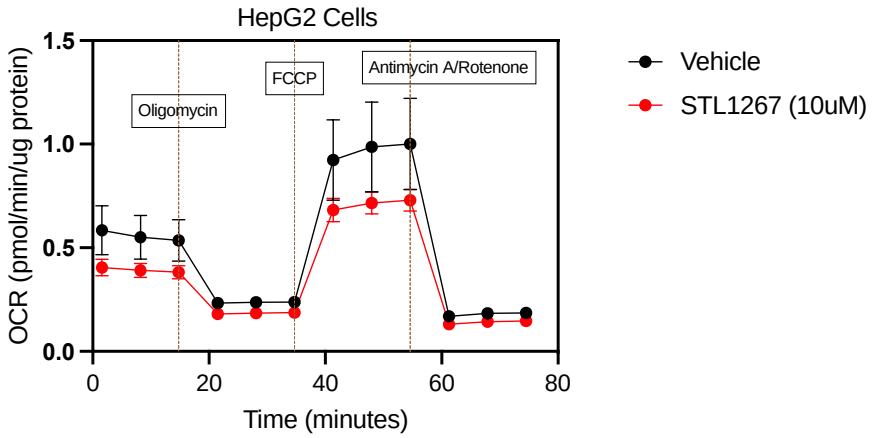

Figure 2.1 **STL1267 induced changes in bioenergetics of HepG2 cells were assessed by Seahorse Flux Analyzer using Cell Mito Stress Kit.** In **a**, there are mitochondrial oxygen consumption curves presented as averages ± standard errors of each measurement time point (n = 9). Initial three measurement points represent basal mitochondrial respiration, the next three points after blocking adenine nucleotide translocating by adding oligomycin represent proton leak-stimulated oxygen consumption, then follow three points representing maximal mitochondrial oxygen consumption capacity when mitochondrial inner membrane is uncoupled by FCCP, and the last three points are for non-mitochondrial oxygen consumption when mitochondrial respiratory chain is inhibited by rotenone and antimycin A. Represented as mean +- SEM.

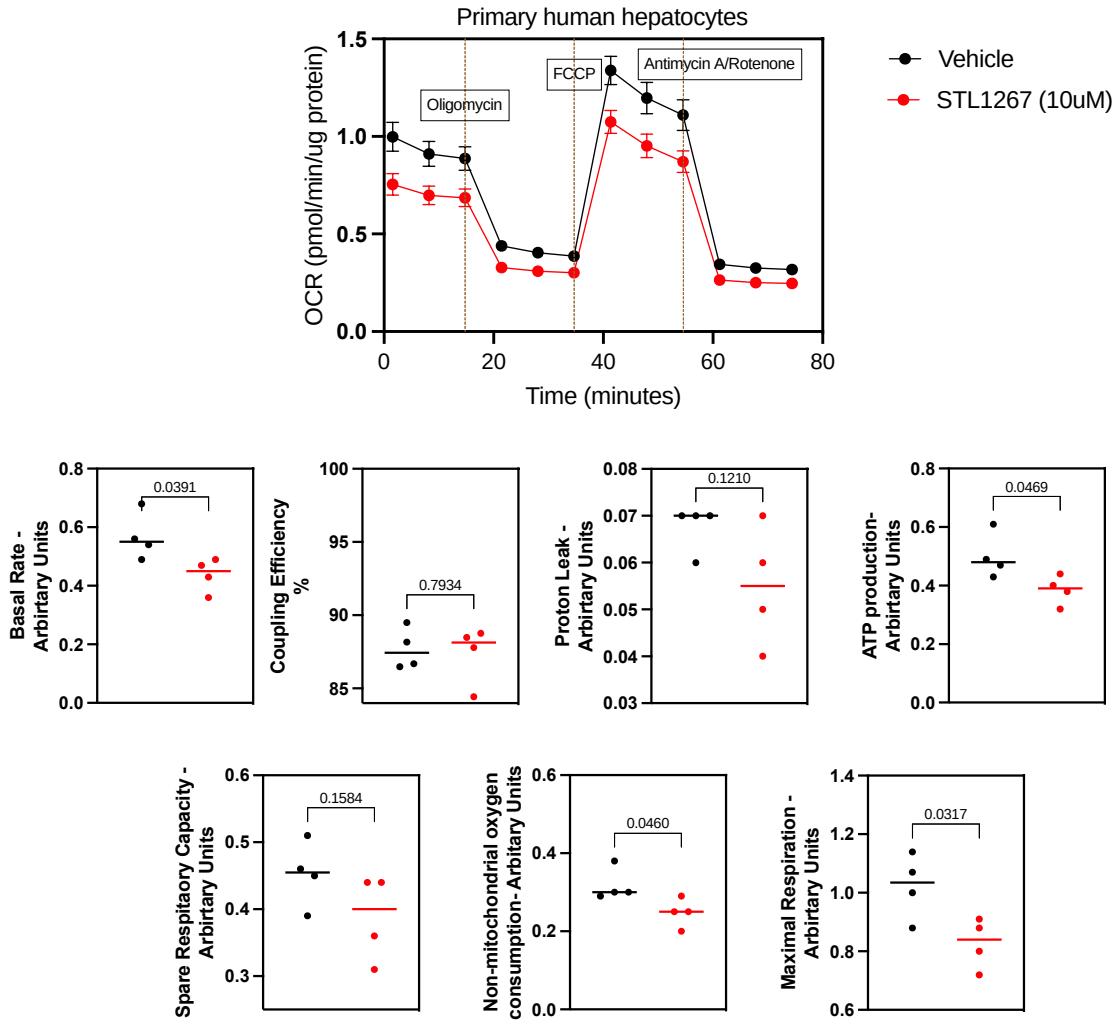

Figure 2.2 **STL1267 induced changes in bioenergetics of primary human hepatocytes cells were assessed by Seahorse Flux Analyzer using Cell Mito Stress Kit.** In a, there are mitochondrial oxygen consumption curves presented as averages ± standard errors of each measurement time point (n = 9). Initial three measurement points represent basal mitochondrial respiration, the next three points after blocking adenine nucleotide translocating by adding oligomycin represent proton leak-stimulated oxygen consumption, then follow three points representing maximal mitochondrial oxygen consumption capacity when mitochondrial inner membrane is uncoupled by FCCP, and the last three points are for non-mitochondrial oxygen consumption when mitochondrial respiratory chain is inhibited by rotenone and antimycin A. The summary data calculated from the curves are shown. Represented as mean +- SEM, and analyzed and plotted in GraphPad Prism using Student's t-test. p-values shown.

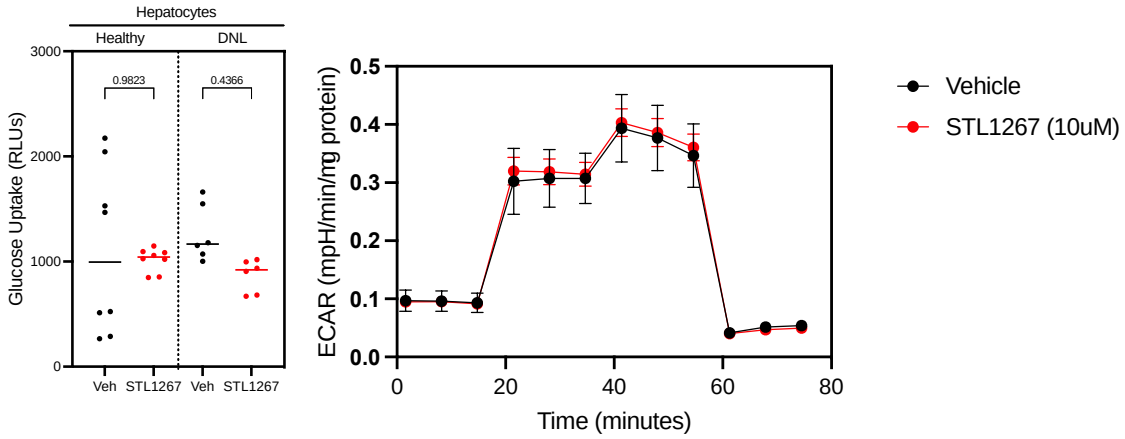

Figure 2.3 **induced changes in glucose metabolism in HepG2 cells**. InGlucose uptake is measured in HepG2s and represented as mean (SEM). **b**, glycolytic rate is measured as extracellular acidification rate and represented as averages ± standard errors of each measurement time point (n = 9). Represented as mean +- SEM, and analyzed and plotted in GraphPad Prism using Student's t-test. p-values shown.

To mimic MASH pathology *in vitro*, HepG2 cells were supplemented with excessive lipids, cholesterol, and glucose, referred to as *de novo* lipogenic (DNL) HepG2s (Fig 2.4). Bodipy 493/503 (Molecular Probes) neutral lipid staining indicated that there was increased lipid accumulation in the DNL cells. Hepatocytes contribute significantly to the pathology of MASLD/MASH through the secretion of ROS (Allameh et al., 2023). In the context of MASH, hepatocytes undergo metabolic dysregulation, often driven by factors such as excessive lipid accumulation. This metabolic imbalance triggers (Fig 2.4) the production of ROS within hepatocytes, leading to oxidative stress. The overproduction of ROS can cause damage to cellular components, including lipids, proteins, and DNA, fostering inflammation and hepatocellular injury. This oxidative stress-induced damage plays a pivotal role in the progression of MASH, contributing to inflammation, fibrosis, and ultimately the development of more severe liver diseases.

DNL hepatocyte cells were then studied for their downstream ROS production for both cellular and mitochondrial specific ROS by staining with ImageIT ROS and MitoSOX dyes, respectively (Fig 2.6). In agreement with the hypothesis, both cellular and mitochondrial ROS were augmented in DNL hepatocytes. Since, mitochondria are a major source of ROS within cells, and we saw that REV-ERBa pharmacological activation can reduce mitochondrial respiration, it was hypothesized that reduced mitochondrial respiration could further reduce oxidative

stress. Upon treatment of DNL hepatocytes with STL1267, we observed a significant reduction in both cellular ROS and mitochondria-specific ROS (Fig 2.7).

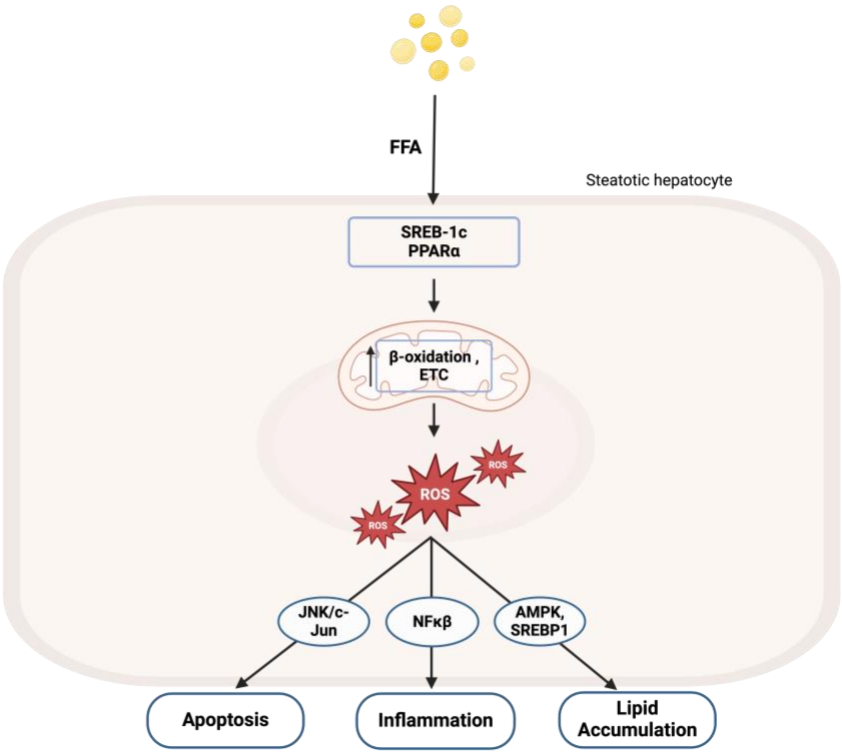

Figure 2.4 **Hepatocyte dysfunction in MASLD.** Excessive intake of free fatty acids leads to increased fatty acid β-oxidation and electron transport chain activity within hepatic mitochondria. Heightened ROS levels activate various protein kinases (such as AMPK, SREBP1, NF-kB, JNK/cJun) and transcription factors. These molecules govern lipid metabolism, inflammation, antioxidant defenses, and hepatocyte apoptosis. Ultimately, alongside insulin resistance, these molecular changes exacerbate fat synthesis within hepatocytes, contributing to the progression of NAFLD. AMPK, Adenosine Monophosphate-activated Protein Kinase; SREBP1, Sterol Regulatory Element-Binding Protein 1; NFκβ, Nuclear Factor-kappa B)

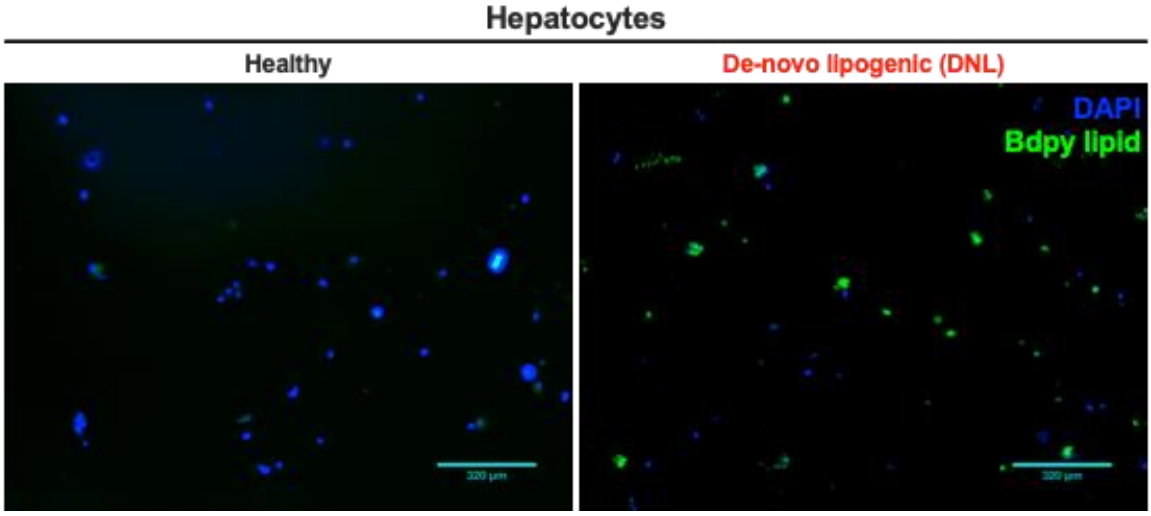

Figure 2.5 **Supplementation of lipids, cholesterol, and glucose increases lipid droplet formation in HepG2s cells** HepG2 cells were cultured in media supplemented with concentrated lipids, cholesterol, and glucose for 5 days. The cells were stained with Bodipy 493/503 (green) and DAPI (blue). Images were taken at 4x magnification.

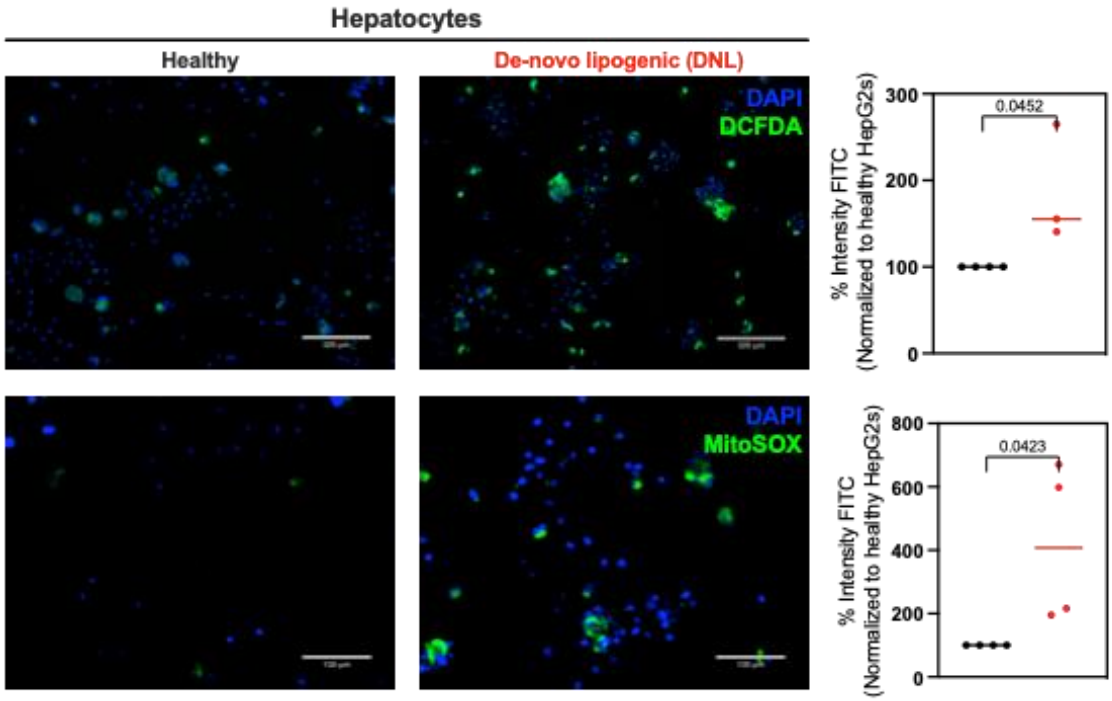

Figure 2.6 **DNL hepatocytes have increased oxidative stress.** HepG2 cells were cultured in media supplemented with concentrated lipids, cholesterol, and glucose for 5 days. The cells were stained with A) ImageIT Live (green) and DAPI (blue) B) MitoSOX (green) and DAPI (blue). Data is represented as mean (SEM) intensity percentage of FITC channel, normalized to healthy hepatocytes. Analyzed and plotted in GraphPad Prism using Student's t-test. p-values shown.

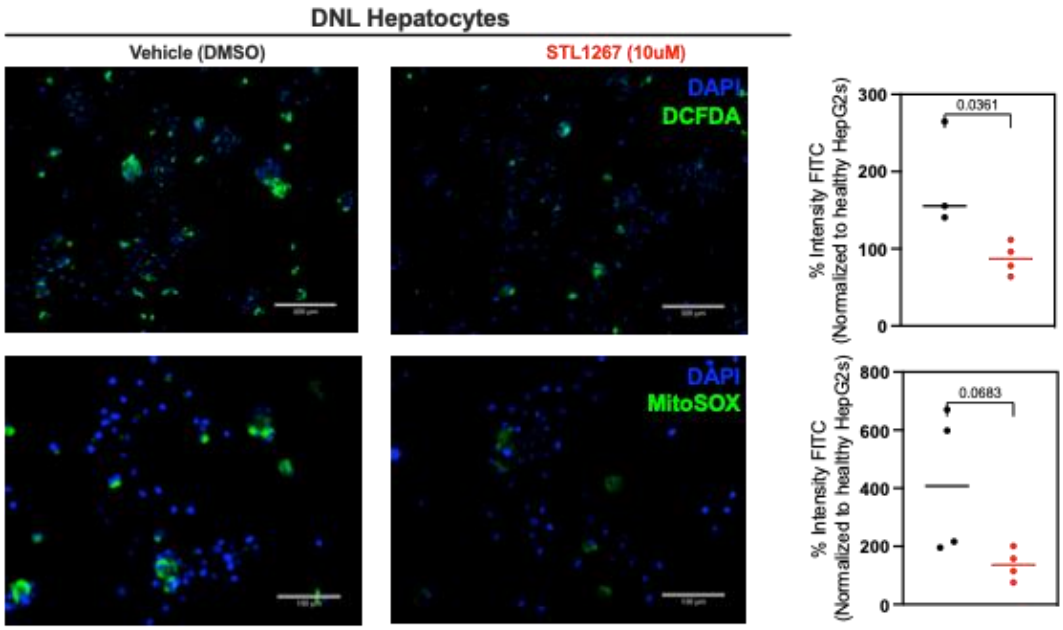

Figure 2.7 **STL1267 treatment attenuates oxidative stress in DNL hepatocytes**. HepG2 cells were cultured in media supplemented with concentrated lipids, cholesterol, and glucose for 5 days. The cells were then treated with either DMSO or STL1267 (10uM) overnight. The cells were stained with A) ImageIT Live (green) and DAPI (blue) B) MitoSOX (green) and DAPI (blue). Data is represented as mean (SEM) intensity percentage of FITC channel, normalized to healthy hepatocytes. Analyzed and plotted in GraphPad Prism using Student's t-test. p-values shown.

The liver is a complex organ composed of various cell types that communicate with each other. REV-ERB mediated changes in mitochondrial respiration in hepatocytes could influence the metabolic and inflammatory status of neighboring cells, such as stellate cells and macrophages via crosstalk or directly. Thus, we sought to assess the effect of STL1267 on stellate cells, as well as macrophages. As expected, REV-ERB pharmacological activation reduced mitochondrial respiration in both LX2 and RAW264.7 cells (Fig 2.8).

Metabolism serves as a fundamental orchestrator of cellular effector function and phenotype, intricately shaping the identity and capabilities of cells. The metabolic pathways within a cell dictate the availability of energy sources, biosynthetic precursors, and redox equivalents, ultimately influencing the cell's ability to carry out specific functions. In immune cells, for instance, the balance between glycolysis and oxidative phosphorylation not only determines energy production but also profoundly impacts effector functions. Cells with a high glycolytic rate often exhibit enhanced pro-inflammatory responses, while those relying more on oxidative phosphorylation may favor anti-inflammatory or quiescent phenotypes. Metabolism directly intersects with signaling pathways, influencing transcriptional programs that define cellular identity and function. Alterations in cellular metabolism can lead to shifts in effector function and phenotype, playing a pivotal role in diverse biological processes, from immune responses to tissue homeostasis and disease states. Thus, it was hypothesized that alterations in mitochondrial respiration in these cells could lead to alterations in downstream effector function

and phenotype. To understand the intimate connection between cellular metabolism and function, each cell type's function was assessed. STL1267 mediated REV-ERB agonism alone could dampen ECM secretion in LX-2 cell (Fig 2.9), suggesting that altered mitochondrial metabolism could affect downstream pathogenic function of these cells.

To understand the broader impact of REV-ERB on various cellular pathways, RNA-sequencing analysis was performed on hepatocyte cell line HepG2 and hepatic stellate cell line LX-2. It was revealed that REV-ERB regulates genes involved in metabolic pathways, including those related to lipid metabolism, as well as inflammation, autophagy, ECM secretion, and mitochondrial function (Fig 2.10, 2.11).

To understand the mechanism of action of this metabolic reprogramming of reduced mitochondrial respiration, REV-ERB's effect on master-regulator HIF-1 was studied. RAW 264.7 macrophages were treated with cobalt chloride to induce HIF-1α stabilization and translocation to the nucleus. These cells were either treated with STL1267 or vehicle. HIF-1α translocation to the nucleus was measured by colocalization with DAPI (Fig 2.12). A reduction in nuclear HIF-1α was observed (yellow) as measured by intensity quantification upon STL1267 treatment, suggesting REV-ERB activation stunts HIF-1 activity. Further, in our livers of MASH mice, STL1267 treatment was able to reduce transcription of HIF-1α target genes such as *Glut-1* and *Vegf,* and HIF-1α activated genes such as *Nrf2* and *SOD1*.

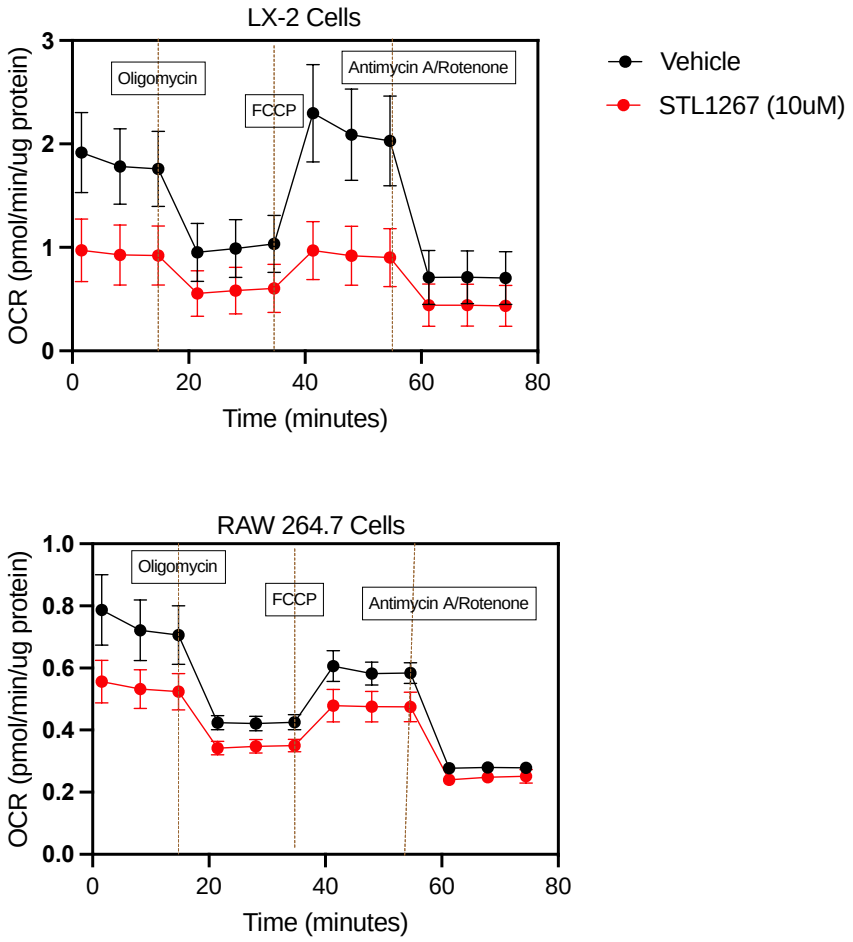

Figure 2.8 **STL1267 induced changes in bioenergetics of LX-2 and RAW 254.7** cells were assessed by Seahorse Flux Analyzer using Cell Mito Stress Kit. In a, there are mitochondrial oxygen consumption curves presented as averages ± standard errors of each measurement time point (n = 9). Initial three measurement points represent basal mitochondrial respiration, the next three points after blocking adenine nucleotide translocating by adding oligomycin represent proton leak-stimulated oxygen consumption, then follow three points representing maximal mitochondrial oxygen consumption capacity when mitochondrial inner membrane is uncoupled by FCCP, and the last three points are for non-mitochondrial oxygen consumption when mitochondrial respiratory chain is inhibited by rotenone and antimycin A.

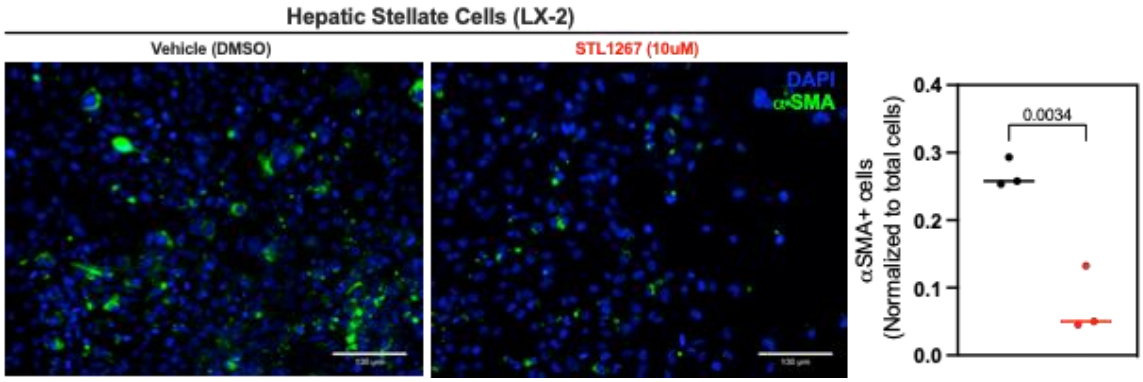

Figure 2.9 **STL1267 treatment attenuates fibrogenic marker (αSMA) in LX2 cells.** Spontaneously activated LX-2 cells were treated with either DMSO or STL1267 (10uM) overnight. The cells were stained for αSMA (green) and DAPI (blue). Data is represented as mean (SEM) of FITC+ cells, normalized to total cell number. Analyzed and plotted in GraphPad Prism using Student's t-test. p-values shown.

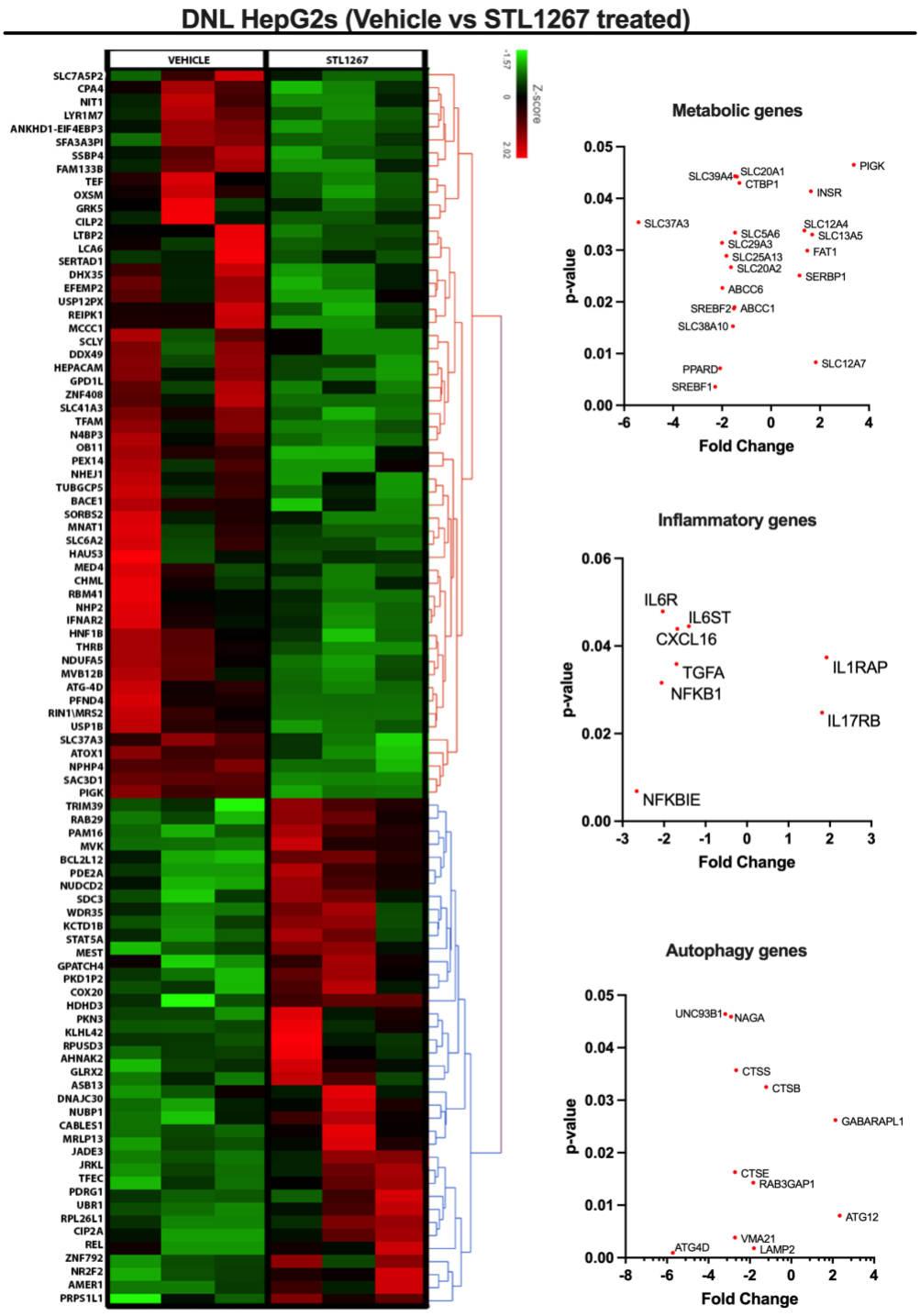

Figure 2.10 **RNA-Seq of HepG2s treated with or without STL1267.** RNA-seq data were pre-processed and analyzed using Picard-STAR pipeline. Using unsupervised hierarchical clustering (HC) analysis based on DEGs, heatmap of the top DEG was plotted. Graphs were plotted for the DEG involved in various processes important in MASLD/MASH.

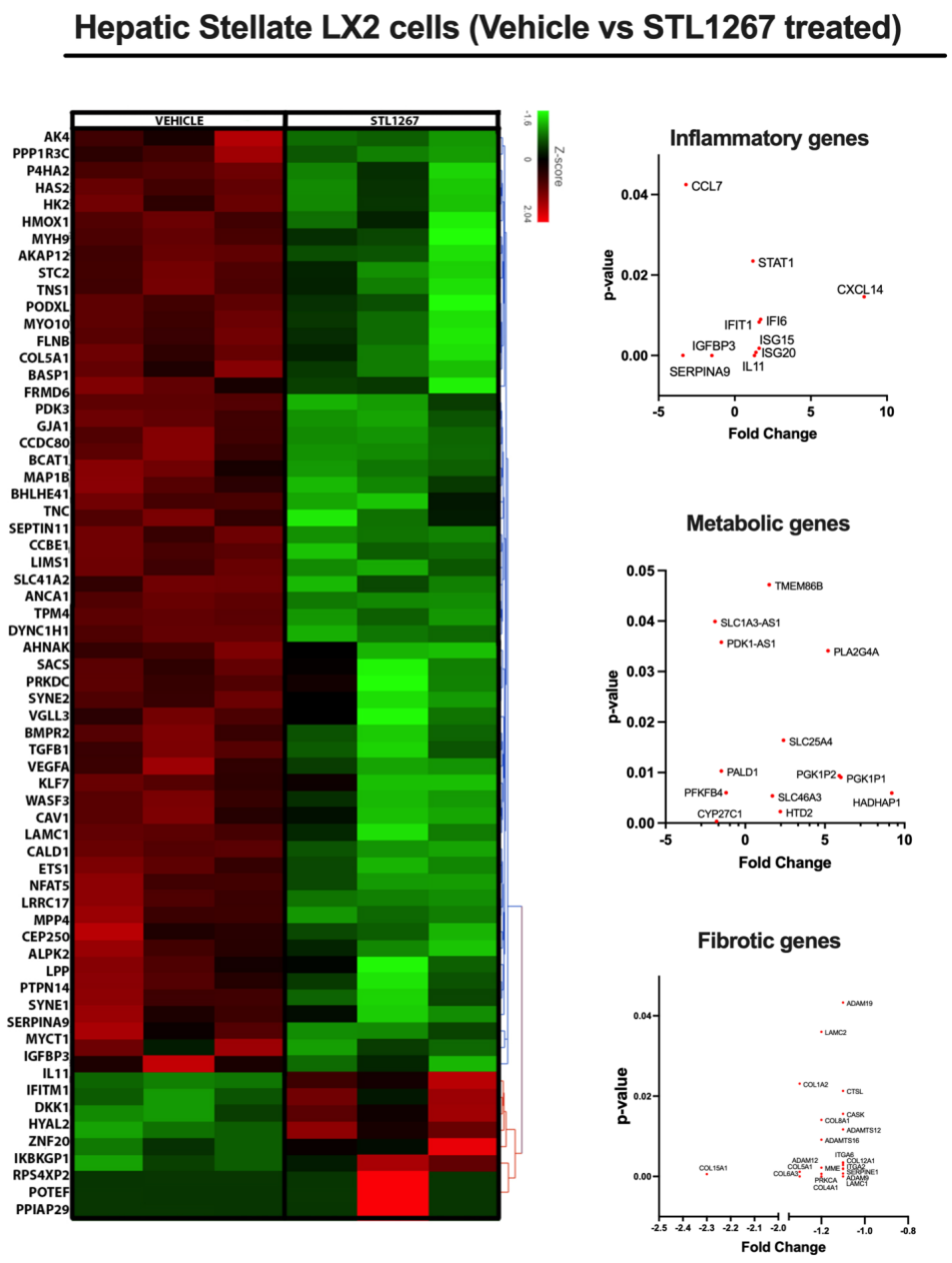

Figure 2.11 **RNA-Seq of LX-2s treated with or without STL1267.** RNA-seq data were pre-processed and analyzed using Picard-STAR pipeline. Using unsupervised hierarchical clustering (HC) analysis based on DEGs, heatmap of the top DEG was plotted. Graphs were plotted for the DEG involved in various processes important in MASLD/MASH.

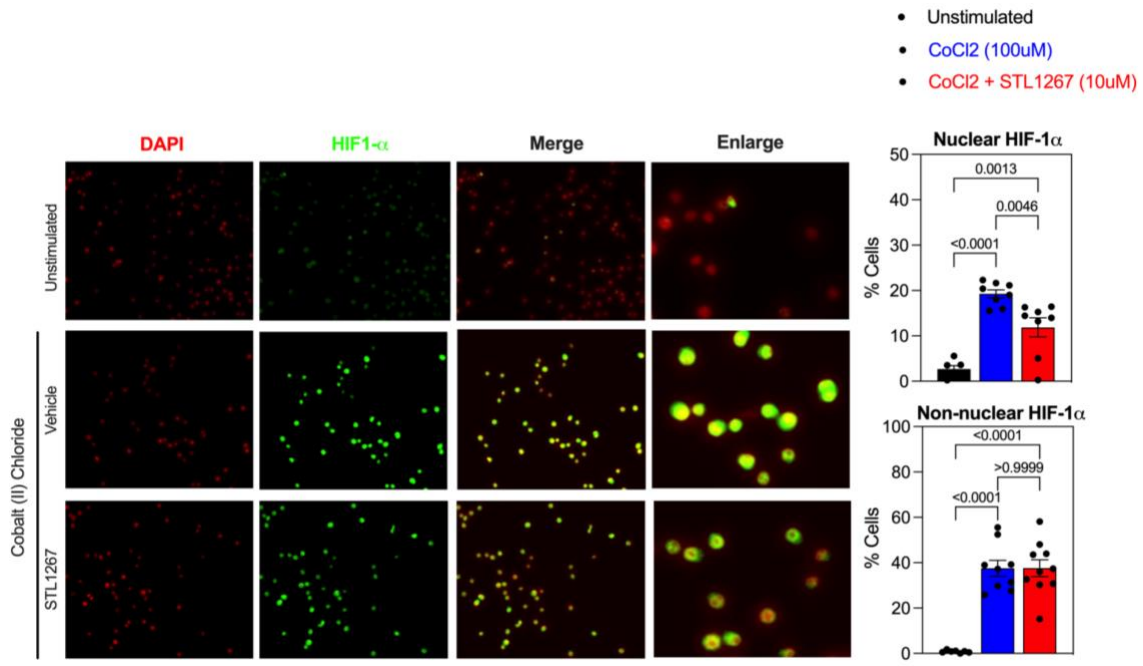

Figure 2.12 **Hypoxia induced nuclear translocation of HIF-1α is attenuated with REV-ERB agonism using STL1267.** Hypoxia was induced with Cobalt (II) Chloride (CoCl2), and cells were treated with either Vehicle (DMSO) or STL1267 (10uM) for overnight. Cells were stained for HIF-1α (Green), and DAPI (Red) was used as a counterstain. For nuclear HIF-1a, total cells threshold and yellow color threshold was plotted, and for non-nuclear HIF-1a green threshold was used.

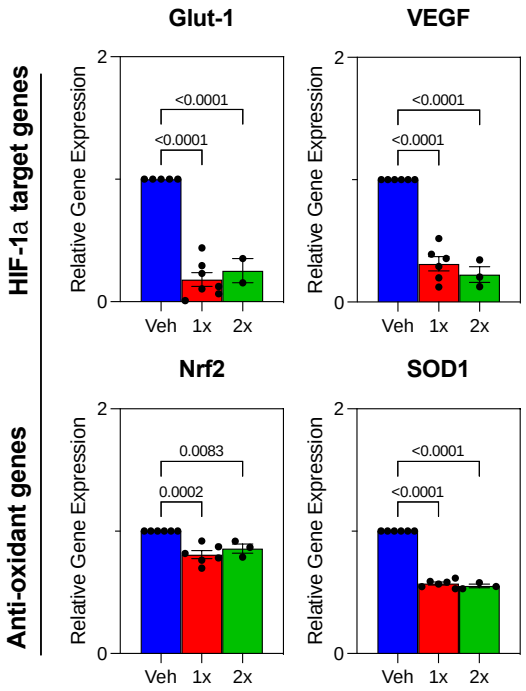

Figure 2.13 **REV-ERBα activation using STL1267 alleviates hypoxia and compensatory antioxidant genes.** qPCR was performed on livers from obese mice fed MASH diet, treated with either vehicle, STL1267 once a day (1x), or STL1267 twice a day (2x). Gene expression was normalized to vehicle. Results were graphed and analyzed in GraphPad Prism by ANOVA and represented as Mean ± SEM (n=3-6).

Chapter Three: Murine models of MASLD/MASH

3.1 Rationale and experimental design

Animal models play a crucial role in understanding the mechanisms underlying liver disease and in testing potential therapeutic interventions. Several approaches have been used to develop MASH models. Modifying the expression of specific genes involved in lipid metabolism, inflammation, or fibrosis can lead to the development of MASH-like conditions. For example, knockout models for genes related to lipid regulation or insulin signaling may mimic aspects of MASH (Febbraio et al., 1999; Liang et al., 2002). Further, administration of chemicals carbon tetrachloride (CCl4) or alterations in diet (methionine-choline deficient) can induce liver injury and steatohepatitis in animals (Rahimi et al., 2022). These models may simulate aspects of human MASH pathology. However, mimicking natural human progression with the use of overnutrition models comprises of feeding animals diets that are high in fat, cholesterol, and/or fructose and can induce obesity, insulin resistance, and liver damage, closely mimicking the metabolic conditions associated with MASH in humans. Examples include high-fat diets, high-fructose diets, or diets deficient in essential nutrients. Since, MASH is a complex condition, the use of a combination of genetic modifications and dietary interventions to create more complex models better reflects the multifactorial nature of human MASH. The use of non-rodent species, such as pigs or primates may provide a more physiologically relevant platform for studying human diseases.

It's important to note that no single model perfectly recapitulates all aspects of human MASH. Often, models are chosen or developed based on the specific aspects of the disease under investigation. Combining different models and approaches allows for a more comprehensive understanding of MASH pathogenesis and potential therapeutic strategies.

Here, we have employed a high fat, high fructose, high cholesterol diet – MASH Diet to induce MASH in mice *in vivo*. Obese leptin$^{ob/ob}$ deficient (*ob/ob*) mice are a commonly used genetic model of obesity and metabolic syndrome. They carry a mutation in the gene that codes for leptin, the hormone responsible for the regulation of appetite and metabolism. As a result, *ob/ob* mice lack functional leptin and exhibit hyperphagia (excessive eating), leading to severe obesity, insulin resistance, and dyslipidemia. When fed a HFHC NASH diet, *ob/ob* mice have been shown to develop and mimic MASH symptoms such as hyperlipidemia, steatosis, and fibrosis (Kristiansen et al., 2016). Like humans with MASH, *ob/ob* mice develop hepatic steatosis, characterized by the accumulation of triglycerides and other lipids within hepatocytes. In addition to steatosis, *ob/ob* mice may also exhibit inflammation and fibrosis in the liver, which are progressive stages of MASH leading to liver damage and cirrhosis. *Ob/ob* mice have a consistent genetic background, reducing variability in experimental results compared to other models or human subjects. This allows for more reproducible studies and easier interpretation of results. However, it's essential to acknowledge some limitations

of using *ob/ob* mice as a MASH model. While *ob/ob* mice develop obesity and metabolic syndrome like humans, their leptin deficiency is not representative of the human condition. In humans, MASH can occur in individuals with normal or elevated leptin levels, implicating additional factors in disease pathogenesis. Further, the pathology of MASH in *ob/ob* mice may not fully recapitulate all aspects of human MASH. For example, the progression to advanced fibrosis and cirrhosis is not as pronounced in *ob/ob* mice. It is also noteworthy that some effects observed in *ob/ob* mice may be due to their leptin deficiency and it thus becomes pertinent to interpret them correctly in the context of MASH.

Thus, the aim of this chapter is to establish and characterize an *ob/ob* MASH diet mouse model and a WT MASH diet model, to study the induced metabolic and inflammatory changes over time. Accordingly, we assessed plasma markers of disease and histopathology of AT and liver. Additionally, we assessed the transcriptional changes to characterize disease progression. In the experimental design, 6-week-old male mice were used throughout. One group of mice was fed a calorie matched control diet that lacked fructose and cholesterol, while the other was fed the HFHC MASH diet. The entire experimental design was performed in both *ob/ob* and WT mice that were matched for sex, timeline, and handling.

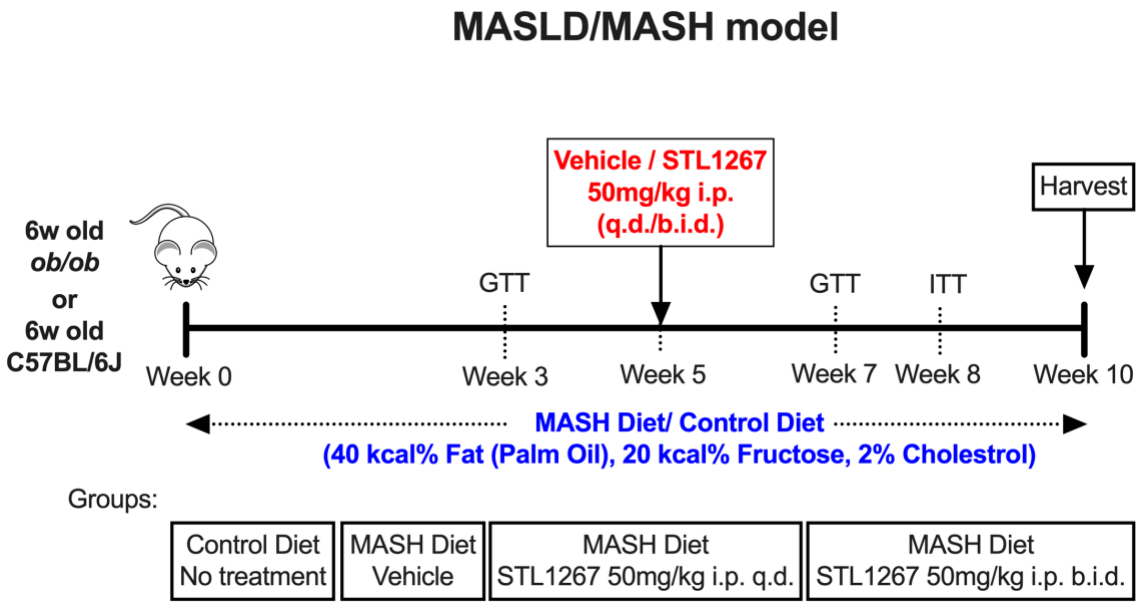

Figure 3.1 **Schematic representation of the MASH ob/ob and B6 model**. Mice were placed on MASH diet or calorie matched control diet. Mice were maintained on this diet throughout the experiment. After 5 weeks, mice on MASH diet were randomly assigned into groups, and were treated with either vehicle (placebo), STL1267 50mg/kg i.p. once a day (q.d.), or STL1267 50mg/kg i.p. twice a day (b.i.d.). During the course of the experiment, i.p.GTT and i.p.ITT were performed. Study was terminated at 10 weeks.

3.2 Results

3.2.1. Model: MASH Leptin^{ob}/ Leptin^{ob} (*ob/ob*) mice

3.2.1.1. Mice sustained elevated plasma metabolic parameters post NASH diet induction

The overall study design is outlined (Figure 3.1). Following a diet induction period of 10 weeks, *ob/ob* mice fed with MASH diet demonstrated increased adiposity as measured by body weight after 1 week till week 10, when compared to animals fed the calorie-matched control diet (CD) (Fig 3.3-A). To eliminate the possibility of a difference in the amount of food consumed, food intake was measured at the end of each week (Fig 3.3-B). There was no observed difference in the amount of food consumed between the CD and MASH diet groups. *Ob/ob* mice that were fed MASH diet showed significant elevations in levels of cholesterol, liver enzymes (ALT, AST, and ALP), as well as circulating TGs and low-density lipoprotein (LDL) when compared to respective control diet fed animals in serum. No significant change in lactate levels was observed, however, a decrease in ALP levels was observed (Fig 3.4).

We report an increase in all major biomarkers associated with disease, including increased TGs in the liver. Further, we performed glucose tolerance and insulin tolerance tests on these mice. We observed that there is no significant increase in

the level of glucose intolerance in mice fed with MASH diet, at either 3weeks or 8 weeks. Similarly, we did not observe significant difference between insulin tolerance in mice fed with MASH diet and CD (Figure 3.5). Together, this suggests that MASH diet in *ob/ob* mice is able to generate metabolic dysregulation similar to human MASH, however, is not enough to induce glucose intolerance and insulin resistance.

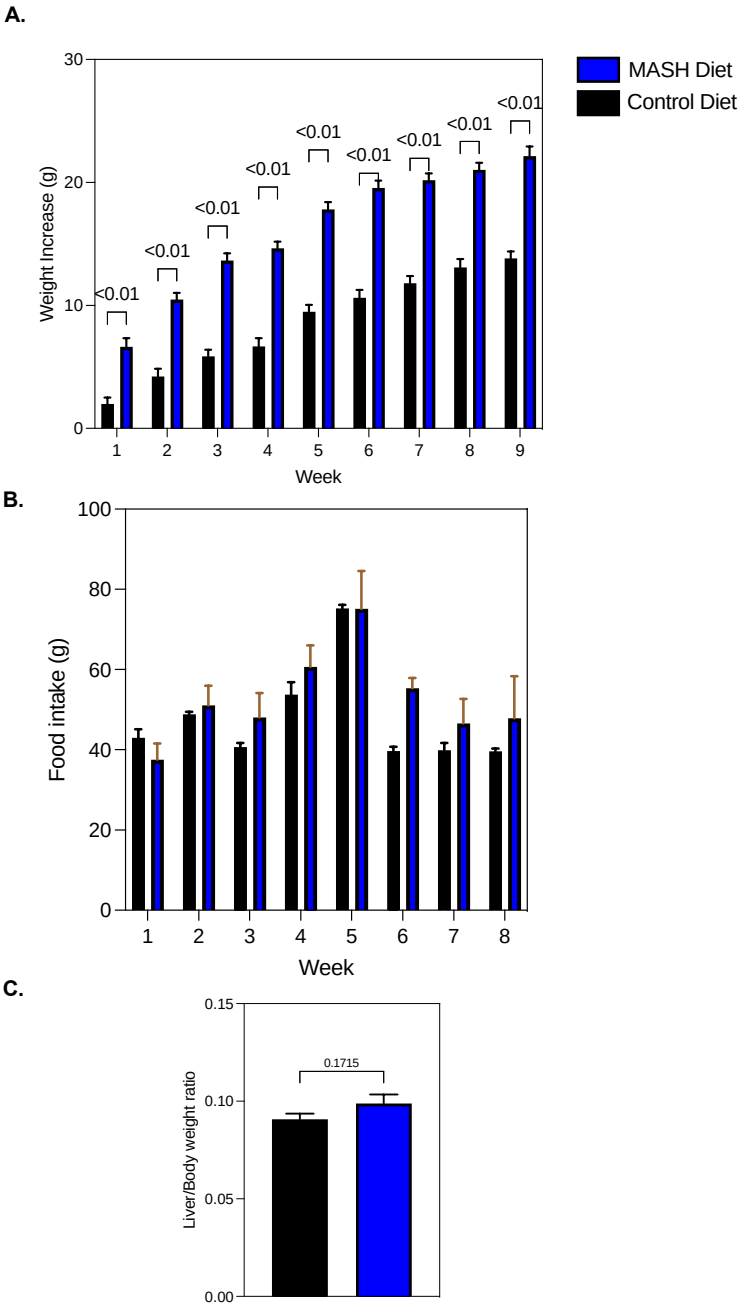

Figure 3.3 **MASH diet induced physiological changes in adiposity in control diet and MASH diet fed mice.** Animals were fed HFHC MASH diet or control diet for 10 weeks (A) Mouse weights per week of diet were measured and normalized to initial weight. Data are presented as mean ± SEM; n = 6-7. p-values indicated (One-way ANOVA). (B) Food intake per week for each cage was measured. Data are presented as mean ± SEM; n = 3 for CD and n = 3-4 for MASH diet, p-values indicated (One-way ANOVA).(C) Liver was harvested at the end of 10 weeks and liver to body weight ratio was plotted as a percentage. Data are presented as mean ± SEM; n = 6-7. p-values indicated (Student's t-test).

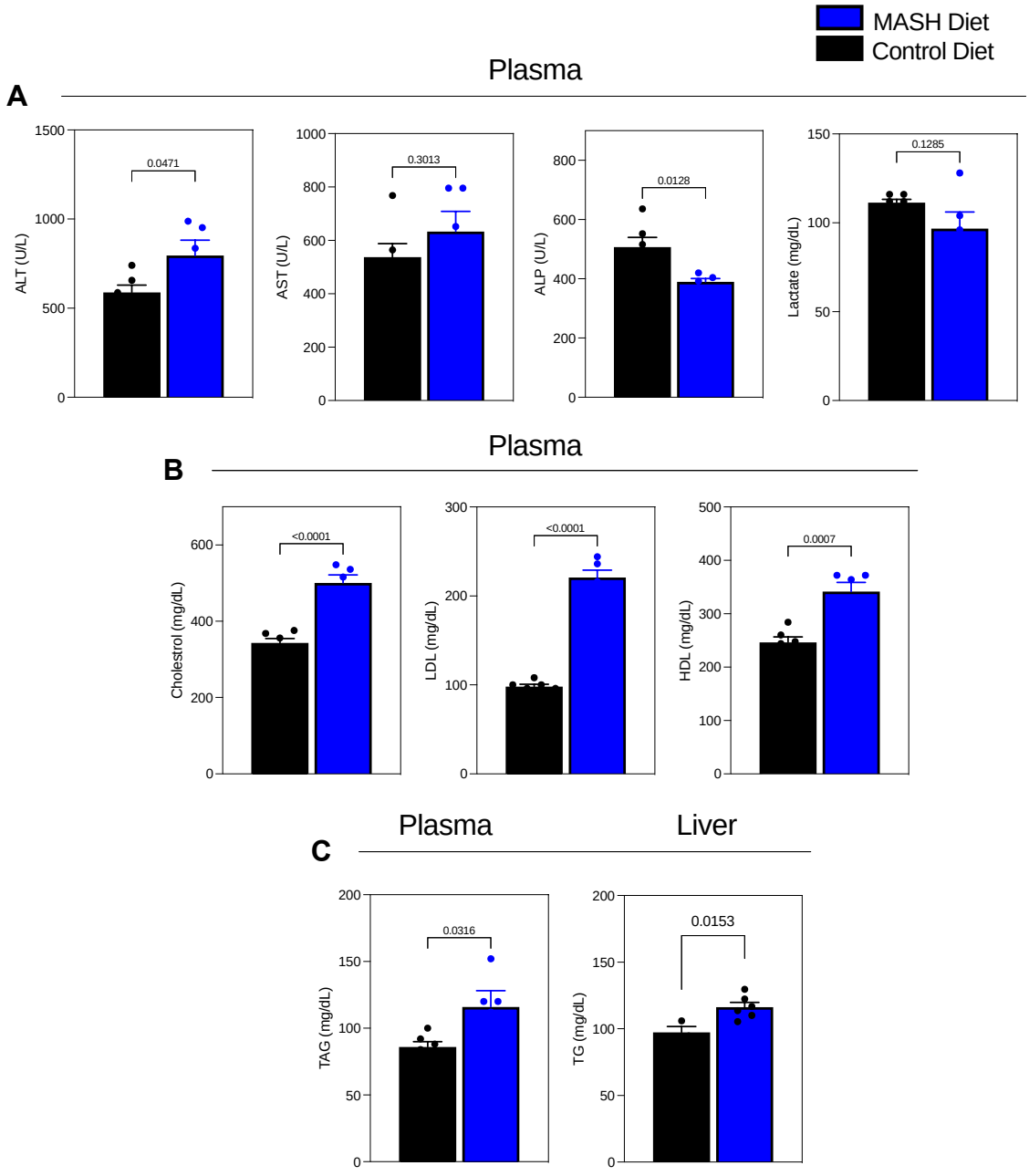

Figure 3.4 **Plasma and metabolic indices were worsened by MASH diet.** Blood plasma was analyzed for liver enzymes (A) as well as circulating metabolic indices – total cholesterol, LDL, and HDL (B) Circulating TGs (left) and Liver TGs (right) were also analyzed. All data are represented as mean ± SEM (n=5-6) and analyzed using student's t-test in GraphPad Prism.

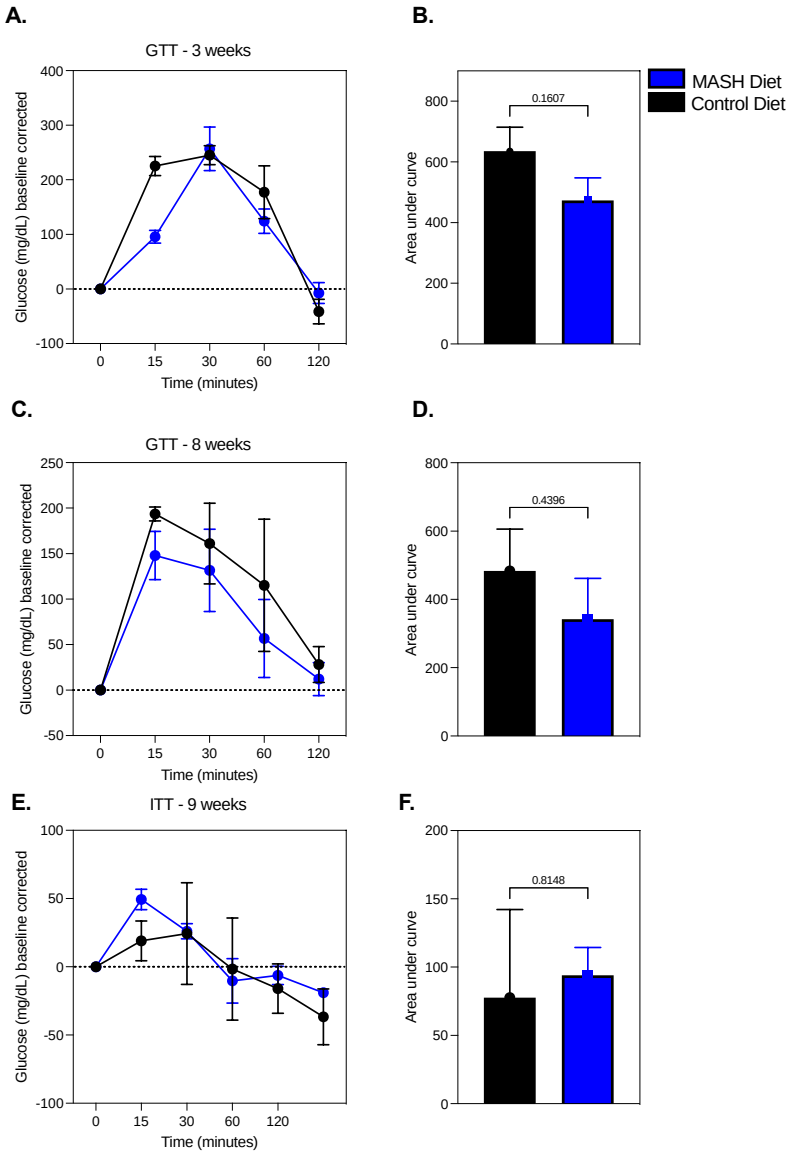

Figure 3.5 **Glucose tolerance test (i.p.GTT) in ob/ob mice in HFHC MASH diet and in control diet.** 6 hour fasted mice were administrated 2.0 g/kg glucose or insulin 0.5U/kg i.p. Blood samples were taken at 0, 15, 30-, 60-, 90- and 120-min. Plasma levels of glucose (A, C, D) were measured. Data are normalized to baseline glucose levels. (B, D, F) Area under curve. Data are presented as mean ± SEM; n = 5-6. *p<0.05 (Student's t-test).

3.2.1.3 Altered liver gene expression after MASH diet-induction

To characterize the effect of 10-week diet induction on global liver gene expression, the transcriptome of control diet vs *ob/ob* MASH mice was analyzed using qPCR of genes involved in fatty liver disease. It is shown that genes linked to lipogenesis, fatty acid uptake, cholesterol biosynthesis, inflammation, and carbohydrate metabolism are robustly induced in *ob/ob* mice fed the MASH diet as compared to animals on the CD (Fig 3.6-3.9). A full list of all the genes and their roles in MASLD/MASH are described in preceding sections (Tables 1.1-1.4)). Further, a large collection of pro-inflammatory factors such as IFNg, TNF, IL-6, IL1β, and Casp-3 were found induced post MASH diet induction in *ob/ob* mice (Fig 3.10).

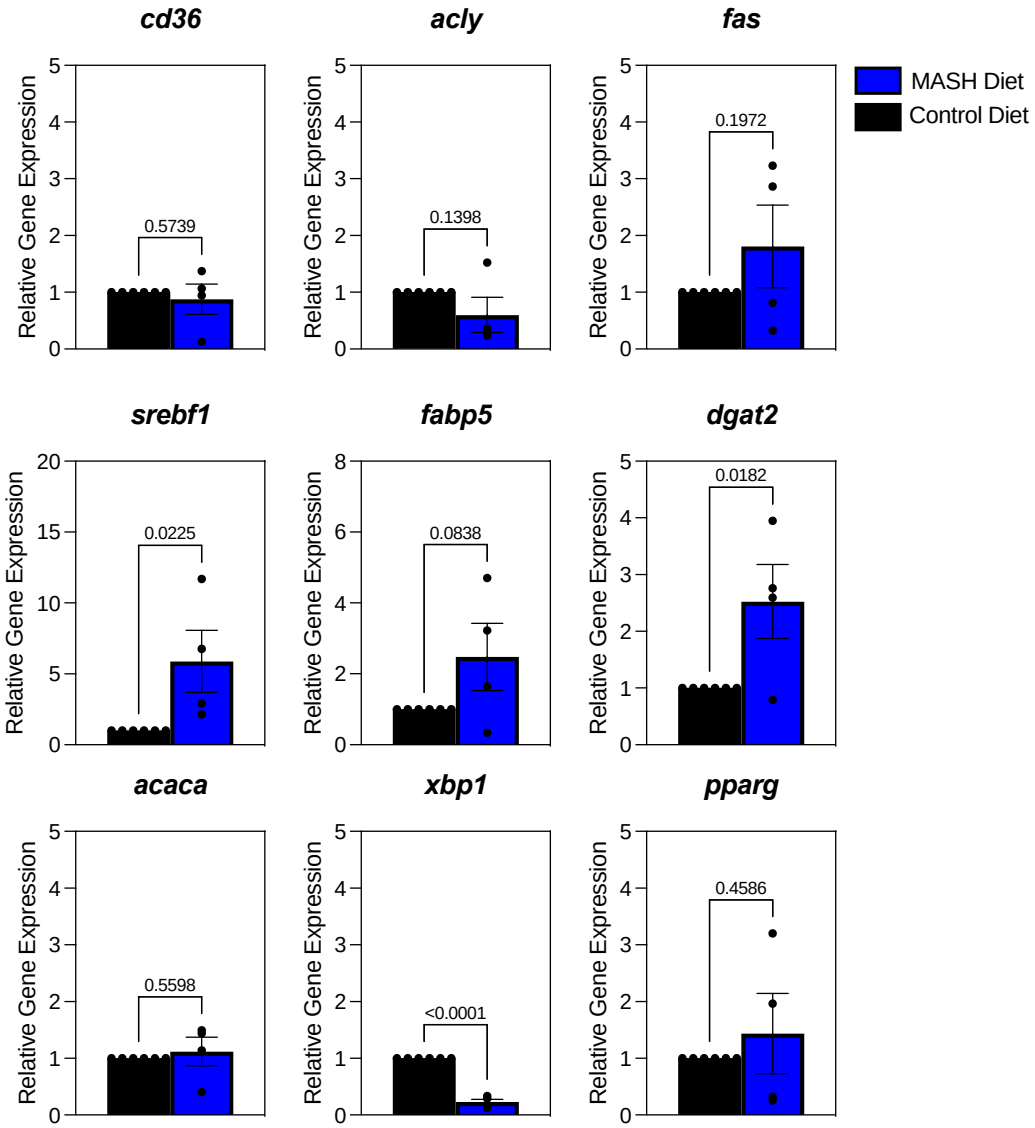

Figure 3.6 **Changes in lipogenic genes in the liver of mice fed MASH diet.** Gene expression of lipogenic genes that are involved in MASLD/MASH in mouse liver tissue. Data are represented as mean ± SEM (n=4-5). p-values are shown, as calculated by student's t-test in GraphPad Prism.

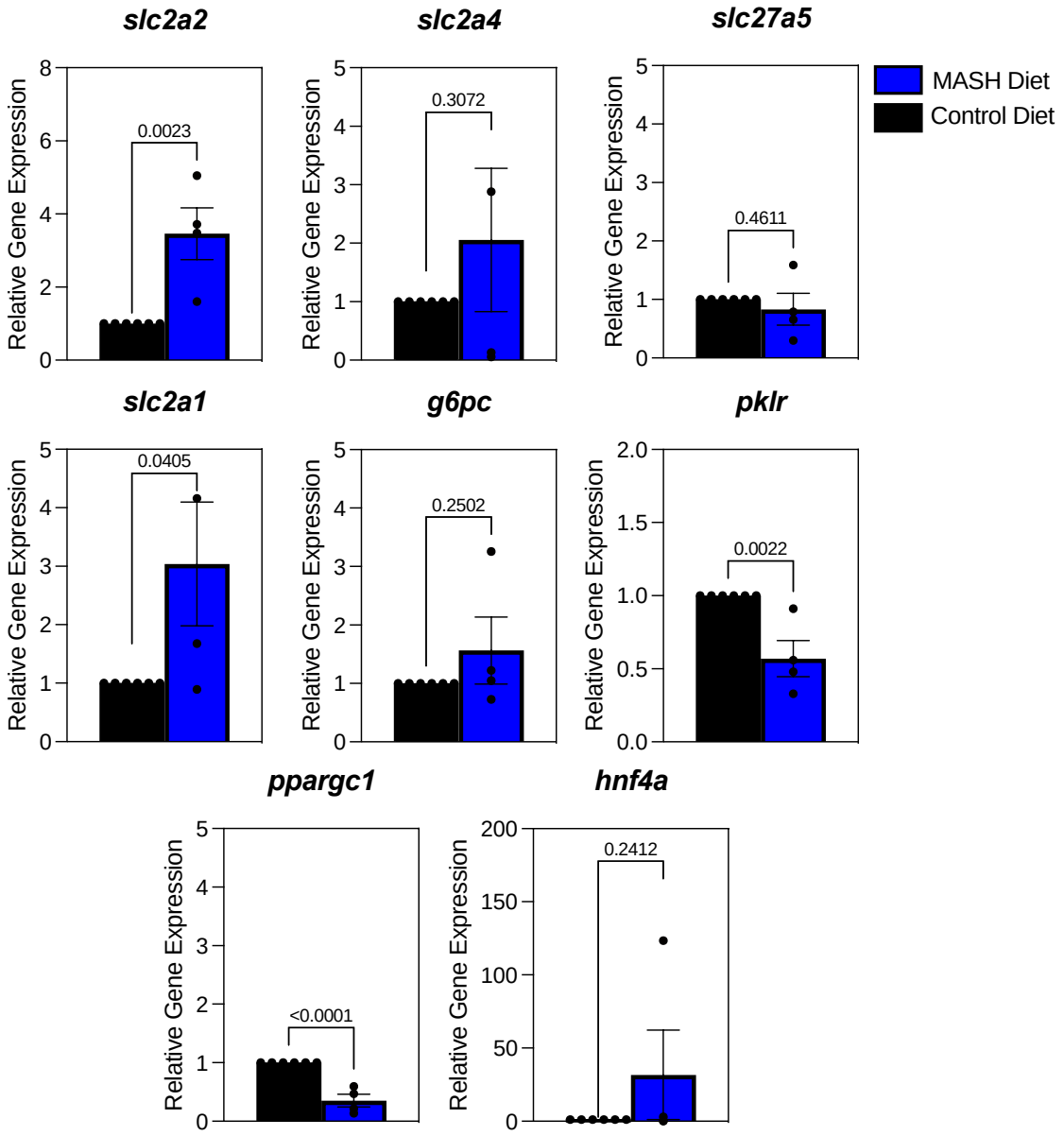

Figure 3.7 **Changes in glucose metabolism genes in the liver of mice fed MASH diet.** Gene expression of genes that are involved in glucose metabolism in MASLD/MASH in mouse liver tissue. Data are represented as mean ± SEM (n=4-5). p-values are shown, as calculated by student's t-test in GraphPad Prism.

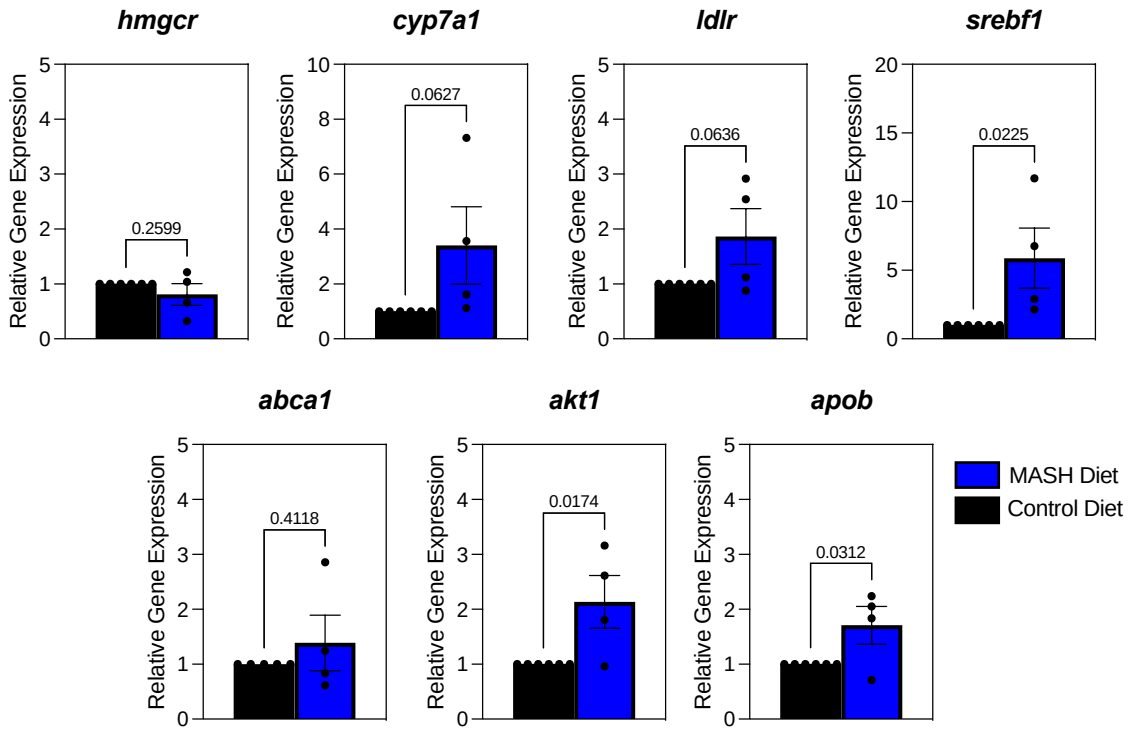

Figure 3.8 **Changes in cholesterol genes in the liver of mice fed MASH diet.** Gene expression of cholesterol genes that are involved in MASLD/MASH in mouse liver tissue. Data are represented as mean ± SEM (n=4-5). p-values are shown, as calculated by student's t-test in GraphPad Prism.

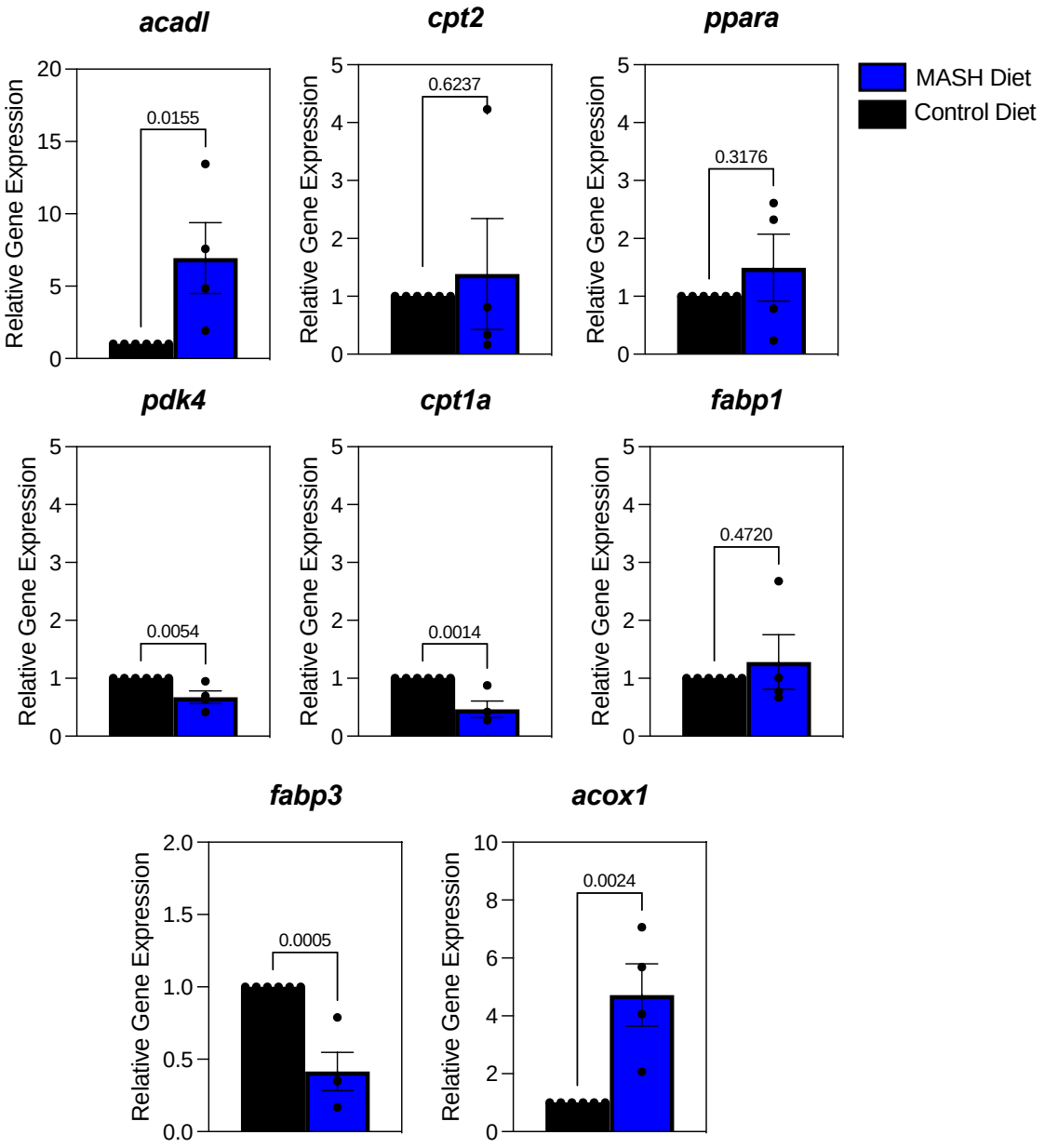

Figure 3.9 **Changes in genes involved in the regulation of fatty acid oxidation the liver of mice fed MASH diet.** Gene expression of FAO genes that are involved in MASLD/MASH in mouse liver tissue. Data are represented as mean ± SEM (n=4-5). p-values are shown, as calculated by student's t-test in GraphPad Prism.

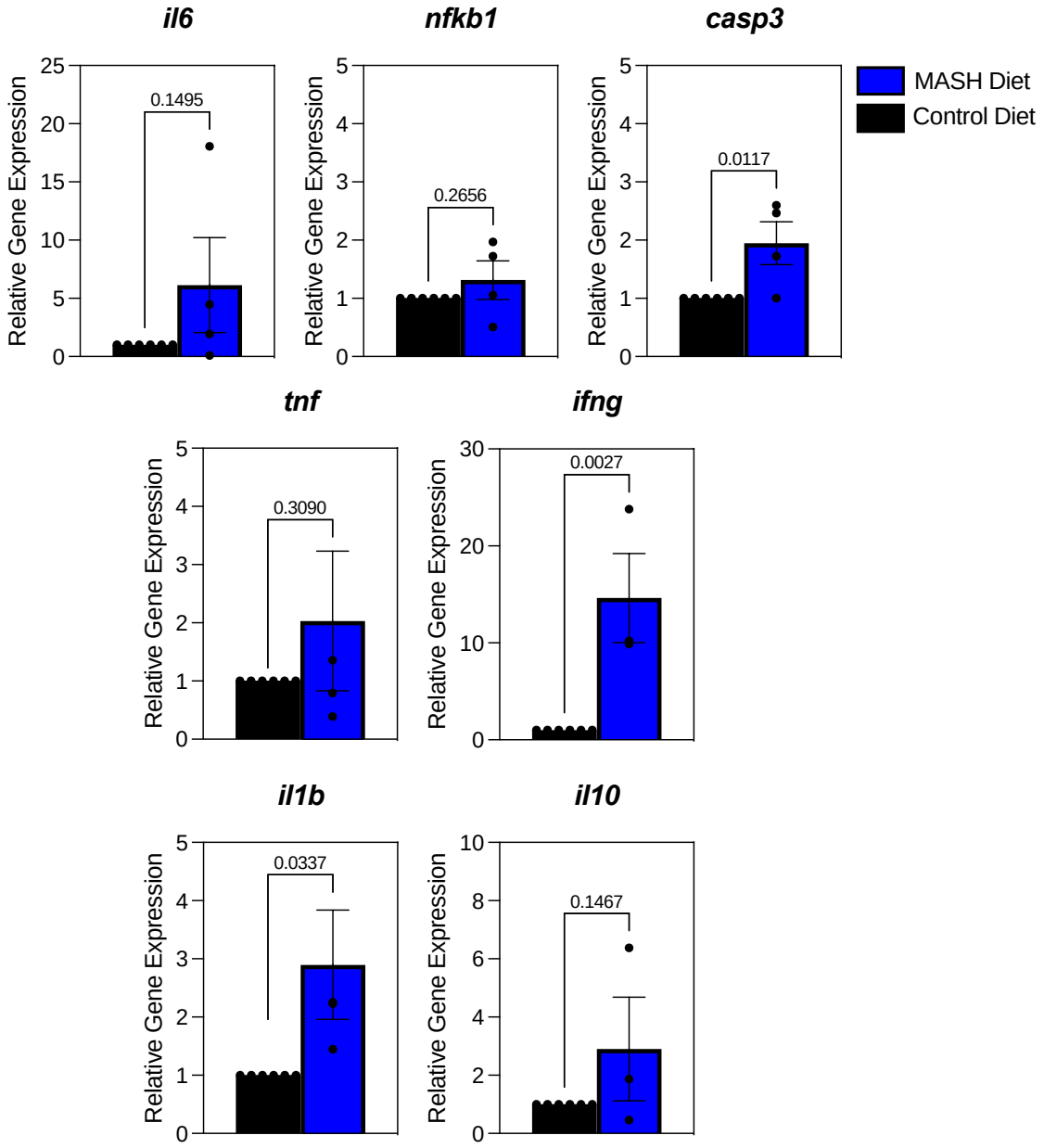

Figure 3.10 **Gene expression changes in inflammatory markers in the liver of mice fed MASH diet.** Gene expression of inflammatory cytokines (IL-6, IL-1β, NFκβ, TNFα, Casp-3) and anti-inflammatory cytokines (IL-10) that are involved in MASLD/MASH in mouse liver tissue. Data are represented as mean ± SEM (n=4-5). p-values are shown, as calculated by student's t-test in GraphPad Prism.

3.2.2 Model: Diet-induced obesity (DIO) MASH B6 mice

3.2.2.1 Mice sustained elevated plasma metabolic parameters post NASH diet induction

We hypothesized that *ob/ob* mice are genetically susceptible to overeating and obesity, which subsequently could be responsible for their overall metabolic syndrome. In order to account for the leptin deficiency, we performed a replicate of our in-vivo model in wild-type B6 mice (Fig 3.1).

We demonstrate that ingestion of the NASH diet over a period of 10 weeks promotes a significant increase in WT mice weights when compared to the control diet group (Fig 3.11-A), however, there was no observed difference in the amount of food consumed between the CD and MASH diet groups (Fig 3.11-B). As a measure of liver dysfunction, plasma was analyzed for various biomarkers (Fig 3.12-A) such as ALT, ASP, and ALP. We observed a trending increase in levels of ALT (p-value 0.0632) and AST (p-value 0.199) in MASH diet group compared to CD. However, similar to *ob/ob* mice we saw a trending decline in ALP levels. We report an increase in all major biomarkers associated with MASH, including increased circulating TC including both HDL and LDL (Fig 3.12-B). Like the *ob/ob* mice, there was no change in serum lactate (Fig 3.12-A). While there was no significant increase in circulating TGs in serum in MASH diet group, we saw

increased amounts of TGs and FFAs in livers of MASH diet fed group (Fig 3.12-C).

Further, we performed glucose tolerance and insulin tolerance tests on these mice (Fig 3.13). We observed that there is a significant increase in the level of glucose intolerance in mice fed with MASH diet for 8 weeks, as observed at 30 min post-injection of glucose, mice fed with MASH diet go through a higher peak in glucose levels. Similarly, we also observed a significant difference between insulin tolerance in mice fed with MASH diet, as observed by glucose levels 15mins post injection of insulin. Together, this suggests that WT mice fed that are fed with MASH diet, develop mild MASH, and can capitulate symptoms such as insulin resistance and glucose intolerance, but a less severe form of MASH, with no significant changes in liver enzymes and circulating TGs.

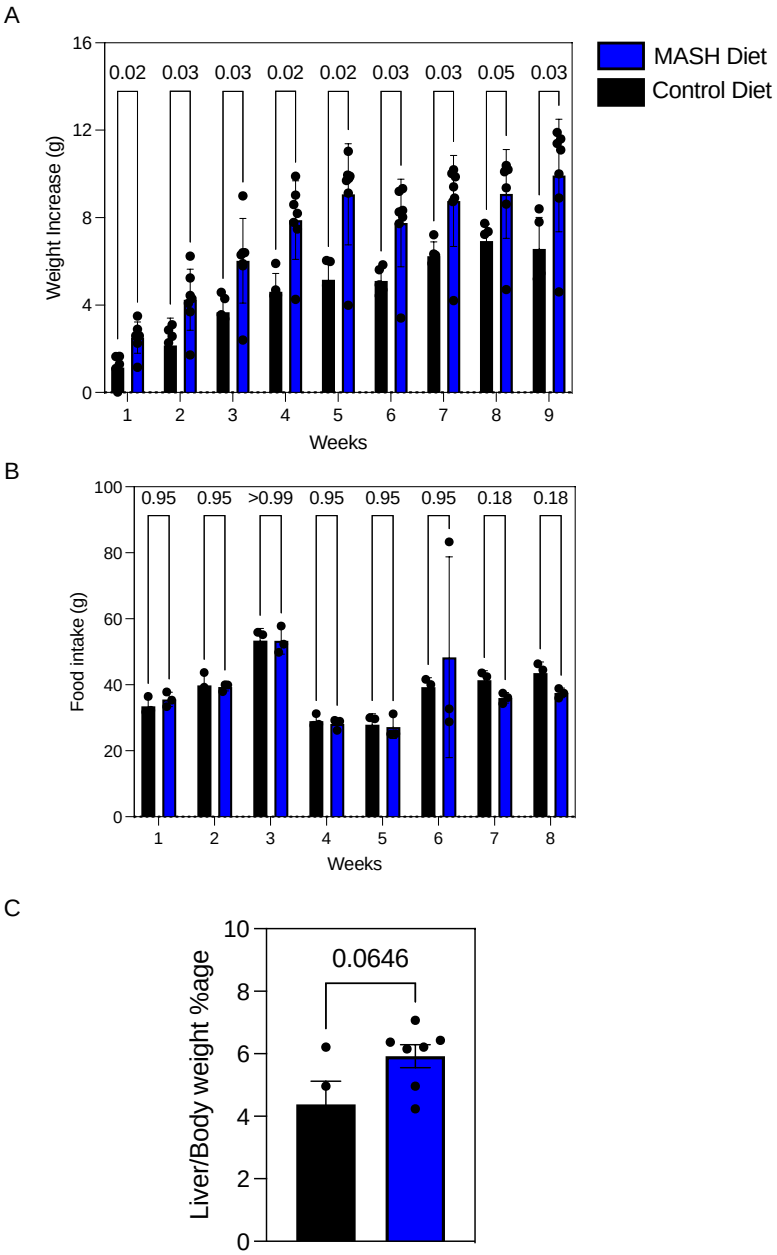

Figure 3.11 **Physiological changes in adiposity in wild-type control diet and MASH diet fed-mice.** Animals were fed HFHC MASH diet for 10 weeks. (A) Mouse weights per week of diet were measured and normalized to initial weight. Data are presented as mean ± SEM; n = 5-6 for CD and n = 9-10 for DIO, p-values indicated (One-way ANOVA). (B) Food intake per week for each cage was measured. Data are presented as mean ± SEM; n = 3 for CD and n = 4-5 for DIO, p-values indicated (One-way ANOVA).(C) Liver was harvested at the end of 10 weeks and liver to body weight ratio was plotted as a percentage. Data are presented as mean ± SEM; n = 5-6 for CD and n = 7-8 for DIO. p-values indicated (Student's t-test).

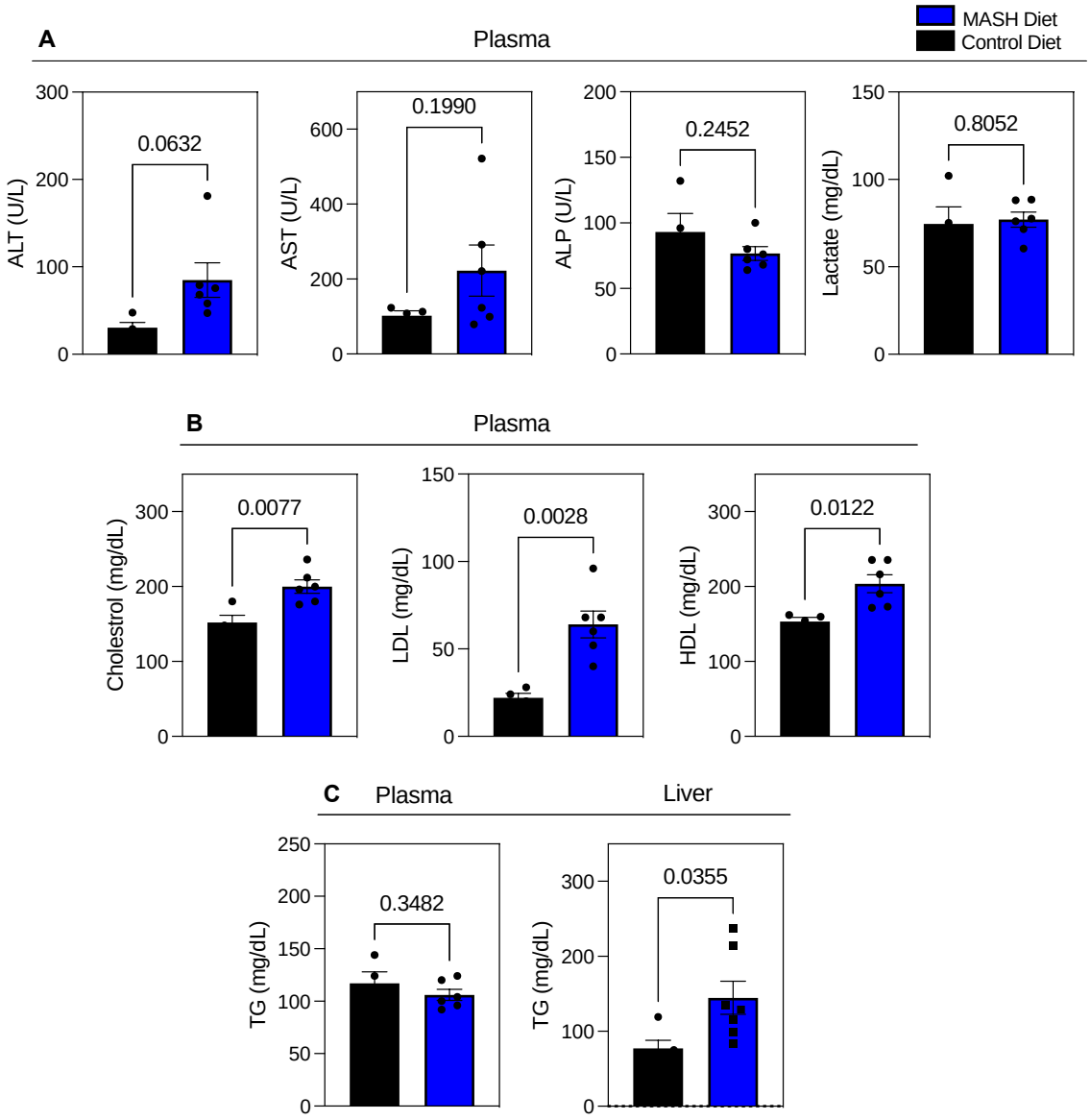

Figure 3.12 **Plasma and metabolic indices were worsened by MASH diet.** Blood plasma was analyzed for liver enzymes (A) as well as circulating metabolic indices – total cholesterol, LDL, and HDL (B) Circulating TGs (left) and Liver TGs (right) were also analyzed. All data are represented as mean ± SEM (n=5-6) and analyzed using student's t-test in GraphPad Prism.

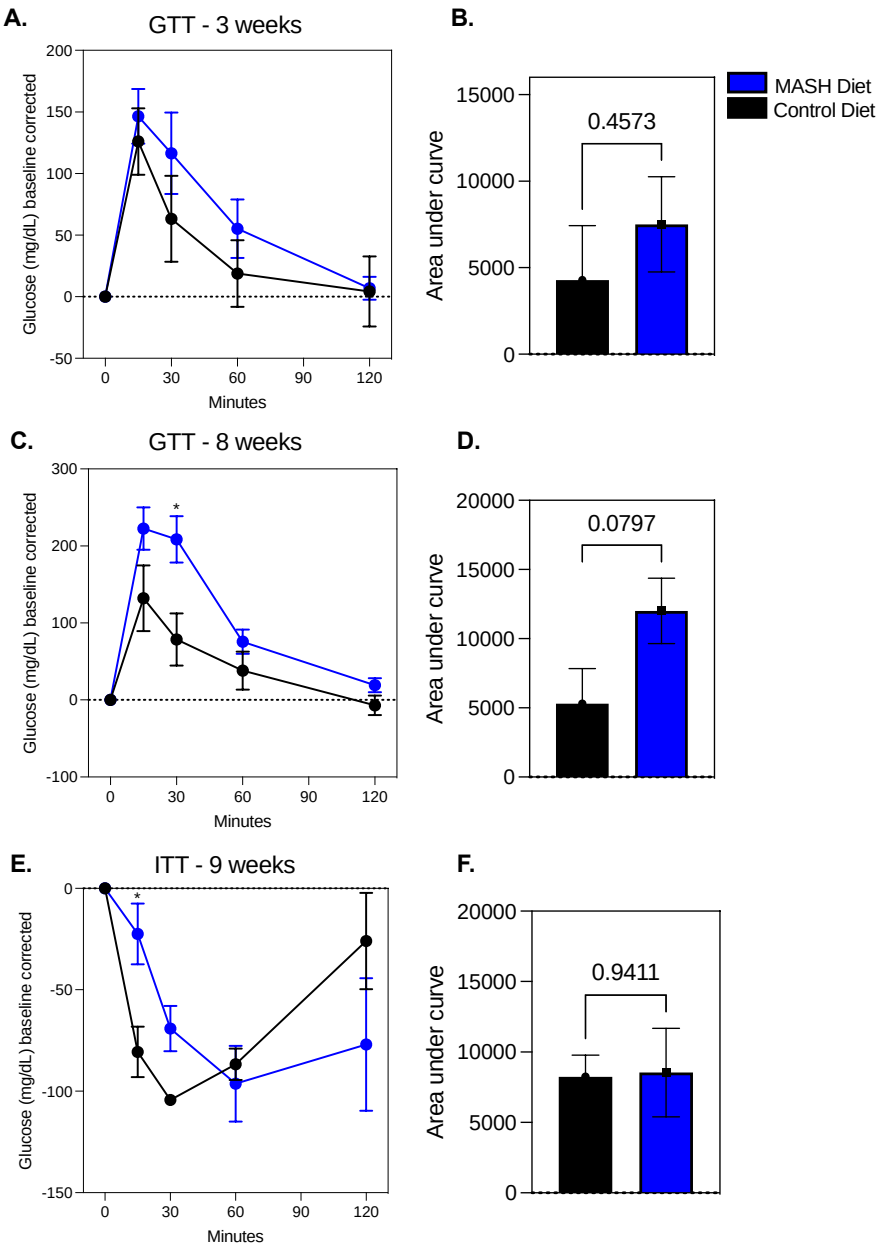

Figure 3.13 **Glucose tolerance test (i.p.GTT) in ob/ob mice in HFHC MASH diet and in control diet.** 6 hour fasted mice were administrated 2.0 g/kg glucose or insulin 0.5U/kg i.p. Blood samples were taken at 0, 15, 30-, 60-, 90- and 120-min. Plasma levels of glucose (A, C, D) were measured. Data are normalized to baseline glucose levels. (B, D, F) Area under curve. Data are presented as mean ± SEM; n = 5-6. *p<0.05 (Student's t-test).

3.2.2.3 Altered liver gene expression post MASH diet-induction

Transcriptionally, MASH diet induced changes were reflected in several pathways, mostly metabolic and inflammatory (Fig 3.14-3.18). We report that there was induction of several important metabolic genes involved in lipogenesis, cholesterol biosynthesis, inflammation, and carbohydrate metabolism in mice that consumed NASH diet suggesting that the model represents significant metabolic dysfunction, similar to ob/ob mice.

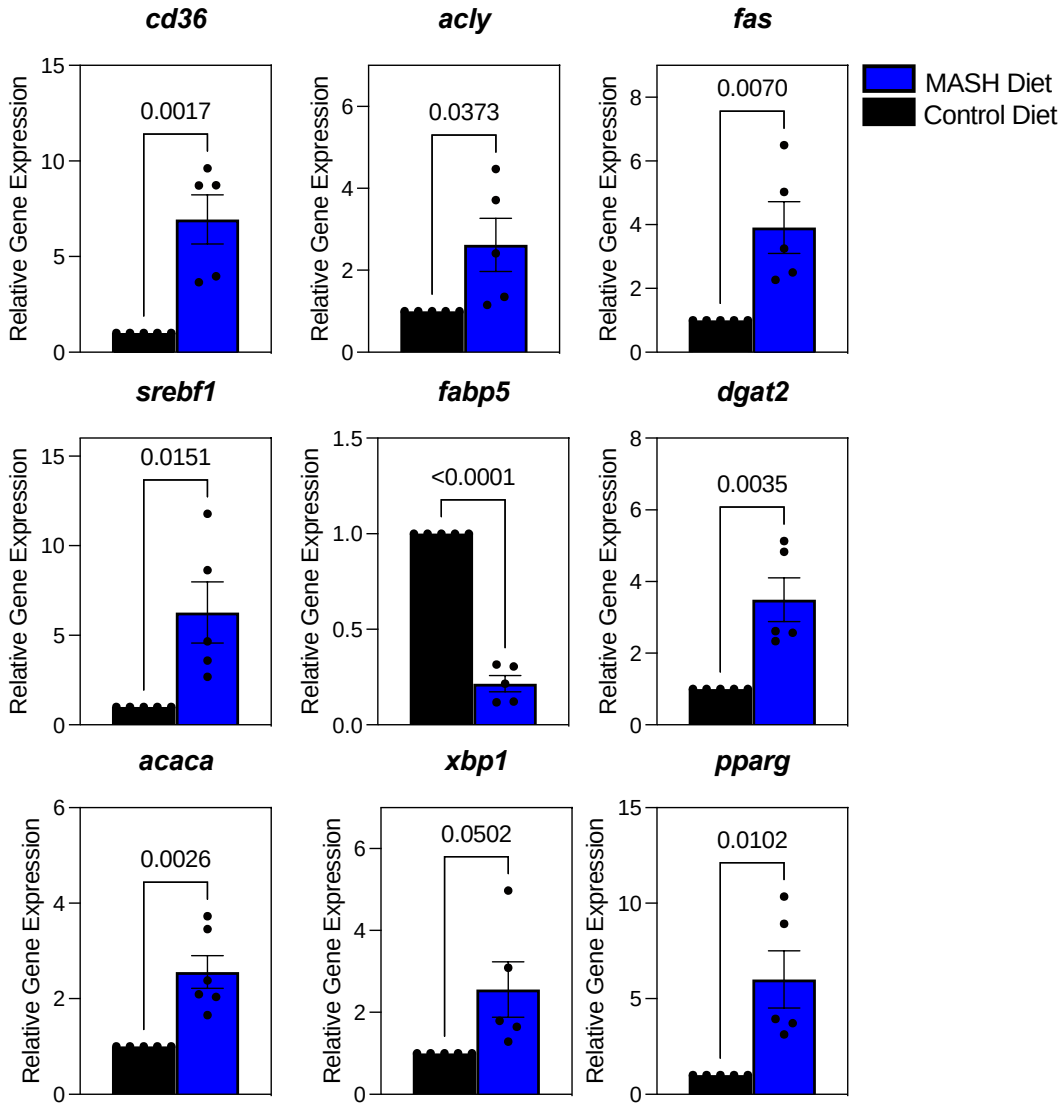

Figure 3.14 **Changes in lipogenic genes in the liver of mice fed MASH diet.** Gene expression of lipogenic genes that are involved in MASLD/MASH in mouse liver tissue. Data are represented as mean ± SEM (n=5-6). p-values are shown, as calculated by student's t-test in GraphPad Prism.

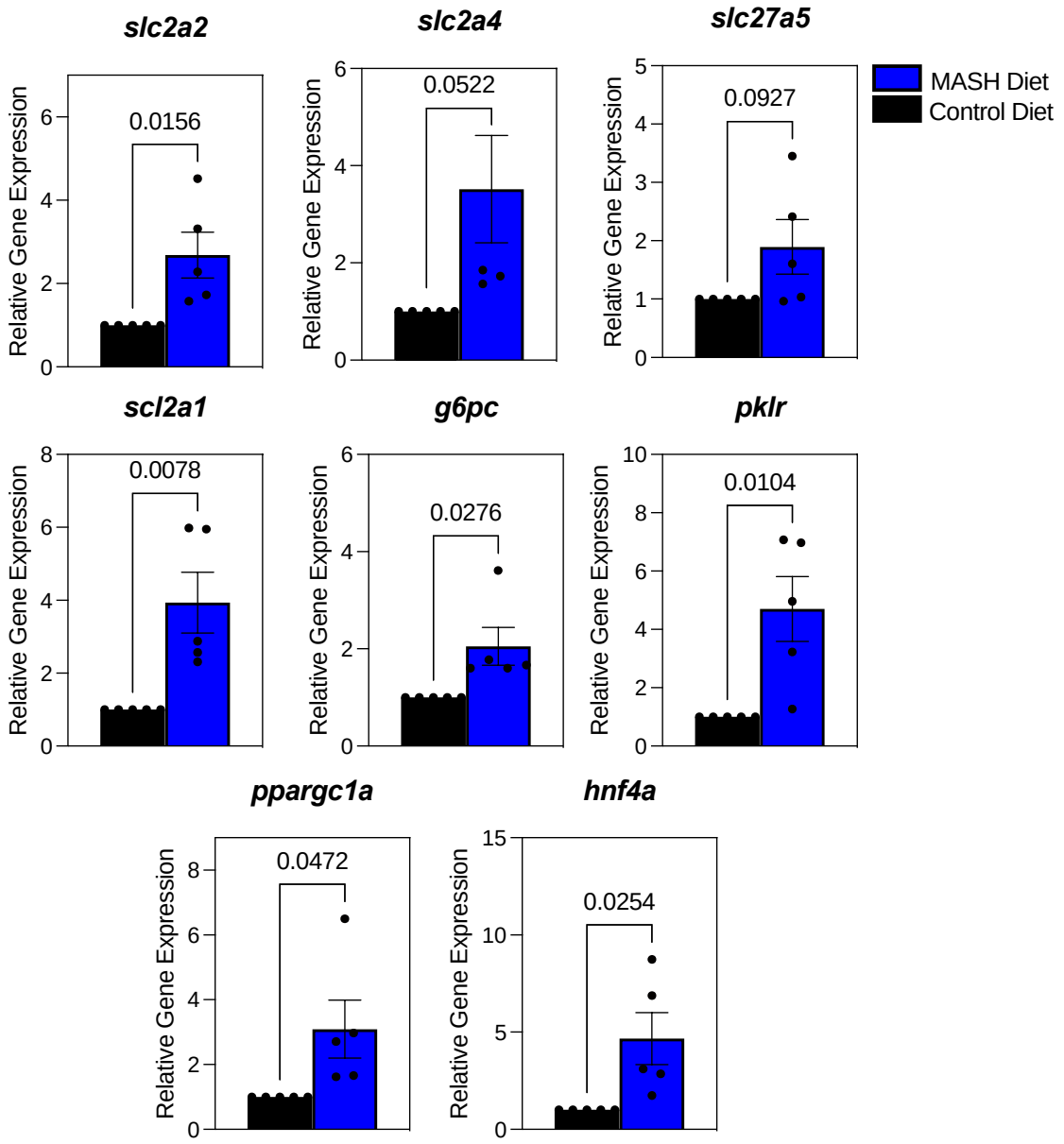

Figure 3.15 **Changes in glucose metabolism genes in the liver of mice fed MASH diet.** Gene expression of genes that are involved in glucose metabolism in MASLD/MASH in mouse liver tissue. Data are represented as mean ± SEM (n=5-6). p-values are shown, as calculated by student's t-test in GraphPad Prism.

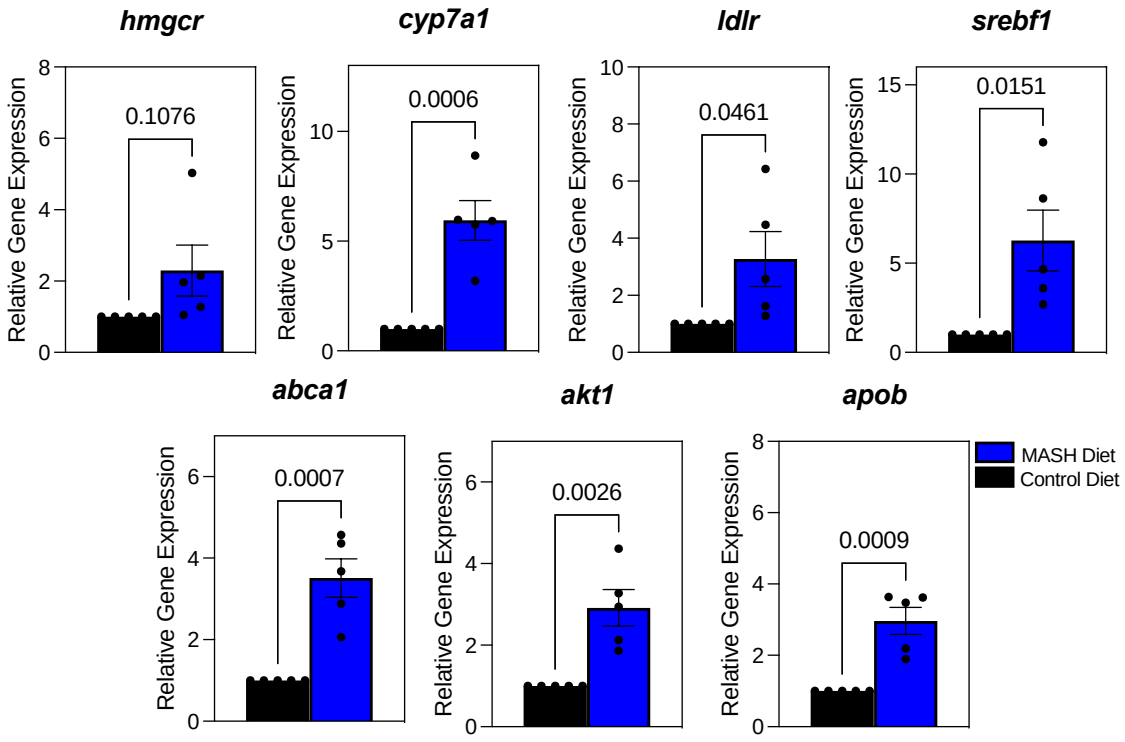

Figure 3.16 **Changes in cholesterol genes in the liver of mice fed MASH diet.** Gene expression of cholesterol genes that are involved in MASLD/MASH in mouse liver tissue. Data are represented as mean ± SEM (n=5-6). p-values are shown, as calculated by student's t-test in GraphPad Prism.

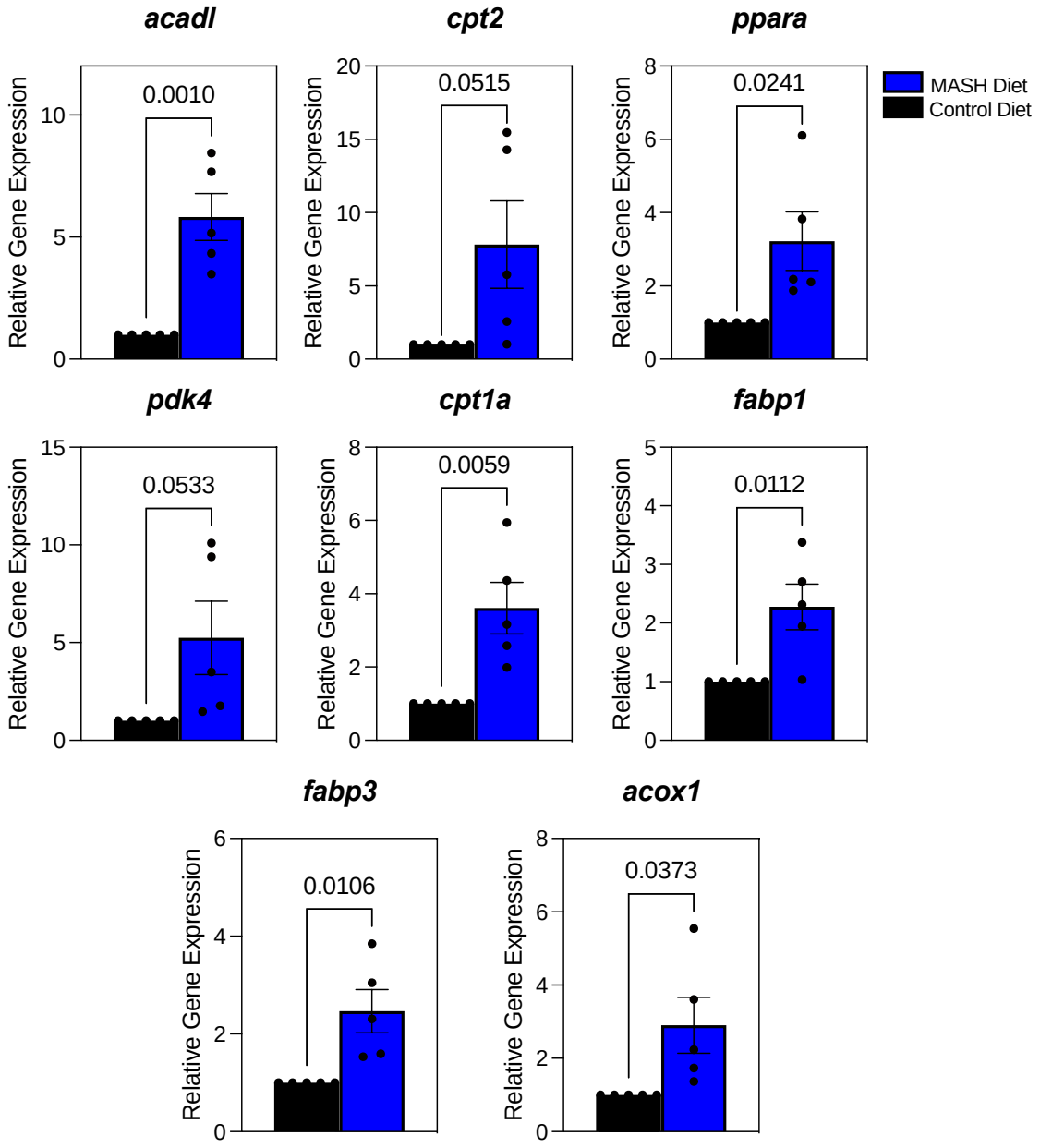

Figure 3.17 **Changes in genes involved in the regulation of fatty acid oxidation the liver of mice fed MASH diet.** Gene expression of FAO genes that are involved in MASLD/MASH in mouse liver tissue. Data are represented as mean ± SEM (n=5-6). p-values are shown, as calculated by student's t-test in GraphPad Prism.

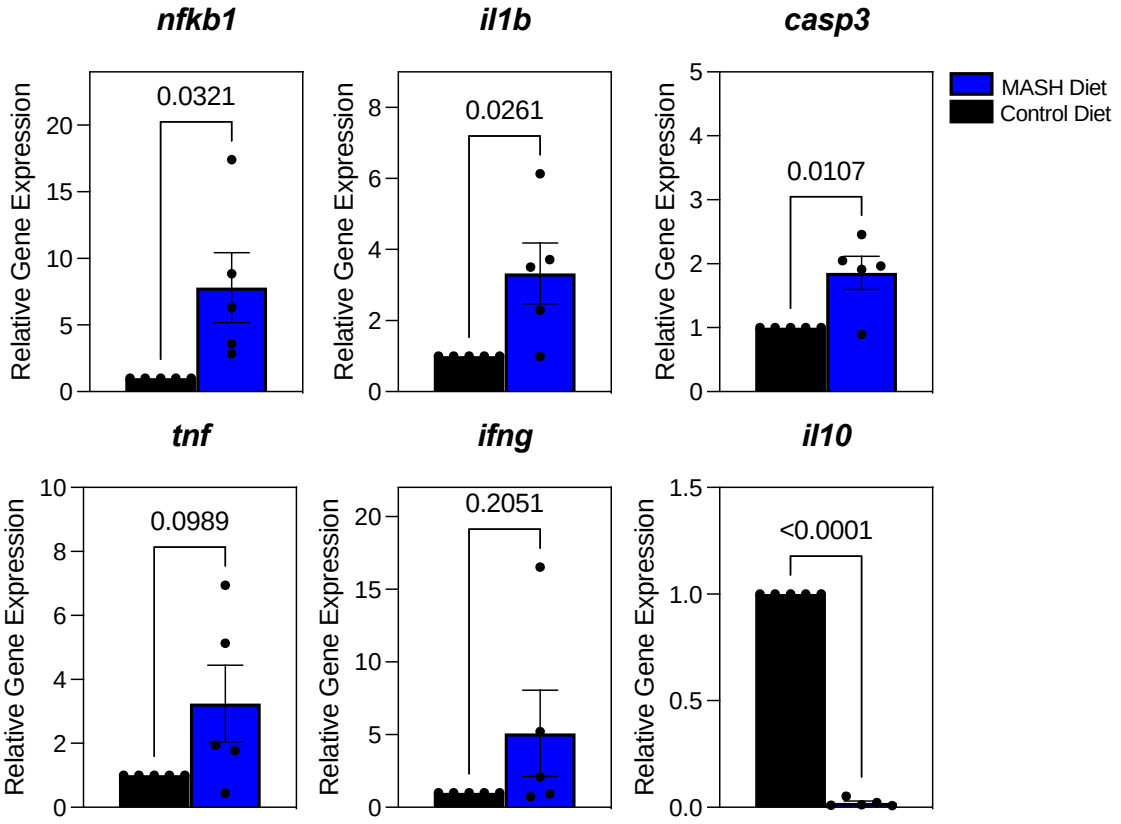

Figure 3.18 **Gene expression changes in inflammatory markers in the liver of mice fed MASH diet.** Gene expression of inflammatory cytokines (IL-6, IL-1β, NFκβ, TNFα, Casp-3) and anti-inflammatory cytokines (IL-10) that are involved in MASLD/MASH in mouse liver tissue. Data are represented as mean ± SEM (n=5-6). p-values are shown, as calculated by student's t-test in GraphPad Prism.

3.2.2.4 Obese and B6 MASH mice demonstrated hepatic steatosis and no fibrosis after MASH diet-induction

As determined by H&E sections, obese MASH mice had altered distribution of lipids. We observed that while there was an increase in micro-steatosis, there was decreased macro-steatosis. Additionally, there was also reduced in hepatic hypertrophy (Fig 3.19) As determined by Gomori's trichrome staining, there was no quantifiable change in fibrosis. (Fig 3.20).

In DIO B6 MASH mice, we saw that there was development of MASH pathology as seen in increased micro-, and macro-steatosis, as well as hypertrophy (Fig 3.21). Similar to obese mice, there was no quantifiable change in fibrosis. (Fig 3.22).

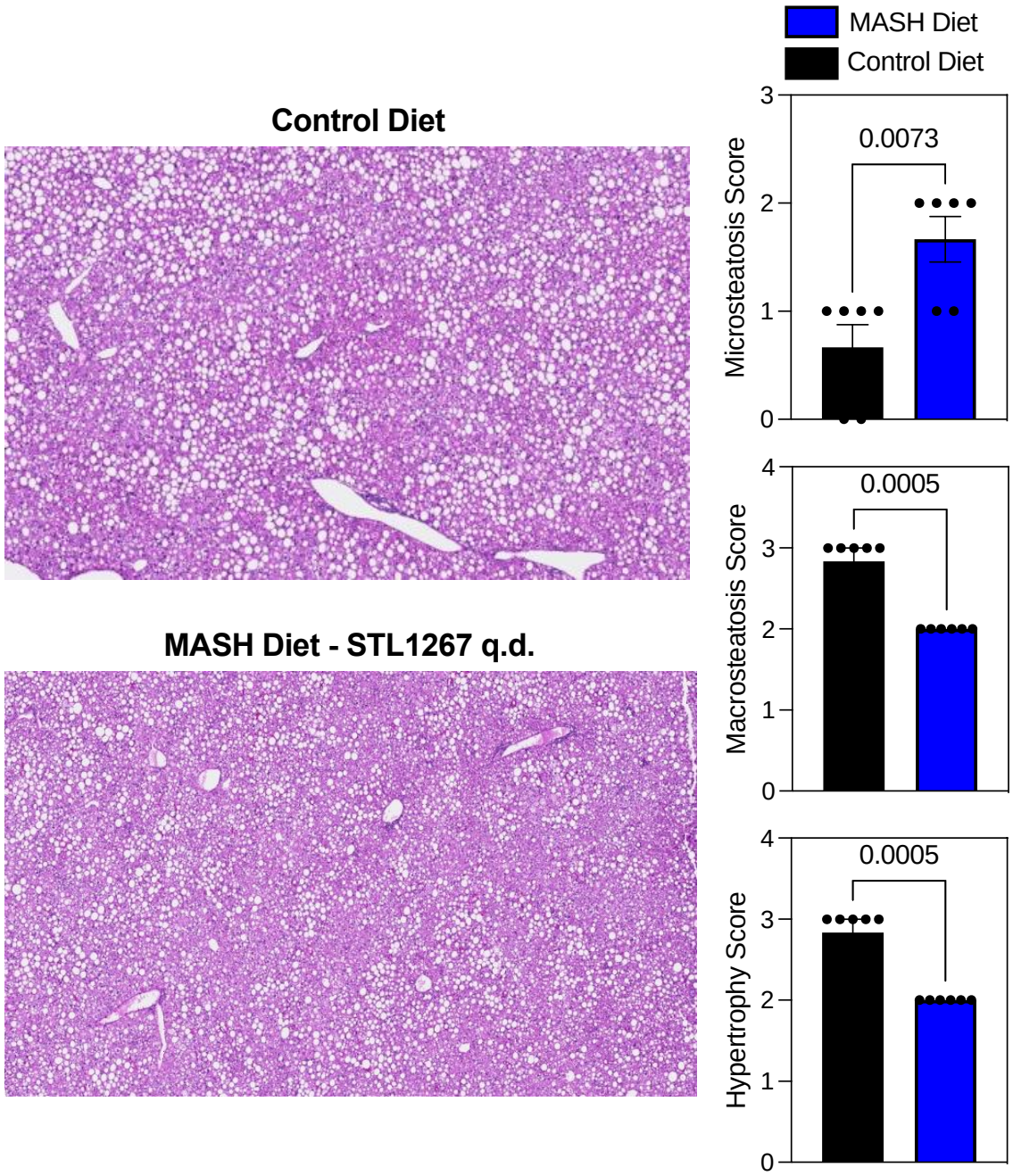

Figure 3.19 **Hepatosteatosis in *ob/ob* mice maintained on MASH diet is altered compared to control diet.** Pathological analysis and scoring from H&E sections of livers suggests that MASH diet fed mice have increased micro-steatosis, and decreased macro-steatosis. MASH diet fed mice also have reduced hepatic hypertrophy.

Control Diet

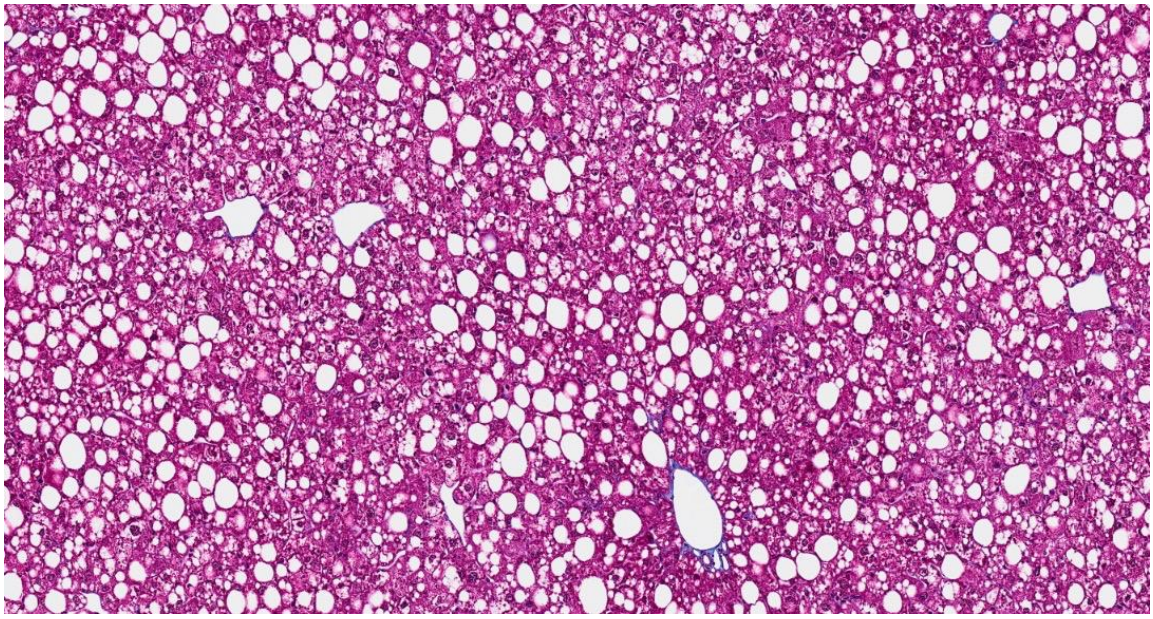

MASH Diet

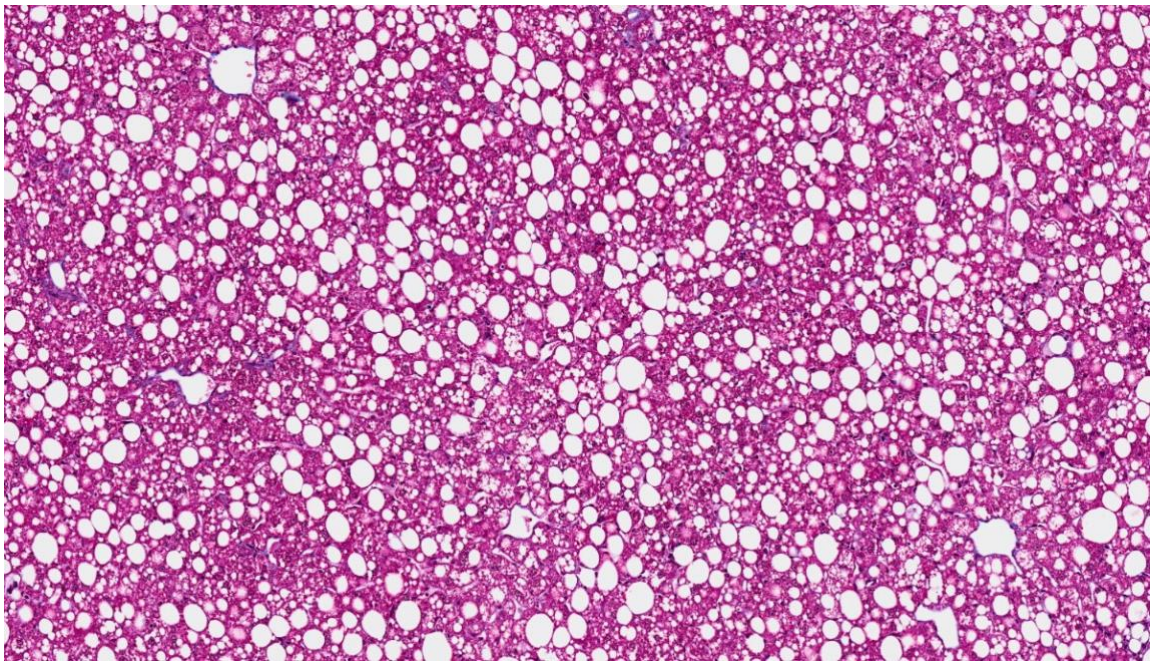

Figure 3.20 **Fibrosis in *ob/ob* mice maintained on MASH diet does not appear altered compared to control diet.** Pathological analysis and scoring from Gomori's Trichrome sections of livers suggests that MASH diet fed mice have not developed excessive fibrosis.

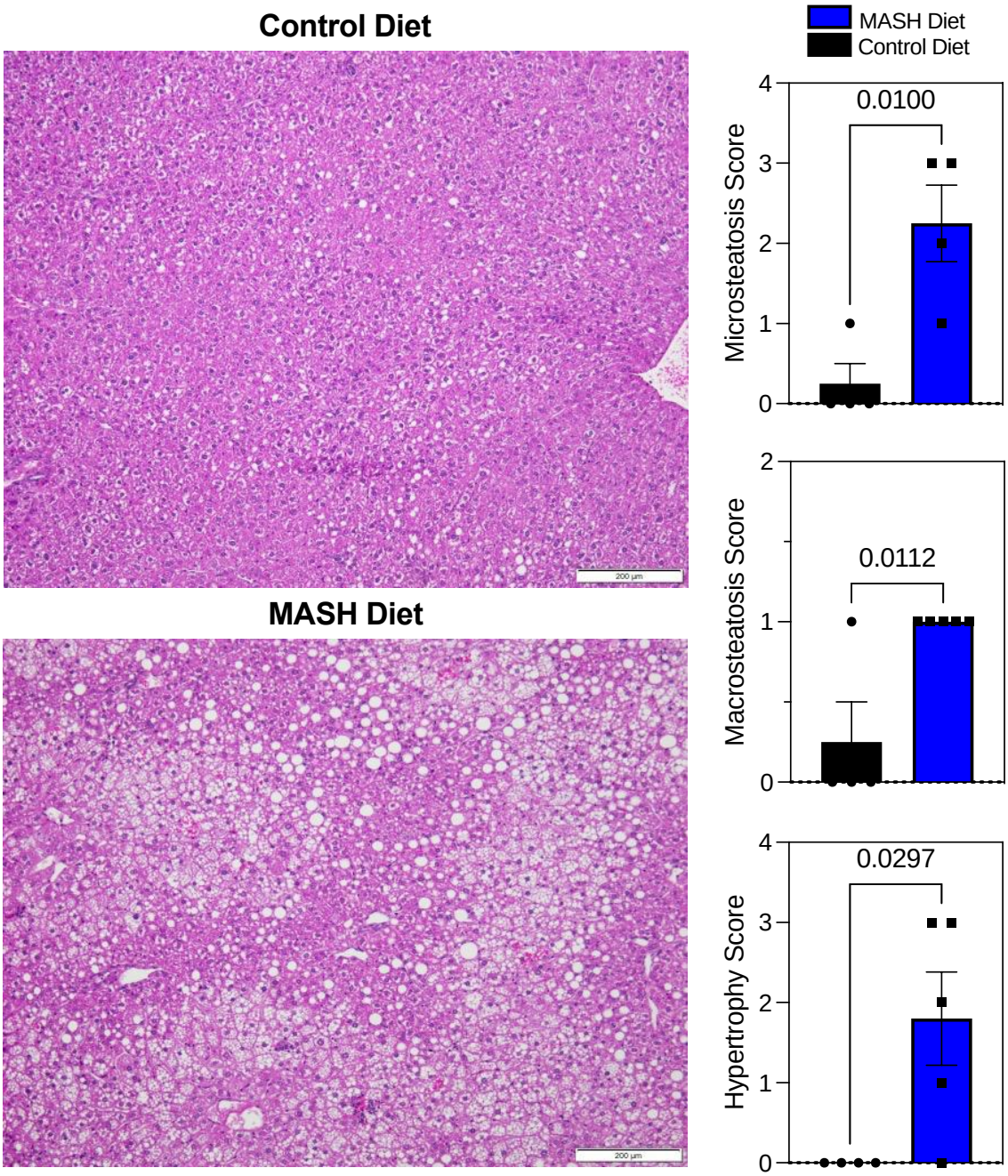

Figure 3.21 **Hepatosteatosis in B6 mice maintained on MASH diet is increased compared to control diet.** Pathological analysis and scoring from H&E sections of livers suggests that MASH diet fed mice have increased micro-steatosis, and macro-steatosis. MASH diet fed mice also have increased hepatic hypertrophy.

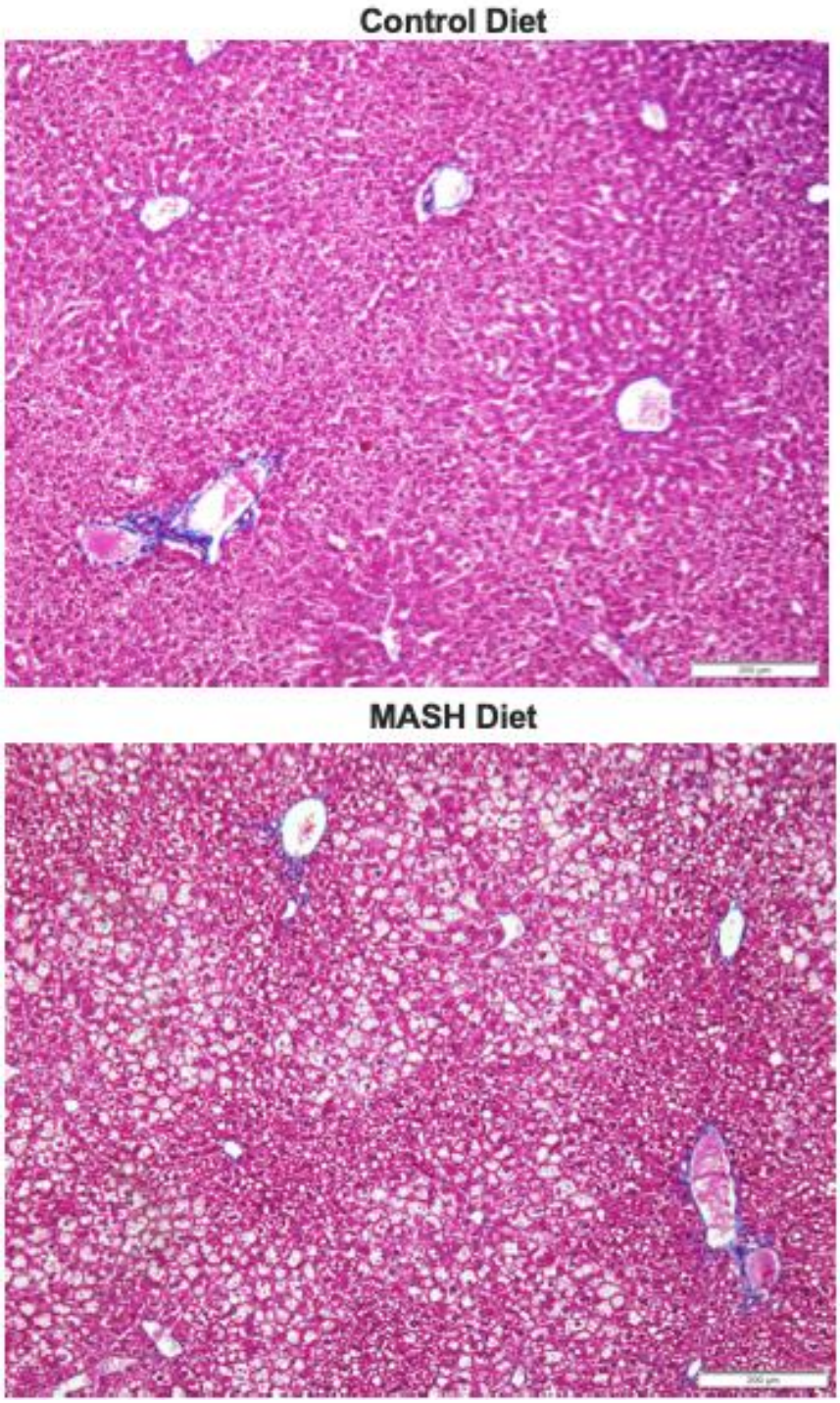

Figure 3.22 **Fibrosis in B6 mice maintained on MASH diet does not appear altered compared to control diet.** Pathological analysis and scoring from Gomori's Trichrome sections of livers suggests that MASH diet fed mice have not developed excessive fibrosis.

Chapter Four: REV-ERBα activation using STL1267 administration *in vivo* alleviates MASH

4.1. Rationale and Experimental Design

Research on REV-ERB in metabolism in the past years has highlighted its role in coordinating various metabolic processes to maintain overall metabolic homeostasis in the body. REV-ERB plays a major role in regulation of genes associated with lipogenesis, metabolism, and inflammation (Hunter et al., 2020). These findings have prompted investigations into the potential of REV-ERB agonists as therapeutic agents for cardio-metabolic diseases, including atherosclerosis often associated with MASLD/MASH.

In our lab's previous studies, we have shown that activation of REV-ERB using SR9009, in a model of murine MASH, alleviates MASH pathology, specifically targeting inflammation and fibrosis. No significant effect on hepatic steatosis was observed (Griffett et al., 2020). In an additional study, it was demonstrated that REV-ERB activation improves metabolic parameters in a DIO model (Solt et al., 2012). Thus, targeting REV-ERB pathways holds promise for the development of novel therapeutic strategies for metabolic disorders such as obesity, diabetes, and dyslipidemia.

SR9009, however, as a pharmacological tool, has poor potency (1μM), solubility, and pharmacokinetic properties. Our collaborators (Murray et al., 2022) developed and characterized STL1267, a novel REV-ERB agonist which has improved potency, selectivity for REV-ERB, as well as an improved pharmacokinetic profile.

It is hypothesized that using the new generation synthetic agonist in-vivo would improve target specific effects as well pharmacological activity. Murray et al characterized STL1267 in-vitro and in-vivo. They administered STL1267 at 50mg/kg i.p. and found that the plasma half-life of the compound was approximately 1.6 hours. They also found that at 50mg/kg, the compound was localized to every major tissue such as plasma, liver, and skeletal muscle, and even the brain. In fact, as a measure of its efficacy, they showed that at 50mg/kg, Bmal1, a target gene for REV-ERB, was successfully repressed when compared to vehicle. Thus, using this characterization, we utilized 50mg/kg i.p. as the initial dosage, injected once and twice a day. The aim of this chapter is to assess and characterize the changes induced by pharmacological activation of REV-ERB, using small molecule ligand STL1267 in MASLD/MASH in-vivo.

4.2. Results

4.2.1. Model: MASH Leptin^{ob}/ Leptin^{ob} (*ob/ob*) mice

4.2.1.1. Plasma and biochemical indices of MASH were improved by STL1267 induced REV-ERB activation

The overall study design is outlined (Fig 3.1). Following a diet induction period of 5 weeks, male *ob/ob* mice fed with MASH diet were treated with 50mg/kg STL1267 i.p. once daily. Mice treated with STL1267 demonstrated no change in adiposity

as measured by body weight, when compared to animals treated with just vehicle (4.1-A). There was no observed difference in the amount of food consumed between the vehicle and STL1267 treated groups (Fig 4.1-B). Further, we observed no change in the liver to body weight ratio upon treatment (Fig 4.1-C). Plasma markers associated with MASH, including ALT, AST, and ALP were all significantly reduced upon STL1267 treatment (Fig 4.2-A). Further, STL1267 reduced MASH induced hypercholesterolemia, as seen by the reduced circulating levels of total cholesterol, including both HDLs and LDLs (Fig 4.2-B). No significant change was observed in circulating triglycerides or lactate levels. This was concurrent with liver triglycerides, with no change between STL1267 treated and vehicle groups (Fig 4.2-C).

Further, we performed glucose tolerance and insulin tolerance tests on these mice (Fig 4.3). While MASH diet did not induce glucose intolerance in *ob/ob* mice, we observed that STL1267 did not rescue glucose intolerance either, as calculated by area under the curve (AUC). Interestingly, however, we saw increased levels of glucose in STL1267 treated mice at 30mins post glucose injection. We did not observe significant improvement in insulin tolerance in mice treated with STL1267. Together, this suggests that STL1267 is able to rescue metabolic parameters associated with MASH, however, is not enough to induce glucose intolerance and insulin resistance in *ob/ob* mice.

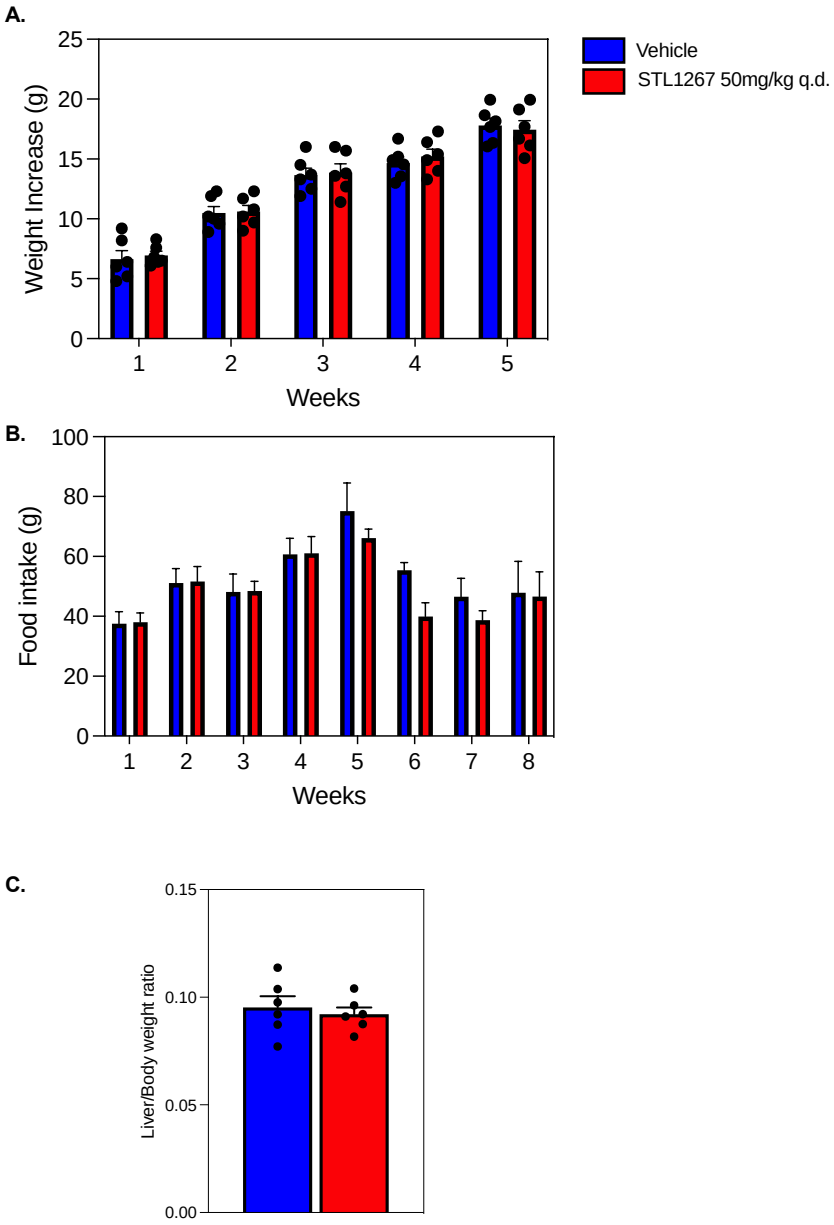

Figure 4.1 **STL1267 induced physiological changes in adiposity in obese control diet and MASH diet fed mice.** Animals that were fed HFHC MASH diet for 10 weeks were treated with 50mg/kg i.p. STL1267 daily for 5 weeks. (A) Mouse weights per week of treatment were measured and normalized to initial weight. Data are presented as mean ± SEM; n = 5-6 for Vehicle and n = 5-6 for STL1267 treated, p-values indicated (One-way ANOVA). (B) Food intake per week for each cage was measured. Data are presented as mean ± SEM; n = 3 for Vehicle and n = 3 for STL1267 treated, p-values indicated (One-way ANOVA). (C) Liver was harvested at the end of 10 weeks and liver to body weight ratio was plotted as a percentage. Data are presented as mean ± SEM; n = 5-6. p-values indicated (Student's t-test).

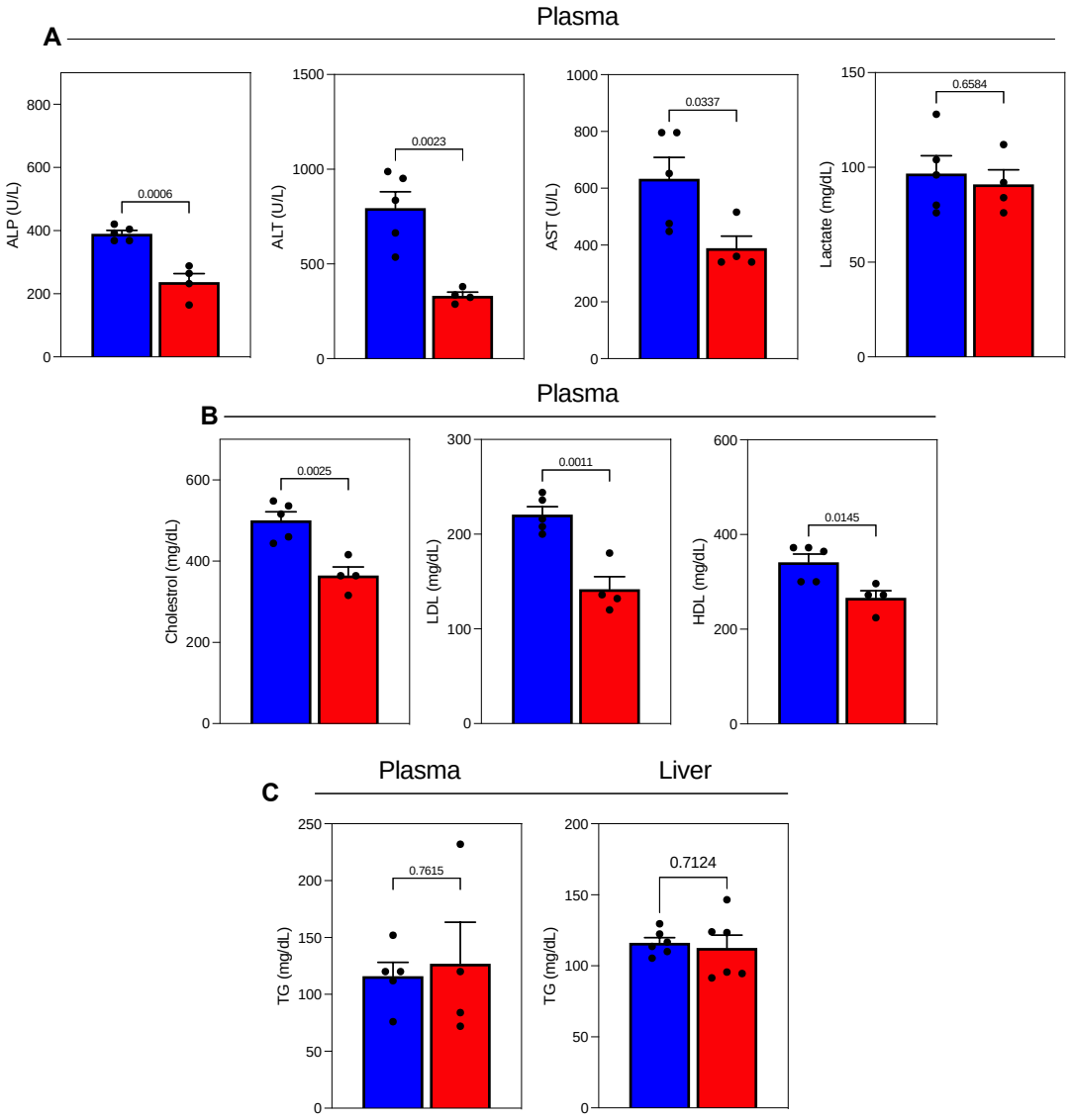

Figure 4.2 **Plasma and metabolic indices of MASH were improved by REV-ERB activation using STL1267.** Blood plasma was analyzed for liver enzymes (A) as well as circulating metabolic indices – total cholesterol, LDL, and HDL (B) Circulating TGs (left) and Liver TGs (right) were also analyzed. All data are represented as mean ± SEM (n=5-6) and analyzed using student's t-test in GraphPad Prism.

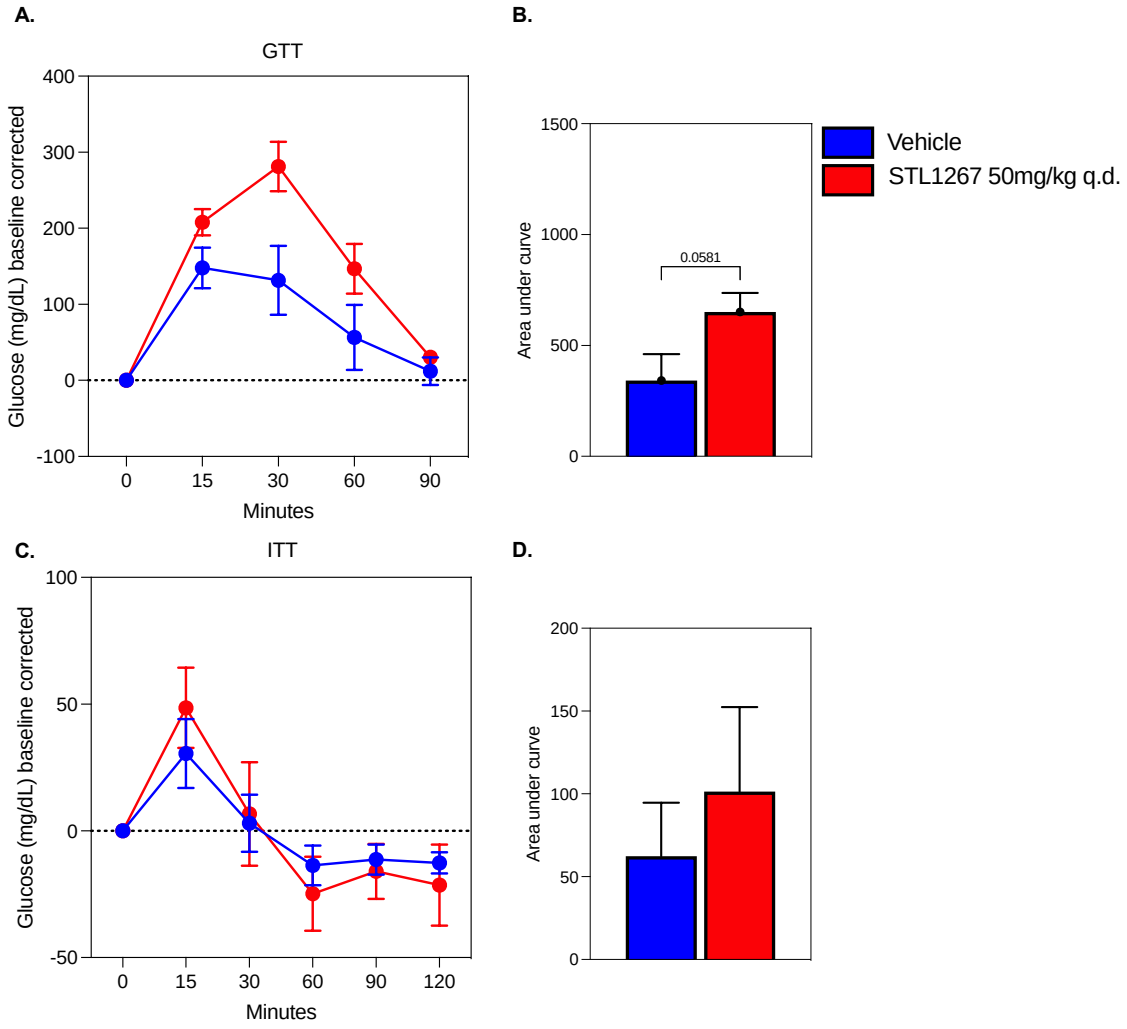

Figure 4.3 **Glucose and insulin tolerance test (i.p.GTT) in obese mice treated with STL1267 or vehicle in HFHC MASH diet.** 6 hour fasted mice were administrated 2.0 g/kg glucose or insulin 0.5U/kg i.p. Blood samples were taken at 0, 15, 30-, 60-, 90- and 120-min. Plasma levels of glucose (A, C) were measured. Data are normalized to baseline glucose levels. Area under curve (B, D). Data are presented as mean ± SEM; n = 5-6. *p<0.05 (Student's t-test)

4.2.1.2. STL1267 administration in-vivo alters metabolic gene expression

To characterize the effect of STL1267 treatment on global liver gene expression, the transcriptome of STL1267 treated and vehicle MASH mice was analyzed using qPCR of genes involved in fatty liver disease (Fig 4.4-4.7). It is shown that genes linked to lipogenesis, fatty acid uptake, cholesterol biosynthesis, inflammation, and carbohydrate metabolism are robustly reduced in MASH *ob/ob* mice treated with STL1267 compared to those animals on vehicle treatment. Further, a large collection of pro-inflammatory factors such as IFNg, TNF, IL-6, IL1b, and Casp-3 were found significantly reduced post STL1267 treatment (Fig 4.8).

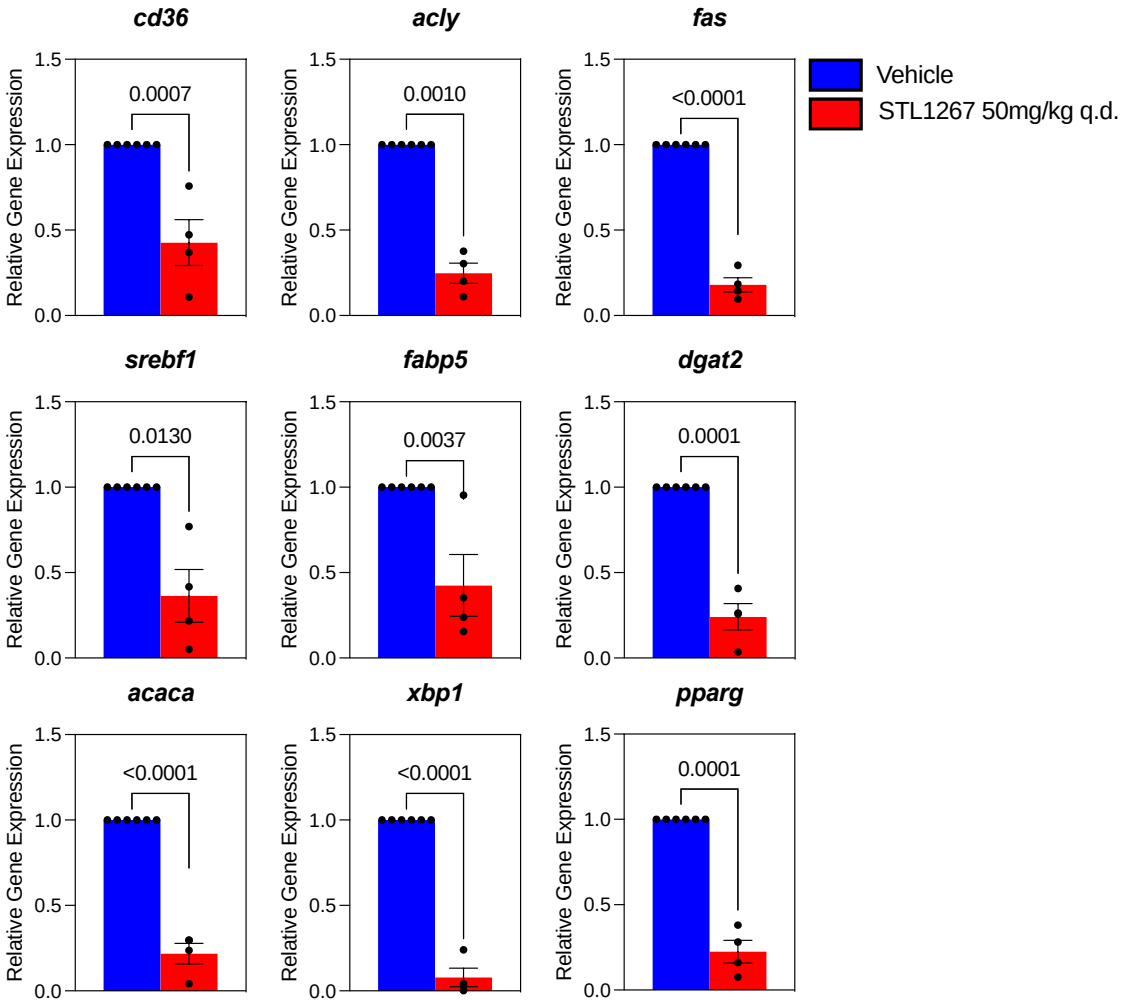

Figure 4.4 **STL1267 induced changes in lipogenic genes in the liver of mice fed MASH diet.** Gene expression of lipogenic genes that are involved in MASLD/MASH in mouse liver tissue. Data are represented as mean ± SEM (n=5-6). p-values are shown, as calculated by student's t-test in GraphPad Prism.

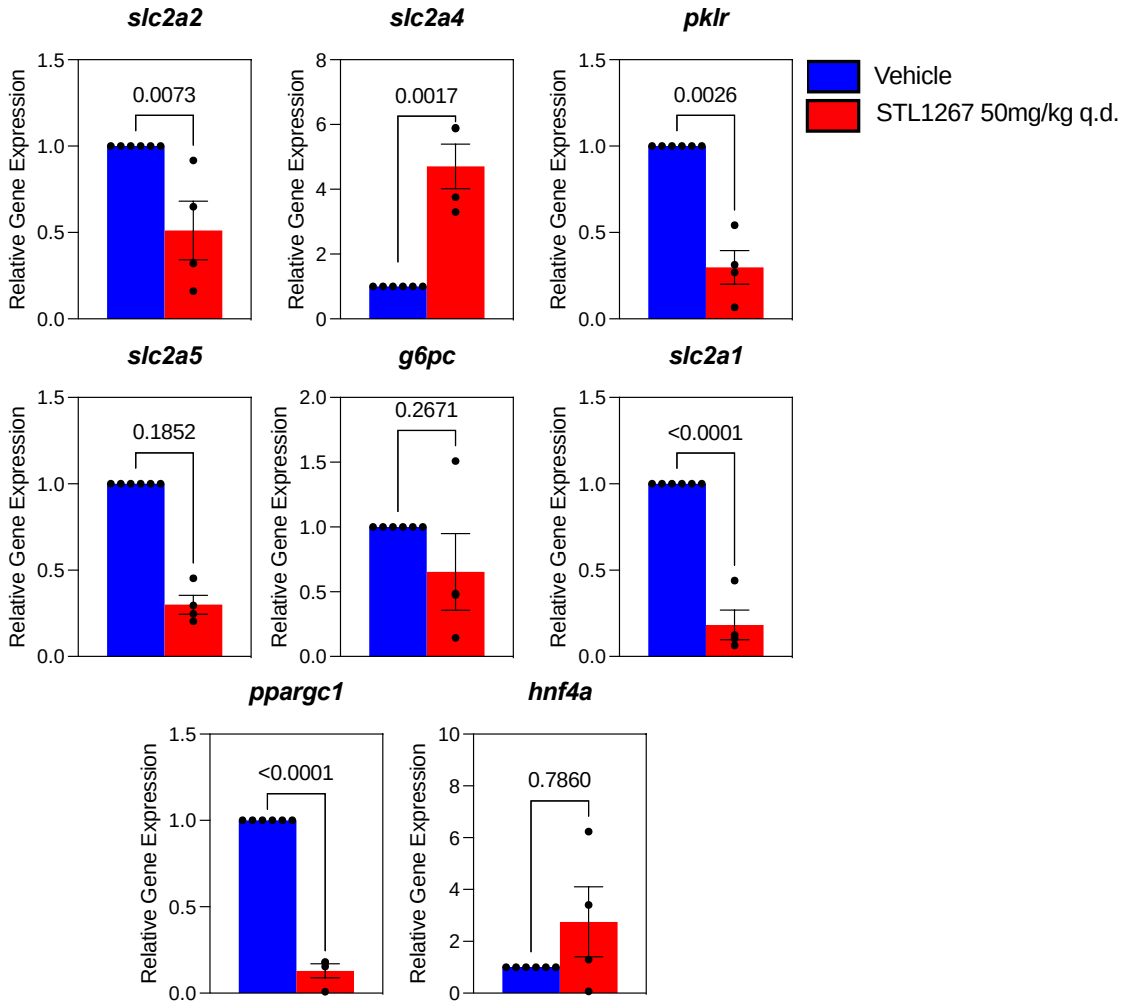

Figure 4.5 **STL1267 induced changes in glucose metabolism genes in the liver of mice fed MASH diet.** Gene expression of genes that are involved in glucose metabolism in MASLD/MASH in mouse liver tissue. Data are represented as mean ± SEM (n=5-6). p-values are shown, as calculated by student's t-test in GraphPad Prism.

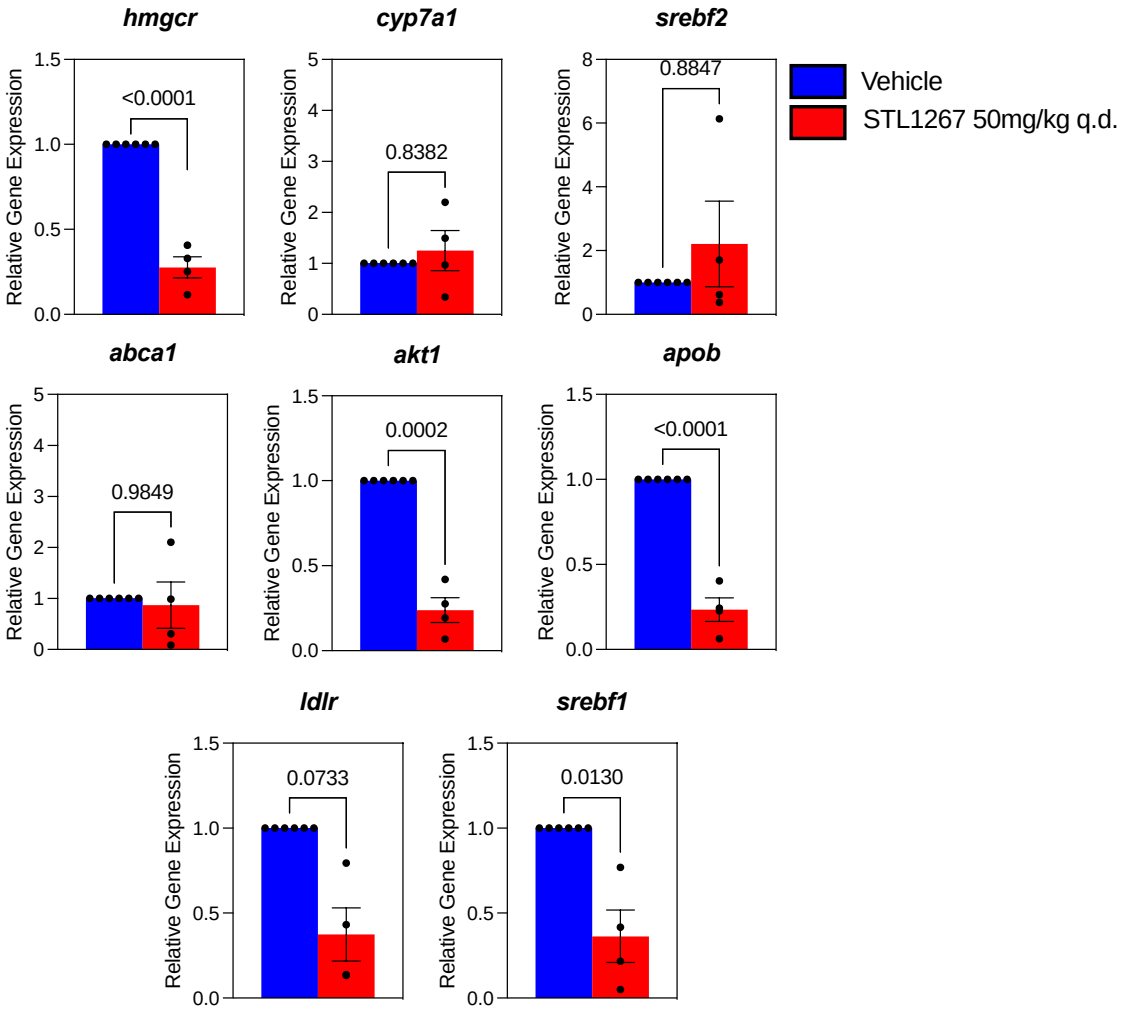

Figure 4.6 **STL1267 induced changes in cholesterol genes in the liver of mice fed MASH diet.** Gene expression of cholesterol genes that are involved in MASLD/MASH in mouse liver tissue. Data are represented as mean ± SEM (n=5-6). p-values are shown, as calculated by student's t-test in GraphPad Prism.

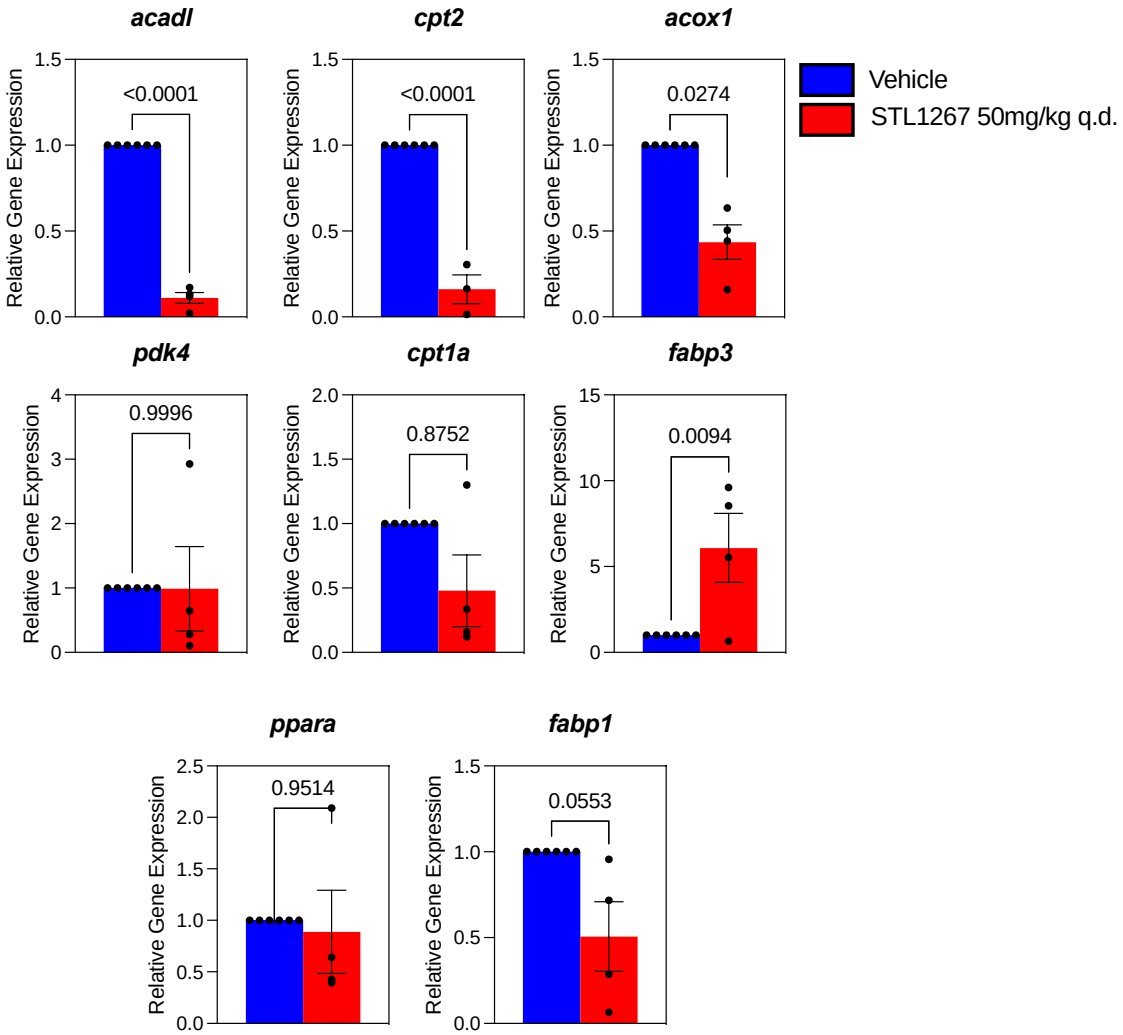

Figure 4.7 **STL1267 induced changes in genes involved in the regulation of fatty acid oxidation the liver of mice fed MASH diet.** Gene expression of FAO genes that are involved in MASLD/MASH in mouse liver tissue. Data are represented as mean ± SEM (n=5-6). p-values are shown, as calculated by student's t-test in GraphPad Prism.

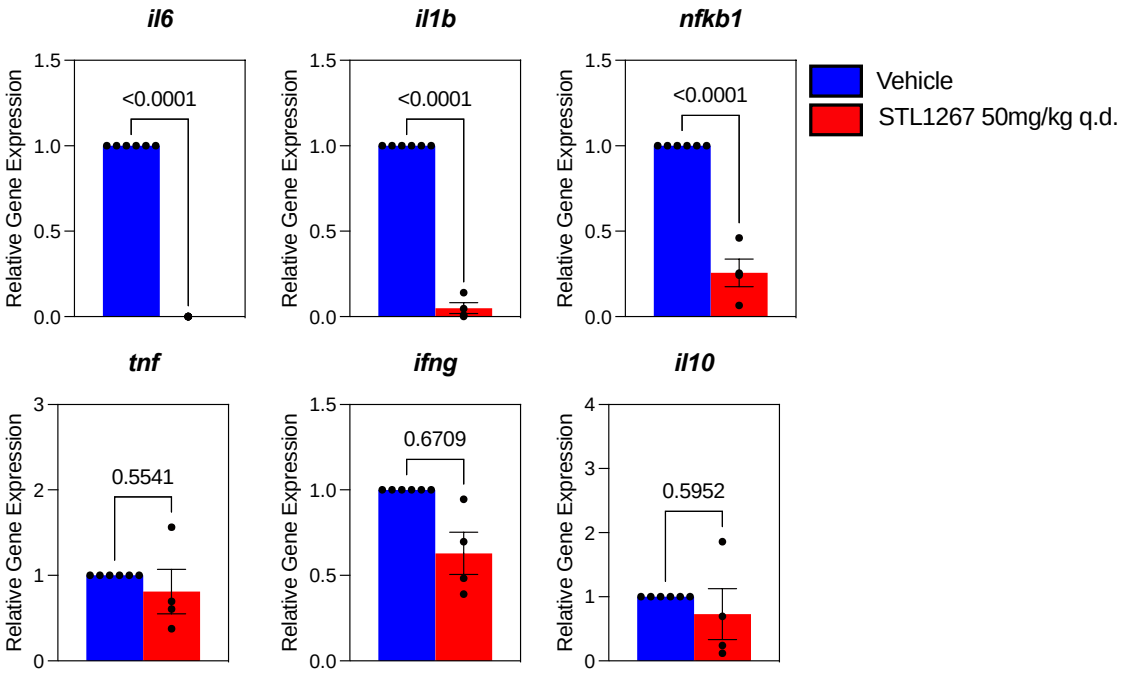

Figure 4.8 **STL1267 induced changes in inflammatory genes in the liver of mice fed MASH diet.** Gene expression of inflammatory cytokines (IL-6, IL-1β, NFκβ, TNFα, Casp-3) and anti-inflammatory cytokines (IL-10) that are involved in MASLD/MASH in mouse liver tissue. Data are represented as mean ± SEM (n=6-10). p-values are shown, as calculated by student's t-test in GraphPad Prism.

Upon initial experimentation with a standard dosage of 50mg/kg, our observations revealed a lack of discernible alterations in the targeted metabolic parameters such as glucose tolerance, inulin tolerance, as well hypertriglyceridemia. This finding prompted a critical reassessment of our approach, leading us to hypothesize that the dosage employed might have been insufficient to evoke significant physiological changes. To thoroughly investigate this hypothesis, we escalated the dosage to 50mg/kg twice a day (b.i.d.), aiming to provoke a more pronounced response and unveil subtler nuances in metabolic regulation.

4.2.1.3. Plasma and biochemical indices of MASH were improved by STL1267 b.i.d. induced REV-ERB activation

Following a diet induction period of 5 weeks, *ob/ob* mice fed with MASH diet were treated with 50mg/kg STL1267 i.p. twice daily. Mice treated with STL1267 demonstrated a trending decline in adiposity as measured by body weight, when compared to animals treated with just vehicle, but were not significantly changed (Fig 4.9-A). There was no significant observed difference in the amount of food consumed between the vehicle and STL1267 treated groups, however due to the loss (Fig 4.9-B). Further, we observed no change in the liver to body weight ratio upon treatment (Fig 4.9-C). Plasma markers associated with MASH, including ALP, ALT were significantly reduced upon STL1267 treatment (Fig 4.10-A). However, there was no significant change in AST levels. Further, similar to STL1267 q.d., STL1267 b.i.d. reduced MASH induced hypercholesterolemia, as

seen by the reduced circulating levels of total cholesterol, including both HDLs and LDLs (Fig 4.10-B). No significant change was observed in circulating triglycerides or lactate levels even with twice a day dosage. However, twice a day dosage was able to reduce liver hypertriglyceridemia significantly (Fig 4.10-C).

Further, we performed glucose tolerance and insulin tolerance tests on these mice. Contrary to our expectations, doubling the dosage led to a deterioration in glucose tolerance (Fig 4.11-A, B). Our analysis revealed a significant increase in glucose levels in animals treated with STL1267 twice a day as compared to vehicle. This unexpected outcome suggests a potential disruption in glucose homeostasis, possibly stemming from exaggerated metabolic responses or altered insulin sensitivity induced by the escalated dosage. We did not observe significant improvement in insulin tolerance in these mice either (Fig 4.11-C, D). Together, this suggests that STL1267 is able to rescue metabolic parameters associated with MASH, however, is not enough to rescue glucose intolerance and insulin resistance in *ob/ob* mice.

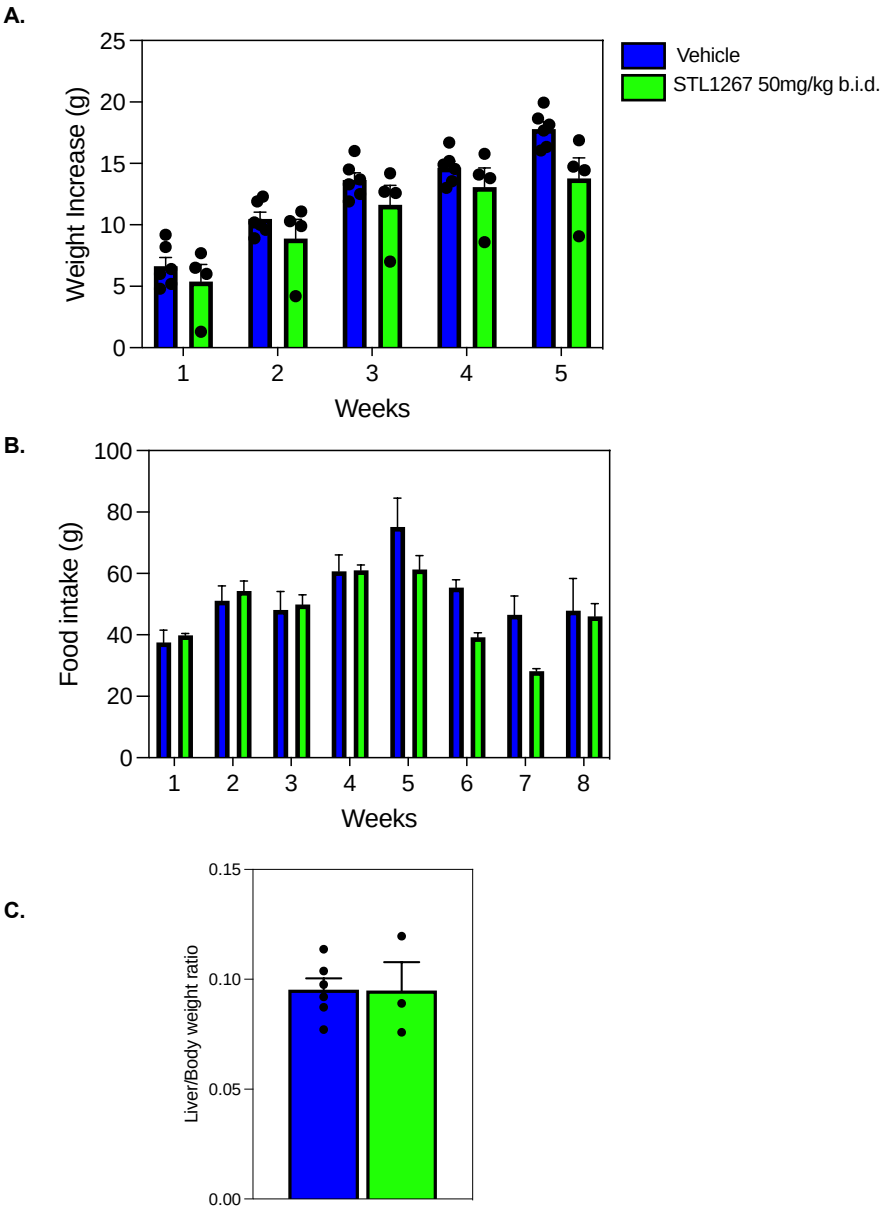

Figure 4.9 **STL1267 twice a day induced physiological changes in adiposity in obese control diet and MASH diet fed mice.** Animals that were fed HFHC MASH diet for 10 weeks were treated with 50mg/kg i.p. STL1267 twice (b.i.d.) daily for 5 weeks. (A) Mouse weights per week of treatment were measured and normalized to initial weight. Data are presented as mean ± SEM; n = 5-6 for Vehicle and n = 3-4 for STL1267 treated, p-values indicated (One-way ANOVA). (B) Food intake per week for each cage was measured. Data are presented as mean ± SEM; n = 3 for Vehicle and n = 2-3 for STL1267 treated, p-values indicated (One-way ANOVA). (C) Liver was harvested at the end of 10 weeks and liver to body weight ratio was plotted as a percentage. Data are presented as mean ± SEM; n = 5-6. p-values indicated (Student's t-test).

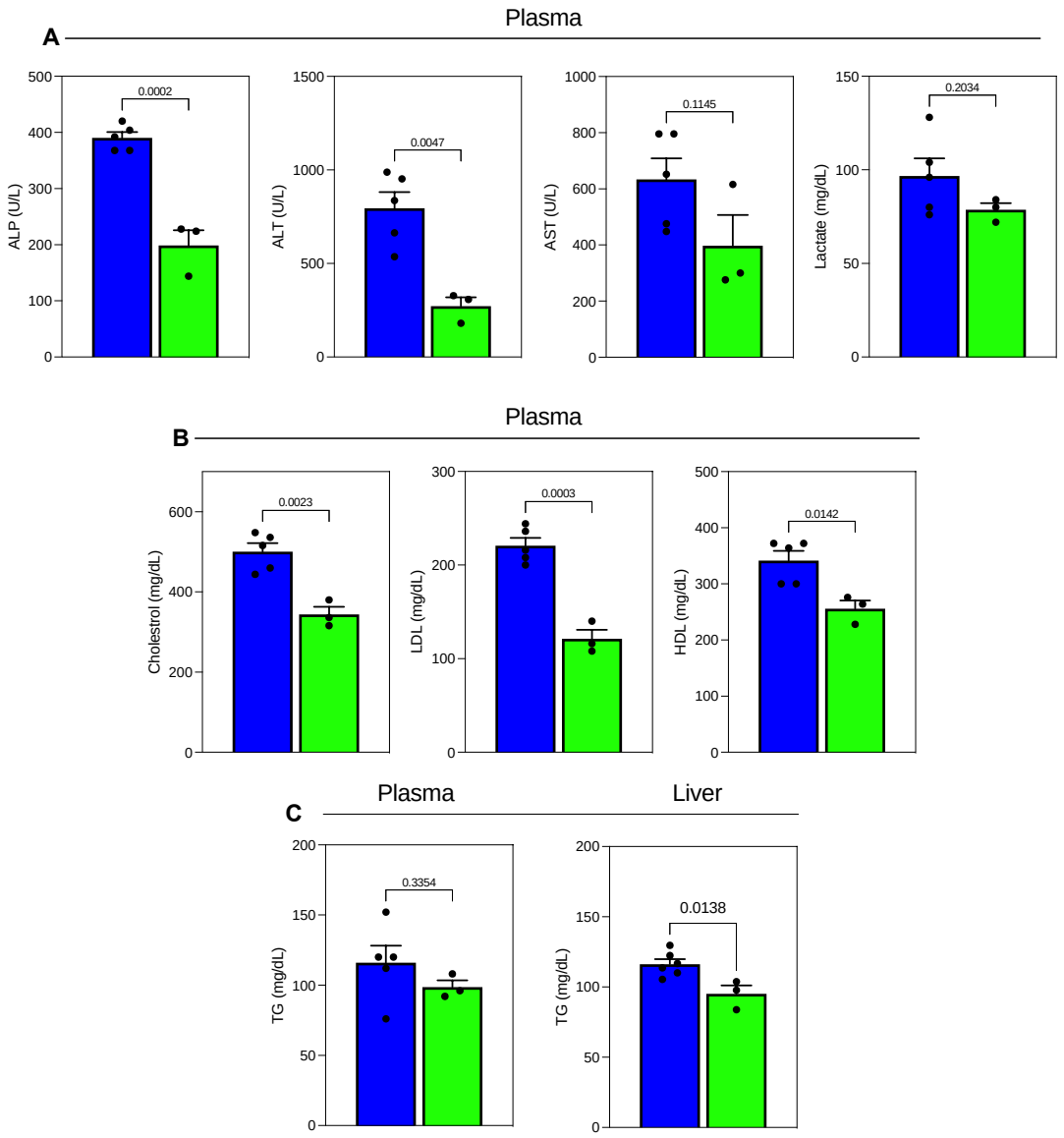

Figure 4.10 **Plasma and metabolic indices of MASH were improved by REV-ERB activation using STL1267 b.i.d.** Blood plasma was analyzed for liver enzymes (A) as well as circulating metabolic indices – total cholesterol, LDL, and HDL (B) Circulating TGs (left) and Liver TGs (right) were also analyzed. All data are represented as mean ± SEM (n=3-6) and analyzed using student's t-test in GraphPad Prism.

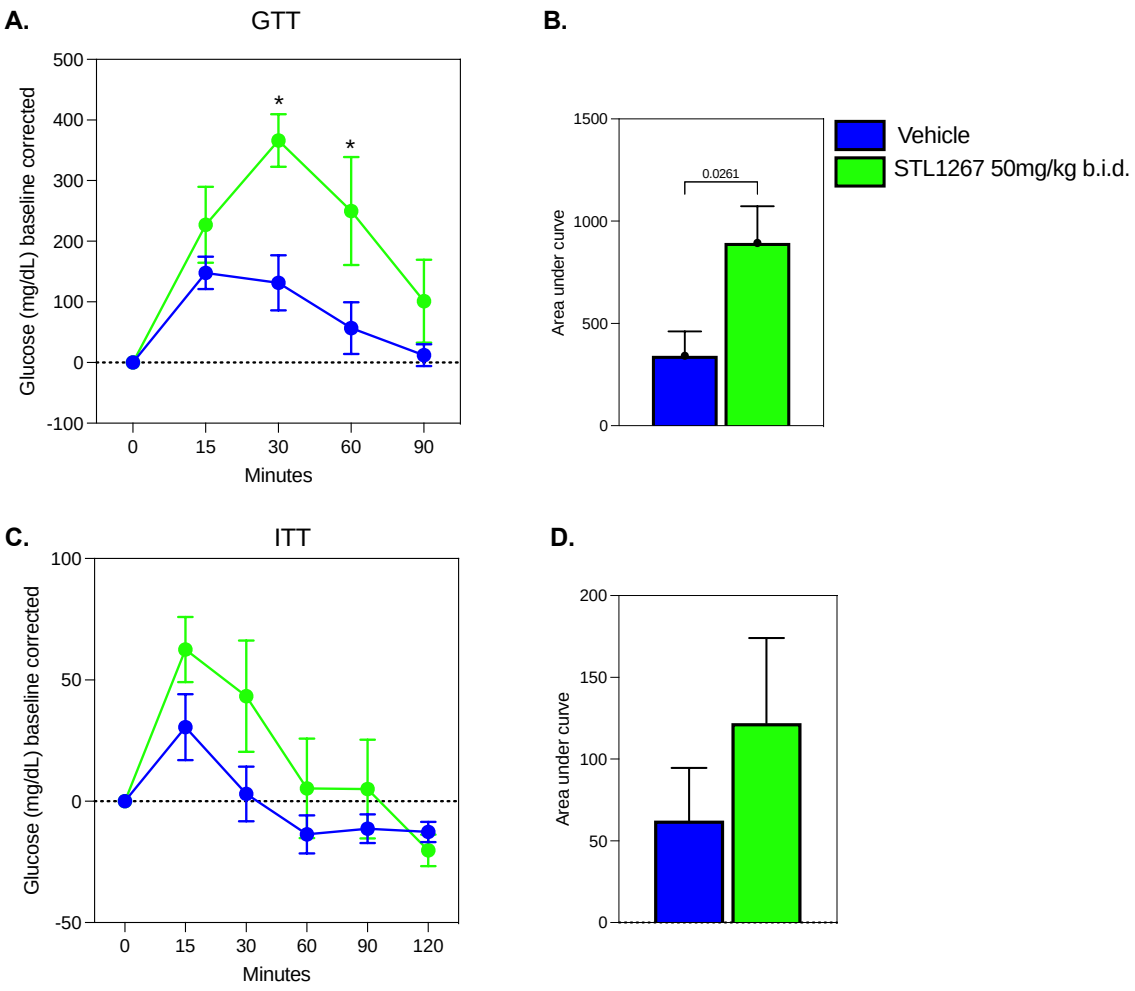

Figure 4.11 **Glucose and insulin tolerance test (i.p.GTT) in obese mice treated with STL1267 b.i.d. or vehicle in HFHC MASH diet.** 6 hour fasted mice were administrated 2.0 g/kg glucose or insulin 0.5U/kg i.p. Blood samples were taken at 0, 15, 30-, 60-, 90- and 120-min. Plasma levels of glucose (A, C) were measured. Data are normalized to baseline glucose levels. Area under curve (B, D). Data are presented as mean ± SEM; n = 3-6. *p<0.05 (Student's t-test)

4.2.1.4. STL1267 administration in-vivo alleviates histological hepatic steatosis and fibrosis

Histological assessments of biopsied liver tissue revealed that control diet animals did not develop fibrosis or steatosis over the 10-week period. However, ob/ob mice presented with high levels of steatosis.

4.2.1.5. STL1267 administration in-vivo alters metabolic gene expression

Following the administration of the standard dosage, we observed a reduction in the expression levels of several metabolic genes, including *Cd36*, *Acly*, *Srebf1*, *Dgat2*, and *Pparg*. However, doubling the dosage resulted in a reversal of this trend, with no significant changes in expression compared to vehicle (Fig 4.12).. This observation suggests that the escalated dosage exerts a stimulatory effect on metabolic gene expression, potentially modulating metabolic pathways associated with lipid metabolism and energy homeostasis. Notably, the effects of doubling the dosage were not limited to lipid metabolism, as evidenced by the comparable expression levels of GLUT2 (*Slc2a2*) and PKLR (*Pklr*) to the vehicle group (Fig 4.13). Interestingly, while the expression of GLUT2 and PKLR remained comparable to the vehicle group, the expression of G6PC was significantly increased in response to the double dosage. Consistent with observations following standard dosage administration, the expression levels of genes associated with cholesterol metabolism remained reduced upon doubling the

dosage (Fig 4.14). This sustained downregulation suggests a robust and persistent modulation of cholesterol pathways. In contrast to the persistent reduction observed in cholesterol genes, doubling the dosage resulted in the normalization of expression levels of FAO genes, such as *Acadl* and a significant increase in *Acox1* as well as *Ppara* in treated mice (Fig 4.15). We observed a significant reduction in the expression levels of inflammatory genes, including IL-6, IL-1β, and NF-κB. post STL1267 b.i.d. treatment similar to q.d (Fig 4.16).

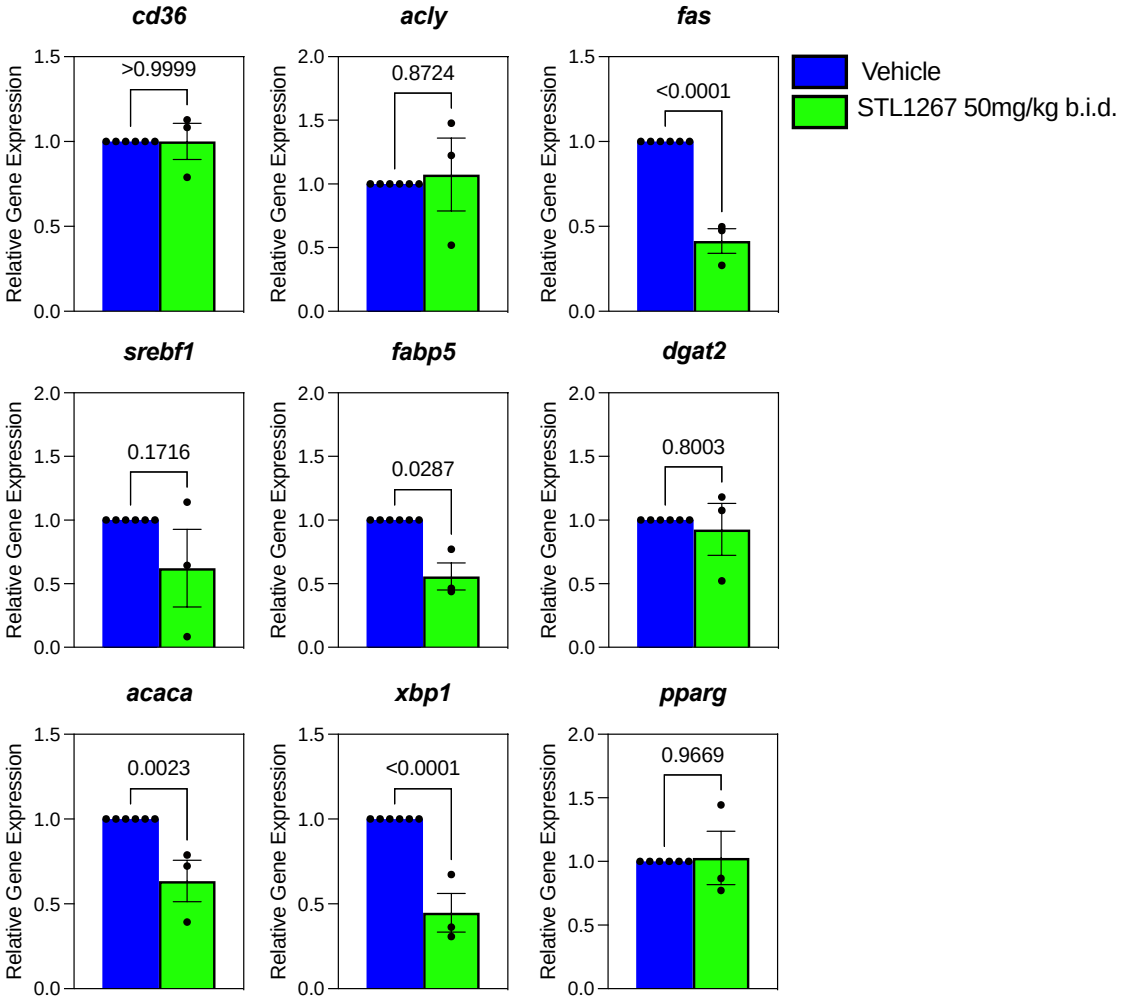

Figure 4.12 **STL1267 induced changes in lipogenic genes in the liver of mice fed MASH diet.** Gene expression of lipogenic genes that are involved in MASLD/MASH in mouse liver tissue. Data are represented as mean ± SEM (n=3-6). p-values are shown, as calculated by student's t-test in GraphPad Prism.

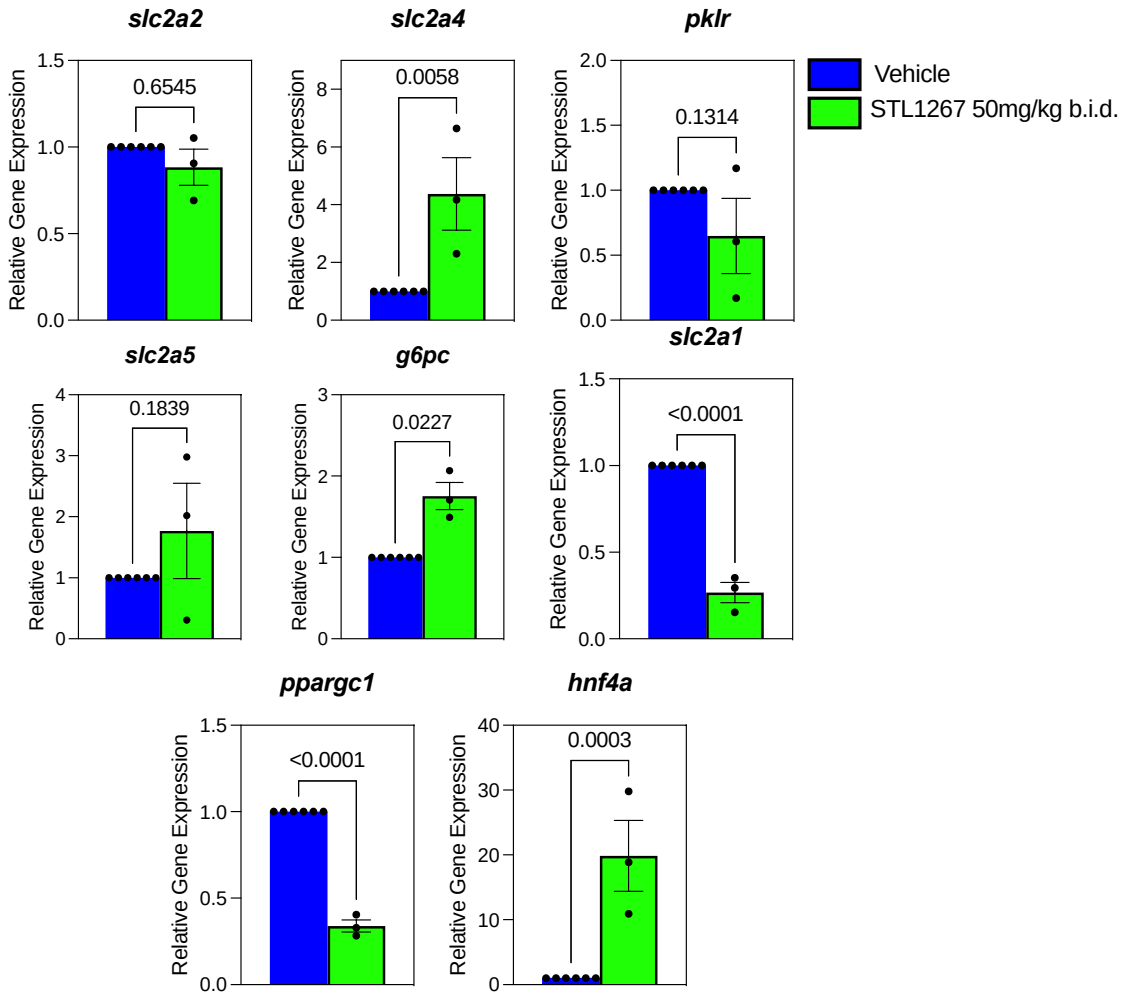

Figure 4.13 **STL1267 induced changes in glucose metabolism genes in the liver of mice fed MASH diet.** Gene expression of genes that are involved in glucose metabolism in MASLD/MASH in mouse liver tissue. Data are represented as mean ± SEM (n=3-6). p-values are shown, as calculated by student's t-test in GraphPad Prism.

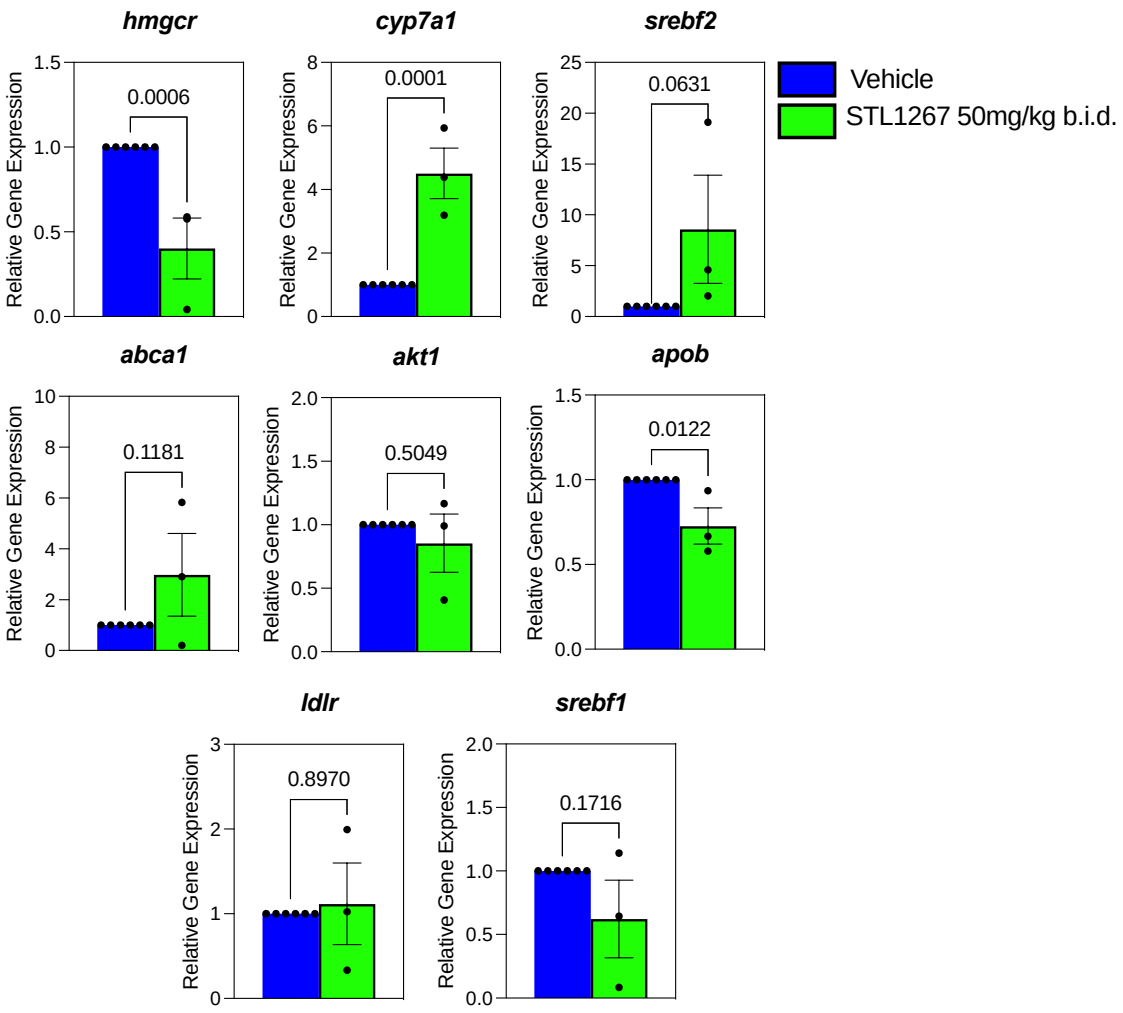

Figure 4.14 **STL1267 induced changes in cholesterol genes in the liver of mice fed MASH diet.** Gene expression of cholesterol genes that are involved in MASLD/MASH in mouse liver tissue. Data are represented as mean ± SEM (n=3-6). p-values are shown, as calculated by student's t-test in GraphPad Prism.

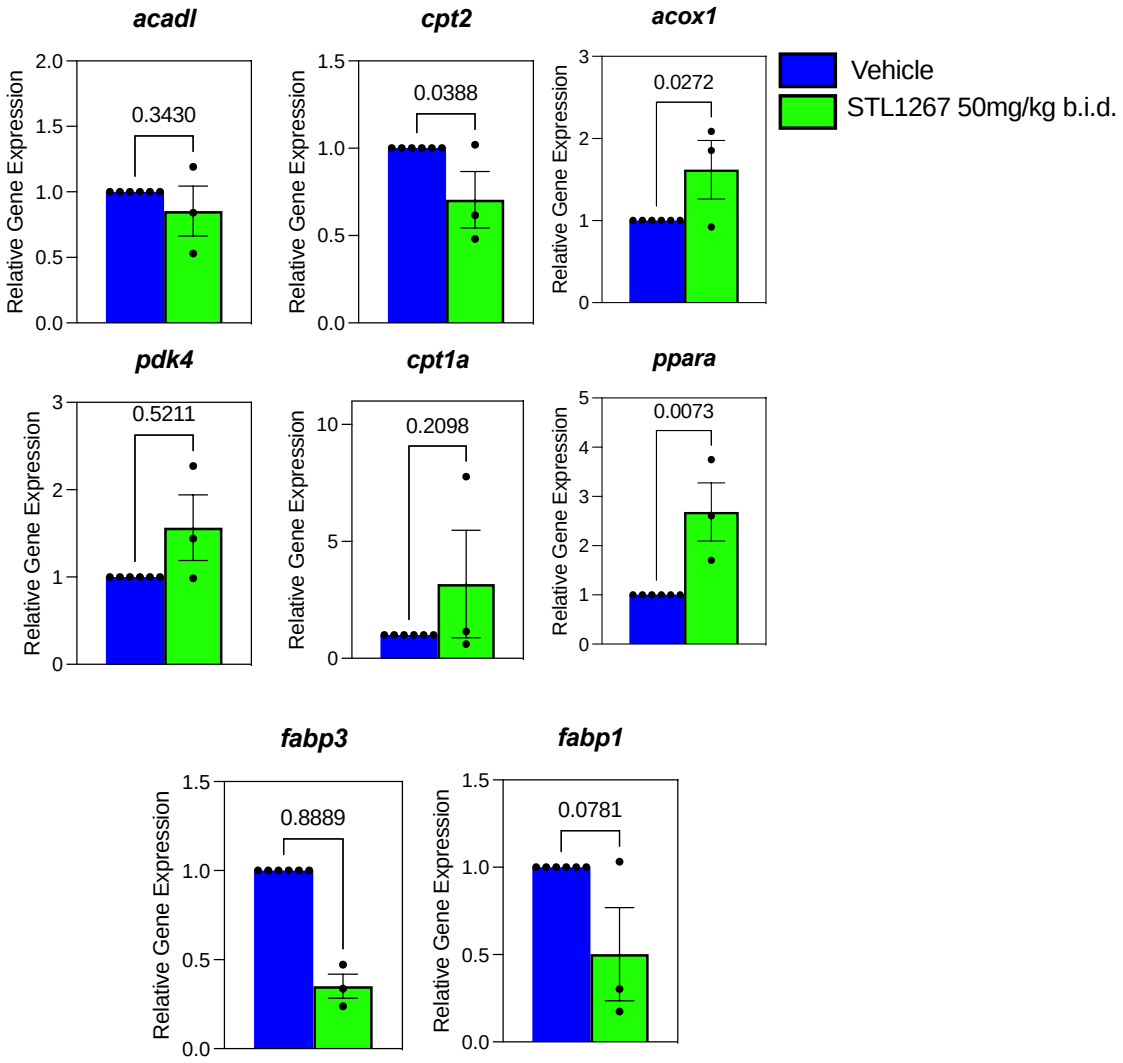

Figure 4.15 **STL1267 induced changes in genes involved in the regulation of fatty acid oxidation the liver of mice fed MASH diet.** Gene expression of FAO genes that are involved in MASLD/MASH in mouse liver tissue. Data are represented as mean ± SEM (n=3-6). p-values are shown, as calculated by student's t-test in GraphPad Prism.

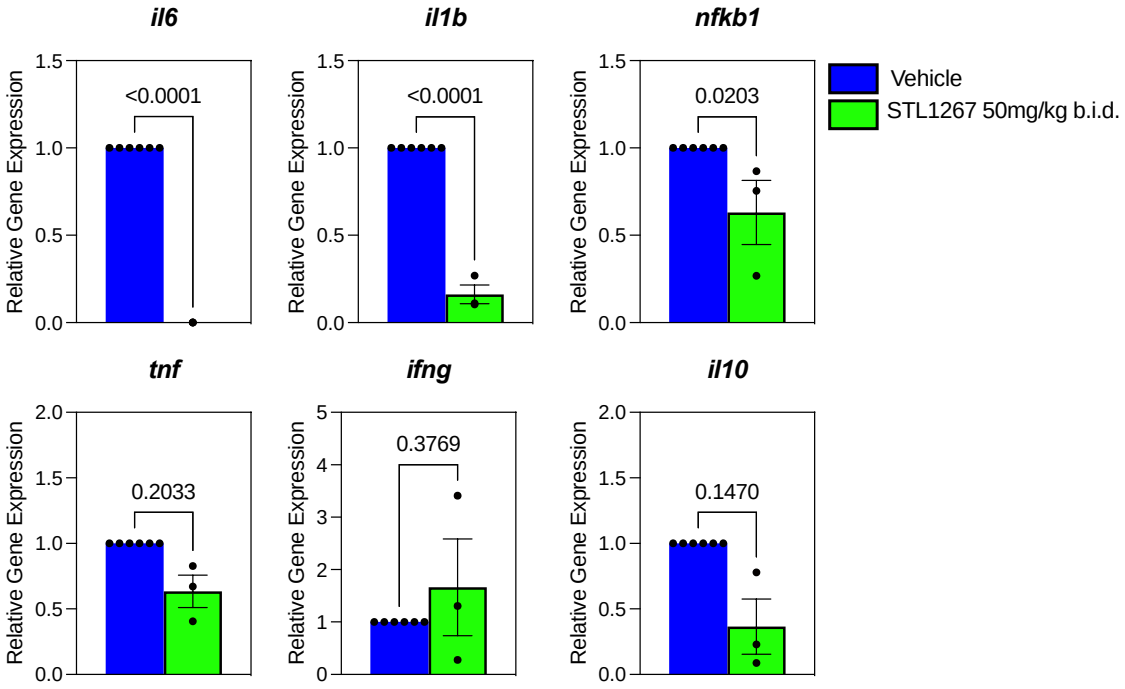

Figure 4.16 **STL1267 induced changes in inflammatory genes in the liver of mice fed MASH diet.** Gene expression of inflammatory cytokines (IL-6, IL-1β, NFκβ, TNFα, Casp-3) and anti-inflammatory cytokines (IL-10) that are involved in MASLD/MASH in mouse liver tissue. Data are represented as mean ± SEM (n=3-6). p-values are shown, as calculated by student's t-test in GraphPad Prism.

Together, escalated dosage causes the exacerbation of glucose intolerance, as well as divergent effects on specific genes involved in metabolism. This underscores the delicate balance in metabolic regulation and highlights the need for cautious consideration when manipulating dosage levels in therapeutic settings. Thus, we continued all further experiments on our standard dosing of 50mg/kg, once a day.

4.2.2. Model: Diet-induced obesity (DIO) MASH B6 mice

4.2.2.1. Plasma and biochemical indices of DIO MASH were improved by STL1267 induced REV-ERB activation

The overall study design is outlined (Fig 3.1). Following a diet induction period of 5 weeks, *ob/ob* mice fed with MASH diet were treated with 50mg/kg STL1267 i.p. once daily. Mice treated with STL1267 demonstrated no change in adiposity as measured by body weight, when compared to animals treated with just vehicle (Fig 4.17-A). There was no observed difference in the amount of food consumed between the vehicle and STL1267 treated groups (Fig 4.17-B). Further, we observed no change in the liver to body weight ratio upon treatment (Fig 4.17-C). Plasma markers associated with MASH, including ALT, AST, and ALP were all significantly reduced upon STL1267 treatment (Fig 4.18-A). Further, STL1267 reduced MASH induced hypercholesterolemia, as seen by the reduced circulating levels of total cholesterol, including both HDLs and LDLs (Fig 4.18-B). No

significant change was observed in circulating triglycerides or lactate levels. This was concurrent with liver triglycerides, with no change between STL1267 treated and vehicle groups (Fig 4.18-C).

Further, we performed glucose tolerance and insulin tolerance tests on these mice (Fig 4.19). While MASH diet did not induce glucose intolerance in *ob/ob* mice, we observed that STL1267 did not rescue glucose intolerance either, as seen by AUC. Interestingly, however, we saw increased levels of glucose in STL1267 treated mice at 30mins post glucose injection. We did not observe significant improvement in insulin tolerance in mice treated with STL1267. Together, this suggests that STL1267 is able to rescue metabolic parameters associated with MASH, however, is not enough to induce glucose intolerance and insulin resistance in *ob/ob* mice.

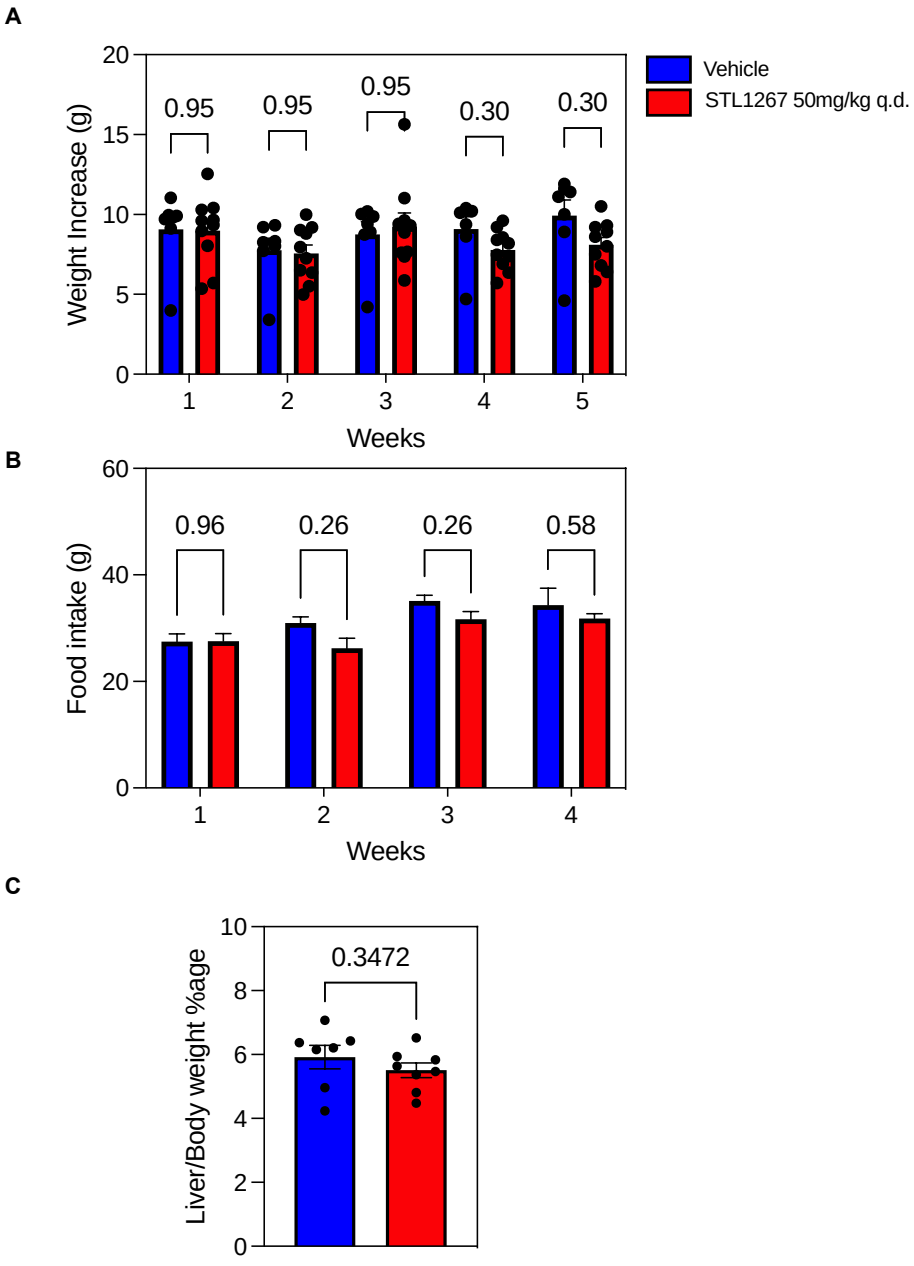

Figure 4.17 **STL1267 induced physiological changes in adiposity in control diet and MASH diet fed B6 mice.** Animals that were fed HFHC MASH diet for 10 weeks were treated with 50mg/kg i.p. STL1267 daily for 5 weeks. (A) Mouse weights per week of treatment were measured and normalized to initial weight. Data are presented as mean ± SEM; n = 5-6 for Vehicle and n = 5-6 for STL1267 treated, p-values indicated (One-way ANOVA). (B) Food intake per week for each cage was measured. Data are presented as mean ± SEM; n = 3 for Vehicle and n = 3 for STL1267 treated, p-values indicated (One-way ANOVA). (C) Liver was harvested at the end of 10 weeks and liver to body weight ratio was plotted as a percentage. Data are presented as mean ± SEM; n = 7-10. p-values indicated (Student's t-test)

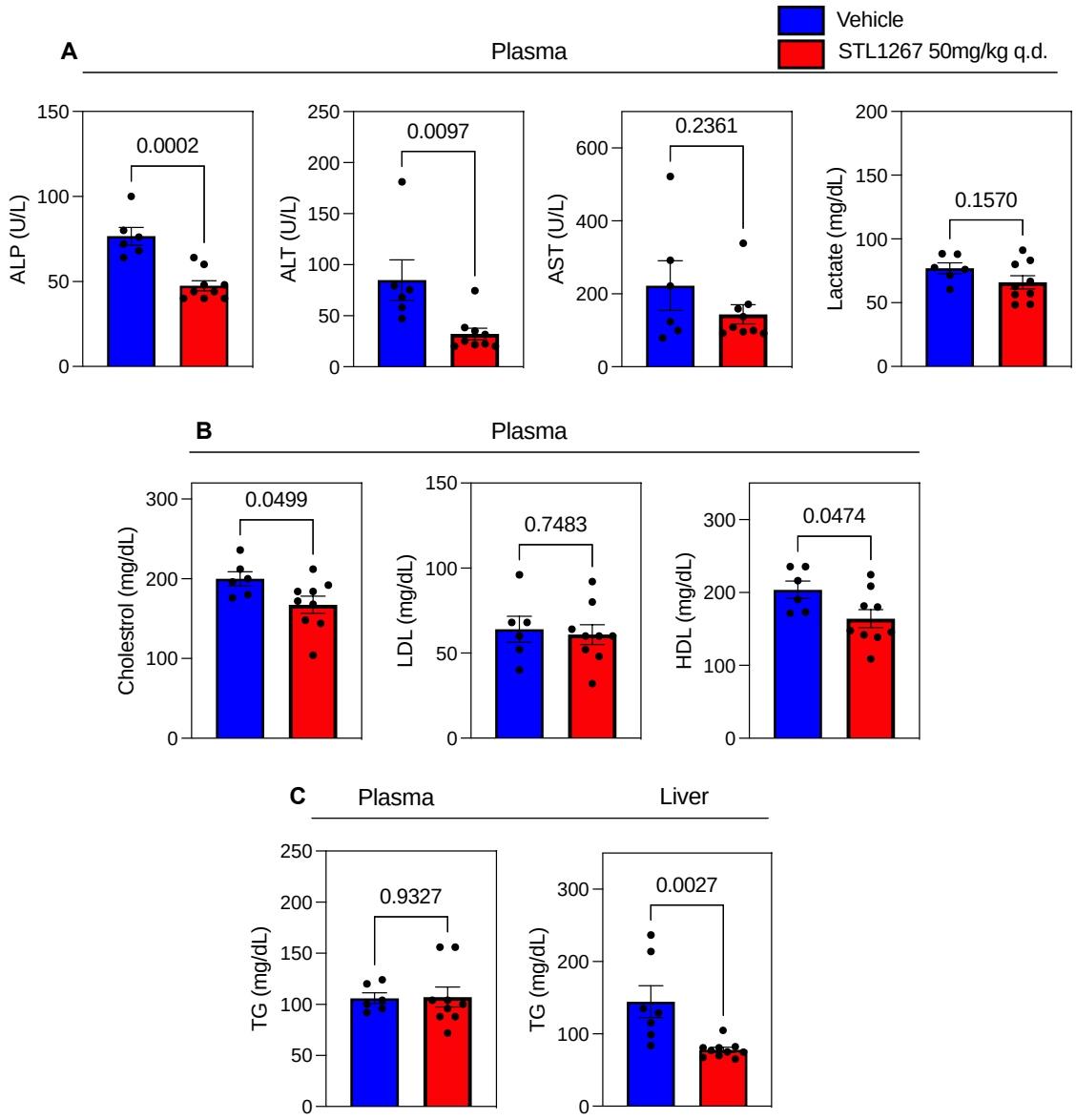

Figure 4.18 **Plasma and metabolic indices of MASH were improved by REV-ERB activation using STL1267 in DIO B6 MASH.** Blood plasma was analyzed for liver enzymes (A) as well as circulating metabolic indices – total cholesterol, LDL, and HDL (B) Circulating TGs (left) and Liver TGs (right) were also analyzed. All data are represented as mean ± SEM (n=6-10) and analyzed using student's t-test in GraphPad Prism.

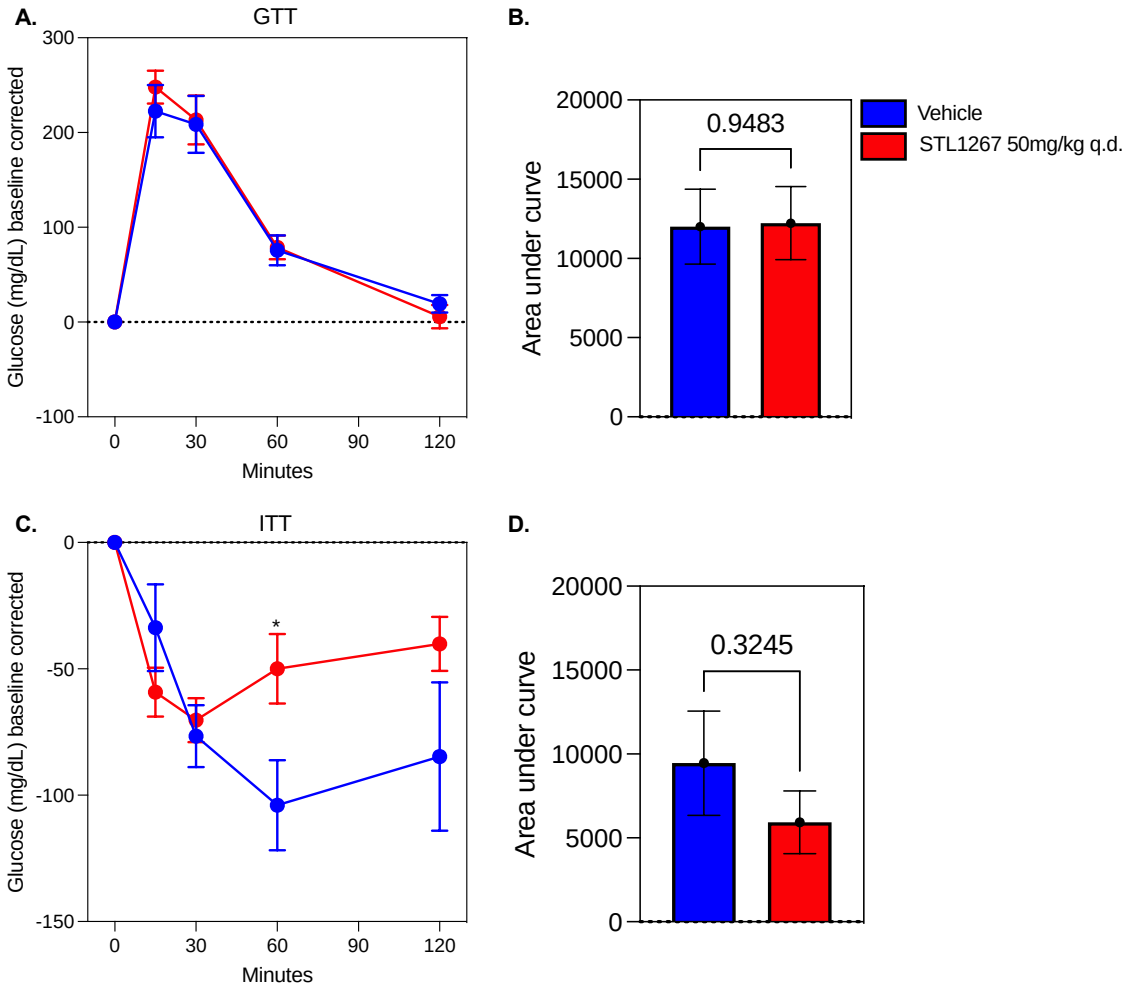

Figure 4.19 **Glucose and insulin tolerance test (i.p.GTT) in DIO B6 MASH mice treated with STL1267 q.d. or vehicle.** 6 hour fasted mice were administrated 2.0 g/kg glucose or insulin 0.5U/kg i.p. Blood samples were taken at 0, 15, 30-, 60-, 90- and 120-min. Plasma levels of glucose (A, C) were measured. Data are normalized to baseline glucose levels. Area under curve (B, D). Data are presented as mean ± SEM; n = 6-10. *p<0.05 (Student's t-test)

4.2.2.2. STL1267 administration in-vivo alters metabolic gene expression in the liver

To characterize the effect of STL1267 treatment on global liver gene expression, the transcriptome of STL1267 treated and vehicle MASH mice was analyzed using qPCR of genes involved in fatty liver disease. It is shown that genes linked to lipogenesis, fatty acid uptake, cholesterol biosynthesis, inflammation, and carbohydrate metabolism are robustly reduced in MASH *ob/ob* mice treated with STL1267 compared to those animals on vehicle treatment (Fig 4.20-4.23). Further, a large collection of pro-inflammatory factors such as IFNg, TNF, IL-6, IL1β, and Casp-3 were found significantly reduced post STL1267 treatment (Fig 4.24).

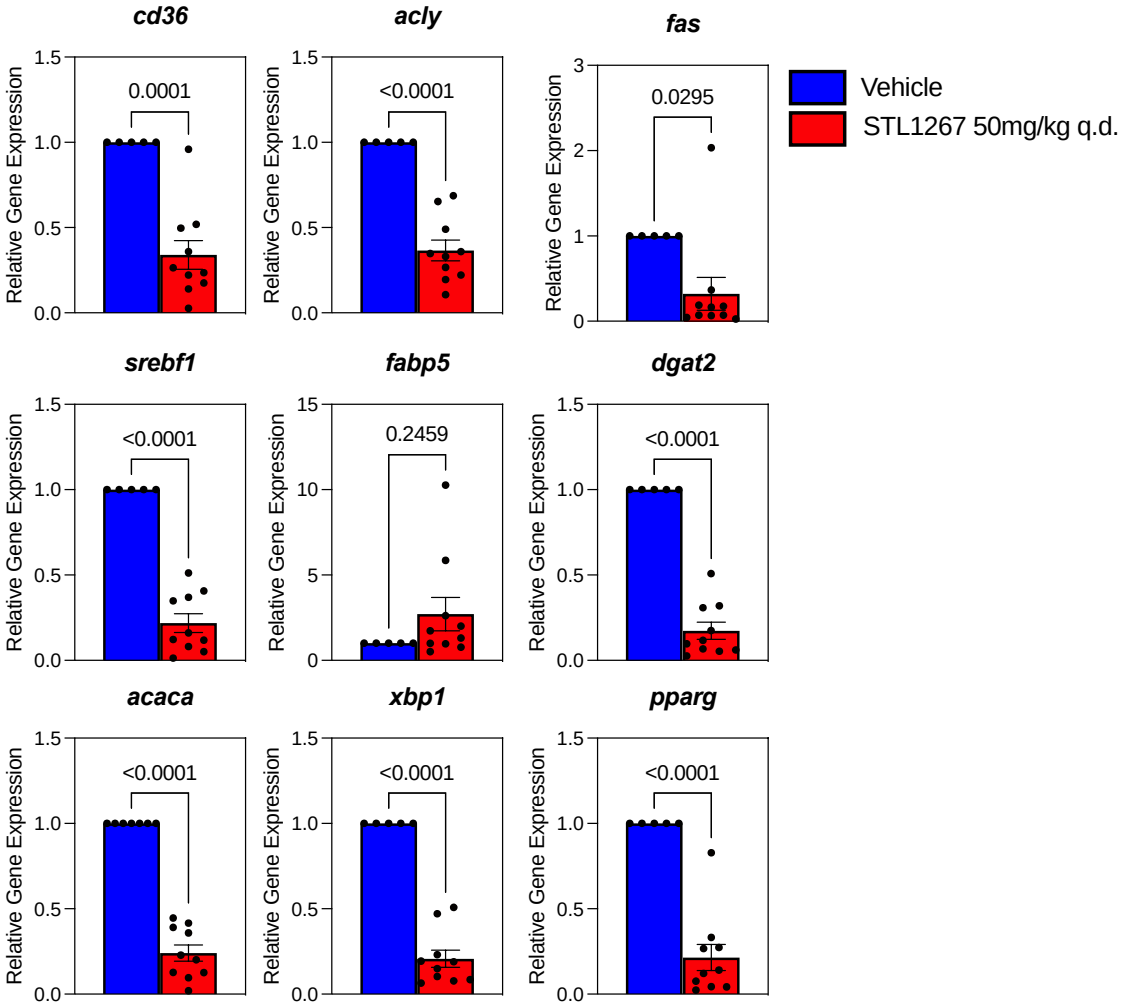

Figure 4.20 **STL1267 induced changes in lipogenic genes in the liver of mice fed MASH diet.** Gene expression of lipogenic genes that are involved in MASLD/MASH in mouse liver tissue. Data are represented as mean ± SEM (n=6-10). p-values are shown, as calculated by student's t-test in GraphPad Prism.

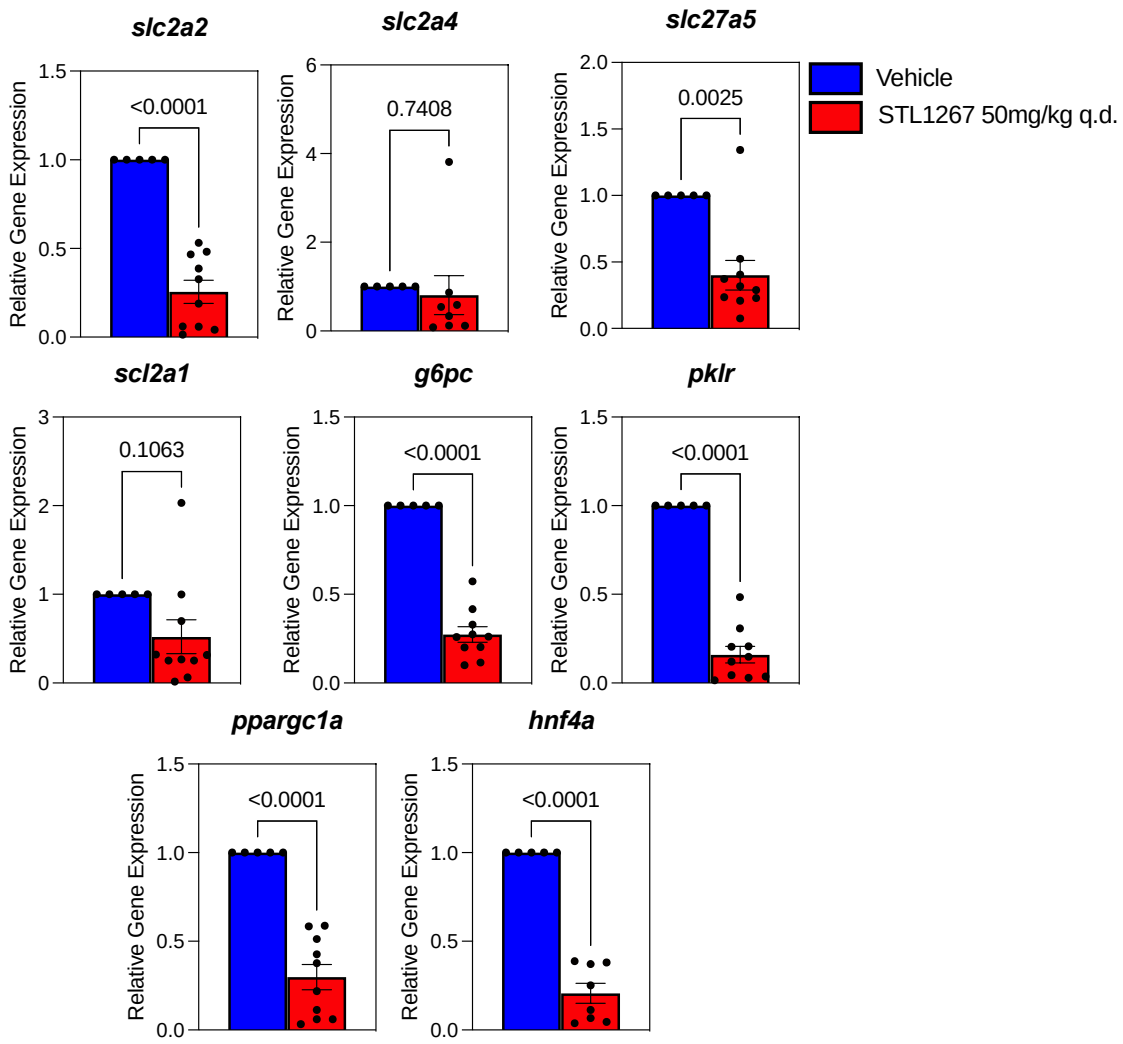

Figure 4.21 **STL1267 induced changes in glucose metabolism genes in the liver of mice fed MASH diet.** Gene expression of genes that are involved in glucose metabolism in MASLD/MASH in mouse liver tissue. Data are represented as mean ± SEM (n=6-10). p-values are shown, as calculated by student's t-test in GraphPad Prism.

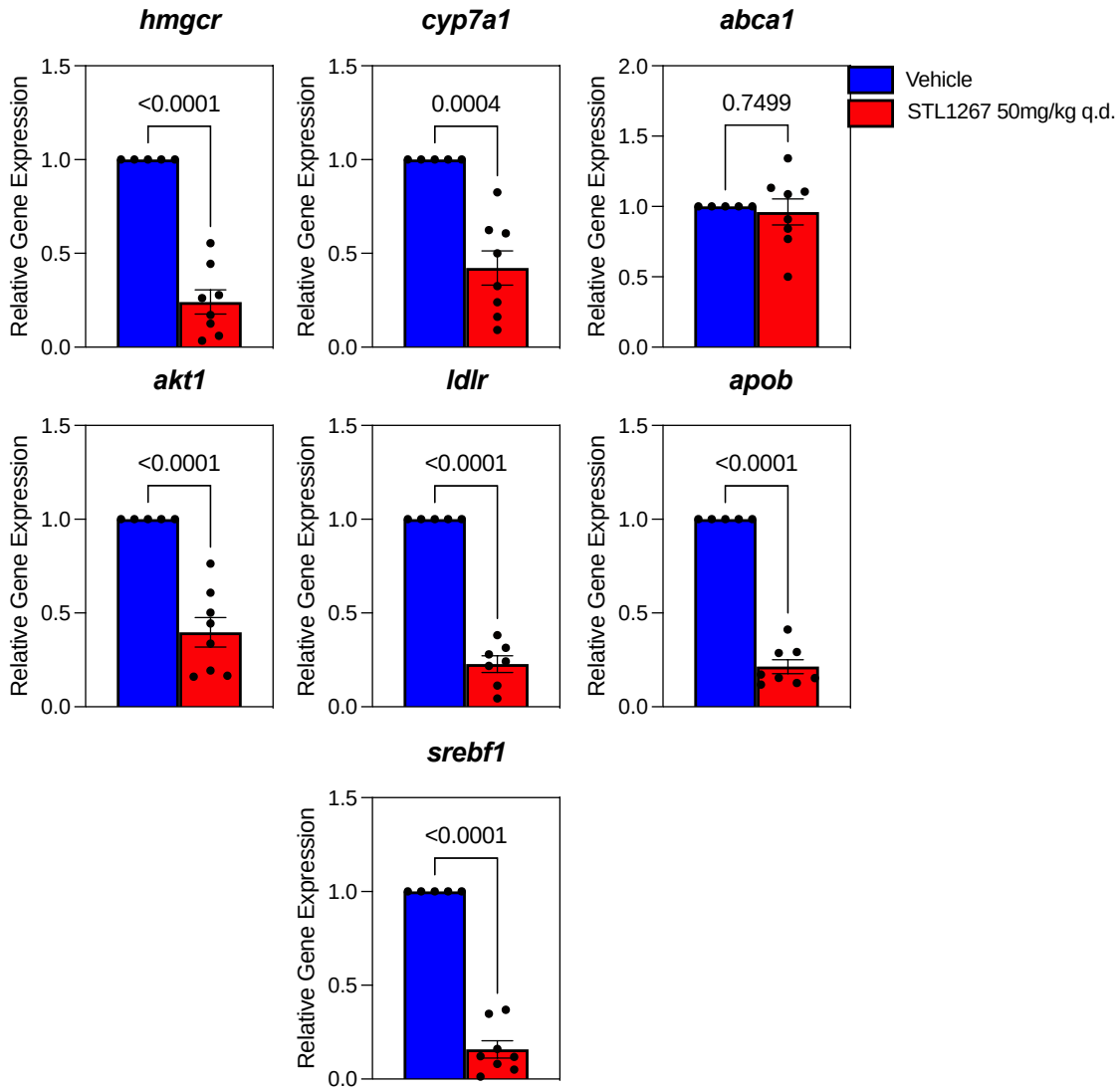

Figure 4.22 **STL1267 induced changes in cholesterol genes in the liver of mice fed MASH diet.** Gene expression of cholesterol genes that are involved in MASLD/MASH in mouse liver tissue. Data are represented as mean ± SEM (n=6-10). p-values are shown, as calculated by student's t-test in GraphPad Prism.

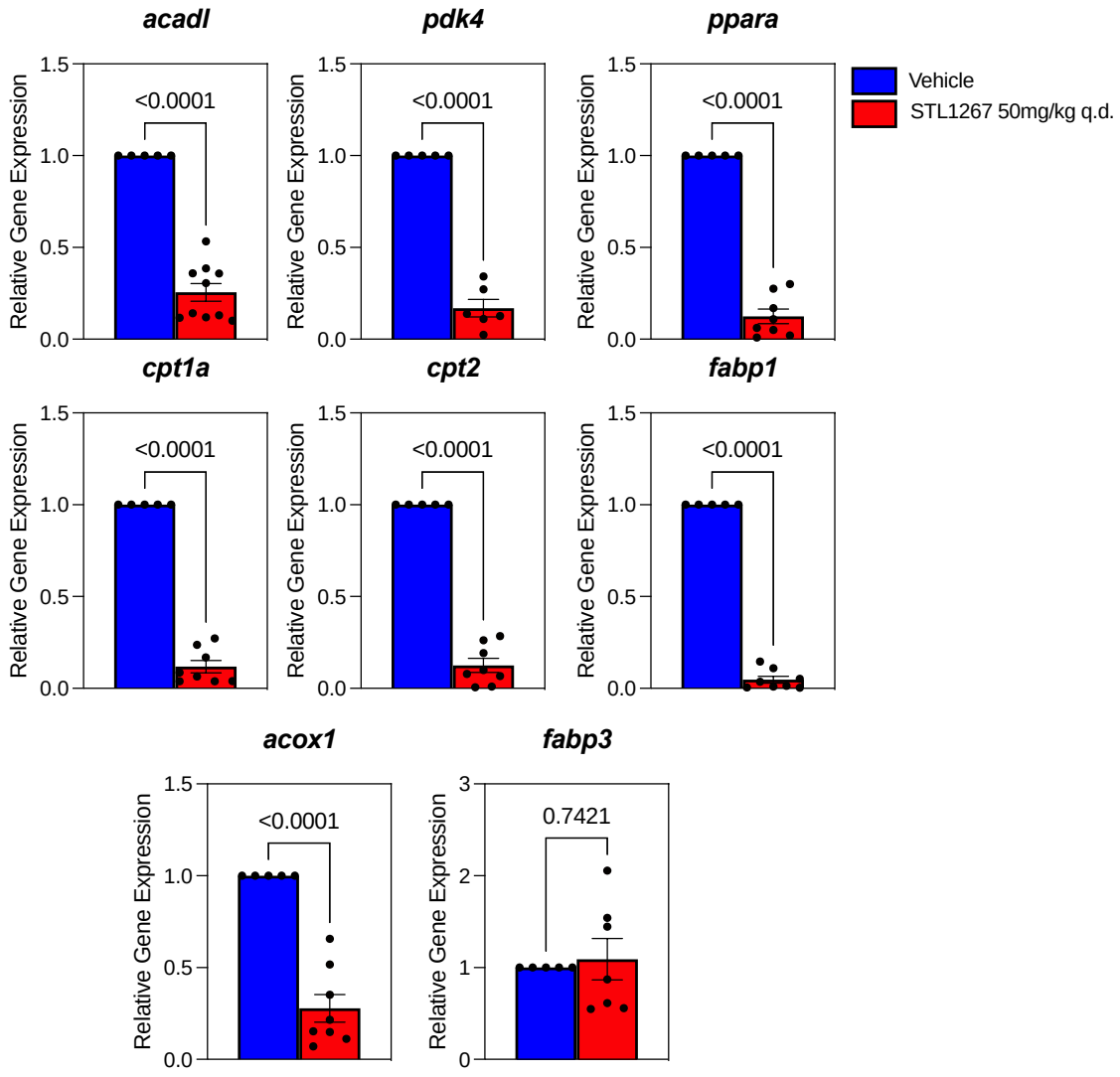

Figure 4.23 **STL1267 induced changes in genes involved in the regulation of fatty acid oxidation the liver of mice fed MASH diet.** Gene expression of FAO genes that are involved in MASLD/MASH in mouse liver tissue. Data are represented as mean ± SEM (n=6-10). p-values are shown, as calculated by student's t-test in GraphPad Prism.

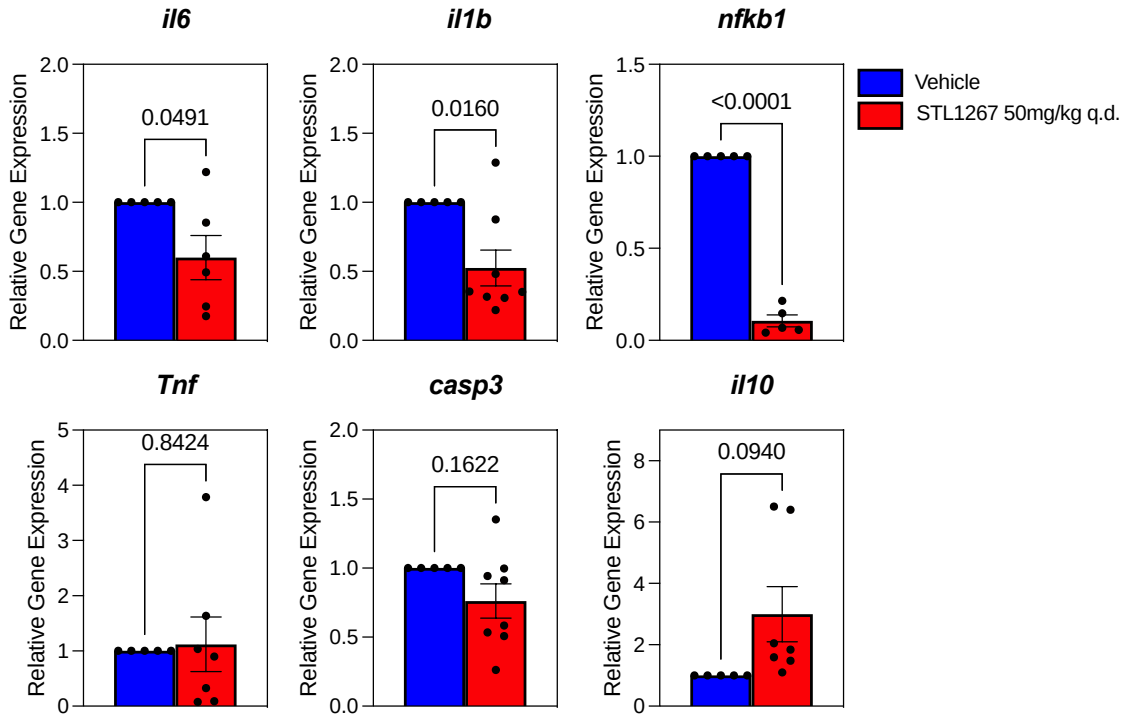

Figure 4.24 **STL1267 induced changes in inflammatory genes in the liver of mice fed MASH diet.** Gene expression of inflammatory cytokines (IL-6, IL-1β, NFκβ, TNFα, Casp-3) and anti-inflammatory cytokines (IL-10) that are involved in MASLD/MASH in mouse liver tissue. Data are represented as mean ± SEM (n=6-10). p-values are shown, as calculated by student's t-test in GraphPad Prism.

4.2.2.3. STL1267 administration in-vivo alleviates histological hepatic steatosis and fibrosis

As determined by H&E sections, obese MASH mice treated with STL1267 q.d as well as b.i.d. had altered distribution of lipids. We observed that while there was no change in micro-steatosis, there was increased macro-steatosis. Additionally, there was also an increase in hepatic hypertrophy (Fig 4.25, 4.27). As determined by Gomori's trichrome staining, there was no quantifiable change in fibrosis, but STL1267 treatment seems to be decreasing fibrotic regions (Fig 4.26, 4.28).

In DIO B6 MASH mice treated with STL1267, we saw that there was improved MASH pathology as seen in reduced micro-, and macro-steatosis, as well as hypertrophy (Fig 4.29). Similar to obese mice, there was no quantifiable change in fibrosis, but STL1267 treatment seems to be decreasing fibrotic regions (Fig 4.30).

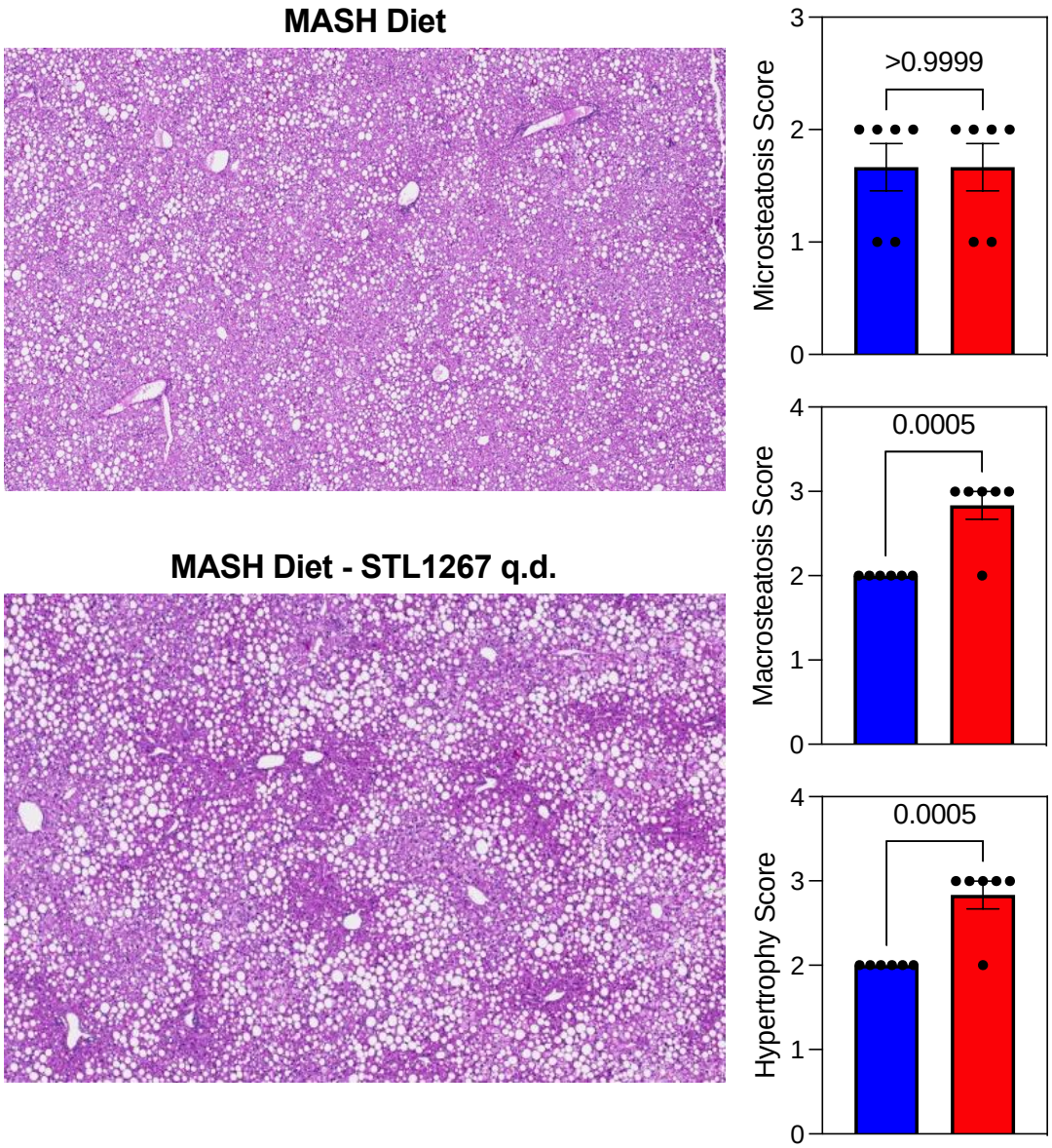

Figure 4.25 **Hepatosteatosis in *ob/ob* mice treated with STL1267 q.d. is altered compared to MASH diet.** Pathological analysis and scoring from H&E sections of livers suggests that STL1267 treated MASH mice have increased macro-steatosis, and increased hepatic hypertrophy.

MASH Diet - Vehicle

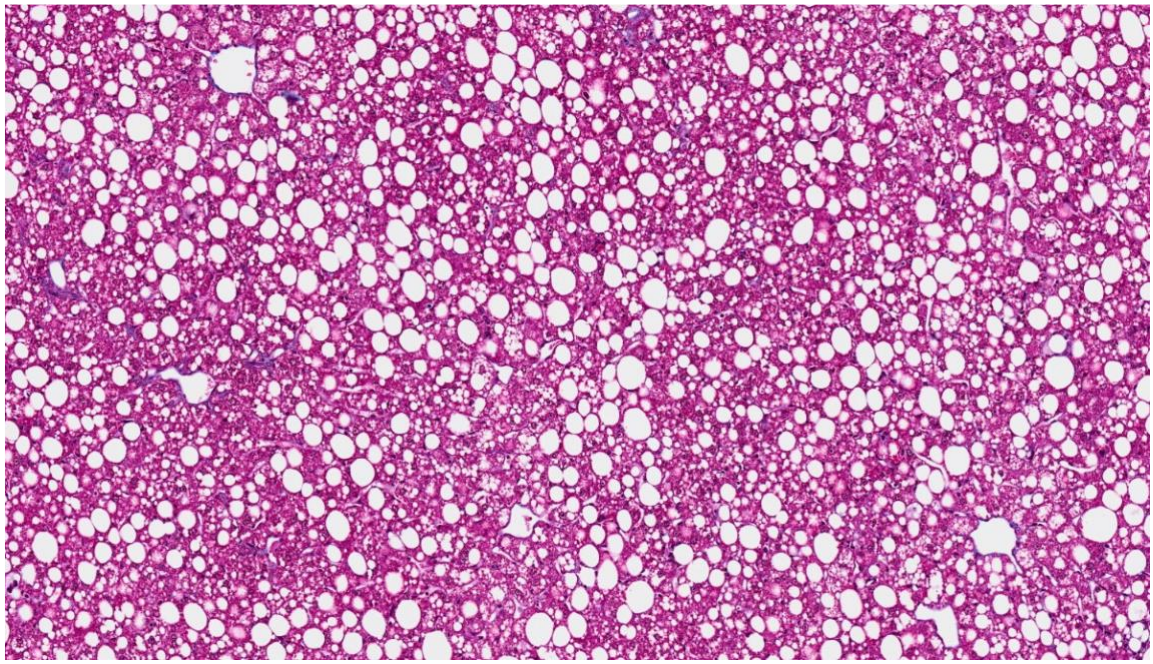

MASH Diet - STL1267 q.d.

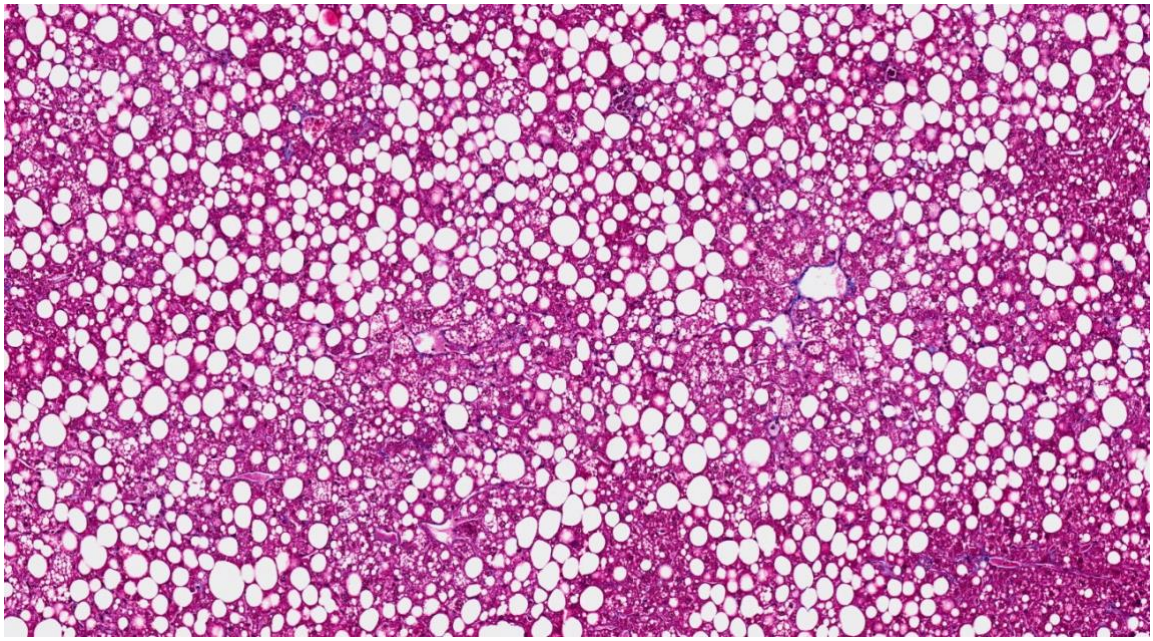

Figure 4.26 **Fibrosis in *ob/ob* mice treated with STL1267 q.d. diet does not appear altered compared to MASH diet.** Pathological analysis and scoring from Gomori's Trichrome sections of livers suggests that mice have not developed excessive fibrosis.

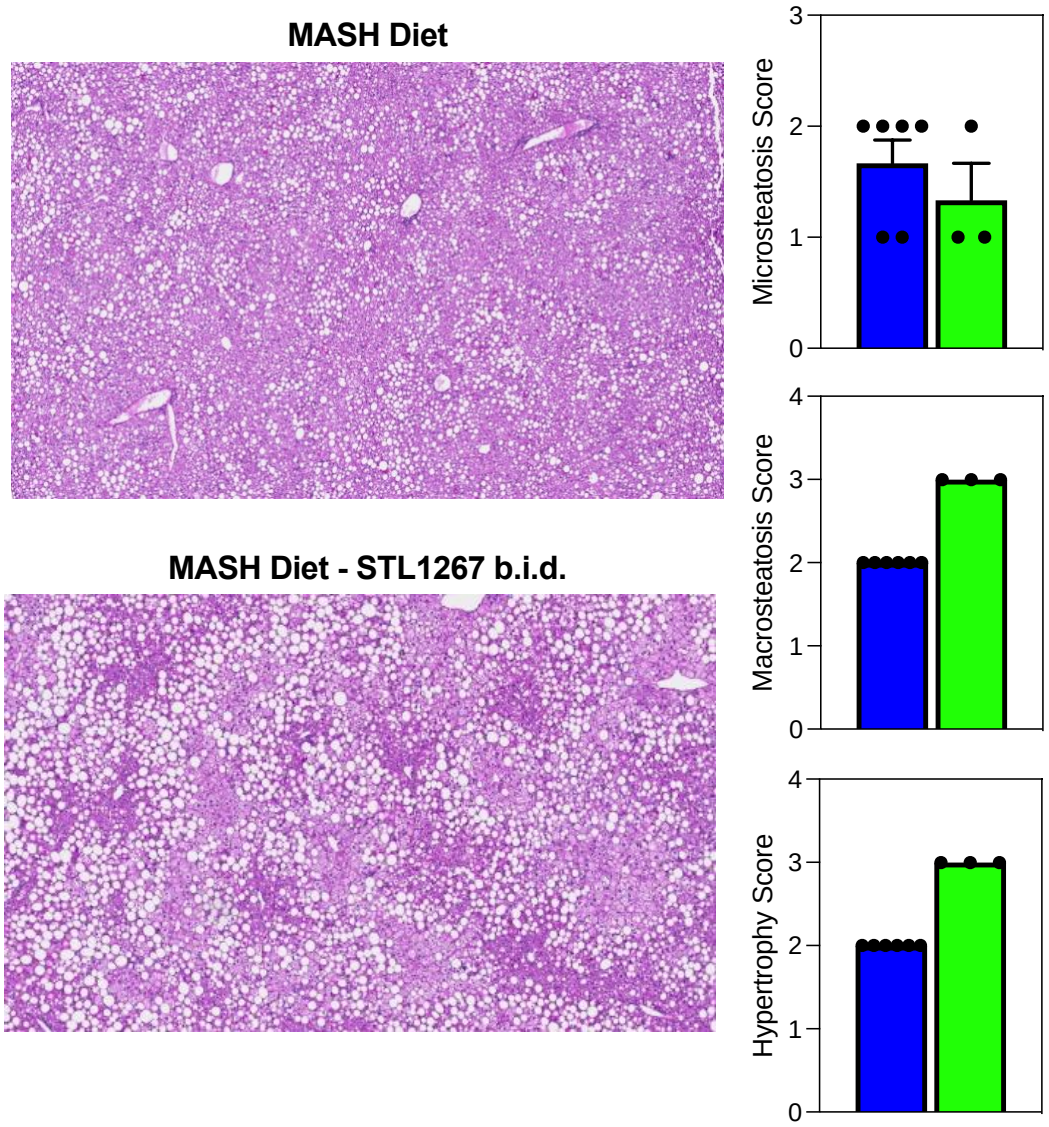

Figure 4.27 **Hepatosteatosis in *ob/ob* mice treated with STL1267 b.i.d. is altered compared to MASH diet vehicle.** Pathological analysis and scoring from H&E sections of livers suggests that STL1267 b.i.d. treated mice have increased macro-steatosis and increased hepatic hypertrophy.

MASH Diet - Vehicle

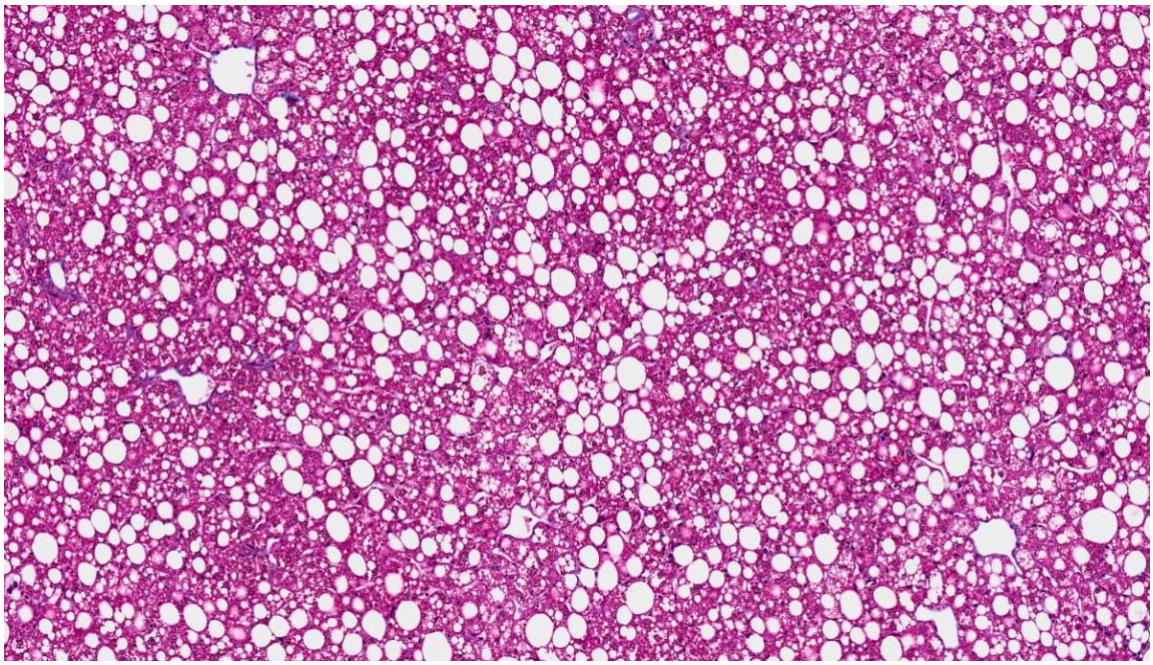

MASH Diet - STL1267 b.i.d.

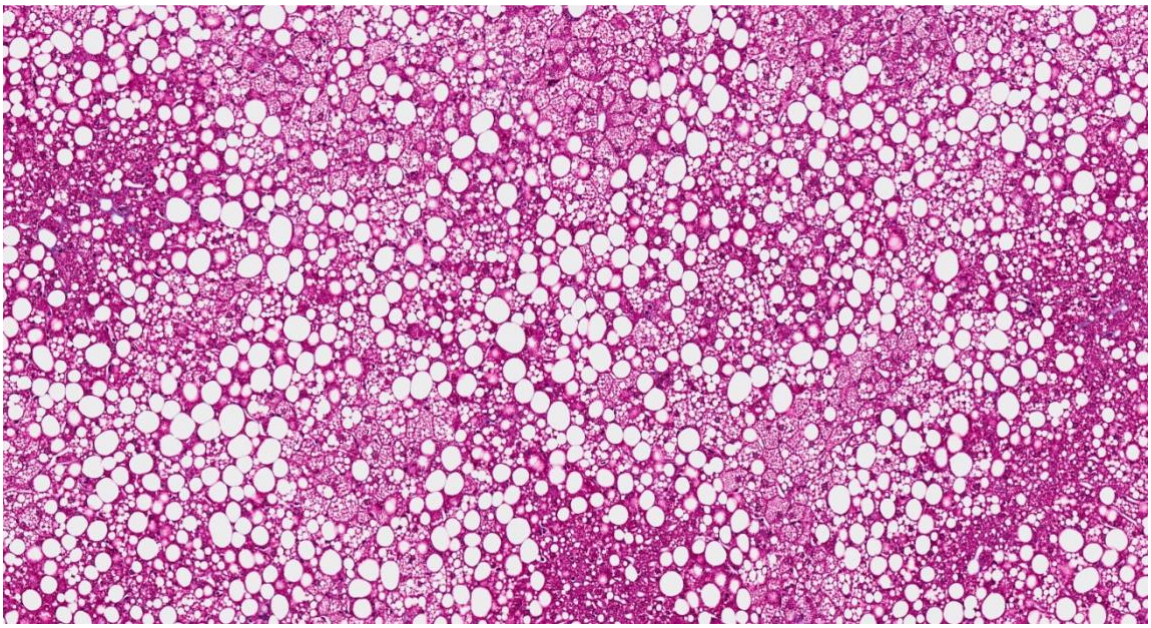

Figure 4.28 **Fibrosis in *ob/ob* mice treated with STL1267 b.i.d. diet does not appear altered compared to MASH diet.** Pathological analysis and scoring from Gomori's Trichrome sections of livers suggests that mice did not develop excessive fibrosis.

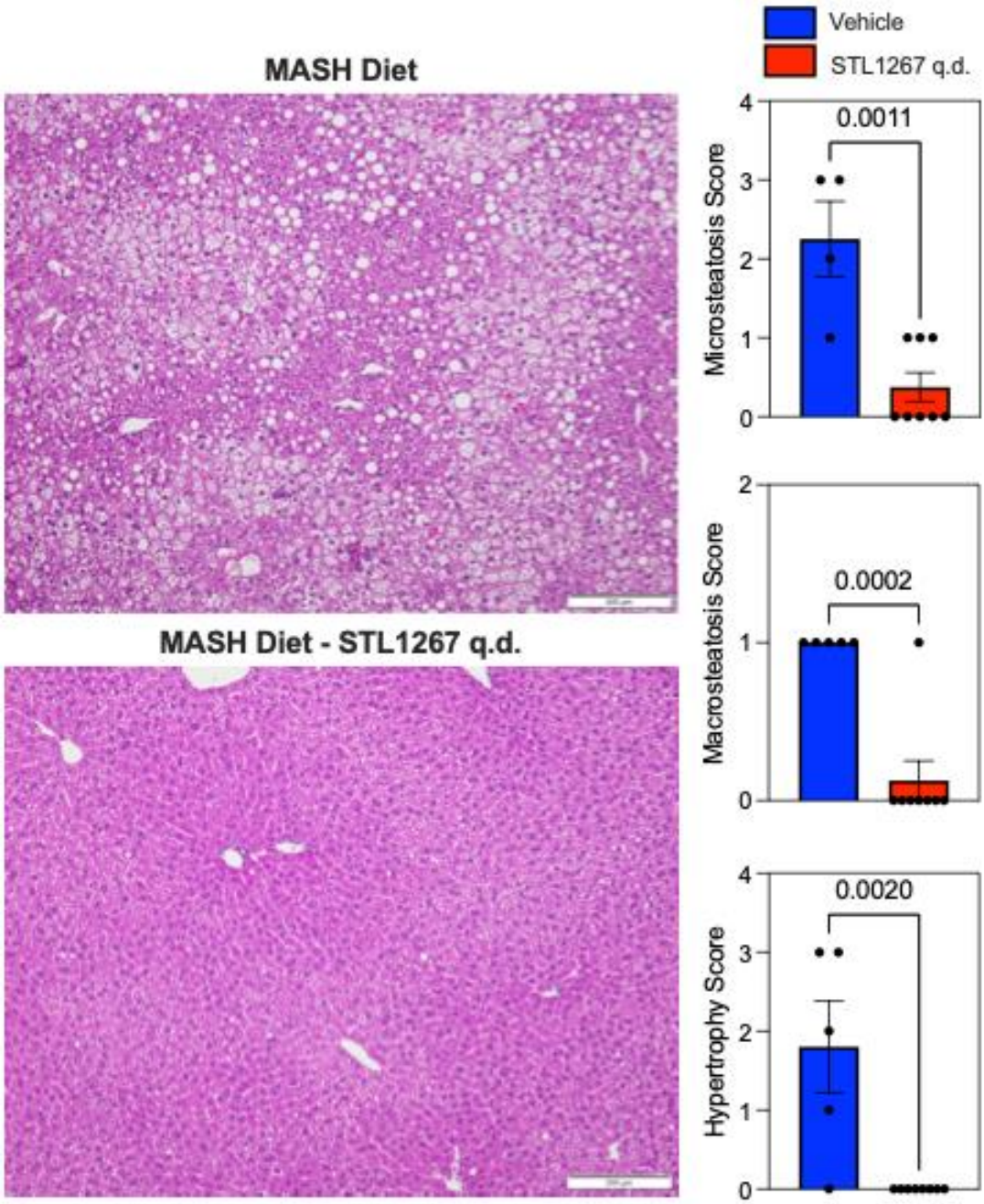

Figure 4.29 **Hepatosteatosis in *B6* mice treated with STL1267 q.d. is altered compared to MASH diet vehicle.** Pathological analysis and scoring from H&E sections of livers suggests that STL1267 q.d. treated mice have reduced micro-steatosis, and macro-steatosis. MASH diet fed mice also have decreased hepatic hypertrophy.

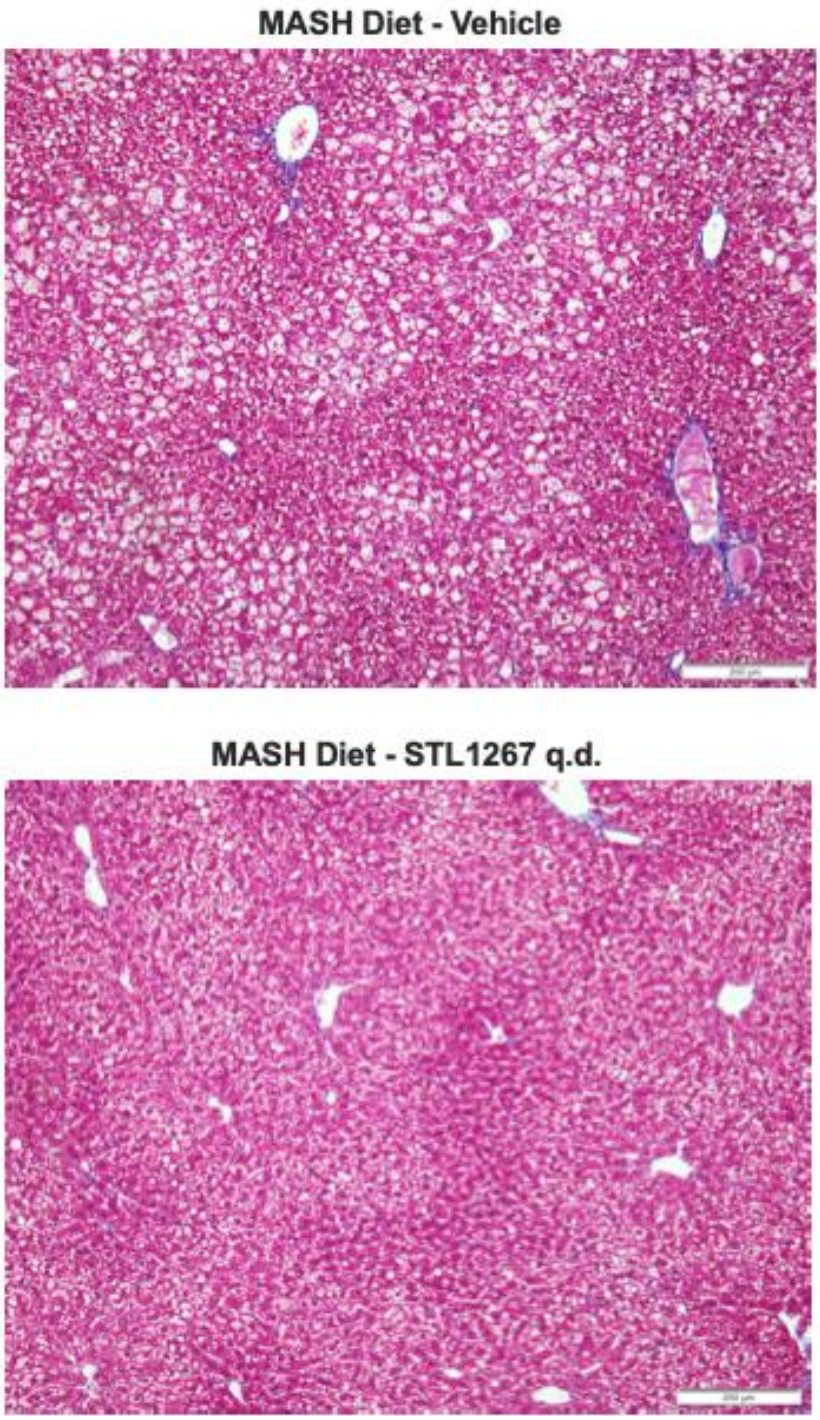

Figure 4.30 **Fibrosis in *B6* mice treated with STL1267 q.d. diet does not appear altered compared to MASH diet.** Pathological analysis and scoring from Gomori's Trichrome sections of livers suggests that MASH diet fed mice did not develop excessive fibrosis.

4.3 Discussion

The aim of this dissertation was to look into the promising therapeutic potential of utilizing REV-ERB synthetic agonist STL1267 as a treatment strategy for MASLD/MASH. MASLD/MASH represents a significant clinical challenge due to its intricate interplay of metabolic dysregulation and hepatic dysfunction. Despite advancements in understanding the pathophysiology of MASLD/MASH, effective therapeutic interventions remain limited, with no approved therapy till date. Our research aimed to address this gap by investigating the role of REV-ERB in MASLD/MASH. The hypothesis underlying our study posited that REV-ERB activation could potentially mitigate metabolic derangements associated with MASLD/MASH, thus offering a novel therapeutic avenue. Specifically, we hypothesized that activation of REV-ERB could induce beneficial alterations in mitochondrial metabolism, thereby ameliorating hepatic dysfunction and metabolic dysregulation characteristic of MASLD/MASH.

Hepatocytes have a multifaceted role in MASLD/MASH. They are the primary site of lipid accumulation initiating the cascade of events leading to metabolic dysfunction, as well as inflammation and fibrosis. Mitochondrial dysfunction in hepatocytes stands as a pivotal aspect of MASLD/MASH pathogenesis. (Gong et al., 2022). Hepatocyte mitochondria undergo structural and functional alterations, manifesting an impaired oxidative phosphorylation, decreased ATP production, and heightened generation of ROS. Moreover, mitochondrial dysfunction disrupts

lipid metabolism, leading to aberrant lipid accumulation within hepatocytes, a defining characteristic of MASLD/MASH. Collectively, mitochondrial dysfunction in hepatocytes plays a central role in MASLD/MASH pathogenesis (Prasun et al., 2021). REV-ERB plays a crucial role in orchestrating mitochondrial function and metabolism. Within mitochondria, REV-ERB modulates key processes involved in energy production, mitochondrial biogenesis, and oxidative metabolism. Through its transcriptional regulatory activity, REV-ERB governs the expression of genes encoding proteins critical for mitochondrial respiration, including those involved in the electron transport chain and oxidative phosphorylation (Woldt et al., 2013). By fine-tuning mitochondrial metabolism, REV-ERB helps maintain cellular energy homeostasis and contributes to the regulation of circadian rhythms, as REV-ERB activity is intricately linked to the circadian clock machinery. Dysregulation of REV-ERB activity has been associated with metabolic disorders, including obesity, insulin resistance, and fatty liver disease, underscoring its importance in mitochondrial function and metabolic health (Griffett et al., 2022). Our hypothesis was that REV-ERB activation affects mitochondrial metabolism in order to mitigate liver pathology.

We aimed to test this hypothesis in HepG2 cells using Seahorse Flux analyzer. Upon treatment with STL1267, HepG2s had a decreased rate of oxygen consumption, indicating a REV-ERB mediated decrease in mitochondrial respiration or OXPHOS (Fig 2.1). This change in cellular metabolism could indicate a shift in substrate utilization, and thus we aimed to check if there was a metabolic

reprogramming towards glycolysis. In STL1267 treated HepG2s, there was no change in glycolytic flux as measured by ECAR in the glycolytic stress test. This was further fortified by the absence of any difference in uptake of glucose between STL1267 treated HepG2s and vehicle treated (Fig 2.3). This was interesting as REV-ERB clearly modulated mitochondrial respiration in these hepatocytes, but was not shifting the cellular metabolism towards glycolysis. This could perhaps indicate the utilization of alternate energy sources such as fatty acids, or a state of cellular quiescence in hepatocytes. However, HepG2 cells are a hepatocellular carcinoma cell line, and may not represent the physiological characteristics of normal hepatocytes, which might especially be true in the context of metabolic reprogramming, pertaining the Warburg effect (Liberti & Locasale, 2016).

In order to further validate these findings, we utilized primary human hepatocytes. We treated them with either vehicle control or STL1267, and saw a similar decrease in mitochondrial respiration (Fig 2.2), and no changes were observed in glycolytic flux of these cells. Suggesting that REV-ERB does indeed play a role in modulating mitochondrial respiration, and does not affect glucose metabolism in these cells.

Since we saw reproducible and similar results in HepG2 and primary human hepatocytes, we decided to use HepG2s for the remaining experiments for ease of modulation. Importantly, MASLD/MASH hepatocytes *in-vivo* are heavily steatotic, marked by increased lipid accumulation. We showed that in-vitro

supplementation of extracellular lipids and cholesterol is able to induce de-novo lipogenesis and increase lipid content (Fig 2.5). As mentioned previously, oxidative stress in hepatocytes is a key hallmark feature of MASLD/MASH, and it plays a major role in promoting lipid peroxidation, DNA damage, and cellular injury. We were able to confirm that *de-novo lipogenic* (DNL) hepatocytes have increased oxidative stress, not just cellularly but also mitochondrial specific, suggesting the presence of mitochondrial dysfunction (Fig 2.6). Since we showed STL1267 attenuates mitochondrial respiration, we hypothesized downstream production of oxidative stress could be attenuated as well. Treatment with STL1267 was able to rescue this oxidative stress, in both cellular ROS as well mitochondria specific ROS, suggesting a prominent mechanism of action for REV-ERB agonism (Fig 2.7).

One key aspect of MASH is the presence of fibrosis. This is mediated by HSC cells in the liver. Their activation involves profound metabolic reprogramming, with mitochondrial metabolism. HSCs undergo a transition from a quiescent, lipid-storing phenotype to an activated, proliferative, and fibrogenic phenotype in response to liver injury or inflammation. Mitochondrial metabolism contributes significantly to the metabolic changes associated with HSC activation (Delgado et al., 2021). We hypothesized that reduction of mitochondrial respiration in HSCs could impair the metabolic reprogramming, thereby attenuating downstream fibrogenic potential. Indeed, STL1267 was able to reduce mitochondrial respiration in LX-2 cells (Fig 2.8), and this correlated with the reduced fibrogenic activation of

these cells, as seen by reduced alpha-SMA (Fig 2.9). Overall, this suggests that REV-ERB activation plays a role on hepatic stellate cells directly via metabolic reprogramming in order to rescue fibrosis. In fact, we were able to extend these findings in another key hallmark of MASH, which is inflammation. In macrophages, we showed that REV-ERB activation was able to reduce OXPHOS, similar to hepatocytes and stellate cells (Fig 2.8). It has been shown and well established that mitochondrial respiration is a major source of ATP for activated macrophages, and is required for maintaining the energy demand that comes with a pro-inflammatory state (Y. Wang et al., 2021). However, there is also a shift of metabolism towards glycolysis in M1 macrophages (Yu et al., 2020). Unlike hepatocytes, REV-ERB activation did in-fact reduce the glycolytic capacity in activated macrophages. Downstream, this correlates with reduced effector function, in this case, inflammatory cytokine secretion. We have previously shown that REV-ERB activation in macrophages (BMDM) reduces pro-inflammatory cytokine secretion (Makhija et al., 2023).

RNAseq analysis on HepG2s treated with STL1267 confirmed a global transcriptome change in genes related to metabolism, inflammation, as well autophagy (Fig 2.10). Suggesting that REV-ERB activation through metabolic reprogramming is able to rescue downstream disease hallmarks such as oxidative stress, inflammation, and autophagy. This was further extended to stellate cells, where we observed major changes in genes related to inflammation, metabolism, and fibrosis (Fig 2.11).

HIF-1α is a key regulator of glycolytic gene expression, promoting glycolysis under hypoxic conditions. Additionally, HIF-1α promotes ROS production by enhancing mitochondrial respiration and electron transport chain activity (Taylor & Scholz, 2022). Since, we observed deduced glycolysis and ROS in macrophages, we hypothesized that REV-ERB activation could affect HIF-1α stability, explaining the reduced glycolysis and ROS.

In hypoxic macrophages treated with REV-ERB agonist STL1267, nuclear translocation of HIF-1α was reduced (Fig 2.12). Further in-line with this, in the liver of MASH mice, we saw HIF-1 target genes such as *Glut-1* and *Vegf* reduced upon STL1267 treatment. HIF-1α activation triggers the expression of genes encoding antioxidant enzymes, such as superoxide dismutase (SOD) and NRF2 (Fig 2.13). This REV-ERB mediated reduction in HIF1α could protect against mitochondrial dysfunction by reducing glycolysis, attenuating ROS production, maintaining mitochondrial dynamics, and preventing excessive mitochondrial biogenesis, to promote cell survival under conditions of metabolic stress in MASLD. However, future experiments are required to successfully conclude this interaction.

In conclusion, the above evidence suggests that REV-ERB agonism, by reducing mitochondrial metabolism in hepatocytes, stellate cells, and macrophages, holds significant therapeutic potential for mitigating MASLD/MASH. By targeting mitochondrial metabolism across multiple cell types involved in liver

pathophysiology, REV-ERB effectively disrupts downstream effector functions of these cells in MASLD, namely oxidative stress, ECM secretion, and pro-inflammatory cytokine release. This intervention relies on metabolic reprogramming to modulate mitochondrial dysfunction in a cell specific manner, which could potentially be via HIF-1α. In order to further elucidate the molecular mechanisms underlying the metabolic effects and for refining therapeutic strategies in MASLD/MASH we utilized *in-vivo* mouse models.

In MASLD mouse models, there is a discernible increase in FAO, OXPHOS, and overall metabolic activity (Lu et al., 2021). NAFLD, characterized by hepatic lipid accumulation and metabolic dysregulation, triggers a compensatory response aimed at restoring metabolic homeostasis. It has been shown previously that this response often entails upregulation of FAO pathways, wherein accumulated lipids are oxidized to generate energy (Diraison et al., 2003) and heightened OXPHOS activity is observed, facilitating the utilization of fatty acids as substrates for ATP production within mitochondria (Sunny et al., 2010). Previous studies from our lab and others have shown that REV-ERB activation using SR9009 alleviates MASLD/MASH pathology (Griffett et al., 2020). However, SR9009 has numerous limitations, as mentioned previously. Briefly, it has poor solubility, potency, as well as recent studies have questioned its specificity. In this study, we administer STL1267 as a therapeutic to alleviate MASLD/MASH mice, expecting better pharmacokinetics and high specificity to REV-ERB. In order to determine the ideal dose of STL1267, 50mg/kg was administered intraperitoneally in MASH mice

either once daily (q.d.) or twice daily (b.i.d.) at ZT1 or at ZT1 and ZT10. Control group was treated with only placebo (vehicle).

We characterized two mouse models of MASLD/MASH, leptin deficient obese MASH, and DIO B6 MASH mice. By administering a REV-ERB activator, we aim to reduce mitochondrial function; fatty acid oxidation in the liver; as well as the enhanced triglyceride synthesis. Thereby alleviating not just mitochondrial dysfunction, but also lipid overload and metabolic stress.

We were able to show that in obese mouse model of MASLD/MASH, there was increased adiposity, and it correlated with increased circulating levels of liver enzyme ALT (Fig 3.3A, 3.4A). Increased lipogenesis is a hallmark of MASLD/MASH, and we observed increased levels of both circulating triglycerides, as well as liver triglycerides (Fig 3.4C). Often, in patients of MASLD/MASH, high postprandial glucose levels are observed, suggesting the presence of impaired glucose metabolism and insulin resistance (Chang et al., 2022). In our obese mice, we found that administration of MASH diet did not worsen glucose tolerance or insulin tolerance (Fig 3.5). To further investigate the metabolic changes, we performed qPCR on the livers from these mice. We observed elevated expression of GLUT2 and GLUT1 transporters (encoded by *Slc2a2* and *Slc2a1*) in the liver (Fig 3.7). This indicates an enhanced capacity for glucose uptake and transport into hepatocytes. GLUT2 primarily facilitates glucose uptake in response to elevated blood glucose levels, whereas GLUT1 is responsible for basal glucose

uptake. Increased expression of these transporters may reflect a compensatory response to maintain glucose homeostasis in the context of altered metabolic conditions or insulin resistance. However, decreased expression of pyruvate kinase L/R (PKLR) suggests a decreased capacity for glycolytic flux and reduced conversion of glucose-derived substrates into pyruvate (Fig 3.7). This downregulation points to decreased phosphoenolpyruvate (PEP) to pyruvate conversion, suggesting its shunting towards alternate pathways, such as lactate production or gluconeogenesis. However, we observed no changes in circulating lactate or gluconeogenic genes such as *G6pc* and *Hnf4α*. However, *Ppargc1a* encoding for PGC-1α which promotes the expression of gluconeogenesis genes through FOXO1 and HNF4α was found to be significantly downregulated (Fig 3.7). Together, it can be concluded that obese mice develop an even worsened glucose metabolism. Leptin-deficient obese mice treated with STL1267 either q.d. or b.i.d. did not show any loss in adiposity as determined by their body weight. Though, there was a trending decline in b.i.d. mice (Fig 4.1A, Fig 4.9A). All circulating liver enzymes, including ALP, ALT, and AST were decreased in STL1267 treated mice irrespective of dosage (Fig 4.2, Fig 4.10). Once daily treatment was able to rescue the altered hepatic glucose uptake as evidenced by GLUT2 and GLUT1 (Fig 4.5). However, decreased expression of pyruvate kinase L/R (PKLR) was not rescued (Fig 4.5). Subsequently, no changes in circulating lactate or liver gluconeogenic genes such as *G6pc* and *Hnf4α* were observed (Fig 4.5). However, *Ppargc1a* encoding for PGC-1α remained severely downregulated (Fig 4.5). Increased dosage in b.i.d. group did not have significant changes on the liver transcriptome,

however, only GLUT1 and PKLR was observed to be rescued (Fig 4.13). Further, increased gluconeogenesis was observed with upregulation of HNF4 and G6PC (Fig 4.13). Neither dosage was able to rescue glucose tolerance and insulin resistance in these MASH obese mice (Fig 4.3, 4.11). Interestingly, in both q.d. and b.i.d. treated mice, glucose levels were increased post 30 minutes in q.d. and an overall increase as evidenced by AUC in b.i.d (Fig 4.3A, Fig 4.11A). No changes were observed in insulin sensitivity in either group (Fig 4.3B, 4.11B). This was expected, however, as the genetic mutation in leptin-deficient *ob/ob* mice leads to severe obesity, hyperphagia, and glucose and insulin metabolism impairment. They often display pre-existing hyperglycemia, and insulin resistance. Additionally, increased adiposity may affect administration, distribution, and absorption of glucose and insulin. Thus, making it difficult to detect subtler changes observed upon pharmacological intervention.

In genes that regulate lipid metabolism, we saw a significant increase in important genes such *fabp5, dgat2,* and *srebf1.* FABP5 is responsible in the uptake, utilization, and transport of fatty acids in the liver of MASH mice (Fig 3.6). DGAT2 is the enzyme that catalyzes the final step in triglyceride synthesis, and SREBF1 is the transcription factor responsible for genes involved in lipid synthesis. This is in agreement with triglyceride levels, which are increased in both circulation as well as liver, suggesting the presence of hyperlipidemia (Fig 3.4; C). STL1267 treatment was able to rescue lipid metabolism, by downregulating genes coding for fatty acid uptake (CD36, FAS), ACLY, SREBF1, DGAT2, ACACA, and PPARG

(Fig 4.4). Interestingly, this rescue was lost in b.i.d. group, where no changes were observed in the above genes, except decreased FAS and FABP5 (Fig 4.12). This could perhaps be explained by liver triglyceride levels, as increased dosage in b.i.d. group was able to reduce TG levels in the liver, and the transcription levels were perhaps normalized after, suggesting a suppression in lipid synthesis and increase in catabolism. However, there was continued repression of lipid synthesis genes in q.d. group and longer treatment would have perhaps yielded significant changes in lipid levels.

We also observed a significant increase in circulating total cholesterol, HDL and LDL in obese mice that were fed MASH diet (Fig 3.4; B). Transcriptionally, this was backed up by the increased expression of ApoB, which is important in the assembly and secretion of lipoproteins such as LDLs and their uptake by other peripheral tissues. Further, Srebf1 was upregulated as well, suggesting the upregulation of downstream genes it regulates in cholesterol biogenesis, namely HMG-CoA. While there was a trending increase in *Cyp7a1* and *Ldlr*, it did not reach statistical significance (p-value > 0.06) (Fig 3.8). STL1267 treatment (q.d. and b.i.d.) was able to rescue increased circulating total cholesterol, HDL, and LDL levels (Fig 4.2; B, Fig 4.10; B). In both q.d and b.i.d. group, genes encoding for enzymes in cholesterol biosynthesis such as HMGCR were downregulated (Fig 4.6, 4.14). CYP7A1 was upregulated in b.i.d. mice suggesting the increased shuttling of cholesterols for bile acid synthesis.

With this documented increase in lipids, fatty acids, and cholesterol, we wanted to investigate the possible changes in lipid catabolism via FAO. The upregulation of *Acox1* (encoding Acyl-CoA oxidase 1) and *Acadl* (encoding Acyl-CoA dehydrogenase, long chain) in the liver, suggests an increased capacity for fatty acid catabolism, potentially indicating a response to elevated fatty acid availability or increased energy demand (Fig 3.9). However, CPT1A is a key enzyme involved in the transport of long-chain fatty acids into the mitochondria for oxidation. Its downregulation suggests a reduced capacity for mitochondrial fatty acid uptake and oxidation (Fig 3.9). This coupled with the downregulation of PDK4 suggests a shift away from FAO as PDK4 in normal state inhibits pyruvate dehydrogenase (PDH), thereby reducing the conversion of pyruvate to acetyl-CoA for entry into the TCA cycle. This could perhaps be a compensatory mechanism for the reduced FA uptake in the mitochondria which precedes mitochondrial dysfunction, characteristic of MASLD to MASH progression. Overall, the observed changes in FAO indicate a complex reprogramming of hepatic lipid metabolism, with a potential shift towards increased reliance on glucose oxidation and altered fatty acid handling upon MASH induction. STL1267 treatment in these mice, reduces genes coding for ACADL, CPT2, and ACOX1 suggesting reduced fatty acid oxidation (Fig 4.7, 4.15). Further, in both q.d. and b.i.d. groups, MASH induced PDK4 and CPT1 downregulation was rescued, but not increased significantly. However, it is of note that PPARα expression was significantly increased in b.i.d. group suggesting continued fatty acid catabolism through oxidation (Fig 4.15).

Previous research has established the role of inflammation in MASLD/MASH. We were able to show upregulation of genes coding for various pro-inflammatory cytokines such as IL-1β and IFNγ (Fig 3.10). We did not see any significant changes in IL-6 transcript levels. Further, anti-inflammatory cytokines such as IL-10 remained unchanged. STL1267 administration revealed an almost complete absence of Il6, Il1β, NFκβ transcripts indicating a stark and unequivocal suppression of gene expression echoed in both q.d. as well as b.i.d. groups (Fig 4.8, 4.16).

Restoring leptin signaling in these leptin-deficient obese mice may ameliorate the observed alterations in gene expression, potentially mitigating metabolic dysfunction and improving lipid metabolism. Thus, correcting for leptin deficiency through the use of wild-type B6 mice is important for accurately characterizing the metabolic changes and identifying REV-ERB activation as a therapeutic for the management of metabolic disorders such as MASLD/MASH. In order to validate our findings, we replicated our experiment in a diet-induced obesity (DIO) model using wild-type B6 mice. Similar to our previous experiment in obese mice, we assessed the expression levels of key genes involved in liver metabolism. However, only q.d. treatment was employed. By using the DIO model in B6 mice, we aimed to validate the relevance of our findings in a different model of obesity and assess the robustness of our observations across different experimental paradigms.

Similar to obese mice, we saw increased mass in our DIO MASH mice (Fig 3.11; A). This was accompanied by a trending increase in the liver/body weight ratio of MASH diet mice (p value = 0.06) (Fig 3.11; C). Circulating levels of liver enzymes ALT and were trending up, however, were not statistically different. Further, we did not observe a significant increase in the circulating triglycerides, as opposed to liver triglycerides which were significantly increased (Fig 3.12; C). STL1267 treatment in B6 MASH mice did not rescue increased mass, however, significant reductions in circulating levels of ALP and ALT were observed (Fig 4.17; A). STL1267 treatment rescued the increased liver triglycerides (Fig 4.18; C). This is in agreement with the transcriptional profile of lipid metabolism genes in the liver. Genes coding for CD36, ACLY, FAS, SREBF1, DGAT2, ACACA as well as PPARG were significantly upregulated in B6 MASH mice (Fig 3.14) and were all consequently downregulated upon STL1267 treatment (Fig 4.20).

Unlike leptin deficient obese mice, MASH diet in B6 mice worsened glucose tolerance post 8 weeks of consumption, as expected (Fig 3.13; C). MASH mice showed increased glucose levels till 30 minutes after glucose administration. This was further extended to insulin resistance as well (Fig 3.13; E). MASH mice were unable to respond to insulin administration and showed increased glucose levels at 15 and 30 minutes. Similar to obese mice, STL1267 in B6 MASH mice did not have any effect on glucose tolerance (Fig 4.19; A). However, STL1267 in B6 MASH mice we observed that mice utilize insulin, as they recovered blood glucose faster 60 minutes post insulin administration (Fig 4.19; C). To further validate these

findings, we checked the glucose metabolic genes in the liver. Similar to obese mice we saw increased GLUT1 and GLUT2 expression (Fig 3.15). However, we also saw that MASH diet in B6 mice increased PGC-1α, HNF4α, PKLR, and G6PC, suggesting possible increased glycolytic flux, gluconeogenesis, as well mitochondrial metabolism. REV-ERB activation using STL1267 was able to reduce gene levels for GLUT2, G6PC, PKLR, PGC-1, as well as HNF4 (Fig 4.21).

We also observed a significant increase in circulating total cholesterol, HDL and LDL in B6 mice that were fed MASH diet (Fig 3.12; B). Transcriptionally, this was backed up by the increased expression of APOB, SREBF1, and ABCA1 (Fig 3.16). There was also a clear induction in *Cyp7a1* and *Ldlr*. Consistent with decreased TC, HDL, and LDL (Fig 4.18; B), STL1267 treated MASH mice had lower levels of transcript for HMGCR, CYP7A1, LDLR, APOB, and SREBF1 (Fig 4.22).

As for lipid catabolism, we saw a significant increase in genes coding for ACADL, CPT2, PDK4, CPT1A, PPARα, FABPs, and ACOX1 (Fig 3.17). The increased expression of all genes related to fatty acid metabolism and mitochondrial function in the liver suggests a shift towards enhanced fatty acid oxidation and mitochondrial metabolism in the liver. This metabolic adaptation may be driven by increased fatty acid availability, altered nutrient utilization, or metabolic demands, reflecting a complex interplay of physiological and metabolic factors influencing hepatic lipid metabolism. With STL1267 we were able to rescue compensatory

mitochondrial overload, and showed decreased ACADL, CPT2, PDK4, CPT1A, PPARα and ACOX1 (Fig 4.23).

As mentioned previously, these metabolic compensatory changes are followed by mitochondrial dysfunction and overload as the disease progresses in severity. This is often marked by inflammation and fibrosis. We observed a significant upregulation in genes coding for proinflammatory markers and cytokines such as NFκβ, IL1β, IL-6 and Casp-3 (Fig 3.18). Additionally, anti-inflammatory cytokine IL-10 was downregulated. STL1267 reduced IL-6, IL-1β, and NFκβ. IL-10 transcript was increased in treated group, but was not statistically significant (Fig 4.24).

Histopathological analysis reveals that MASH induction in obese mice induced reduced hypertrophy, the opposite was seen in B6 mice. This could be due to factors such as increased cell death and fibrosis, the opposite effect may be observed in WT mice, where MASH-induced inflammation and liver injury stimulate compensatory hepatocyte proliferation and hypertrophy. In the context of MASH, micro-steatosis is often associated with more severe liver pathology and inflammation compared to macro-steatosis. In obese mice, we observed increased micro-steatosis and reduced macro-steatosis. This could be explained by increased lipolysis or lipophagy. However, these changes though statistically significant, are too subtle to be biologically relevant. Nevertheless, STL1267 was able to rescue steatosis in both obese and B6 MASH models, consistent with reduced triglyceride levels.

Collectively, the observed changes suggest a metabolic shift that consequently contributes to an overall increase in cellular metabolism, reflective of the liver's effort to cope with lipid overload and metabolic stress in NAFLD mouse models (Satapati et al., 2012). Such metabolic alterations precede the loss in mitochondrial flexibility leading to mitochondrial dysfunction and severe MASH. REV-ERB activation using STL1267 mitigates this transition from metabolic alterations to mitochondrial dysfunction and severe metabolic-associated steatohepatitis (MASH) in our mouse models, by targeting mitochondrial function and metabolic flexibility. Furthermore, the pharmacological activation of REV-ERBα could also have systemic effects beyond the liver, influencing metabolic pathways in peripheral tissues such as skeletal muscle and adipose tissue. This systemic metabolic improvement may contribute to overall metabolic health and attenuate the progression of NAFLD to more severe stages, and needs to be investigated further.

Future Directions

Performing RNAseq and metabolomics on adipose and liver tissues will provide a multi-dimensional view of the molecular landscape underlying therapeutic effects of REV-ERB activation. RNAseq will allow us to identify differentially expressed genes (DEGs). This will shed light on key pathways and biological processes modulated by the REV-ERB activation, shedding light on its mechanisms of action,

in context of MASLD/MASH. Additionally, it will also offer insight into AT liver cross talk.

By the use of metabolomics on liver and AT from our mouse models, we will identify metabolic pathways that are perturbed in response to REV-ERB activation using STL1267. This holistic view of metabolic changes, combined with the gene expression data obtained from RNAseq, pwill provide a deeper understanding of the physiological consequences of treatment.

Further, pathway analysis and network modeling will help with the elucidation of complex interactions within major metabolic tissues such as AT and liver.

Investigating the interaction between REV-ERB and factor HIF-1α using ChiP qPCR will provide insights into their interactive effects on gene regulation. By analyzing the occupancy of REV-ERB on HIF-1α we can decipher the molecular mechanisms underlying their interaction and its impact on cellular processes. Our data suggests that REV-ERB regulates HIF-1α, which is purported to have mito-protective effects. Utilizing cell culture models, we aim to evaluate the impact of HIF-1α on mitochondrial function and integrity in hepatocytes.

Chapter Five – REV-ERB activation as a novel pharmacological approach for treating inflammatory pain

Makhija S, Griffett JD, Veerakanellore GB, Burris TP, Elgendy B, Griffett K. REV-ERB activation as a novel pharmacological approach for treating inflammatory pain. Front Pharmacol. 2023 Apr 19;14:1171931.
doi: 10.3389/fphar.2023.1171931. PMID: 37153791; PMCID: PMC10154555.

5.1. Introduction

Chronic pain affects the lives of people worldwide and has significant implications on healthcare (Eccles and Davies, 2021). Conventional therapeutics oftentimes are insufficient in long-term pain management and can result in an array of adverse effects (Janakiram et al., 2019). As pain accompanies a wide variety of chronic diseases and is highly subjective, it is important to target pathways that play a significant role in the development and maintenance of pain stemming from different conditions. The NLR family pyrin domain containing 3 (NLRP3) inflammasome has been implicated as a major driver of pain by increasing the processing of the pro-inflammatory cytokine, interleukin 1 beta (IL-1β) (Elzinga et

al., 2019). Chronic activation of the inflammasome leads to upregulation of NFκB-driven inflammation which results in the recruitment of additional inflammatory molecules and cells (e.g., mast cells, neutrophils, microglia, etc.) and the initiation of an inflammatory microenvironment. Numerous studies have shown that regardless of the pain pathology, chronic activation of NLRP3 is always a factor in the development and maintenance of pain (Ren and Torres, 2009; Zhou and Zhou, 2014; Muley et al., 2016; Sommer et al., 2018; De Prá et al., 2019; Elzinga et al., 2019).

REV-ERBα and REV-ERBβ (encoded by the genes *NR1D1 and NR1D2,* respectively) are members of the nuclear receptor superfamily of transcription factors (Raghuram et al., 2007). The REV-ERBs regulate a wide variety of physiological processes including circadian rhythm, lipid and glucose metabolism, and inflammatory pathways of the innate and adaptive immune systems. Both REV-ERBs are quite unique from the other nuclear receptors as they lack a carboxy-terminal activation of function-2 region from their ligand binding domains, and therefore can only act as a repressor of transcription by recruiting the NCoR (Figure 1A). Because of this, REV-ERB agonists enhance repression of direct target genes.

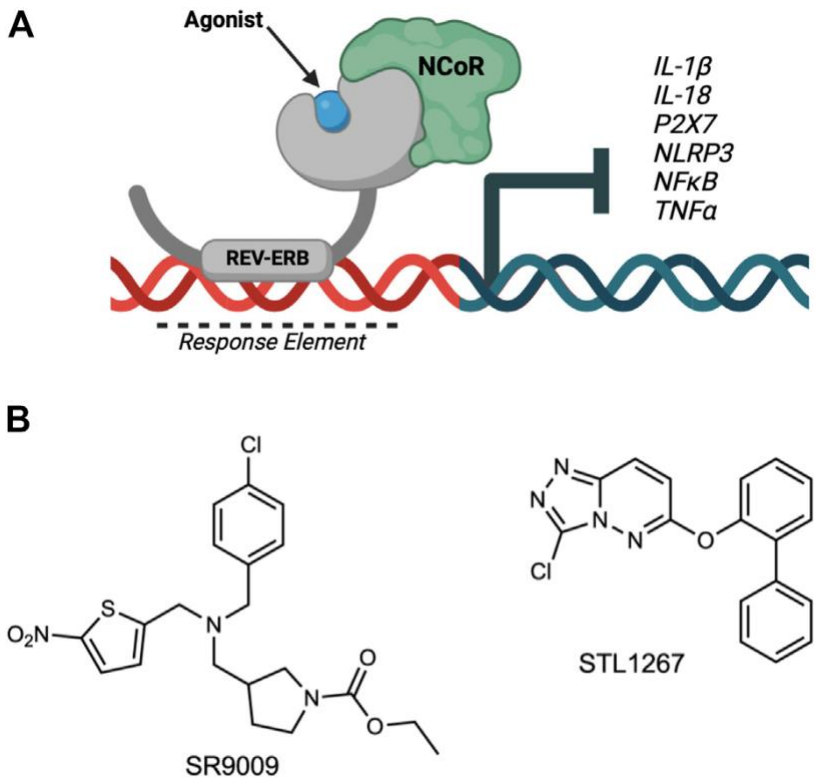

Figure 5.1 **Overview of REV-ERB regulation of inflammatory components involved in pain.** (A) The nuclear receptor REV-ERB recognizes sequences within the promoter of its target genes (Response Element) and binds DNA via its DNA-binding domain. Upon binding of a ligand, REV-ERB undergoes a conformational change and recruits the NCoR corepressor, causing the repression of transcription of its target genes including NLRP3, IL-1β, and other pro-inflammatory cytokines and pathway genes. (B) Structures of two REV-ERB agonists: SR9009 and STL1267.

REV-ERB activity can be modulated with small molecule ligands to drive changes in the transcription of its direct target genes. For example, several studies demonstrated that the REV-ERB agonist SR9009 can effectively suppress the transcription of *IL-1β* and *NLRP3,* two genes that are REV-ERB targets (Pourcet et al., 2018; Duez and Pourcet, 2021). Based on this role of REV-ERB in regulating inflammatory pathways, we sought to evaluate if suppression of the inflammasome via REV-ERB activation had analgesic potential.

Recently, we described a novel small molecule agonist for REV-ERB, STL1267, with greater potency and selectivity for REV-ERB than SR9009 (Murray et al., 2022). For our studies, we compared the STL1267 compound to the first-generation *in vivo* REV-ERB agonist, SR9009, to evaluate direct REV-ERB effects on inflammation and pain. In the current study, we first validated the previous work demonstrating that REV-ERB regulates inflammatory processes by confirming effects in bone marrow-derived macrophages in *Nr1d1* $^{-/-}$ mice, as well as in human monocytes. We then investigated whether pharmacological activation of REV-ERB by small molecule ligands (SR9009 and STL1267) could suppress activation of the inflammasome in human microglia cells, which are more relative to pain associated with nerve damage. Finally, we confirmed our findings in an acute inflammatory pain model to demonstrate that activation of REV-ERB has efficacy as an inflammatory pain therapeutic.

5.2. Results

5.2.1. REV-ERB agonists suppress pro-inflammatory cytokines and the NLRP3 inflammasome in LPS-stimulated macrophages.

Previous studies have shown that activating REV-ERB, either pharmacologically or by overexpression, can suppress IL-1β and other pro-inflammatory cytokines in several inflammatory models (Gibbs et al., 2012; Pourcet et al., 2018; Guo et al., 2019; Morioka et al., 2019; Hong et al., 2021). Conversely, genetic loss of function of REV-ERB leads to enhanced IL-1β expression. Here, we wanted to evaluate the efficacy of the novel REV-ERB agonist STL1267 to suppress the NLRP3 inflammasome in LPS-stimulated macrophages as compared to SR9009. First, we validated previous studies that demonstrated the loss of REV-ERBα led to an increase in the expression of pro-inflammatory molecules including NLRP3. We assessed the pro-inflammatory markers, *IL-1β*, *IL-18*, and *Nlrp3* in bone marrow-derived macrophages (BMDMs) from *Nr1d1* $^{-/-}$ mice and wild-type mice by QPCR. As shown in Figure 2A, mice lacking REV-ERBα had significant increases in the expression of the three pro-inflammatory genes, suggesting that the activation of REV-ERB suppresses inflammation.

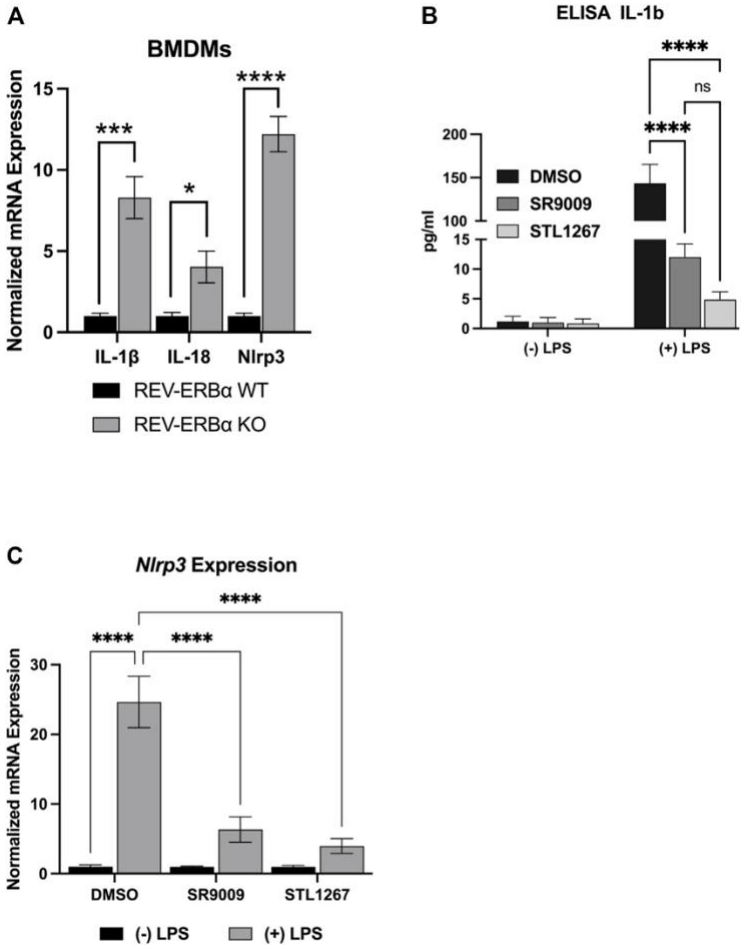

Figure 5.2 **In vitro model of REV-ERB anti-inflammatory actions.** (A) Mouse bone marrow derived macrophages from Nr1d1−/− (n = 7) and wildtype (n = 12) mice. Both male and female mice were used for this study and no sex-specific differences were noted. (B) IL 1β ELISA results for differentiated Thp-1 cells. (C) NLRP3gene expression results of the differentiated Thp-1 cells. Results were graphed and analyzed in Graphpad Prism by ANOVA and represented as Mean ± SEM.

We then investigated the action of SR9009 and STL1267 on suppression of the inflammasome by differentiating Thp-1 monocytes by priming with PMA, allowing the cells to recover in PMA-free media, then stimulating the cells with LPS and IFNγ. During the last 24-h of the recovery period, either DMSO, 10 μM SR9009, or 10 μM STL1267 was added to the media as a "pre-treatment." Control cells were pre-treated with compounds but not stimulated with LPS. We then evaluated IL-1β release by removing media and performing an ELISA. As Figure 2B shows, Thp-1 cells that did not receive LPS stimulation secreted low amounts of IL-1β regardless of the pre-treatment. As expected, we observed a significant increase in IL-1β in DMSO-treated LPS-stimulated cells. Moreover, the REV-ERB agonists SR9009 and STL1267 both significantly reduced the amount of secreted IL-1β in the LPS-stimulated cells, validating that REV-ERB activation is anti-inflammatory. Total RNA was isolated from the same cells to evaluate changes in gene expression of various pro-inflammatory cytokines and the NLRP3 inflammasome. Figure 2C shows that upon LPS stimulation of the cells, the expression of *Nlrp3* is significantly increased however both REV-ERB agonists significantly suppress the expression of the inflammasome in this model.

5.2.2. NLRP3 inflammasome activation is suppressed in human microglia by REV-ERB agonists.

Once we validated previous studies that demonstrated REV-ERB regulates inflammasome activation and expression of several pro-inflammatory molecules,

we then evaluated the anti-inflammatory activity in a human microglia cell line, HMC3. As resident macrophages of the central nervous system (CNS), microglia have been implicated in the activation and sensation of pain in humans (Clark et al., 2010; Rhie et al., 2020; Ren and Illes, 2022). We hypothesized that the suppression of these factors via REV-ERB pharmacological activation may provide analgesic effects by reducing inflammation. To test our hypothesis that REV-ERB agonists suppress inflammation in microglia, we performed a similar experiment as described with the Thp-1 cells.

HMC3 cells were pre-treated with either DMSO, 10 μM SR9009, or 10 μM STL1267 for 24-h, then stimulated with LPS for an additional 24-h. Media was collected for ELISA analysis while the cells were fixed and immunostained for NLRP3 or collected for QPCR analysis. As shown in Figure 3A, we observed a significant decrease in NLRP3 staining in both the SR9009 and STL1267-treated cells as compared to DMSO treated cells, which is consistent with our previous Thp-1 cell data. We also observed no significant changes in cells without LPS-stimulation (Supplementary Figure S1). A control containing no primary antibody was also performed to confirm the green signal was due to the presence of NLRP3 (Supplementary Figure S2). The media was collected from all the plates and we performed the Pro-Quantum IL-1β immunoassay to evaluate whether the REV-ERB agonists could suppress the secretion of IL-1β, a key mediator of inflammation and NLRP3 activation. We found that 10 μM SR9009 significantly suppressed the secretion of this cytokine following LPS stimulation, and STL1267 pre-treatment reduced IL-1β to levels consistent with no LPS

stimulation (Figure 3B). This clearly shows that the potency and efficacy of the STL1267 is superior to that of SR9009 in this model, consistent with our previous pharmacological characterization of STL1267 (Murray et al., 2022). We then performed QPCR to evaluate the expression of *NLRP3, IL-1β,* and *IL-18* in the cells following REV-ERB agonist treatment. As shown in Figure 3C, both REV-ERB agonists significantly suppress the expression of *NLRP3, IL-1β,* and *IL-18* in the LPS-stimulated cells. Our data suggests that not only is REV-ERB a regulator of inflammation in the periphery as described by numerous labs, the pharmacological activation of REV-ERB has significant effects on suppressing inflammation in the CNS, which may play a role in pain and other chronic inflammatory conditions (Gibbs et al., 2012; Amir et al., 2018; Pourcet et al., 2018; Baxter and Ray, 2019; Chang et al., 2019; Amir et al., 2020; Hong et al., 2021; Gray and Gibbs, 2022).

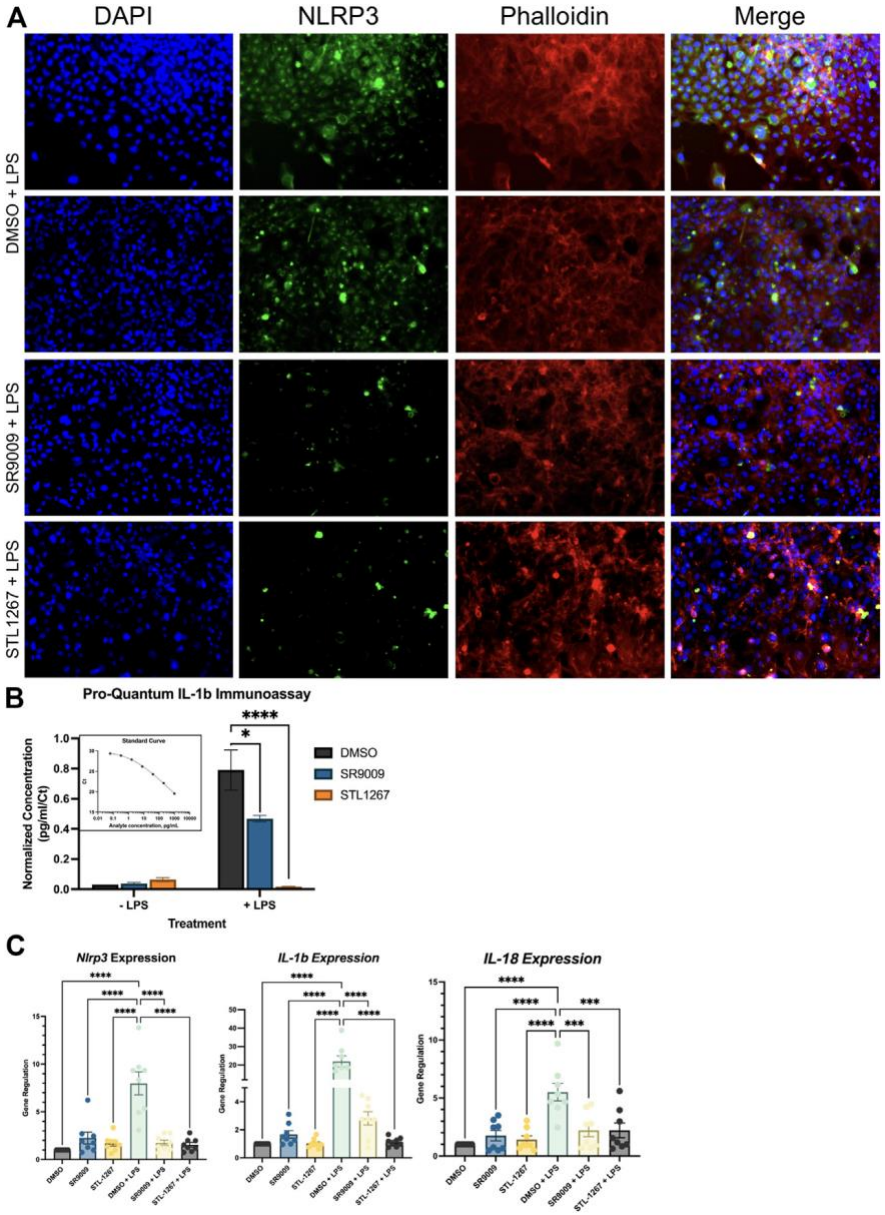

Figure 5.3 **REV-ERB agonists have an anti-inflammatory effect on a human microglia cell line.** (A) Immunostaining of LPS-stimulated HMC3 cells treated with either DMSO, SR9009, or STL1267. Cells were immunostained for NLRP3 (green) and counterstained with DAPI (Blue) and Actin (Phalloidin; Red) to verify cellular occupancy of NLRP3. (B) ELISA assay evaluating the secretion of IL-1β into the cell culture media. Results are shown as pg/mL normalized to Ct value of IL-1β per the ThermoFisher protocol using the Connect cloud software and graphed in Graphpad Prism. (C) Gene expression results for NLRP3, IL-1β, and IL-18. For all cell-based experiments, an n = 6 for each condition was used. Experiments were performed on three different occasions by different researchers, and the results were analyzed separately by ANOVA and represented by Mean ± SEM.

5.2.3. A single dose of REV-ERB agonist reduces pain behavior in Sprague-Dawley rats

Given that inflammation plays a major role in the development of pain conditions, we sought to investigate whether suppressing the NLRP3 inflammasome via the REV-ERB agonists SR9009 and STL1267 will be analgesic in an inflammatory pain model. To perform these assays, we used 21 female Sprague-Dawley rats and assessed baseline sensitivity to both mechanical and thermal stimuli by Von Frey filament assay and hot plate. The following day, rats were administered either vehicle, SR9009, or STL1267 via intraperitoneal injection, rested for 1 h, then administered λ-Carrageenan subcutaneously into the left footpad to induce the acute inflammatory response (saline was injected into the right footpad as an internal control) (Allen and Yaksh, 2004; McCarson, 2015). This method produces a localized inflammatory response characterized by redness, swelling, het, reduced function, and hypersensitivity (as demonstrated by hyperagesia and/or allodynia), and can be used to assess efficacy of anti-inflammatory molecules (Fehrenbacher et al., 2012). At 4-, 24-, and 48-hpi, rats were assessed for mechanical and thermal hypersensitivity, and footpad thickness as shown in Figure 4A.

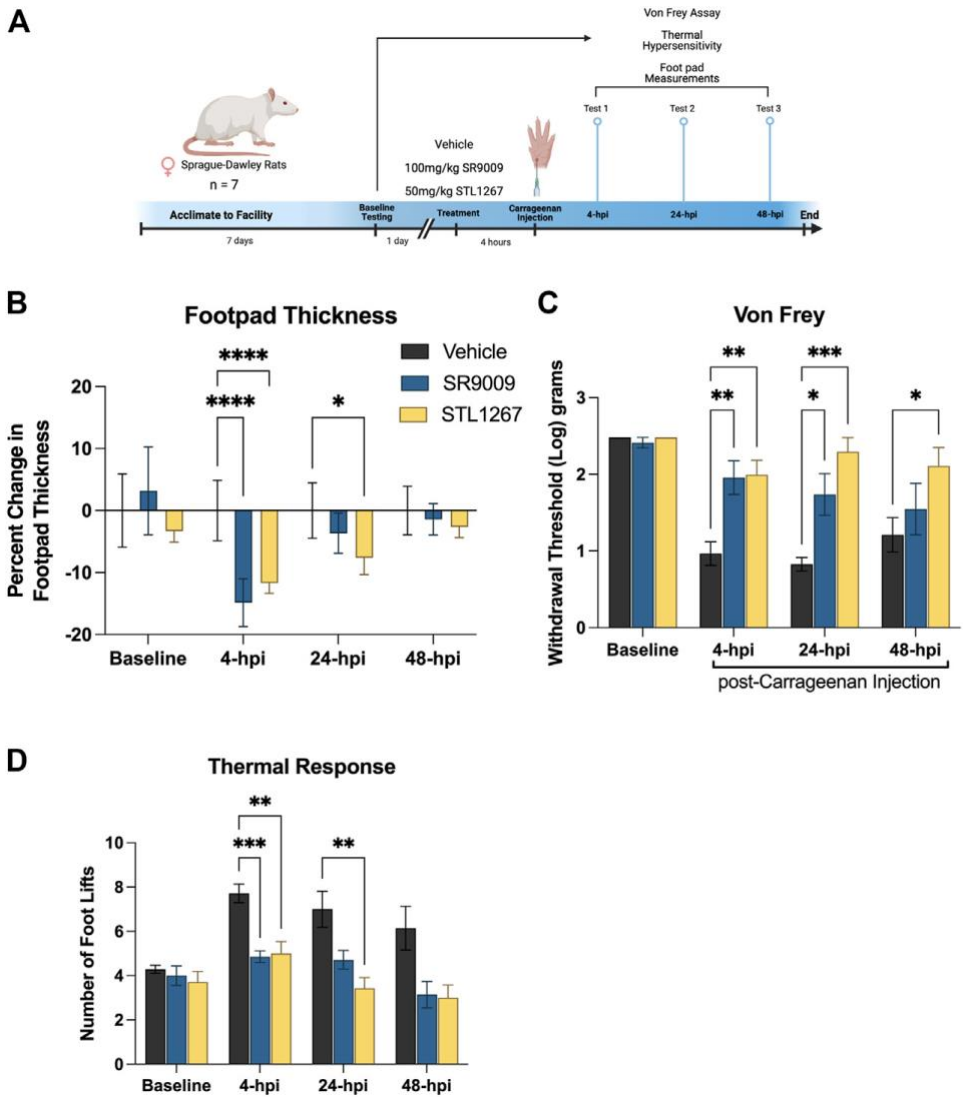

Figure 5.4 **REV-ERB agonists suppress pain behavior in a rat model of acute inflammatory pain.** (A) Schematic of the rat model used to evaluate the efficacy of REV-ERB agonists SR9009 and STL1267 in acute inflammatory pain. (B) Measurement of the inflammatory response following a single injection of REVERB agonist (i.p.) and carrageenan injection in the rat hind paw.Measurements were taken with a digital caliper and normalized as the change in thickness as a percentage to the baseline measurements. (C) Mechanical hypersensitivity was measured using a Von Frey filament. (D) Thermal hypersensitivity was also tested on these animals following a single injection of REV ERB agonist (i.p.) and evaluated by recording the number of foot lifts over a 30-s interval. Data was analyzed in Graphpad Prism using ANOVA with Dunnett's post-hoc test and represented by Mean ± SD.

Measurements of footpad thickness show that a single administration of REV-ERB agonist (either SR9009 or STL1267) was sufficient to reduce footpad inflammation driven by *λ*-Carrageenan injection at 4-hpi (Figure 4B). STL1267 continued to suppress footpad inflammation at 24-hpi, suggesting that it may be more efficacious at the 50 mg/kg dose as compared to SR9009 which was given at 100 mg/kg, as determined by our previous work with these compounds (Solt et al., 2012; Murray et al., 2022). By 48-hpi, there was no significant change in footpad thickness as compared to the vehicle control group, which was expected given the rats only received a single dose of REV-ERB agonists and the compounds should have been completely metabolized by this time.

Mechanical hypersensitivity evaluated by Von Frey filaments is a standard assay performed to evaluate analgesic activity of compounds (Allen and Yaksh, 2004).The withdrawal threshold measurement at baseline suggests that there were no differences among groups, however at 4- and 24-hpi both groups treated with REV-ERB agonists displayed significantly higher withdrawal thresholds as compared to the vehicle control group (Figure 4C). At 48-hpi, although footpad thickness was not significantly affected, the group administered the single dose of STL1267 displayed a significant increase in paw withdrawal threshold as compared to the vehicle control group, suggesting that the administration of REV-ERB agonists may provide analgesic activity in inflammatory pain models.

Evaluating the response to a thermal stimulus represents an additional aspect of quantitative sensory testing, which may facilitate the findings of our REV-ERB compounds in a translational manner. Thermal hyperalgesia is a common pathology in a number of human pain states, and is often used to evaluate novel small molecules. We evaluated the thermal response threshold of the animals using a hotplate set to 55°C. The number of foot lifts over a thirty-second period was recorded and shows that administration of REV-ERB agonists significantly reduced the number of foot lifts at 4-hpi (Figure 4D). At 24-hpi, SR9009 reduced the number of foot lifts but was not significant compared to the vehicle group. However, STL1267 did continue to show efficacy in this assay at 24-hpi. By 48-hpi, the number of foot lifts was still less than the control group although not significant.

5.3. Discussion

It is well known that chronic pain conditions are associated with inflammation and represents a major healthcare concern worldwide (Chen et al., 2021). Recent evidence points to chronic inflammation due to inflammasome activation in local inflamed tissues, peripheral nerves, or even the CNS (spinal cord) as a driver of the initiation and maintenance of chronic pain (He et al., 2019; Chen et al., 2021; Griffett, 2022). One such pro-inflammatory driver of pain is the cytokine IL-1β, which can incidentally contribute to pain by both increasing local inflammatory responses and by direct activation of nociceptors to elicit action

potentials which initiates pain sensations (Chen et al., 2021). The activity of IL-1β is tightly regulated via the NLRP3 inflammasome. The inflammasome is a large multicomponent molecule that consists of NLRP3, ASC adaptors, and caspase enzymes, and is present primarily in immune cells including macrophages and microglia, although several recent studies have demonstrated its presence in neurons of the sensory nervous system (Baldwin et al., 2016; Caseley et al., 2020). The activation of the NLRP3 inflammasome is mediated through toll-like receptors (TLRs) and various cytokine receptors resulting in the NFκB-mediated upregulation of NLRP3 and IL-1β transcription. The chronic activation of NLRP3 has been implicated in a variety of disorders including atherosclerosis, auto-immune disorders (e.g., multiple sclerosis), and Alzheimer's disease (Eren and Özören, 2019).

Previous studies have shown a direct regulation of both NLRP3 and IL-1β by REV-ERB. In collaboration with the Duez and Stalls group, we determined that there are several REV-ERB response elements in the promoter of the *Nlrp3* gene in mice, with corresponds with the human genome (Pourcet et al., 2018). The NLRP3 inflammasome is tightly regulated by a variety of physiological factors including circadian rhythms, as a direct result of REV-ERB (Duez and Pourcet, 2021). This work not only validated the direct control of inflammation in macrophages by REV-ERB, but also addressed the concepts that inflammation is a highly regulated process. Dysregulation of inflammatory mediators including NLRP3 can lead to a variety of diseases. Understanding the role that chronic

NLRP3 inflammasome plays in the initiation and maintenance of pain conditions, we sought to evaluate whether the pharmacological activation of REV-ERB with small molecule agonists alleviated pain behaviors.

We first validated previously published data to confirm that loss of REV-ERB leads to increases in inflammatory mediators by evaluating the differences in pro-inflammatory cytokines (*IL-1β* and *IL-18*) and *Nlrp3* gene expression in mouse BMDMs from both REV-ERBα-null animals and wildtype (C57Bl/6J) animals. We confirmed that the loss of REV-ERB in these animals correlated with an increase in inflammatory molecule expression by QPCR. These results allowed us to develop our hypothesis that REV-ERB may play a role in pain driven by inflammation. We then wanted to evaluate the effects of pharmacological activation of REV-ERB in human monocytes, since these cells can recapitulate NLRP3 activity as seen in a variety of inflammatory diseases. We therefore used a standard procedure of differentiating Thp-1 cells towards an inflammatory macrophage phenotype and evaluated the effects of our small molecule REV-ERB agonists on inflammatory mediators. Our results not only validated previously published results demonstrating the anti-inflammatory effects of REV-ERB agonist SR9009, it also demonstrated that the new compound, STL-1267, has greater efficacy in these models as compared to SR9009 (Morioka et al., 2016; Morioka et al., 2021; Murray et al., 2022).

Since we are interested in the potential analgesic properties of REV-ERB agonists, we then decided to evaluate the effects on inflammatory molecules in a human microglia cell line. Microglia activation has been implicated as a key driver of a variety of pain conditions including chemotherapy-induced neuropathy, generalized inflammatory pain, migraine, and diabetic peripheral neuropathy pain (Sommer et al., 2018; Morioka et al., 2021). Upon nerve injury, microglia are capable of surrounding cell bodies of neurons and dorsal root ganglia and serve as a source of inflammatory mediators (e.g., IL-1β, IL-18, TNF-α, chemokines, etc.) thereby directing a neuroinflammatory response. Without access to human primary microglia, the HMC3 cell line provides a translational approach to test whether the compounds can suppress neuroinflammation. Immunostaining for NLRP3 in these cells displayed a significant reduction of NLRP3 expression, suggesting that pharmacological activation of REV-ERB with small molecules can suppress NLRP3 activity in microglia. This finding has implications in numerous diseases in which microglia play a key role. We also compared expression of NLRP3 to cells that were not stimulated with LPS to confirm the immunostaining methods. While these results are clear, we also confirmed the reduction of NLRP3 expression by evaluating the secretion of IL-1β by ELISA as well as determined that the REV-ERB agonists downregulated the expression of *NLRP3*, *IL-1β,* and *IL-18* by QPCR from these cells. From our results, we confirmed previous data suggesting that REV-ERB directly regulates the expression of *NLRP3* and hypothesized that if REV-ERB agonists can suppress

the activation of inflammatory microglia, then we may observe analgesic activity in an inflammatory pain model.

To test this hypothesis, we contracted a research organization to blindly perform an acute inflammatory assay on rats in which the rats would only receive a single intraperitoneal injection of either vehicle, SR9009, or STL1267 an hour prior to carrageenan footpad injection. The CRO routinely performed these assays in rats, and this provided an additional model to validate the effects of REV-ERB activation in inflammatory pain, allowing us to confirm the translational value of REV-ERB. STL1267 is more soluble and stable in the vehicle as compared to SR9009, has increased potency as characterized in radioligand binding assays and luciferase co-transfection assays, and has improved pharmacokinetic properties and half-life (Murray et al., 2022).

The mechanical Von Frey test is a widely used method to evaluate mechanical allodynia in laboratory animals and remains to be the gold standard in determining mechanical thresholds in pain models. Likewise, the hotplate method can be used to evaluate heat thresholds (hypersensitivity) in animal models. Since a constant heat stimulus is applied, several nocifensive behaviors were used to evaluate the analgesic potential of the REV-ERB compounds including licking, jumping, hind paw withdrawal, and leaning. We found that in the acute inflammatory model, a single dose of REV-ERB agonist was sufficient to reduce the initial inflammation that occurred as a result of footpad λ-Carrageenan

injection. Interestingly, we observed significant differences in the withdrawal threshold following the carrageenan injection in both treatment groups suggesting that the compounds had an analgesic effect in the mechanical Von Frey assay. A similar effect was found in the thermal response assay, confirming our hypothesis that REV-ERB mediated repression of inflammatory processes has analgesic activities.

Pain is a multifaceted and diverse problem that can be attributed to a variety of pathologies. Likewise, evaluating pain in animal models presents some difficulties as we are limited to evaluating behaviors to assess pain levels. However, these models have provided key data that suggests there is translational value in targeting the REV-ERB receptor for inflammatory pain. While considerably more work needs to be performed to evaluate the role that REV-ERB plays in analgesia, we believe that this may have potential therapeutic implications in pain driven by inflammatory processes. Here, we explored how pharmacological activation of REV-ERB effects inflammatory processes of pain, mainly via macrophage and microglial-type processes of activating the NLRP3 inflammasome. These compounds will need to be explored in the future to evaluate the efficacy of analgesia in pain models less dependent on inflammatory processes, and the mechanisms involved are yet to be understood.

Given the issues of opioid misuse worldwide, it is imperative that new, non-opioid, effective therapeutics for chronic pain are developed and evaluated. One

area that will need to be evaluated in the future is whether REV-ERB compounds that have efficacy in pain models affect the addiction or reward pathways. While we are not able to perform these experiments currently, we have previously published data that demonstrates the SR9009 series of REV-ERB agonists are non-addictive in a conditioned place preference (CPP) assay (Banerjee et al., 2014). That data also confirmed an “anti-addictive” effect of combining a REV-ERB agonist with cocaine in the CPP assay, suggesting that targeting REV-ERB for analgesia may be a safer alternative than opioid therapy (Banerjee et al., 2014). Further work in this area will need to be performed. Additionally, it is important to note that animal models have successfully predicted the usefulness of several commonly used treatments for pain including ibuprofen and morphine. The human processing and interpretation of pain is different from the animals commonly used in the laboratory. Likewise, disparities in therapeutic efficacy between rodents and humans may be attributed to differences in pharmacokinetics/pharmacodynamics (PK/PD) between species (Muley et al., 2016). While our current understanding of the translational value and predictive capacity of these compounds is limited, this work provides important biological information depicting the role that the nuclear receptor REV-ERB plays in inflammatory pain. Overall, the data presented here suggests that pharmacological activation of REV-ERB with small molecule ligands may have analgesic activity in models of acute inflammatory pain.

Chapter Six: Materials and Methods

6.1 Cell culture

HepG2 liver hepatocarcinoma cell line was purchased from American Type Culture Collection (Rockville, MD). The cells were maintained in Eagle's Minimum Essential Media (EMEM) (Cellgro) supplemented with 10% fetal bovine serum, and ITS. RAW 264.7 cells and LX-2 cells were cultured in DMEM supplemented with 10% fetal bovine serum. Where mentioned, RAW cells were stimulated with 100ng/mL LPS for respective timepoints. The human monocyte cell line, Thp-1, was purchased from ATCC (Catalog #TIB-202), maintained in a humidified incubator at 37°C with 5% CO2, and cultured in antibiotic-free RPMI media supplemented with 10% FBS. Cells were tested for *mycoplasma* regularly as a quality control.

To differentiate Thp-1 cells, cells were primed for 24 h in media supplemented with Paramethoxyamphetamine (PMA; Sigma P1585). After priming, cells were washed and plated in fresh PMA-free culture media in 100 mm polystyrene dishes for 72 h. For the last 24-h, dimethylsulfoxide (DMSO), SR9009 (10 μM), or STL1267 (10 μM) was added to the media as a "pre-treatment." The media was replaced with culture media containing 20 ng/mL interferon gamma (IFNγ) and 250 ng/mL lipopolysaccharide (LPS) for 48 h.

To determine whether SR9009 or STL1267 could suppress the release of IL-1β, we performed an ELISA (ThermoFisher A35574) as per manufacturer's protocol (*n* = 6) from media removed from the cell culture dishes. For gene expression analysis, total RNA was isolated from the cells using Qiagen RNeasy kit per manufacturer's protocol. Bio-Rad iScript cDNA synthesis kit was used to reverse transcribe up to 1 µg of cDNA for QPCR analysis using SYBR green (Invitrogen Power SYBR) using the ddCt method on the QuantStudio5 384-well QPCR system (Applied Biosystems). Genes normalized to 36b4 housekeeping gene for all experiments using fold-change analysis and plotted on Graphpad Prism software.

The human microglia cell line, HMC3, were a gift from Dr. Rajesh Amin (Auburn University). Cells were cultured in DMEM with 10% FBS (Corning) and 2.5 mM L-Glutamine (Gibco) without antibiotics and maintained in a humidified chamber at 37°C with 5% CO_2. Cells were tested for *mycoplasma* regularly as a quality control. Cells were seeded in 12-well tissue culture-treated plates (Corning) at 1,00,000 cells/mL in normal cell media. The following day, cells were pre-treated with either DMSO, SR9009, or STL1267 at 10 µM and incubated overnight. The next day, cells were stimulated with 100 ng/mL LPS or Media (control) in the continued presence of compound treatment. Media was collected the following day for ELISA analysis and cells were either immunostained or collected for QPCR as described above.

HepG2 cells cultured in EMEM, were supplemented with additional lipids, cholesterol, and high glucose to make them de-novolipogenic. Bodipy lipid staining was performed as per manufacturer's instructions where mentioned.

Primary human hepatocytes were obtained from AnaBios and cultured per manufacturer's instructions in media provided by manufacturer. (1141; AnaBios)

6.2 Seahorse XFp Metabolic Flux Assays

80,000 cells were seeded in each well of the XFp mini cell culture plate in 200uL of 10% DMEM, and incubated overnight at 37C 5% CO2. The top and bottom wells were left with no cells to use as background correction. The cells were treated with respective treatments, as mentioned. The culture was replaced with 180uL of XF assay medium and incubated for 1 hr at 37C without CO2. Glycolytic stress test or MitoStress test was performed per manufacturer's instructions. (103010, 103017; Agilent)

6.3 Glucose uptake assay

Glucose uptake was measured in HepG2 cells according to manufacturer's instructions using Glucose Uptake-Glo assay. (J1341; Promega)

6.4 DCFDA/MitoSOX

100,000 cells were seeded in each well of a 6well plate, and allowed to incubate overnight at 37C, 5% CO2. The cells were then treated as mentioned. 500uL 25uM

H2DCFDA in PBS/ 1uM of MitoSOX Green was added to the wells, and incubated protected from light at 37C, nonCO2. The cells were washed thrice with warm PBS, and counterstained with DAPI. Images were acquired immediately using Discover Echo Revolve microscope.

6.5 Immunofluorescence staining

Following removal of the cell media, cells were rinsed three times with cold 1X PBS, then fixed with 4% paraformaldehyde (PFA) in phosphate buffered saline (PBS; pH 7.4) for 10 min at 37°C. PFA was removed, and the cells were gently washed three times with 1X PBS. Cells were permeabilized by incubating in 0.1% Triton X-100 in 1X PBS at room temperature for 15 min. Following permeabilization, cells were again washed in 1X PBS three times then blocked in 2% BSA in 1X PBS at room temperature for 1 h. Cells were stained for NLRP3 (ThermoFisher MA5-32255) or αSMA (19245T, Cell Signaling Technology). Cells were washed three times with 1X PBS then incubated with secondary antibody (per manufacturer's protocol; ThermoFisher A11008) and counterstained with phalloidin where mentioned (ThermoFisher B3475) in 0.1% BSA in 1X PBS for 45 min. Cells were washed three times with 1X PBS and fluoromount media (ThermoFisher P36971) was added to each well to cover the cells. The Discover Echo Revolve microscope system was used to image the cells.

6.6 RNA sequencing and data analysis

Total RNA from HepG2 and LX-2 were extracted using RNeasy plus Universal Kits (QIAGEN, MD). The quality of RNA was assessed before being processed for library preparation using Bioanalyzer (Agilent Technologies). The whole transcriptome was amplified, and the library was constructed using TruSeq Stranded mRNA (Illumina; San Diego, CA). Quantitative assessment of library was done using Qubit 2.0 fluorometer (Invitrogen) and evaluated on the high-sensitivity DNA chip (Agilent Technologies). Libraries were sequenced on a NovaSeq 6000 platform (Illumina) using a pair-end 50 bp sequencing strategy. RNA sequencing data were preprocessed and analyzed using the Picard-STAR-limma pipeline. Raw read counts and fragments per kilobase of transcript per million (FPKM) mapped reads abundance were estimated at the transcript and gene levels. Principal component analysis (PCA) was used to identify outliers. Both upregulated and downregulated gene sets are reported on three GO subcategories: biological process (BP), cellular component (CC), and molecular function (MF). FDR q-values were estimated to correct the *P*-values for the multiple testing issue. Data was plotted at a fold change cut off of 1.5.

6.7 Animals

Obese leptin deficient (ob/ob), WT C5BL6 (B6) mice, and *Nr1d1* knockout mice were purchased from Jackson Laboratory (Bar Harbor, ME). All mice were housed and maintained in Washington University in St. Louis and Auburn University College of Veterinary Medicine Animal Housing Facility. Experimental protocols

were approved by the Animal Care and Use Committee of the Auburn University, Auburn, AL, and Washington University in St. Louis. Bone marrow-derived macrophages (BMDMs) were collected following rapid cervical dislocation from femurs and tibias and immediately analyzed by quantitative polymerase chain reaction (QPCR).

6.8 MASH Model

Upon receipt, 2 mice were housed in each standard cage with huts and placed on MASH diet (D09100301; Research Diets) or calorie matched control diet (S09100304; Research Diets) (Trevaskis et al., 2012). Mice were maintained on this diet throughout the experiment. Mice were handled and weighed weekly while acclimating to the diet. After 5 weeks, mice were randomly assigned into groups (n = 6-10) and dosing was started. Mice were weighed daily, and food-intake was monitored weekly. At the termination of the study, mice were fasted and euthanized by CO_2 and blood was collected by cardiac puncture for clinical chemistry analysis at Scripps Florida Metabolism Core (Roche COBAS instrument) and metabolic analysis (Stanbio). Tissues were collected and flash-frozen in liquid nitrogen for gene expression, or placed in 10% neutral buffered formalin (NBF) (16004119; VWR) for paraffin-embedding (Auburn University Histology) or 4% Paraformaldehyde in PBS (PFA) for cryo-sectioning.

6.9 Compounds and Dosing

STL1267 was formulated as 50mg/kg at 10mg/ml in 10% DMSO, 10% Tween-80 (Sigma), 80% PBS. Both vehicle (10% DMSO, 10% Tween 80 (Sigma), 80% PBS) and STL1267 were filter sterilized (Millipore Steriflip) prior to dosing. Mice were given once and twice daily i.p. injections within two hours of “lights on” (ZT0-ZT1) and 2 hours before “lights off” (ZT10-ZT12). Dosing was performed for 5 weeks by the same researcher. SR9009 was formulated as previously published (Solt et al., 2012).

6.10 λ-Carrageenan injections for acute inflammatory pain

All animal housing and research procedures involving rats were done at CARE Research, LLC. The standards for animal husbandry and care followed are those found in the Guide for the Care and Use of Laboratory Animals, eighth edition, Revised 201 (the Guide). Animal welfare for this study was in compliance with the U.S. Department of Agriculture’s (USDA) Animal Welfare Act (9 CFR Parts 1, 2, and 3), the Guide and CARE Research SOPs. Twenty-one female Sprague-Dawley rats were purchased from Charles River and allowed to acclimate to the testing facility for 7 days. Prior to dosing, all rats were subjected to baseline withdrawal response behavior testing (Von Frey filament and thermal response threshold to a heat source) and footpad thickness measurements using a digital caliper on the left hindfoot. Body weights were recorded pre-dose to determine appropriate dosing volumes. On the first day of the experiment, rats were administered a single dose of either vehicle control (10% DMSO; 12%

CremophoreEL; 78% PBS), 100 mg/kg SR9009, or 50 mg/kg STL1267 via intraperitoneal injection. Dosing was determined by our previous work in which we evaluated different vehicles and performed pharmacokinetic analysis (Murray et al., 2022). Injection of compounds occurred as close to “lights on” as possible (i.e., 7 a.m.). One hour after compound administration, rats were given an injection of *λ*-Carrageenan into the left hind paw (1cc syringe loaded with 100ul of 2.0% carrageenan (w/v), subcutaneous injection into plantar footpad) under light isoflurane anesthesia to induce the inflammatory response. Since *λ*-Carrageenan is reported to induce peak inflammatory response within 3–5 h, the first set of testing occurred within this period. Testing then occurred again at approximately 24 h post-injection (hpi) of λ-carrageenan and finally at approximately 48-hpi.

6.11 Von Frey filament testing

Withdrawal responses were measured using Von Frey filaments at the injection site at baseline testing, ∼4-hpi, ∼24-hpi, and ∼48-hpi for all 21 rats. The “ascending stimulus” method was used to determine an estimate for the mechanical threshold. For testing, the rats were placed in clear metabolism cages with the base removed to give access to the wire mesh floor. While in the testing chamber, Von Frey filaments were applied to the plantar surface of the injected hind paw in a series of ascending forces (von Frey filaments are plastic hairs of calibrated diameters, 5 cm long and are fixed on hand-held applicators). The chosen filament was applied to the plantar surface of the hind left paw until the filament was seen to bend. The procedure was repeated five consecutive times on

the left hind foot of each animal. The expected response was a paw withdrawal, sudden flinching, or paw licking. The response was considered positive if at least three expected responses were observed out of five trials. The procedure was started again on each animal with the next filament of greater force. The procedure was repeated until a rat gave a positive response on two consecutive filaments. Once a positive response was given on two consecutive filaments, testing was stopped on that animal. The gram value of the lower filament that gave a positive response was considered the paw withdrawal threshold for the animal.

6.12 Thermal response threshold to a heat source (Hot plate)

In this test, the surface of the heat source was heated to a constant temperature of approximately 55°C verified by an infrared thermometer. A large glass beaker (10,000 mL) was placed on the heat source and the bottom of the beaker measured for temperature with the infrared thermometer. Each rat was placed into the beaker and a timer was activated. Each rat remained on the heat source for 30 s. During that time, the number of times the carrageenan injected hind left foot was lifted from the heat source was recorded. If there was no response observed by 30 s, the test was stopped, and the rat returned to its cage.

6.13 Footpad thickness measurements

Footpad thickness was measured from the top of the foot to the base of the central pad by digital calipers.

6.14 Liver Biochemical Assessment

Free fatty acids and triglycerides were measured in the liver samples per manufacturer's instructions. Briefly, 50mg of liver tissue was lysed in RIPA buffer and homogenized using a tissue homogenizer. The lysate was used fresh to measure free fatty acid and triglyceride content. (2100430; Stanbio) (K612; BioVision)

6.15 ipGTT and ipITT

For intraperitoneal glucose tolerance test (ipGTT), mice were transferred to clean cages and fasted for 6 hours. Mice were weighed, baseline blood glucose was taken, then mice were given either an injection of glucose solution in PBS (2g/kg body weight) or Insulin (0.5U/kg) in PBS. Blood glucose levels were subsequently repeated at 15-, 30-, 60-, 90-, and 120-minutes following the injection of glucose. Mean blood glucose levels (mg/dL) are reported as well as the area under the curve (AUC) which was analyzed by two-tailed student's t-test in Graphpad prism. Following the ipGTT, mice were given access to food *ad libitum*.

6.16 Histological analysis

Formalin fixed liver tissues were processed, and paraffin embedded. 4 microns thick, hematoxylin and eosin (H&E) and Gomori's trichrome sections were used for evaluation. Liver slides were scanned using the Aperio ScanScope scanner

(Vista, CA). A board-certified pathologist evaluated liver H&E slides based on a modified NAFLD scoring system for rodent models (Liang et al., 2014). Evaluation criteria included macrovesicular steatosis, microvesicular steatosis, hepatocellular hypertrophy, and inflammation.

6.17 Gene Expression

Total RNA was isolated from liver using the trizol (Invitrogen) method (Griffett et al., 2013). Samples were analyzed by QPCR using Fatty Liver and Fibrosis QPCR array plates (Bio-Rad; 384-well format) and PowerUp SYBR reagent (A25778; Thermofisher Scientific) per manufacturer's protocol. Data was analyzed on the PrimePCR software supplied by Bio-Rad. Multiple reference genes were utilized (including Gapdh, ActinB, and Cyclophillin) for analysis(Griffett et al., 2015). Results were plotted in GraphPad prism software as relative expression normalized to control using mean +/- SEM.

Primers were purchased from Integrated DNA Technologies (IDT) and checked for specificity using NCBI Primer-BLAST as follows:

Human *NLRP3* Forward: 5′-CATGAGTGCTGCTTCGACAT-3′

Human *NLRP3* Reverse: 5′-CGACTCCTGAGTCTCCCAAG-3′

Human *36B4* Forward: 5′- CGACCTGGAAGTCCAACTAC-3′

Human *36B4* Reverse: 5′- ATCTGCTGCATCTGCTTG-3′

Human *Il-1β* Forward: 5′- CACCACTACAGCAAGGGCTTCA-3′

Human *Il-1β* Reverse: 5′- GCATCTTCCTCAGCTTGTCCAT-3′

Human *Il-18* Forward: 5′- TCCTTGATGTTATCAGGAGGATTCA-3′

Human *Il-18* Reverse: 5′- GCTGTAACTATCTCTGTGAAGTGTG-3′

Mouse *Il-1β* Forward: 5′-GCAACTGTTCCTGAACTCA-3′

Mouse *Il-1β* Reverse: 5′-CTCGGAGCCTGTAGTGCAG-3′

Mouse *Il-18* Forward: 5′- CTGGAGCTGCTGACAGGCCTGA-3′

Mouse *Il-18* Reverse: 5′- GCCCAGGAACAATGGCTGCCAT-3′

Mouse *Nlrp3* Forward: 5′- GCCTCACCTCACACAGCTGCTG-3′

Mouse *Nlrp3* Reverse: 5′- TTGGCGATCTGTGCGTGGTGAC-3′

Mouse *36b4* Forward: 5′- AGATTCGGGATATGCTGTTGGC-3′

Mouse *36b4* Reverse: 5′- TCGGGTCCTAGACCAGTGTTC-3′

6.18 Statistics

All data are expressed as mean +/- SEM (n = 4 or greater). All expression statistical analysis was performed using ANOVA with Tukey's post-hoc analysis in GraphPad prism software. Weekly mouse weights and food intake data was analyzed by two-way ANOVA followed by Sidak's multiple comparisons at the 95% confidence level. For ipGTT, area under the curve (AUC) was generated and the data was analyzed by two-tailed student's t-test in GraphPad prism software. P-values are reported as numerals. Significance is considered at $p<0.05$. P-value for GTT and ITT is as follows: * $p \leq 0.05$, ** $p \leq 0.01$, *** $p \leq 0.001$, and **** $p \leq 0.0001$.

References

Aagaard, M. M., Siersbaek, R., & Mandrup, S. (2011). Molecular basis for gene-specific transactivation by nuclear receptors. *Biochim Biophys Acta*, *1812*(8), 824-835. https://doi.org/10.1016/j.bbadis.2010.12.018

Adams, D. H., & Eksteen, B. (2006). Aberrant homing of mucosal T cells and extra-intestinal manifestations of inflammatory bowel disease. *Nat Rev Immunol*, *6*(3), 244-251. https://doi.org/10.1038/nri1784

Adlanmerini, M., & Lazar, M. A. (2023). The REV-ERB Nuclear Receptors: Timekeepers for the Core Clock Period and Metabolism. *Endocrinology*, *164*(6). https://doi.org/10.1210/endocr/bqad069

Akazawa, Y., Cazanave, S., Mott, J. L., Elmi, N., Bronk, S. F., Kohno, S., Charlton, M. R., & Gores, G. J. (2010). Palmitoleate attenuates palmitate-induced Bim and PUMA up-regulation and hepatocyte lipoapoptosis. *J Hepatol*, *52*(4), 586-593. https://doi.org/10.1016/j.jhep.2010.01.003

Al-Dayyat, H. M., Rayyan, Y. M., & Tayyem, R. F. (2018). Non-alcoholic fatty liver disease and associated dietary and lifestyle risk factors. *Diabetes Metab Syndr*, *12*(4), 569-575. https://doi.org/10.1016/j.dsx.2018.03.016

Alexander, M., Loomis, A. K., Fairburn-Beech, J., van der Lei, J., Duarte-Salles, T., Prieto-Alhambra, D., Ansell, D., Pasqua, A., Lapi, F., Rijnbeek, P., Mosseveld, M., Avillach, P., Egger, P., Kendrick, S., Waterworth, D. M., Sattar, N., & Alazawi, W. (2018). Real-world data reveal a diagnostic gap in

non-alcoholic fatty liver disease. *BMC Med*, *16*(1), 130. https://doi.org/10.1186/s12916-018-1103-x

Alexander, S. P., Cidlowski, J. A., Kelly, E., Mathie, A., Peters, J. A., Veale, E. L., Armstrong, J. F., Faccenda, E., Harding, S. D., Pawson, A. J., Southan, C., Davies, J. A., Coons, L., Fuller, P. J., Korach, K. S., & Young, M. J. (2021). THE CONCISE GUIDE TO PHARMACOLOGY 2021/22: Nuclear hormone receptors. *Br J Pharmacol*, *178 Suppl 1*(Suppl 1), S246-S263. https://doi.org/10.1111/bph.15540

Allameh, A., Niayesh-Mehr, R., Aliarab, A., Sebastiani, G., & Pantopoulos, K. (2023). Oxidative Stress in Liver Pathophysiology and Disease. *Antioxidants (Basel)*, *12*(9). https://doi.org/10.3390/antiox12091653

Alves-Bezerra, M., & Cohen, D. E. (2017). Triglyceride Metabolism in the Liver. *Compr Physiol*, *8*(1), 1-8. https://doi.org/10.1002/cphy.c170012

Amador, A., Campbell, S., Kazantzis, M., Lan, G., Burris, T. P., & Solt, L. A. (2018). Distinct roles for REV-ERBalpha and REV-ERBbeta in oxidative capacity and mitochondrial biogenesis in skeletal muscle. *PLoS One*, *13*(5), e0196787. https://doi.org/10.1371/journal.pone.0196787

Amir, M., Chaudhari, S., Wang, R., Campbell, S., Mosure, S. A., Chopp, L. B., Lu, Q., Shang, J., Pelletier, O. B., He, Y., Doebelin, C., Cameron, M. D., Kojetin, D. J., Kamenecka, T. M., & Solt, L. A. (2018). REV-ERBalpha Regulates T(H)17 Cell Development and Autoimmunity. *Cell Rep*, *25*(13), 3733-3749 e3738. https://doi.org/10.1016/j.celrep.2018.11.101

Anstee, Q. M., Targher, G., & Day, C. P. (2013). Progression of NAFLD to diabetes mellitus, cardiovascular disease or cirrhosis. *Nat Rev Gastroenterol Hepatol*, *10*(6), 330-344. https://doi.org/10.1038/nrgastro.2013.41

Aranda, A., & Pascual, A. (2001). Nuclear hormone receptors and gene expression. *Physiol Rev*, *81*(3), 1269-1304. https://doi.org/10.1152/physrev.2001.81.3.1269

Armstrong, M. J., Houlihan, D. D., Bentham, L., Shaw, J. C., Cramb, R., Olliff, S., Gill, P. S., Neuberger, J. M., Lilford, R. J., & Newsome, P. N. (2012). Presence and severity of non-alcoholic fatty liver disease in a large prospective primary care cohort. *J Hepatol*, *56*(1), 234-240. https://doi.org/10.1016/j.jhep.2011.03.020

Asif, S., Kim, R. Y., Fatica, T., Sim, J., Zhao, X., Oh, Y., Denoncourt, A., Cheung, A. C., Downey, M., Mulvihill, E. E., & Kim, K. H. (2022). Hmgcs2-mediated ketogenesis modulates high-fat diet-induced hepatosteatosis. *Mol Metab*, *61*, 101494. https://doi.org/10.1016/j.molmet.2022.101494

Bajotto, G., Murakami, T., Nagasaki, M., Qin, B., Matsuo, Y., Maeda, K., Ohashi, M., Oshida, Y., Sato, Y., & Shimomura, Y. (2006). Increased expression of hepatic pyruvate dehydrogenase kinases 2 and 4 in young and middle-aged Otsuka Long-Evans Tokushima Fatty rats: induction by elevated levels of free fatty acids. *Metabolism*, *55*(3), 317-323. https://doi.org/10.1016/j.metabol.2005.09.014

Balsalobre, A., Damiola, F., & Schibler, U. (1998). A serum shock induces circadian gene expression in mammalian tissue culture cells. *Cell*, *93*(6), 929-937. https://doi.org/10.1016/s0092-8674(00)81199-x

Benbrook, D. M., Chambon, P., Rochette-Egly, C., & Asson-Batres, M. A. (2014). History of retinoic acid receptors. *Subcell Biochem*, *70*, 1-20. https://doi.org/10.1007/978-94-017-9050-5_1

Berger, J., & Moller, D. E. (2002). The mechanisms of action of PPARs. *Annu Rev Med*, *53*, 409-435. https://doi.org/10.1146/annurev.med.53.082901.104018

Bhatia, L. S., Curzen, N. P., Calder, P. C., & Byrne, C. D. (2012). Non-alcoholic fatty liver disease: a new and important cardiovascular risk factor? *Eur Heart J*, *33*(10), 1190-1200. https://doi.org/10.1093/eurheartj/ehr453

Bhattacharjee, J., Kirby, M., Softic, S., Miles, L., Salazar-Gonzalez, R. M., Shivakumar, P., & Kohli, R. (2017). Hepatic Natural Killer T-cell and CD8+ T-cell Signatures in Mice with Nonalcoholic Steatohepatitis. *Hepatol Commun*, *1*(4), 299-310. https://doi.org/10.1002/hep4.1041

Bieghs, V., Walenbergh, S. M., Hendrikx, T., van Gorp, P. J., Verheyen, F., Olde Damink, S. W., Masclee, A. A., Koek, G. H., Hofker, M. H., Binder, C. J., & Shiri-Sverdlov, R. (2013). Trapping of oxidized LDL in lysosomes of Kupffer cells is a trigger for hepatic inflammation. *Liver Int*, *33*(7), 1056-1061. https://doi.org/10.1111/liv.12170

Blais, P., Husain, N., Kramer, J. R., Kowalkowski, M., El-Serag, H., & Kanwal, F. (2015). Nonalcoholic fatty liver disease is underrecognized in the primary

care setting. *Am J Gastroenterol*, *110*(1), 10-14. https://doi.org/10.1038/ajg.2014.134

Bookout, A. L., Jeong, Y., Downes, M., Yu, R. T., Evans, R. M., & Mangelsdorf, D. J. (2006). Anatomical profiling of nuclear receptor expression reveals a hierarchical transcriptional network. *Cell*, *126*(4), 789-799. https://doi.org/10.1016/j.cell.2006.06.049

Breuer, D. A., Pacheco, M. C., Washington, M. K., Montgomery, S. A., Hasty, A. H., & Kennedy, A. J. (2020). CD8(+) T cells regulate liver injury in obesity-related nonalcoholic fatty liver disease. *Am J Physiol Gastrointest Liver Physiol*, *318*(2), G211-G224. https://doi.org/10.1152/ajpgi.00040.2019

Browning, J. D., Szczepaniak, L. S., Dobbins, R., Nuremberg, P., Horton, J. D., Cohen, J. C., Grundy, S. M., & Hobbs, H. H. (2004). Prevalence of hepatic steatosis in an urban population in the United States: impact of ethnicity. *Hepatology*, *40*(6), 1387-1395. https://doi.org/10.1002/hep.20466

Bugge, A., Feng, D., Everett, L. J., Briggs, E. R., Mullican, S. E., Wang, F., Jager, J., & Lazar, M. A. (2012). Rev-erbalpha and Rev-erbbeta coordinately protect the circadian clock and normal metabolic function. *Genes Dev*, *26*(7), 657-667. https://doi.org/10.1101/gad.186858.112

Burke, L., Downes, M., Carozzi, A., Giguere, V., & Muscat, G. E. (1996). Transcriptional repression by the orphan steroid receptor RVR/Rev-erb beta is dependent on the signature motif and helix 5 in the E region: functional evidence for a biological role of RVR in myogenesis. *Nucleic Acids Res*, *24*(18), 3481-3489. https://doi.org/10.1093/nar/24.18.3481

Burris, T. P., de Vera, I. M. S., Cote, I., Flaveny, C. A., Wanninayake, U. S., Chatterjee, A., Walker, J. K., Steinauer, N., Zhang, J., Coons, L. A., Korach, K. S., Cain, D. W., Hollenberg, A. N., Webb, P., Forrest, D., Jetten, A. M., Edwards, D. P., Grimm, S. L., Hartig, S., . . . Cidlowski, J. A. (2023). International Union of Basic and Clinical Pharmacology CXIII: Nuclear Receptor Superfamily-Update 2023. *Pharmacol Rev*, *75*(6), 1233-1318. https://doi.org/10.1124/pharmrev.121.000436

Butt, T. R., & Walfish, P. G. (1996). Human nuclear receptor heterodimers: opportunities for detecting targets of transcriptional regulation using yeast. *Gene Expr*, *5*(4-5), 255-268. https://www.ncbi.nlm.nih.gov/pubmed/8723391

Byrne, C. D., & Targher, G. (2015). NAFLD: a multisystem disease. *J Hepatol*, *62*(1 Suppl), S47-64. https://doi.org/10.1016/j.jhep.2014.12.012

Caldeira da Silva, C. C., Cerqueira, F. M., Barbosa, L. F., Medeiros, M. H., & Kowaltowski, A. J. (2008). Mild mitochondrial uncoupling in mice affects energy metabolism, redox balance and longevity. *Aging Cell*, *7*(4), 552-560. https://doi.org/10.1111/j.1474-9726.2008.00407.x

Canto, C., Houtkooper, R. H., Pirinen, E., Youn, D. Y., Oosterveer, M. H., Cen, Y., Fernandez-Marcos, P. J., Yamamoto, H., Andreux, P. A., Cettour-Rose, P., Gademann, K., Rinsch, C., Schoonjans, K., Sauve, A. A., & Auwerx, J. (2012). The NAD(+) precursor nicotinamide riboside enhances oxidative metabolism and protects against high-fat diet-induced obesity. *Cell Metab*, *15*(6), 838-847. https://doi.org/10.1016/j.cmet.2012.04.022

Carter, E. L., Gupta, N., & Ragsdale, S. W. (2016). High Affinity Heme Binding to a Heme Regulatory Motif on the Nuclear Receptor Rev-erbbeta Leads to Its Degradation and Indirectly Regulates Its Interaction with Nuclear Receptor Corepressor. *J Biol Chem*, *291*(5), 2196-2222. https://doi.org/10.1074/jbc.M115.670281

Chambon, P. (1996). A decade of molecular biology of retinoic acid receptors. *FASEB J*, *10*(9), 940-954. https://www.ncbi.nlm.nih.gov/pubmed/8801176

Chandra, V., Huang, P., Hamuro, Y., Raghuram, S., Wang, Y., Burris, T. P., & Rastinejad, F. (2008). Structure of the intact PPAR-gamma-RXR- nuclear receptor complex on DNA. *Nature*, *456*(7220), 350-356. https://doi.org/10.1038/nature07413

Chang, C., Loo, C. S., Zhao, X., Solt, L. A., Liang, Y., Bapat, S. P., Cho, H., Kamenecka, T. M., Leblanc, M., Atkins, A. R., Yu, R. T., Downes, M., Burris, T. P., Evans, R. M., & Zheng, Y. (2019). The nuclear receptor REV-ERBalpha modulates Th17 cell-mediated autoimmune disease. *Proc Natl Acad Sci U S A*, *116*(37), 18528-18536. https://doi.org/10.1073/pnas.1907563116

Chang, X., Bian, H., Xia, M., Zhu, X., Sun, X., Yang, X., Gao, J., Lin, H., Yan, H., & Gao, X. (2022). Postprandial glucose is correlated with an increasing risk of liver fibrosis in Chinese patients with nonalcoholic fatty liver disease. *Diabetes Metab*, *48*(6), 101377. https://doi.org/10.1016/j.diabet.2022.101377

Chen, X., Li, L., Liu, X., Luo, R., Liao, G., Li, L., Liu, J., Cheng, J., Lu, Y., & Chen, Y. (2018). Oleic acid protects saturated fatty acid mediated lipotoxicity in hepatocytes and rat of non-alcoholic steatohepatitis. *Life Sci*, *203*, 291-304. https://doi.org/10.1016/j.lfs.2018.04.022

Cho, H., Zhao, X., Hatori, M., Yu, R. T., Barish, G. D., Lam, M. T., Chong, L. W., DiTacchio, L., Atkins, A. R., Glass, C. K., Liddle, C., Auwerx, J., Downes, M., Panda, S., & Evans, R. M. (2012). Regulation of circadian behaviour and metabolism by REV-ERB-alpha and REV-ERB-beta. *Nature*, *485*(7396), 123-127. https://doi.org/10.1038/nature11048

Comporti, M., & Saccocci, C. (1965). [Stimulation of the lipid peroxidation of rat liver homogenates by low concentration of CC1-4 in vitro]. *Boll Soc Ital Biol Sper*, *41*(18), 1066-1069. https://www.ncbi.nlm.nih.gov/pubmed/5896464 (Stimolazione della perossidazione lipidica di omogenati di fegato di ratto da parte di basse concentrazioni di CC1-4 in vitro.)

Croci, I., Byrne, N. M., Chachay, V. S., Hills, A. P., Clouston, A. D., O'Moore-Sullivan, T. M., Prins, J. B., Macdonald, G. A., & Hickman, I. J. (2016). Independent effects of diet and exercise training on fat oxidation in non-alcoholic fatty liver disease. *World J Hepatol*, *8*(27), 1137-1148. https://doi.org/10.4254/wjh.v8.i27.1137

Cui, W., Matsuno, K., Iwata, K., Ibi, M., Matsumoto, M., Zhang, J., Zhu, K., Katsuyama, M., Torok, N. J., & Yabe-Nishimura, C. (2011). NOX1/nicotinamide adenine dinucleotide phosphate, reduced form (NADPH) oxidase promotes proliferation of stellate cells and aggravates

liver fibrosis induced by bile duct ligation. *Hepatology*, *54*(3), 949-958. https://doi.org/10.1002/hep.24465

Cuzick, J., Sestak, I., Cawthorn, S., Hamed, H., Holli, K., Howell, A., Forbes, J. F., & Investigators, I.-I. (2015). Tamoxifen for prevention of breast cancer: extended long-term follow-up of the IBIS-I breast cancer prevention trial. *Lancet Oncol*, *16*(1), 67-75. https://doi.org/10.1016/S1470-2045(14)71171-4

de la Cruz-Lopez, K. G., Castro-Munoz, L. J., Reyes-Hernandez, D. O., Garcia-Carranca, A., & Manzo-Merino, J. (2019). Lactate in the Regulation of Tumor Microenvironment and Therapeutic Approaches. *Front Oncol*, *9*, 1143. https://doi.org/10.3389/fonc.2019.01143

De Mei, C., Ercolani, L., Parodi, C., Veronesi, M., Lo Vecchio, C., Bottegoni, G., Torrente, E., Scarpelli, R., Marotta, R., Ruffili, R., Mattioli, M., Reggiani, A., Wade, M., & Grimaldi, B. (2015). Dual inhibition of REV-ERBbeta and autophagy as a novel pharmacological approach to induce cytotoxicity in cancer cells. *Oncogene*, *34*(20), 2597-2608. https://doi.org/10.1038/onc.2014.203

de Vera, I. M. S., Zheng, J., Novick, S., Shang, J., Hughes, T. S., Brust, R., Munoz-Tello, P., Gardner, W. J., Jr., Marciano, D. P., Kong, X., Griffin, P. R., & Kojetin, D. J. (2017). Synergistic Regulation of Coregulator/Nuclear Receptor Interaction by Ligand and DNA. *Structure*, *25*(10), 1506-1518 e1504. https://doi.org/10.1016/j.str.2017.07.019

Delezie, J., Dumont, S., Dardente, H., Oudart, H., Grechez-Cassiau, A., Klosen, P., Teboul, M., Delaunay, F., Pevet, P., & Challet, E. (2012). The nuclear receptor REV-ERBalpha is required for the daily balance of carbohydrate and lipid metabolism. *FASEB J*, *26*(8), 3321-3335. https://doi.org/10.1096/fj.12-208751

Delgado, M. E., Cardenas, B. I., Farran, N., & Fernandez, M. (2021). Metabolic Reprogramming of Liver Fibrosis. *Cells*, *10*(12). https://doi.org/10.3390/cells10123604

Ding, G., Li, X., Hou, X., Zhou, W., Gong, Y., Liu, F., He, Y., Song, J., Wang, J., Basil, P., Li, W., Qian, S., Saha, P., Wang, J., Cui, C., Yang, T., Zou, K., Han, Y., Amos, C. I., . . . Sun, Z. (2021). REV-ERB in GABAergic neurons controls diurnal hepatic insulin sensitivity. *Nature*, *592*(7856), 763-767. https://doi.org/10.1038/s41586-021-03358-w

Diraison, F., Yankah, V., Letexier, D., Dusserre, E., Jones, P., & Beylot, M. (2003). Differences in the regulation of adipose tissue and liver lipogenesis by carbohydrates in humans. *J Lipid Res*, *44*(4), 846-853. https://doi.org/10.1194/jlr.M200461-JLR200

Doggrell, S. A. (2008). Clinical trials with thiazolidinediones in subjects with Type 2 diabetes--is pioglitazone any different from rosiglitazone? *Expert Opin Pharmacother*, *9*(3), 405-420. https://doi.org/10.1517/14656566.9.3.405

Dongiovanni, P., Petta, S., Mannisto, V., Mancina, R. M., Pipitone, R., Karja, V., Maggioni, M., Kakela, P., Wiklund, O., Mozzi, E., Grimaudo, S., Kaminska, D., Rametta, R., Craxi, A., Fargion, S., Nobili, V., Romeo, S., Pihlajamaki,

J., & Valenti, L. (2015). Statin use and non-alcoholic steatohepatitis in at risk individuals. *J Hepatol*, *63*(3), 705-712. https://doi.org/10.1016/j.jhep.2015.05.006

Dumas, B., Harding, H. P., Choi, H. S., Lehmann, K. A., Chung, M., Lazar, M. A., & Moore, D. D. (1994). A new orphan member of the nuclear hormone receptor superfamily closely related to Rev-Erb. *Mol Endocrinol*, *8*(8), 996-1005. https://doi.org/10.1210/mend.8.8.7997240

Elmore, S. P., Qian, T., Grissom, S. F., & Lemasters, J. J. (2001). The mitochondrial permeability transition initiates autophagy in rat hepatocytes. *FASEB J*, *15*(12), 2286-2287. https://doi.org/10.1096/fj.01-0206fje

European Association for the Study of the, L., European Association for the Study of, D., & European Association for the Study of, O. (2016). EASL-EASD-EASO Clinical Practice Guidelines for the management of non-alcoholic fatty liver disease. *J Hepatol*, *64*(6), 1388-1402. https://doi.org/10.1016/j.jhep.2015.11.004

European Association for the Study of the Liver. Electronic address, e. e. e., Clinical Practice Guideline, P., Chair, representative, E. G. B., & Panel, m. (2021). EASL Clinical Practice Guidelines on non-invasive tests for evaluation of liver disease severity and prognosis - 2021 update. *J Hepatol*, *75*(3), 659-689. https://doi.org/10.1016/j.jhep.2021.05.025

Fang, B., Mane-Padros, D., Bolotin, E., Jiang, T., & Sladek, F. M. (2012). Identification of a binding motif specific to HNF4 by comparative analysis of

multiple nuclear receptors. *Nucleic Acids Res*, *40*(12), 5343-5356. https://doi.org/10.1093/nar/gks190

Febbraio, M., Abumrad, N. A., Hajjar, D. P., Sharma, K., Cheng, W., Pearce, S. F., & Silverstein, R. L. (1999). A null mutation in murine CD36 reveals an important role in fatty acid and lipoprotein metabolism. *J Biol Chem*, *274*(27), 19055-19062. https://doi.org/10.1074/jbc.274.27.19055

Ferraris, R. P., Choe, J. Y., & Patel, C. R. (2018). Intestinal Absorption of Fructose. *Annu Rev Nutr*, *38*, 41-67. https://doi.org/10.1146/annurev-nutr-082117-051707

Fischer, A., & Smiesko, M. (2019). Ligand Pathways in Nuclear Receptors. *J Chem Inf Model*, *59*(7), 3100-3109. https://doi.org/10.1021/acs.jcim.9b00360

Fletcher, J. A., Deja, S., Satapati, S., Fu, X., Burgess, S. C., & Browning, J. D. (2019). Impaired ketogenesis and increased acetyl-CoA oxidation promote hyperglycemia in human fatty liver. *JCI Insight*, *5*(11). https://doi.org/10.1172/jci.insight.127737

Fontaine, C., Rigamonti, E., Pourcet, B., Duez, H., Duhem, C., Fruchart, J. C., Chinetti-Gbaguidi, G., & Staels, B. (2008). The nuclear receptor Rev-erbalpha is a liver X receptor (LXR) target gene driving a negative feedback loop on select LXR-induced pathways in human macrophages. *Mol Endocrinol*, *22*(8), 1797-1811. https://doi.org/10.1210/me.2007-0439

Foretz, M., Guichard, C., Ferre, P., & Foufelle, F. (1999). Sterol regulatory element binding protein-1c is a major mediator of insulin action on the hepatic

expression of glucokinase and lipogenesis-related genes. *Proc Natl Acad Sci U S A*, *96*(22), 12737-12742. https://doi.org/10.1073/pnas.96.22.12737

Freeman, S. L., Kwon, H., Portolano, N., Parkin, G., Venkatraman Girija, U., Basran, J., Fielding, A. J., Fairall, L., Svistunenko, D. A., Moody, P. C. E., Schwabe, J. W. R., Kyriacou, C. P., & Raven, E. L. (2019). Heme binding to human CLOCK affects interactions with the E-box. *Proc Natl Acad Sci U S A*, *116*(40), 19911-19916. https://doi.org/10.1073/pnas.1905216116

Geldof, L., Deventer, K., Roels, K., Tudela, E., & Van Eeno, P. (2016). In Vitro Metabolic Studies of REV-ERB Agonists SR9009 and SR9011. *Int J Mol Sci*, *17*(10). https://doi.org/10.3390/ijms17101676

Geng, Y., Faber, K. N., de Meijer, V. E., Blokzijl, H., & Moshage, H. (2021). How does hepatic lipid accumulation lead to lipotoxicity in non-alcoholic fatty liver disease? *Hepatol Int*, *15*(1), 21-35. https://doi.org/10.1007/s12072-020-10121-2

Ghyselinck, N. B., & Duester, G. (2019). Retinoic acid signaling pathways. *Development*, *146*(13). https://doi.org/10.1242/dev.167502

Go, Y., Jeong, J. Y., Jeoung, N. H., Jeon, J. H., Park, B. Y., Kang, H. J., Ha, C. M., Choi, Y. K., Lee, S. J., Ham, H. J., Kim, B. G., Park, K. G., Park, S. Y., Lee, C. H., Choi, C. S., Park, T. S., Lee, W. N., Harris, R. A., & Lee, I. K. (2016). Inhibition of Pyruvate Dehydrogenase Kinase 2 Protects Against Hepatic Steatosis Through Modulation of Tricarboxylic Acid Cycle Anaplerosis and Ketogenesis. *Diabetes*, *65*(10), 2876-2887. https://doi.org/10.2337/db16-0223

Gong, J., Tu, W., Liu, J., & Tian, D. (2022). Hepatocytes: A key role in liver inflammation. *Front Immunol*, *13*, 1083780. https://doi.org/10.3389/fimmu.2022.1083780

Gorski, J., Toft, D., Shyamala, G., Smith, D., & Notides, A. (1968). Hormone receptors: studies on the interaction of estrogen with the uterus. *Recent Prog Horm Res*, *24*, 45-80. https://doi.org/10.1016/b978-1-4831-9827-9.50008-3

Grant, D., Yin, L., Collins, J. L., Parks, D. J., Orband-Miller, L. A., Wisely, G. B., Joshi, S., Lazar, M. A., Willson, T. M., & Zuercher, W. J. (2010). GSK4112, a small molecule chemical probe for the cell biology of the nuclear heme receptor Rev-erbalpha. *ACS Chem Biol*, *5*(10), 925-932. https://doi.org/10.1021/cb100141y

Griffett, K., Bedia-Diaz, G., Elgendy, B., & Burris, T. P. (2020). REV-ERB agonism improves liver pathology in a mouse model of NASH. *PLoS One*, *15*(10), e0236000. https://doi.org/10.1371/journal.pone.0236000

Griffett, K., Hayes, M. E., Boeckman, M. P., & Burris, T. P. (2022). The role of REV-ERB in NASH. *Acta Pharmacol Sin*, *43*(5), 1133-1140. https://doi.org/10.1038/s41401-022-00883-w

Griffett, K., Solt, L. A., El-Gendy Bel, D., Kamenecka, T. M., & Burris, T. P. (2013). A liver-selective LXR inverse agonist that suppresses hepatic steatosis. *ACS Chem Biol*, *8*(3), 559-567. https://doi.org/10.1021/cb300541g

Griffett, K., Welch, R. D., Flaveny, C. A., Kolar, G. R., Neuschwander-Tetri, B. A., & Burris, T. P. (2015). The LXR inverse agonist SR9238 suppresses fibrosis

in a model of non-alcoholic steatohepatitis. *Mol Metab*, *4*(4), 353-357. https://doi.org/10.1016/j.molmet.2015.01.009

Griffin, P., Dimitry, J. M., Sheehan, P. W., Lananna, B. V., Guo, C., Robinette, M. L., Hayes, M. E., Cedeno, M. R., Nadarajah, C. J., Ezerskiy, L. A., Colonna, M., Zhang, J., Bauer, A. Q., Burris, T. P., & Musiek, E. S. (2019). Circadian clock protein Rev-erbalpha regulates neuroinflammation. *Proc Natl Acad Sci U S A*, *116*(11), 5102-5107. https://doi.org/10.1073/pnas.1812405116

Grontved, L., Waterfall, J. J., Kim, D. W., Baek, S., Sung, M. H., Zhao, L., Park, J. W., Nielsen, R., Walker, R. L., Zhu, Y. J., Meltzer, P. S., Hager, G. L., & Cheng, S. Y. (2015). Transcriptional activation by the thyroid hormone receptor through ligand-dependent receptor recruitment and chromatin remodelling. *Nat Commun*, *6*, 7048. https://doi.org/10.1038/ncomms8048

Guan, S., Zhao, L., & Peng, R. (2022). Mitochondrial Respiratory Chain Supercomplexes: From Structure to Function. *Int J Mol Sci*, *23*(22). https://doi.org/10.3390/ijms232213880

Guillaumond, F., Dardente, H., Giguere, V., & Cermakian, N. (2005). Differential control of Bmal1 circadian transcription by REV-ERB and ROR nuclear receptors. *J Biol Rhythms*, *20*(5), 391-403. https://doi.org/10.1177/0748730405277232

Guo, D. K., Zhu, Y., Sun, H. Y., Xu, X. Y., Zhang, S., Hao, Z. B., Wang, G. H., Mu, C. C., & Ren, H. G. (2019). Pharmacological activation of REV-ERBalpha represses LPS-induced microglial activation through the NF-kappaB

pathway. *Acta Pharmacol Sin*, *40*(1), 26-34. https://doi.org/10.1038/s41401-018-0064-0

Handa, P., Vemulakonda, A., Kowdley, K. V., Uribe, M., & Mendez-Sanchez, N. (2016). Mitochondrial DNA from hepatocytes as a ligand for TLR9: Drivers of nonalcoholic steatohepatitis? *World J Gastroenterol*, *22*(31), 6965-6971. https://doi.org/10.3748/wjg.v22.i31.6965

Harley, I. T., Stankiewicz, T. E., Giles, D. A., Softic, S., Flick, L. M., Cappelletti, M., Sheridan, R., Xanthakos, S. A., Steinbrecher, K. A., Sartor, R. B., Kohli, R., Karp, C. L., & Divanovic, S. (2014). IL-17 signaling accelerates the progression of nonalcoholic fatty liver disease in mice. *Hepatology*, *59*(5), 1830-1839. https://doi.org/10.1002/hep.26746

Haukeland, J. W., Konopski, Z., Eggesbo, H. B., von Volkmann, H. L., Raschpichler, G., Bjoro, K., Haaland, T., Loberg, E. M., & Birkeland, K. (2009). Metformin in patients with non-alcoholic fatty liver disease: a randomized, controlled trial. *Scand J Gastroenterol*, *44*(7), 853-860. https://doi.org/10.1080/00365520902845268

Her, Z., Tan, J. H. L., Lim, Y. S., Tan, S. Y., Chan, X. Y., Tan, W. W. S., Liu, M., Yong, K. S. M., Lai, F., Ceccarello, E., Zheng, Z., Fan, Y., Chang, K. T. E., Sun, L., Chang, S. C., Chin, C. L., Lee, G. H., Dan, Y. Y., Chan, Y. S., . . . Chen, Q. (2020). CD4(+) T Cells Mediate the Development of Liver Fibrosis in High Fat Diet-Induced NAFLD in Humanized Mice. *Front Immunol*, *11*, 580968. https://doi.org/10.3389/fimmu.2020.580968

Hill, K. K., Roemer, S. C., Churchill, M. E., & Edwards, D. P. (2012). Structural and functional analysis of domains of the progesterone receptor. *Mol Cell Endocrinol*, *348*(2), 418-429. https://doi.org/10.1016/j.mce.2011.07.017

Hin Tang, J. J., Hao Thng, D. K., Lim, J. J., & Toh, T. B. (2020). JAK/STAT signaling in hepatocellular carcinoma. *Hepat Oncol*, *7*(1), HEP18. https://doi.org/10.2217/hep-2020-0001

Hoene, M., Kappler, L., Kollipara, L., Hu, C., Irmler, M., Bleher, D., Hoffmann, C., Beckers, J., Hrabe de Angelis, M., Haring, H. U., Birkenfeld, A. L., Peter, A., Sickmann, A., Xu, G., Lehmann, R., & Weigert, C. (2021). Exercise prevents fatty liver by modifying the compensatory response of mitochondrial metabolism to excess substrate availability. *Mol Metab*, *54*, 101359. https://doi.org/10.1016/j.molmet.2021.101359

Horie, Y., Suzuki, A., Kataoka, E., Sasaki, T., Hamada, K., Sasaki, J., Mizuno, K., Hasegawa, G., Kishimoto, H., Iizuka, M., Naito, M., Enomoto, K., Watanabe, S., Mak, T. W., & Nakano, T. (2004). Hepatocyte-specific Pten deficiency results in steatohepatitis and hepatocellular carcinomas. *J Clin Invest*, *113*(12), 1774-1783. https://doi.org/10.1172/JCI20513

Horlein, A. J., Naar, A. M., Heinzel, T., Torchia, J., Gloss, B., Kurokawa, R., Ryan, A., Kamei, Y., Soderstrom, M., Glass, C. K., & et al. (1995). Ligand-independent repression by the thyroid hormone receptor mediated by a nuclear receptor co-repressor. *Nature*, *377*(6548), 397-404. https://doi.org/10.1038/377397a0

Hunter, A. L., Pelekanou, C. E., Adamson, A., Downton, P., Barron, N. J., Cornfield, T., Poolman, T. M., Humphreys, N., Cunningham, P. S., Hodson, L., Loudon, A. S. I., Iqbal, M., Bechtold, D. A., & Ray, D. W. (2020). Nuclear receptor REVERBalpha is a state-dependent regulator of liver energy metabolism. *Proc Natl Acad Sci U S A*, *117*(41), 25869-25879. https://doi.org/10.1073/pnas.2005330117

Hunter, A. L., Pelekanou, C. E., Barron, N. J., Northeast, R. C., Grudzien, M., Adamson, A. D., Downton, P., Cornfield, T., Cunningham, P. S., Billaud, J. N., Hodson, L., Loudon, A. S., Unwin, R. D., Iqbal, M., Ray, D. W., & Bechtold, D. A. (2021). Adipocyte NR1D1 dictates adipose tissue expansion during obesity. *Elife*, *10*. https://doi.org/10.7554/eLife.63324

Inzaugarat, M. E., Johnson, C. D., Holtmann, T. M., McGeough, M. D., Trautwein, C., Papouchado, B. G., Schwabe, R., Hoffman, H. M., Wree, A., & Feldstein, A. E. (2019). NLR Family Pyrin Domain-Containing 3 Inflammasome Activation in Hepatic Stellate Cells Induces Liver Fibrosis in Mice. *Hepatology*, *69*(2), 845-859. https://doi.org/10.1002/hep.30252

Ishimoto, T., Lanaspa, M. A., Rivard, C. J., Roncal-Jimenez, C. A., Orlicky, D. J., Cicerchi, C., McMahan, R. H., Abdelmalek, M. F., Rosen, H. R., Jackman, M. R., MacLean, P. S., Diggle, C. P., Asipu, A., Inaba, S., Kosugi, T., Sato, W., Maruyama, S., Sanchez-Lozada, L. G., Sautin, Y. Y., . . . Johnson, R. J. (2013). High-fat and high-sucrose (western) diet induces steatohepatitis that is dependent on fructokinase. *Hepatology*, *58*(5), 1632-1643. https://doi.org/10.1002/hep.26594

Janich, P., Arpat, A. B., Castelo-Szekely, V., Lopes, M., & Gatfield, D. (2015). Ribosome profiling reveals the rhythmic liver translatome and circadian clock regulation by upstream open reading frames. *Genome Res*, *25*(12), 1848-1859. https://doi.org/10.1101/gr.195404.115

Jensen, E. V., Desombre, E. R., Kawashima, T., Suzuki, T., Kyser, K., & Jungblut, P. W. (1967). Estrogen-binding substances of target tissues. *Science*, *158*(3800), 529-530. https://doi.org/10.1126/science.158.3800.529-c

Jensen, E. V., Suzuki, T., Kawashima, T., Stumpf, W. E., Jungblut, P. W., & DeSombre, E. R. (1968). A two-step mechanism for the interaction of estradiol with rat uterus. *Proc Natl Acad Sci U S A*, *59*(2), 632-638. https://doi.org/10.1073/pnas.59.2.632

Jiang, J. X., Venugopal, S., Serizawa, N., Chen, X., Scott, F., Li, Y., Adamson, R., Devaraj, S., Shah, V., Gershwin, M. E., Friedman, S. L., & Torok, N. J. (2010). Reduced nicotinamide adenine dinucleotide phosphate oxidase 2 plays a key role in stellate cell activation and liver fibrogenesis in vivo. *Gastroenterology*, *139*(4), 1375-1384. https://doi.org/10.1053/j.gastro.2010.05.074

Khan, S. H., Braet, S. M., Koehler, S. J., Elacqua, E., Anand, G. S., & Okafor, C. D. (2022). Ligand-induced shifts in conformational ensembles that describe transcriptional activation. *Elife*, *11*. https://doi.org/10.7554/eLife.80140

Kim, D., Kim, W., Joo, S. K., Kim, J. H., Harrison, S. A., Younossi, Z. M., & Ahmed, A. (2019). Predictors of nonalcoholic steatohepatitis and significant fibrosis

in non-obese nonalcoholic fatty liver disease. *Liver Int*, *39*(2), 332-341. https://doi.org/10.1111/liv.13983

Kim, G. A., Moon, J. H., & Kim, W. (2023). Critical appraisal of metabolic dysfunction-associated steatotic liver disease: Implication of Janus-faced modernity. *Clin Mol Hepatol*, *29*(4), 831-843. https://doi.org/10.3350/cmh.2023.0277

Kim, J., Park, I., Jang, S., Choi, M., Kim, D., Sun, W., Choe, Y., Choi, J. W., Moon, C., Park, S. H., Choe, H. K., & Kim, K. (2022). Pharmacological Rescue with SR8278, a Circadian Nuclear Receptor REV-ERBalpha Antagonist as a Therapy for Mood Disorders in Parkinson's Disease. *Neurotherapeutics*, *19*(2), 592-607. https://doi.org/10.1007/s13311-022-01215-w

Kohjima, M., Enjoji, M., Higuchi, N., Kato, M., Kotoh, K., Yoshimoto, T., Fujino, T., Yada, M., Yada, R., Harada, N., Takayanagi, R., & Nakamuta, M. (2007). Re-evaluation of fatty acid metabolism-related gene expression in nonalcoholic fatty liver disease. *Int J Mol Med*, *20*(3), 351-358. https://www.ncbi.nlm.nih.gov/pubmed/17671740

Kohjima, M., Higuchi, N., Kato, M., Kotoh, K., Yoshimoto, T., Fujino, T., Yada, M., Yada, R., Harada, N., Enjoji, M., Takayanagi, R., & Nakamuta, M. (2008). SREBP-1c, regulated by the insulin and AMPK signaling pathways, plays a role in nonalcoholic fatty liver disease. *Int J Mol Med*, *21*(4), 507-511. https://www.ncbi.nlm.nih.gov/pubmed/18360697

Kojetin, D., Wang, Y., Kamenecka, T. M., & Burris, T. P. (2011). Identification of SR8278, a synthetic antagonist of the nuclear heme receptor REV-ERB. *ACS Chem Biol*, *6*(2), 131-134. https://doi.org/10.1021/cb1002575

Koliaki, C., Szendroedi, J., Kaul, K., Jelenik, T., Nowotny, P., Jankowiak, F., Herder, C., Carstensen, M., Krausch, M., Knoefel, W. T., Schlensak, M., & Roden, M. (2015). Adaptation of hepatic mitochondrial function in humans with non-alcoholic fatty liver is lost in steatohepatitis. *Cell Metab*, *21*(5), 739-746. https://doi.org/10.1016/j.cmet.2015.04.004

Koyama, Y., & Brenner, D. A. (2017). Liver inflammation and fibrosis. *J Clin Invest*, *127*(1), 55-64. https://doi.org/10.1172/JCI88881

Kristiansen, M. N., Veidal, S. S., Rigbolt, K. T., Tolbol, K. S., Roth, J. D., Jelsing, J., Vrang, N., & Feigh, M. (2016). Obese diet-induced mouse models of nonalcoholic steatohepatitis-tracking disease by liver biopsy. *World J Hepatol*, *8*(16), 673-684. https://doi.org/10.4254/wjh.v8.i16.673

Kumar, N., Solt, L. A., Wang, Y., Rogers, P. M., Bhattacharyya, G., Kamenecka, T. M., Stayrook, K. R., Crumbley, C., Floyd, Z. E., Gimble, J. M., Griffin, P. R., & Burris, T. P. (2010). Regulation of adipogenesis by natural and synthetic REV-ERB ligands. *Endocrinology*, *151*(7), 3015-3025. https://doi.org/10.1210/en.2009-0800

Laitinen, S., Fontaine, C., Fruchart, J. C., & Staels, B. (2005). The role of the orphan nuclear receptor Rev-Erb alpha in adipocyte differentiation and function. *Biochimie*, *87*(1), 21-25. https://doi.org/10.1016/j.biochi.2004.12.006

Latham, T., Mackay, L., Sproul, D., Karim, M., Culley, J., Harrison, D. J., Hayward, L., Langridge-Smith, P., Gilbert, N., & Ramsahoye, B. H. (2012). Lactate, a product of glycolytic metabolism, inhibits histone deacetylase activity and promotes changes in gene expression. *Nucleic Acids Res*, *40*(11), 4794-4803. https://doi.org/10.1093/nar/gks066

Lazar, M. A., Hodin, R. A., Darling, D. S., & Chin, W. W. (1989). A novel member of the thyroid/steroid hormone receptor family is encoded by the opposite strand of the rat c-erbA alpha transcriptional unit. *Mol Cell Biol*, *9*(3), 1128-1136. https://doi.org/10.1128/mcb.9.3.1128-1136.1989

Lazarus, J. V., Anstee, Q. M., Hagstrom, H., Cusi, K., Cortez-Pinto, H., Mark, H. E., Roden, M., Tsochatzis, E. A., Wong, V. W., Younossi, Z. M., Zelber-Sagi, S., Romero-Gomez, M., & Schattenberg, J. M. (2021). Defining comprehensive models of care for NAFLD. *Nat Rev Gastroenterol Hepatol*, *18*(10), 717-729. https://doi.org/10.1038/s41575-021-00477-7

Le Martelot, G., Claudel, T., Gatfield, D., Schaad, O., Kornmann, B., Lo Sasso, G., Moschetta, A., & Schibler, U. (2009). REV-ERBalpha participates in circadian SREBP signaling and bile acid homeostasis. *PLoS Biol*, *7*(9), e1000181. https://doi.org/10.1371/journal.pbio.1000181

Lee, J., Kim, D. E., Griffin, P., Sheehan, P. W., Kim, D. H., Musiek, E. S., & Yoon, S. Y. (2020). Inhibition of REV-ERBs stimulates microglial amyloid-beta clearance and reduces amyloid plaque deposition in the 5XFAD mouse model of Alzheimer's disease. *Aging Cell*, *19*(2), e13078. https://doi.org/10.1111/acel.13078

Lee, S., & Dong, H. H. (2017). FoxO integration of insulin signaling with glucose and lipid metabolism. *J Endocrinol*, *233*(2), R67-R79. https://doi.org/10.1530/JOE-17-0002

Lee, Y., Hirose, H., Ohneda, M., Johnson, J. H., McGarry, J. D., & Unger, R. H. (1994). Beta-cell lipotoxicity in the pathogenesis of non-insulin-dependent diabetes mellitus of obese rats: impairment in adipocyte-beta-cell relationships. *Proc Natl Acad Sci U S A*, *91*(23), 10878-10882. https://doi.org/10.1073/pnas.91.23.10878

Legaki, A. I., Moustakas, II, Sikorska, M., Papadopoulos, G., Velliou, R. I., & Chatzigeorgiou, A. (2022). Hepatocyte Mitochondrial Dynamics and Bioenergetics in Obesity-Related Non-Alcoholic Fatty Liver Disease. *Curr Obes Rep*, *11*(3), 126-143. https://doi.org/10.1007/s13679-022-00473-1

Li, F., Hao, X., Chen, Y., Bai, L., Gao, X., Lian, Z., Wei, H., Sun, R., & Tian, Z. (2017). The microbiota maintain homeostasis of liver-resident gammadeltaT-17 cells in a lipid antigen/CD1d-dependent manner. *Nat Commun*, *7*, 13839. https://doi.org/10.1038/ncomms13839

Li, S., Liu, C., Li, N., Hao, T., Han, T., Hill, D. E., Vidal, M., & Lin, J. D. (2008). Genome-wide coactivation analysis of PGC-1alpha identifies BAF60a as a regulator of hepatic lipid metabolism. *Cell Metab*, *8*(2), 105-117. https://doi.org/10.1016/j.cmet.2008.06.013

Liang, G., Yang, J., Horton, J. D., Hammer, R. E., Goldstein, J. L., & Brown, M. S. (2002). Diminished hepatic response to fasting/refeeding and liver X receptor agonists in mice with selective deficiency of sterol regulatory

element-binding protein-1c. *J Biol Chem*, *277*(11), 9520-9528. https://doi.org/10.1074/jbc.M111421200

Liang, N., Damdimopoulos, A., Goni, S., Huang, Z., Vedin, L. L., Jakobsson, T., Giudici, M., Ahmed, O., Pedrelli, M., Barilla, S., Alzaid, F., Mendoza, A., Schroder, T., Kuiper, R., Parini, P., Hollenberg, A., Lefebvre, P., Francque, S., Van Gaal, L., . . . Fan, R. (2019). Hepatocyte-specific loss of GPS2 in mice reduces non-alcoholic steatohepatitis via activation of PPARalpha. *Nat Commun*, *10*(1), 1684. https://doi.org/10.1038/s41467-019-09524-z

Liang, W., Menke, A. L., Driessen, A., Koek, G. H., Lindeman, J. H., Stoop, R., Havekes, L. M., Kleemann, R., & van den Hoek, A. M. (2014). Establishment of a general NAFLD scoring system for rodent models and comparison to human liver pathology. *PLoS One*, *9*(12), e115922. https://doi.org/10.1371/journal.pone.0115922

Liberti, M. V., & Locasale, J. W. (2016). The Warburg Effect: How Does it Benefit Cancer Cells? *Trends Biochem Sci*, *41*(3), 211-218. https://doi.org/10.1016/j.tibs.2015.12.001

Lim, J. S., Mietus-Snyder, M., Valente, A., Schwarz, J. M., & Lustig, R. H. (2010). The role of fructose in the pathogenesis of NAFLD and the metabolic syndrome. *Nat Rev Gastroenterol Hepatol*, *7*(5), 251-264. https://doi.org/10.1038/nrgastro.2010.41

Linden, A. G., Li, S., Choi, H. Y., Fang, F., Fukasawa, M., Uyeda, K., Hammer, R. E., Horton, J. D., Engelking, L. J., & Liang, G. (2018). Interplay between ChREBP and SREBP-1c coordinates postprandial glycolysis and

lipogenesis in livers of mice. *J Lipid Res*, *59*(3), 475-487. https://doi.org/10.1194/jlr.M081836

Liu, C., Tao, Q., Sun, M., Wu, J. Z., Yang, W., Jian, P., Peng, J., Hu, Y., Liu, C., & Liu, P. (2010). Kupffer cells are associated with apoptosis, inflammation and fibrotic effects in hepatic fibrosis in rats. *Lab Invest*, *90*(12), 1805-1816. https://doi.org/10.1038/labinvest.2010.123

Liu, G., Zhou, L., Zhang, H., Chen, R., Zhang, Y., Li, L., Lu, J. Y., Jiang, H., Liu, D., Qi, S., Jiang, Y. M., Yin, K., Xie, Z., Shi, Y., Liu, Y., Cao, X., Chen, Y. X., Zou, D., & Zhang, W. J. (2017). Regulation of hepatic lipogenesis by the zinc finger protein Zbtb20. *Nat Commun*, *8*, 14824. https://doi.org/10.1038/ncomms14824

Liu, J., Jiang, S., Zhao, Y., Sun, Q., Zhang, J., Shen, D., Wu, J., Shen, N., Fu, X., Sun, X., Yu, D., Chen, J., He, J., Shi, T., Ding, Y., Fang, L., Xue, B., & Li, C. (2018). Geranylgeranyl diphosphate synthase (GGPPS) regulates non-alcoholic fatty liver disease (NAFLD)-fibrosis progression by determining hepatic glucose/fatty acid preference under high-fat diet conditions. *J Pathol*, *246*(3), 277-288. https://doi.org/10.1002/path.5131

Liu, Y., Lin, H., Jiang, L., Shang, Q., Yin, L., Lin, J. D., Wu, W. S., & Rui, L. (2020). Hepatic Slug epigenetically promotes liver lipogenesis, fatty liver disease, and type 2 diabetes. *J Clin Invest*, *130*(6), 2992-3004. https://doi.org/10.1172/JCI128073

Lombard, D. B., Tishkoff, D. X., & Bao, J. (2011). Mitochondrial sirtuins in the regulation of mitochondrial activity and metabolic adaptation. *Handb Exp Pharmacol*, *206*, 163-188. https://doi.org/10.1007/978-3-642-21631-2_8

Lonard, D. M., & O'Malley, B. W. (2006). The expanding cosmos of nuclear receptor coactivators. *Cell*, *125*(3), 411-414. https://doi.org/10.1016/j.cell.2006.04.021

Lu, Q., Tian, X., Wu, H., Huang, J., Li, M., Mei, Z., Zhou, L., Xie, H., & Zheng, S. (2021). Metabolic Changes of Hepatocytes in NAFLD. *Front Physiol*, *12*, 710420. https://doi.org/10.3389/fphys.2021.710420

Ma, X., Hua, J., Mohamood, A. R., Hamad, A. R., Ravi, R., & Li, Z. (2007). A high-fat diet and regulatory T cells influence susceptibility to endotoxin-induced liver injury. *Hepatology*, *46*(5), 1519-1529. https://doi.org/10.1002/hep.21823

Makhija, S., Griffett, J. D., Veerakanellore, G. B., Burris, T. P., Elgendy, B., & Griffett, K. (2023). REV-ERB activation as a novel pharmacological approach for treating inflammatory pain. *Front Pharmacol*, *14*, 1171931. https://doi.org/10.3389/fphar.2023.1171931

Matta-Camacho, E., Banerjee, S., Hughes, T. S., Solt, L. A., Wang, Y., Burris, T. P., & Kojetin, D. J. (2014). Structure of REV-ERBbeta ligand-binding domain bound to a porphyrin antagonist. *J Biol Chem*, *289*(29), 20054-20066. https://doi.org/10.1074/jbc.M113.545111

Mazzarino, M., Rizzato, N., Stacchini, C., de la Torre, X., & Botre, F. (2018). A further insight into the metabolic profile of the nuclear receptor Rev-erb

agonist, SR9009. *Drug Test Anal*, *10*(11-12), 1670-1681. https://doi.org/10.1002/dta.2538

McCullough, A., Previs, S., & Kasumov, T. (2018). Stable isotope-based flux studies in nonalcoholic fatty liver disease. *Pharmacol Ther*, *181*, 22-33. https://doi.org/10.1016/j.pharmthera.2017.07.008

Miyajima, N., Horiuchi, R., Shibuya, Y., Fukushige, S., Matsubara, K., Toyoshima, K., & Yamamoto, T. (1989). Two erbA homologs encoding proteins with different T3 binding capacities are transcribed from opposite DNA strands of the same genetic locus. *Cell*, *57*(1), 31-39. https://doi.org/10.1016/0092-8674(89)90169-4

Montagner, A., Polizzi, A., Fouche, E., Ducheix, S., Lippi, Y., Lasserre, F., Barquissau, V., Regnier, M., Lukowicz, C., Benhamed, F., Iroz, A., Bertrand-Michel, J., Al Saati, T., Cano, P., Mselli-Lakhal, L., Mithieux, G., Rajas, F., Lagarrigue, S., Pineau, T., . . . Guillou, H. (2016). Liver PPARalpha is crucial for whole-body fatty acid homeostasis and is protective against NAFLD. *Gut*, *65*(7), 1202-1214. https://doi.org/10.1136/gutjnl-2015-310798

Mooli, R. G. R., & Ramakrishnan, S. K. (2022). Emerging Role of Hepatic Ketogenesis in Fatty Liver Disease. *Front Physiol*, *13*, 946474. https://doi.org/10.3389/fphys.2022.946474

Moore, M. P., Cunningham, R. P., Meers, G. M., Johnson, S. A., Wheeler, A. A., Ganga, R. R., Spencer, N. M., Pitt, J. B., Diaz-Arias, A., Swi, A. I. A., Hammoud, G. M., Ibdah, J. A., Parks, E. J., & Rector, R. S. (2022).

Compromised hepatic mitochondrial fatty acid oxidation and reduced markers of mitochondrial turnover in human NAFLD. *Hepatology*, *76*(5), 1452-1465. https://doi.org/10.1002/hep.32324

Murray, M. H., Valfort, A. C., Koelblen, T., Ronin, C., Ciesielski, F., Chatterjee, A., Veerakanellore, G. B., Elgendy, B., Walker, J. K., Hegazy, L., & Burris, T. P. (2022). Structural basis of synthetic agonist activation of the nuclear receptor REV-ERB. *Nat Commun*, *13*(1), 7131. https://doi.org/10.1038/s41467-022-34892-4

Myint, M., Oppedisano, F., De Giorgi, V., Kim, B. M., Marincola, F. M., Alter, H. J., & Nesci, S. (2023). Inflammatory signaling in NASH driven by hepatocyte mitochondrial dysfunctions. *J Transl Med*, *21*(1), 757. https://doi.org/10.1186/s12967-023-04627-0

Nieto, N., Friedman, S. L., & Cederbaum, A. I. (2002). Stimulation and proliferation of primary rat hepatic stellate cells by cytochrome P450 2E1-derived reactive oxygen species. *Hepatology*, *35*(1), 62-73. https://doi.org/10.1053/jhep.2002.30362

Noel, R., Song, X., Shin, Y., Banerjee, S., Kojetin, D., Lin, L., Ruiz, C. H., Cameron, M. D., Burris, T. P., & Kamenecka, T. M. (2012). Synthesis and SAR of tetrahydroisoquinolines as Rev-erbalpha agonists. *Bioorg Med Chem Lett*, *22*(11), 3739-3742. https://doi.org/10.1016/j.bmcl.2012.04.023

Nogueira, M. A., Oliveira, C. P., Ferreira Alves, V. A., Stefano, J. T., Rodrigues, L. S., Torrinhas, R. S., Cogliati, B., Barbeiro, H., Carrilho, F. J., & Waitzberg, D. L. (2016). Omega-3 polyunsaturated fatty acids in treating non-alcoholic

steatohepatitis: A randomized, double-blind, placebo-controlled trial. *Clin Nutr*, *35*(3), 578-586. https://doi.org/10.1016/j.clnu.2015.05.001

Orasanu, G., Ziouzenkova, O., Devchand, P. R., Nehra, V., Hamdy, O., Horton, E. S., & Plutzky, J. (2008). The peroxisome proliferator-activated receptor-gamma agonist pioglitazone represses inflammation in a peroxisome proliferator-activated receptor-alpha-dependent manner in vitro and in vivo in mice. *J Am Coll Cardiol*, *52*(10), 869-881. https://doi.org/10.1016/j.jacc.2008.04.055

Ou, H., Fu, Y., Liao, W., Zheng, C., & Wu, X. (2019). Association between Smoking and Liver Fibrosis among Patients with Nonalcoholic Fatty Liver Disease. *Can J Gastroenterol Hepatol*, *2019*, 6028952. https://doi.org/10.1155/2019/6028952

Paik, Y. H., Iwaisako, K., Seki, E., Inokuchi, S., Schnabl, B., Osterreicher, C. H., Kisseleva, T., & Brenner, D. A. (2011). The nicotinamide adenine dinucleotide phosphate oxidase (NOX) homologues NOX1 and NOX2/gp91(phox) mediate hepatic fibrosis in mice. *Hepatology*, *53*(5), 1730-1741. https://doi.org/10.1002/hep.24281

Panasyuk, G., Espeillac, C., Chauvin, C., Pradelli, L. A., Horie, Y., Suzuki, A., Annicotte, J. S., Fajas, L., Foretz, M., Verdeguer, F., Pontoglio, M., Ferre, P., Scoazec, J. Y., Birnbaum, M. J., Ricci, J. E., & Pende, M. (2012). PPARgamma contributes to PKM2 and HK2 expression in fatty liver. *Nat Commun*, *3*, 672. https://doi.org/10.1038/ncomms1667

Papazyan, R., Zhang, Y., & Lazar, M. A. (2016). Genetic and epigenomic mechanisms of mammalian circadian transcription. *Nat Struct Mol Biol*, *23*(12), 1045-1052. https://doi.org/10.1038/nsmb.3324

Pardee, K. I., Xu, X., Reinking, J., Schuetz, A., Dong, A., Liu, S., Zhang, R., Tiefenbach, J., Lajoie, G., Plotnikov, A. N., Botchkarev, A., Krause, H. M., & Edwards, A. (2009). The structural basis of gas-responsive transcription by the human nuclear hormone receptor REV-ERBbeta. *PLoS Biol*, *7*(2), e43. https://doi.org/10.1371/journal.pbio.1000043

Pariollaud, M., Gibbs, J. E., Hopwood, T. W., Brown, S., Begley, N., Vonslow, R., Poolman, T., Guo, B., Saer, B., Jones, D. H., Tellam, J. P., Bresciani, S., Tomkinson, N. C., Wojno-Picon, J., Cooper, A. W., Daniels, D. A., Trump, R. P., Grant, D., Zuercher, W., . . . Ray, D. W. (2018). Circadian clock component REV-ERBalpha controls homeostatic regulation of pulmonary inflammation. *J Clin Invest*, *128*(6), 2281-2296. https://doi.org/10.1172/JCI93910

Park, S. H., Helsley, R. N., Fadhul, T., Willoughby, J. L. S., Noetzli, L., Tu, H. C., Solheim, M. H., Fujisaka, S., Pan, H., Dreyfuss, J. M., Bons, J., Rose, J., King, C. D., Schilling, B., Lusis, A. J., Pan, C., Gupta, M., Kulkarni, R. N., Fitzgerald, K., . . . Softic, S. (2023). Fructose Induced KHK-C Increases ER Stress and Modulates Hepatic Transcriptome to Drive Liver Disease in Diet-Induced and Genetic Models of NAFLD. *bioRxiv*. https://doi.org/10.1101/2023.01.27.525605

Patel, P. J., Banh, X., Horsfall, L. U., Hayward, K. L., Hossain, F., Johnson, T., Stuart, K. A., Brown, N. N., Saad, N., Clouston, A., Irvine, K. M., Russell, A. W., Valery, P. C., Williams, S., & Powell, E. E. (2018). Underappreciation of non-alcoholic fatty liver disease by primary care clinicians: limited awareness of surrogate markers of fibrosis. *Intern Med J*, *48*(2), 144-151. https://doi.org/10.1111/imj.13667

Penvose, A., Keenan, J. L., Bray, D., Ramlall, V., & Siggers, T. (2019). Comprehensive study of nuclear receptor DNA binding provides a revised framework for understanding receptor specificity. *Nat Commun*, *10*(1), 2514. https://doi.org/10.1038/s41467-019-10264-3

Pereira, R. M., Botezelli, J. D., da Cruz Rodrigues, K. C., Mekary, R. A., Cintra, D. E., Pauli, J. R., da Silva, A. S. R., Ropelle, E. R., & de Moura, L. P. (2017). Fructose Consumption in the Development of Obesity and the Effects of Different Protocols of Physical Exercise on the Hepatic Metabolism. *Nutrients*, *9*(4). https://doi.org/10.3390/nu9040405

Perez-Carreras, M., Del Hoyo, P., Martin, M. A., Rubio, J. C., Martin, A., Castellano, G., Colina, F., Arenas, J., & Solis-Herruzo, J. A. (2003). Defective hepatic mitochondrial respiratory chain in patients with nonalcoholic steatohepatitis. *Hepatology*, *38*(4), 999-1007. https://doi.org/10.1053/jhep.2003.50398

Perry, R. J., Samuel, V. T., Petersen, K. F., & Shulman, G. I. (2014). The role of hepatic lipids in hepatic insulin resistance and type 2 diabetes. *Nature*, *510*(7503), 84-91. https://doi.org/10.1038/nature13478

Perry, R. J., Zhang, D., Zhang, X. M., Boyer, J. L., & Shulman, G. I. (2015). Controlled-release mitochondrial protonophore reverses diabetes and steatohepatitis in rats. *Science*, *347*(6227), 1253-1256. https://doi.org/10.1126/science.aaa0672

Pett, J. P., Korencic, A., Wesener, F., Kramer, A., & Herzel, H. (2016). Feedback Loops of the Mammalian Circadian Clock Constitute Repressilator. *PLoS Comput Biol*, *12*(12), e1005266. https://doi.org/10.1371/journal.pcbi.1005266

Phelan, C. A., Gampe, R. T., Jr., Lambert, M. H., Parks, D. J., Montana, V., Bynum, J., Broderick, T. M., Hu, X., Williams, S. P., Nolte, R. T., & Lazar, M. A. (2010). Structure of Rev-erbalpha bound to N-CoR reveals a unique mechanism of nuclear receptor-co-repressor interaction. *Nat Struct Mol Biol*, *17*(7), 808-814. https://doi.org/10.1038/nsmb.1860

Pittala, S., Krelin, Y., Kuperman, Y., & Shoshan-Barmatz, V. (2019). A Mitochondrial VDAC1-Based Peptide Greatly Suppresses Steatosis and NASH-Associated Pathologies in a Mouse Model. *Mol Ther*, *27*(10), 1848-1862. https://doi.org/10.1016/j.ymthe.2019.06.017

Pourcet, B., Zecchin, M., Ferri, L., Beauchamp, J., Sitaula, S., Billon, C., Delhaye, S., Vanhoutte, J., Mayeuf-Louchart, A., Thorel, Q., Haas, J. T., Eeckhoute, J., Dombrowicz, D., Duhem, C., Boulinguiez, A., Lancel, S., Sebti, Y., Burris, T. P., Staels, B., & Duez, H. M. (2018). Nuclear Receptor Subfamily 1 Group D Member 1 Regulates Circadian Activity of NLRP3 Inflammasome to

Reduce the Severity of Fulminant Hepatitis in Mice. *Gastroenterology*, *154*(5), 1449-1464 e1420. https://doi.org/10.1053/j.gastro.2017.12.019

Prasun, P., Ginevic, I., & Oishi, K. (2021). Mitochondrial dysfunction in nonalcoholic fatty liver disease and alcohol related liver disease. *Transl Gastroenterol Hepatol*, *6*, 4. https://doi.org/10.21037/tgh-20-125

Preitner, N., Damiola, F., Lopez-Molina, L., Zakany, J., Duboule, D., Albrecht, U., & Schibler, U. (2002). The orphan nuclear receptor REV-ERBalpha controls circadian transcription within the positive limb of the mammalian circadian oscillator. *Cell*, *110*(2), 251-260. https://doi.org/10.1016/s0092-8674(02)00825-5

Raghuram, S., Stayrook, K. R., Huang, P., Rogers, P. M., Nosie, A. K., McClure, D. B., Burris, L. L., Khorasanizadeh, S., Burris, T. P., & Rastinejad, F. (2007). Identification of heme as the ligand for the orphan nuclear receptors REV-ERBalpha and REV-ERBbeta. *Nat Struct Mol Biol*, *14*(12), 1207-1213. https://doi.org/10.1038/nsmb1344

Rahimi, S., Angaji, S. A., Majd, A., Hatami, B., & Baghaei, K. (2022). A fast and accurate mouse model for inducing non-alcoholic steatohepatitis. *Gastroenterol Hepatol Bed Bench*, *15*(4), 406-414. https://doi.org/10.22037/ghfbb.v15i4.2593

Rai, R. P., Liu, Y., Iyer, S. S., Liu, S., Gupta, B., Desai, C., Kumar, P., Smith, T., Singhi, A. D., Nusrat, A., Parkos, C. A., Monga, S. P., Czaja, M. J., Anania, F. A., & Raeman, R. (2020). Blocking integrin alpha(4)beta(7)-mediated CD4 T cell recruitment to the intestine and liver protects mice from western

diet-induced non-alcoholic steatohepatitis. *J Hepatol*, *73*(5), 1013-1022. https://doi.org/10.1016/j.jhep.2020.05.047

Ramakrishnan, S. N., & Muscat, G. E. (2006). The orphan Rev-erb nuclear receptors: a link between metabolism, circadian rhythm and inflammation? *Nucl Recept Signal*, *4*, e009. https://doi.org/10.1621/nrs.04009

Rau, M., Schilling, A. K., Meertens, J., Hering, I., Weiss, J., Jurowich, C., Kudlich, T., Hermanns, H. M., Bantel, H., Beyersdorf, N., & Geier, A. (2016). Progression from Nonalcoholic Fatty Liver to Nonalcoholic Steatohepatitis Is Marked by a Higher Frequency of Th17 Cells in the Liver and an Increased Th17/Resting Regulatory T Cell Ratio in Peripheral Blood and in the Liver. *J Immunol*, *196*(1), 97-105. https://doi.org/10.4049/jimmunol.1501175

Ray, K. (2021). Examining the prevalence of NAFLD and NASH in a US cohort. *Nat Rev Gastroenterol Hepatol*, *18*(5), 286. https://doi.org/10.1038/s41575-021-00446-0

Raza, G. S., Sodum, N., Kaya, Y., & Herzig, K. H. (2022). Role of Circadian Transcription Factor Rev-Erb in Metabolism and Tissue Fibrosis. *Int J Mol Sci*, *23*(21). https://doi.org/10.3390/ijms232112954

Reitz, C. J., Alibhai, F. J., Khatua, T. N., Rasouli, M., Bridle, B. W., Burris, T. P., & Martino, T. A. (2019). SR9009 administered for one day after myocardial ischemia-reperfusion prevents heart failure in mice by targeting the cardiac inflammasome. *Commun Biol*, *2*, 353. https://doi.org/10.1038/s42003-019-0595-z

Renaud, J. P., Harris, J. M., Downes, M., Burke, L. J., & Muscat, G. E. (2000). Structure-function analysis of the Rev-erbA and RVR ligand-binding domains reveals a large hydrophobic surface that mediates corepressor binding and a ligand cavity occupied by side chains. *Mol Endocrinol*, *14*(5), 700-717. https://doi.org/10.1210/mend.14.5.0444

Rui, L. (2014). Energy metabolism in the liver. *Compr Physiol*, *4*(1), 177-197. https://doi.org/10.1002/cphy.c130024

Saeed, A., Yang, J., Heegsma, J., Groen, A. K., van Mil, S. W. C., Paulusma, C. C., Zhou, L., Wang, B., & Faber, K. N. (2019). Farnesoid X receptor and bile acids regulate vitamin A storage. *Sci Rep*, *9*(1), 19493. https://doi.org/10.1038/s41598-019-55988-w

Said, A., Gagovic, V., Malecki, K., Givens, M. L., & Nieto, F. J. (2013). Primary care practitioners survey of non-alcoholic fatty liver disease. *Ann Hepatol*, *12*(5), 758-765. https://www.ncbi.nlm.nih.gov/pubmed/24018493

Satapati, S., Kucejova, B., Duarte, J. A., Fletcher, J. A., Reynolds, L., Sunny, N. E., He, T., Nair, L. A., Livingston, K. A., Fu, X., Merritt, M. E., Sherry, A. D., Malloy, C. R., Shelton, J. M., Lambert, J., Parks, E. J., Corbin, I., Magnuson, M. A., Browning, J. D., & Burgess, S. C. (2015). Mitochondrial metabolism mediates oxidative stress and inflammation in fatty liver. *J Clin Invest*, *125*(12), 4447-4462. https://doi.org/10.1172/JCI82204

Schattenberg, J. M., Lazarus, J. V., Newsome, P. N., Serfaty, L., Aghemo, A., Augustin, S., Tsochatzis, E., de Ledinghen, V., Bugianesi, E., Romero-Gomez, M., Bantel, H., Ryder, S. D., Boursier, J., Leroy, V., Crespo, J.,

Castera, L., Floros, L., Atella, V., Mestre-Ferrandiz, J., . . . Ratziu, V. (2021). Disease burden and economic impact of diagnosed non-alcoholic steatohepatitis in five European countries in 2018: A cost-of-illness analysis. *Liver Int*, *41*(6), 1227-1242. https://doi.org/10.1111/liv.14825

Seebacher, F., Zeigerer, A., Kory, N., & Krahmer, N. (2020). Hepatic lipid droplet homeostasis and fatty liver disease. *Semin Cell Dev Biol*, *108*, 72-81. https://doi.org/10.1016/j.semcdb.2020.04.011

Serviddio, G., Bellanti, F., Tamborra, R., Rollo, T., Capitanio, N., Romano, A. D., Sastre, J., Vendemiale, G., & Altomare, E. (2008). Uncoupling protein-2 (UCP2) induces mitochondrial proton leak and increases susceptibility of non-alcoholic steatohepatitis (NASH) liver to ischaemia-reperfusion injury. *Gut*, *57*(7), 957-965. https://doi.org/10.1136/gut.2007.147496

Sever, R., & Glass, C. K. (2013). Signaling by nuclear receptors. *Cold Spring Harb Perspect Biol*, *5*(3), a016709. https://doi.org/10.1101/cshperspect.a016709

Shannon, C. E., Ragavan, M., Palavicini, J. P., Fourcaudot, M., Bakewell, T. M., Valdez, I. A., Ayala, I., Jin, E. S., Madesh, M., Han, X., Merritt, M. E., & Norton, L. (2021). Insulin resistance is mechanistically linked to hepatic mitochondrial remodeling in non-alcoholic fatty liver disease. *Mol Metab*, *45*, 101154. https://doi.org/10.1016/j.molmet.2020.101154

Soares-da-Silva, P. (1986). Evidence for a non-precursor dopamine pool in noradrenergic neurones of the dog mesenteric artery. *Naunyn Schmiedebergs Arch Pharmacol*, *333*(3), 219-223. https://doi.org/10.1007/BF00512932

Solt, L. A., Wang, Y., Banerjee, S., Hughes, T., Kojetin, D. J., Lundasen, T., Shin, Y., Liu, J., Cameron, M. D., Noel, R., Yoo, S. H., Takahashi, J. S., Butler, A. A., Kamenecka, T. M., & Burris, T. P. (2012). Regulation of circadian behaviour and metabolism by synthetic REV-ERB agonists. *Nature*, *485*(7396), 62-68. https://doi.org/10.1038/nature11030

Stujanna, E. N., Murakoshi, N., Tajiri, K., Xu, D., Kimura, T., Qin, R., Feng, D., Yonebayashi, S., Ogura, Y., Yamagami, F., Sato, A., Nogami, A., & Aonuma, K. (2017). Rev-erb agonist improves adverse cardiac remodeling and survival in myocardial infarction through an anti-inflammatory mechanism. *PLoS One*, *12*(12), e0189330. https://doi.org/10.1371/journal.pone.0189330

Sun, X., Seidman, J. S., Zhao, P., Troutman, T. D., Spann, N. J., Que, X., Zhou, F., Liao, Z., Pasillas, M., Yang, X., Magida, J. A., Kisseleva, T., Brenner, D. A., Downes, M., Evans, R. M., Saltiel, A. R., Tsimikas, S., Glass, C. K., & Witztum, J. L. (2020). Neutralization of Oxidized Phospholipids Ameliorates Non-alcoholic Steatohepatitis. *Cell Metab*, *31*(1), 189-206 e188. https://doi.org/10.1016/j.cmet.2019.10.014

Sunny, N. E., Parks, E. J., Browning, J. D., & Burgess, S. C. (2011). Excessive hepatic mitochondrial TCA cycle and gluconeogenesis in humans with nonalcoholic fatty liver disease. *Cell Metab*, *14*(6), 804-810. https://doi.org/10.1016/j.cmet.2011.11.004

Sutti, S., & Albano, E. (2020). Adaptive immunity: an emerging player in the progression of NAFLD. *Nat Rev Gastroenterol Hepatol*, *17*(2), 81-92. https://doi.org/10.1038/s41575-019-0210-2

Svegliati-Baroni, G., Saccomanno, S., van Goor, H., Jansen, P., Benedetti, A., & Moshage, H. (2001). Involvement of reactive oxygen species and nitric oxide radicals in activation and proliferation of rat hepatic stellate cells. *Liver*, *21*(1), 1-12. https://doi.org/10.1034/j.1600-0676.2001.210101.x

Tang, Y., Bian, Z., Zhao, L., Liu, Y., Liang, S., Wang, Q., Han, X., Peng, Y., Chen, X., Shen, L., Qiu, D., Li, Z., & Ma, X. (2011). Interleukin-17 exacerbates hepatic steatosis and inflammation in non-alcoholic fatty liver disease. *Clin Exp Immunol*, *166*(2), 281-290. https://doi.org/10.1111/j.1365-2249.2011.04471.x

Targher, G., Bertolini, L., Padovani, R., Rodella, S., Tessari, R., Zenari, L., Day, C., & Arcaro, G. (2007). Prevalence of nonalcoholic fatty liver disease and its association with cardiovascular disease among type 2 diabetic patients. *Diabetes Care*, *30*(5), 1212-1218. https://doi.org/10.2337/dc06-2247

Taylor, C. T., & Scholz, C. C. (2022). The effect of HIF on metabolism and immunity. *Nat Rev Nephrol*, *18*(9), 573-587. https://doi.org/10.1038/s41581-022-00587-8

Teboul, M., & Delaunay, F. (2003). [The orphan nuclear receptor Rev-erb alpha is a major component of the circadian clock]. *Med Sci (Paris)*, *19*(4), 411-413. https://doi.org/10.1051/medsci/2003194411 (Le recepteur nucleaire orphelin Rev-erb alpha oscille entre repression et activation.)

Tontonoz, P., & Mangelsdorf, D. J. (2003). Liver X receptor signaling pathways in cardiovascular disease. *Mol Endocrinol*, *17*(6), 985-993. https://doi.org/10.1210/me.2003-0061

Torres-Hernandez, A., Wang, W., Nikiforov, Y., Tejada, K., Torres, L., Kalabin, A., Adam, S., Wu, J., Lu, L., Chen, R., Lemmer, A., Camargo, J., Hundeyin, M., Diskin, B., Aykut, B., Kurz, E., Kochen Rossi, J. A., Khan, M., Liria, M., . . . Miller, G. (2020). gammadelta T Cells Promote Steatohepatitis by Orchestrating Innate and Adaptive Immune Programming. *Hepatology*, *71*(2), 477-494. https://doi.org/10.1002/hep.30952

Trevaskis, J. L., Griffin, P. S., Wittmer, C., Neuschwander-Tetri, B. A., Brunt, E. M., Dolman, C. S., Erickson, M. R., Napora, J., Parkes, D. G., & Roth, J. D. (2012). Glucagon-like peptide-1 receptor agonism improves metabolic, biochemical, and histopathological indices of nonalcoholic steatohepatitis in mice. *Am J Physiol Gastrointest Liver Physiol*, *302*(8), G762-772. https://doi.org/10.1152/ajpgi.00476.2011

Van Wagner, L. B., & Rinella, M. E. (2011). The role of insulin-sensitizing agents in the treatment of nonalcoholic steatohepatitis. *Therap Adv Gastroenterol*, *4*(4), 249-263. https://doi.org/10.1177/1756283X11403809

Vander Haar, E., Lee, S. I., Bandhakavi, S., Griffin, T. J., & Kim, D. H. (2007). Insulin signalling to mTOR mediated by the Akt/PKB substrate PRAS40. *Nat Cell Biol*, *9*(3), 316-323. https://doi.org/10.1038/ncb1547

Vieira, E., Marroqui, L., Batista, T. M., Caballero-Garrido, E., Carneiro, E. M., Boschero, A. C., Nadal, A., & Quesada, I. (2012). The clock gene Rev-

erbalpha regulates pancreatic beta-cell function: modulation by leptin and high-fat diet. *Endocrinology*, *153*(2), 592-601. https://doi.org/10.1210/en.2011-1595

Vieira, E., Marroqui, L., Figueroa, A. L., Merino, B., Fernandez-Ruiz, R., Nadal, A., Burris, T. P., Gomis, R., & Quesada, I. (2013). Involvement of the clock gene Rev-erb alpha in the regulation of glucagon secretion in pancreatic alpha-cells. *PLoS One*, *8*(7), e69939. https://doi.org/10.1371/journal.pone.0069939

Wang, H., Zhang, H., Wang, Y., Brown, Z. J., Xia, Y., Huang, Z., Shen, C., Hu, Z., Beane, J., Ansa-Addo, E. A., Huang, H., Tian, D., & Tsung, A. (2021). Regulatory T-cell and neutrophil extracellular trap interaction contributes to carcinogenesis in non-alcoholic steatohepatitis. *J Hepatol*, *75*(6), 1271-1283. https://doi.org/10.1016/j.jhep.2021.07.032

Wang, S., Kozai, M., Mita, H., Cai, Z., Masum, M. A., Ichii, O., Takada, K., & Inaba, M. (2021). REV-ERB agonist suppresses IL-17 production in gammadeltaT cells and improves psoriatic dermatitis in a mouse model. *Biomed Pharmacother*, *144*, 112283. https://doi.org/10.1016/j.biopha.2021.112283

Wang, S., Lin, Y., Yuan, X., Li, F., Guo, L., & Wu, B. (2018). REV-ERBalpha integrates colon clock with experimental colitis through regulation of NF-kappaB/NLRP3 axis. *Nat Commun*, *9*(1), 4246. https://doi.org/10.1038/s41467-018-06568-5

Wang, T., Chen, K., Yao, W., Zheng, R., He, Q., Xia, J., Li, J., Shao, Y., Zhang, L., Huang, L., Qin, L., Xu, M., Zhang, Z., Pan, D., Li, Z., & Huang, F. (2021).

Acetylation of lactate dehydrogenase B drives NAFLD progression by impairing lactate clearance. *J Hepatol*, *74*(5), 1038-1052. https://doi.org/10.1016/j.jhep.2020.11.028

Wang, Y., Li, N., Zhang, X., & Horng, T. (2021). Mitochondrial metabolism regulates macrophage biology. *J Biol Chem*, *297*(1), 100904. https://doi.org/10.1016/j.jbc.2021.100904

Watanabe, M., Houten, S. M., Wang, L., Moschetta, A., Mangelsdorf, D. J., Heyman, R. A., Moore, D. D., & Auwerx, J. (2004). Bile acids lower triglyceride levels via a pathway involving FXR, SHP, and SREBP-1c. *J Clin Invest*, *113*(10), 1408-1418. https://doi.org/10.1172/JCI21025

Welch, R. D., Guo, C., Sengupta, M., Carpenter, K. J., Stephens, N. A., Arnett, S. A., Meyers, M. J., Sparks, L. M., Smith, S. R., Zhang, J., Burris, T. P., & Flaveny, C. A. (2017). Rev-Erb co-regulates muscle regeneration via tethered interaction with the NF-Y cistrome. *Mol Metab*, *6*(7), 703-714. https://doi.org/10.1016/j.molmet.2017.05.001

Westermaier, Y., Ruiz-Carmona, S., Theret, I., Perron-Sierra, F., Poissonnet, G., Dacquet, C., Boutin, J. A., Ducrot, P., & Barril, X. (2017). Binding mode prediction and MD/MMPBSA-based free energy ranking for agonists of REV-ERBalpha/NCoR. *J Comput Aided Mol Des*, *31*(8), 755-775. https://doi.org/10.1007/s10822-017-0040-7

Wilson, C. G., Tran, J. L., Erion, D. M., Vera, N. B., Febbraio, M., & Weiss, E. J. (2016). Hepatocyte-Specific Disruption of CD36 Attenuates Fatty Liver and

Improves Insulin Sensitivity in HFD-Fed Mice. *Endocrinology*, *157*(2), 570-585. https://doi.org/10.1210/en.2015-1866

Woldt, E., Sebti, Y., Solt, L. A., Duhem, C., Lancel, S., Eeckhoute, J., Hesselink, M. K., Paquet, C., Delhaye, S., Shin, Y., Kamenecka, T. M., Schaart, G., Lefebvre, P., Neviere, R., Burris, T. P., Schrauwen, P., Staels, B., & Duez, H. (2013). Rev-erb-alpha modulates skeletal muscle oxidative capacity by regulating mitochondrial biogenesis and autophagy. *Nat Med*, *19*(8), 1039-1046. https://doi.org/10.1038/nm.3213

Wolf Greenstein, A., Majumdar, N., Yang, P., Subbaiah, P. V., Kineman, R. D., & Cordoba-Chacon, J. (2017). Hepatocyte-specific, PPARgamma-regulated mechanisms to promote steatosis in adult mice. *J Endocrinol*, *232*(1), 107-121. https://doi.org/10.1530/JOE-16-0447

Wolf, M. J., Adili, A., Piotrowitz, K., Abdullah, Z., Boege, Y., Stemmer, K., Ringelhan, M., Simonavicius, N., Egger, M., Wohlleber, D., Lorentzen, A., Einer, C., Schulz, S., Clavel, T., Protzer, U., Thiele, C., Zischka, H., Moch, H., Tschop, M., . . . Heikenwalder, M. (2014). Metabolic activation of intrahepatic CD8+ T cells and NKT cells causes nonalcoholic steatohepatitis and liver cancer via cross-talk with hepatocytes. *Cancer Cell*, *26*(4), 549-564. https://doi.org/10.1016/j.ccell.2014.09.003

Wu, N., Yin, L., Hanniman, E. A., Joshi, S., & Lazar, M. A. (2009). Negative feedback maintenance of heme homeostasis by its receptor, Rev-erbalpha. *Genes Dev*, *23*(18), 2201-2209. https://doi.org/10.1101/gad.1825809

Xian, H., Watari, K., Sanchez-Lopez, E., Offenberger, J., Onyuru, J., Sampath, H., Ying, W., Hoffman, H. M., Shadel, G. S., & Karin, M. (2022). Oxidized DNA fragments exit mitochondria via mPTP- and VDAC-dependent channels to activate NLRP3 inflammasome and interferon signaling. *Immunity*, *55*(8), 1370-1385 e1378. https://doi.org/10.1016/j.immuni.2022.06.007

Xiao, N., & DeFranco, D. B. (1997). Overexpression of unliganded steroid receptors activates endogenous heat shock factor. *Mol Endocrinol*, *11*(9), 1365-1374. https://doi.org/10.1210/mend.11.9.9976

Xu, G. X., Wei, S., Yu, C., Zhao, S. Q., Yang, W. J., Feng, Y. H., Pan, C., Yang, K. X., & Ma, Y. (2023). Activation of Kupffer cells in NAFLD and NASH: mechanisms and therapeutic interventions. *Front Cell Dev Biol*, *11*, 1199519. https://doi.org/10.3389/fcell.2023.1199519

Xu, X., So, J. S., Park, J. G., & Lee, A. H. (2013). Transcriptional control of hepatic lipid metabolism by SREBP and ChREBP. *Semin Liver Dis*, *33*(4), 301-311. https://doi.org/10.1055/s-0033-1358523

Yamaguchi, K., Yang, L., McCall, S., Huang, J., Yu, X. X., Pandey, S. K., Bhanot, S., Monia, B. P., Li, Y. X., & Diehl, A. M. (2007). Inhibiting triglyceride synthesis improves hepatic steatosis but exacerbates liver damage and fibrosis in obese mice with nonalcoholic steatohepatitis. *Hepatology*, *45*(6), 1366-1374. https://doi.org/10.1002/hep.21655

Yang, G., Lee, H. E., & Lee, J. Y. (2016). A pharmacological inhibitor of NLRP3 inflammasome prevents non-alcoholic fatty liver disease in a mouse model

induced by high fat diet. *Sci Rep*, *6*, 24399. https://doi.org/10.1038/srep24399

Yecies, J. L., Zhang, H. H., Menon, S., Liu, S., Yecies, D., Lipovsky, A. I., Gorgun, C., Kwiatkowski, D. J., Hotamisligil, G. S., Lee, C. H., & Manning, B. D. (2011). Akt stimulates hepatic SREBP1c and lipogenesis through parallel mTORC1-dependent and independent pathways. *Cell Metab*, *14*(1), 21-32. https://doi.org/10.1016/j.cmet.2011.06.002

Yin, L., Wu, N., & Lazar, M. A. (2010). Nuclear receptor Rev-erbalpha: a heme receptor that coordinates circadian rhythm and metabolism. *Nucl Recept Signal*, *8*, e001. https://doi.org/10.1621/nrs.08001

Yin, Y., Kong, D., He, K., & Xia, Q. (2021). Regeneration and activation of liver progenitor cells in liver cirrhosis. *Genes Dis*, *8*(5), 623-628. https://doi.org/10.1016/j.gendis.2020.07.016

Yoshikawa, T., Shimano, H., Amemiya-Kudo, M., Yahagi, N., Hasty, A. H., Matsuzaka, T., Okazaki, H., Tamura, Y., Iizuka, Y., Ohashi, K., Osuga, J., Harada, K., Gotoda, T., Kimura, S., Ishibashi, S., & Yamada, N. (2001). Identification of liver X receptor-retinoid X receptor as an activator of the sterol regulatory element-binding protein 1c gene promoter. *Mol Cell Biol*, *21*(9), 2991-3000. https://doi.org/10.1128/MCB.21.9.2991-3000.2001

Yu, Q., Wang, Y., Dong, L., He, Y., Liu, R., Yang, Q., Cao, Y., Wang, Y., Jia, A., Bi, Y., & Liu, G. (2020). Regulations of Glycolytic Activities on Macrophages Functions in Tumor and Infectious Inflammation. *Front Cell Infect Microbiol*, *10*, 287. https://doi.org/10.3389/fcimb.2020.00287

Yu, X., Rollins, D., Ruhn, K. A., Stubblefield, J. J., Green, C. B., Kashiwada, M., Rothman, P. B., Takahashi, J. S., & Hooper, L. V. (2013). TH17 cell differentiation is regulated by the circadian clock. *Science*, *342*(6159), 727-730. https://doi.org/10.1126/science.1243884

Zhang, L., Zhang, R., Tien, C. L., Chan, R. E., Sugi, K., Fu, C., Griffin, A. C., Shen, Y., Burris, T. P., Liao, X., & Jain, M. K. (2017). REV-ERBalpha ameliorates heart failure through transcription repression. *JCI Insight*, *2*(17). https://doi.org/10.1172/jci.insight.95177

Zhang, Y., Li, Y., Mu, T., Tong, N., & Cheng, P. (2021). Hepatic stellate cells specific liposomes with the Toll-like receptor 4 shRNA attenuates liver fibrosis. *J Cell Mol Med*, *25*(2), 1299-1313. https://doi.org/10.1111/jcmm.16209

Zhang, Y., Papazyan, R., Damle, M., Fang, B., Jager, J., Feng, D., Peed, L. C., Guan, D., Sun, Z., & Lazar, M. A. (2017). The hepatic circadian clock fine-tunes the lipogenic response to feeding through RORalpha/gamma. *Genes Dev*, *31*(12), 1202-1211. https://doi.org/10.1101/gad.302323.117

Zhou, Y., Wang, S., Li, Y., Yu, S., & Zhao, Y. (2017). SIRT1/PGC-1alpha Signaling Promotes Mitochondrial Functional Recovery and Reduces Apoptosis after Intracerebral Hemorrhage in Rats. *Front Mol Neurosci*, *10*, 443. https://doi.org/10.3389/fnmol.2017.00443